

DEVELOPMENT, EVALUATION, AND APPLICATION OF CHROMATOGRAPHIC RESOLUTION
ENHANCEMENT STRATEGIES

by

GARRETT HELLINGHAUSEN

Presented to the Faculty of the Graduate School of
The University of Texas at Arlington in Partial Fulfillment
of the Requirements for the Degree of

DOCTOR OF PHILOSOPHY

THE UNIVERSITY OF TEXAS AT ARLINGTON

December 2019

copyright

Abstract

Development, Evaluation, And Application of Chromatographic Resolution Enhancement Strategies

Garrett Hellinghausen, PhD

The University of Texas at Arlington, 2019

Supervising Professor: Daniel W. Armstrong

With the emergence of advanced separation technologies, like high-efficiency stationary phases bonded with superficially porous particles, or sub-2 μm fully porous particles, faster and more effective methodologies are possible for liquid chromatographic analyses. Such advanced approaches can be easily applied to achiral separations but require more extensive optimization for chiral separations. Chiral molecules are subjected to extensive characterization of their enantiomeric pharmacological properties due to requirements of the Food and Drug Administration. Herein, fundamental chiral method development strategies are thoroughly discussed for hundreds of small molecules using conventional and newly synthesized chiral selectors bonded to high-efficiency supports. In these strategies the principle of complementary behavior is utilized, in which a separation can be obtained just by switching the chiral selector. These methodologies were developed with cyclofructans, cyclodextrins, and macrocyclic glycopeptides as chiral selectors. A variety of organic modifiers and additives were investigated for each selector to determine the best screening protocol, which is often the optimal separation condition. Solvents compatible with mass spectrometry were primarily used to promote sensitive biological enantiomeric analysis. Utilizing these strategies led to the development of modified selectors to target separations of specific analytes, like nicotine. Applications were reported, including the determination of high levels of an unnatural nicotine enantiomer in commercial products that has not been deemed safe. Despite the increased efficiency from small, superficially porous particles and high selectivity from novel selectors, chromatographic peak overlap can still be observed in some cases. Quantitation becomes more inaccurate as chromatographic resolution decreases, especially with asymmetric peaks because peak

integration becomes ambiguous. Conventional strategies to increase chromatographic resolution focus on the use of high efficiency supports bonded to novel selectors analyzed with high resolution instruments. Instead, mathematical approaches were applied after data collection or post-signal acquisition. Signal processing is well established in optical and nuclear magnetic resonance spectroscopy. Herein, these principles have been applied to chromatography data. While there is a focus of using these techniques for fast ultra-high-pressure liquid chromatographic analysis, they can be applied to any chromatographic data (i.e., gas, liquid, supercritical fluid, capillary electrophoresis, etc.). Mathematical approaches using derivatives or power law can enhance resolution of overlapping peaks, usually by reducing peak widths and reduce background noise. These techniques maintain the retention time and area of each peak that is needed for accurate quantitation. It has been shown that there is minimal error ($< 1\%$) in processed peak areas when the overlapping pair is separated enough to distinguish the peaks' maximum (a resolution = ~ 0.8). Derivatives and power law are also useful for impurity and peak purity analysis. Once automated and integrated within chromatography data software, these techniques will revolutionize the chromatography field in a way that is similar to previous spectroscopy advancements. The advantages and limitations of each technique have been determined to facilitate the appropriate use of post-acquisition signal processing resolution enhancement strategies.

Acknowledgements

I would like to acknowledge the individuals who have encouraged and supported me during my graduate research work. First, to Professor Armstrong for the opportunity and guidance he gave to work in his research group. He taught me to question reported literature. As he would say, “Paper never refused ink.” His knowledge of separations and encouragement to present research at conferences has certainly put me in a position for success as an analytical chemist. Research scientists, Dr. J.T. Lee and Dr. Farooq Wahab have always been available for advice and provided ideas and support for my research. I would also like to extend my appreciation to all my co-authors at UTA including Daipayan Roy, Dr. Yadi Wang, Dr. Choyce Weatherly, Dr. Diego Lopez, Elizabeth Readell, and Abiud Portillo. My sincerest gratitude to Dr. Zach Breitbach, who provided me with the opportunity to gain experience and expand my skill set as an intern at AbbVie Pharmaceuticals. Thanks to my committee members who have provided constructive advice to my research and future career. Last, and most important, thanks must be given to my family. My parents and sisters have always supported me in my pursuits. Even if they never fully understood “chiral separations” they never dismissed my enthusiasm. My wife, Maddie, was present through every aspect of my graduate research. Her support, kindness, and encouragement provided the foundation for my success. Without these individuals, this dissertation would not be possible.

I dedicate this dissertation to my parents, Holly and Doug, and my wife, Maddie.

Contents

Abstract	i
Acknowledgements.....	iii
List of Illustrations	x
List of Tables	xiii
Chapter 1	1
Introduction.....	1
1.1 Resolution and the focus on selectivity in chiral separations.....	1
1.2 Updating screening methodologies with new technologies	2
1.3 Post-acquisition signal processing	4
1.4 Organization of dissertation	5
1.5 References.....	6
Chapter 2.....	8
Effective methodologies for enantiomeric separations of 150 pharmacology and toxicology related 1°, 2°, and 3° amines with core-shell chiral stationary phases.....	8
2.1 Abstract	8
2.2 Introduction.....	8
2.3 Experimental	10
2.4 Results and discussion	21
2.5 Conclusions.....	28
2.6 References.....	28
Chapter 3.....	31

Evaluation of the Edman degradation product of vancomycin bonded to core-shell particles as a new HPLC chiral stationary phase	31
3.1 Abstract	31
3.2 Introduction.....	31
3.3 Materials and methods	33
3.4 Results and discussion	36
3.5 Conclusions.....	45
3.6 References.....	45
Chapter 4.....	48
Evaluation of Nicotine in Tobacco Free Nicotine Commercial Products: Nicotine Enantiomers in Tobacco Free Nicotine	48
4.1 Abstract	48
4.2 Introduction.....	48
4.3 Experimental	51
4.4 Results and discussion	53
4.5 Conclusions.....	57
4.6 References.....	58
Chapter 5.....	60
A comprehensive methodology for the chiral separation of 40 tobacco alkaloids and their carcinogenic E/Z-(R,S)-tobacco-specific nitrosamine metabolites	60
5.1 Abstract	60
5.2 Introduction.....	60

5.3 Materials and methods	65
5.4 Results.....	69
5.5 Discussion	76
5.6 References.....	79
Chapter 6.....	83
Mass Spectrometry-Compatible Enantiomeric Separations of 100 Pesticides Using Core–Shell Chiral Stationary Phases and Evaluation of Iterative Curve Fitting Models for Overlapping Peaks	83
6.1 Abstract	83
6.2 Introduction.....	83
6.3 Experimental	85
6.4 Results and discussion	87
6.5 Concluding remarks	100
6.6 References.....	101
Chapter 7.....	103
Increasing chromatographic resolution of analytical signals using derivative enhancement approach	103
7.1 Abstract	103
7.2 Introduction.....	103
7.3 Theory	105
7.4 Materials and methods	107
7.5 Results and discussion	109
7.6 Conclusions.....	121
7.7 References.....	121

Chapter 8.....	124
Improving visualization of trace components for quantification using a power law based integration approach.....	124
8.1 Abstract	124
8.2 Introduction.....	125
8.3 Materials and methods	128
8.4 Results and discussion	129
8.5 Conclusions.....	139
8.6 References.....	140
Chapter 9.....	143
Progress in Peak Processing.....	143
9.1 Abstract	143
9.2 Introduction.....	143
9.3 Discussion.....	146
9.4 Conclusions.....	158
9.5 References.....	159
Chapter 10.....	160
Separating 101 Compounds in Less than 60 Seconds: <i>Operating Above Normal Peak Capacity Limits with Signal Processing</i>	160
10.1 Abstract.....	160
10.2 Introduction.....	160
10.3 Materials and methods	163

10.4 Results and discussion	166
10.5 Conclusions.....	174
10.6 References.....	174
Chapter 11.....	177
Summary and Future Outlook.....	177
Appendix A: Chapter co-authors & citations.....	178
Appendix B: Rights and permissions.....	179

List of Illustrations

Chapter 1 Figure 1. Structures of chiral selectors	3
Chapter 2 Figure 1. Method development of chiral amines.....	21
Chapter 2 Figure 2. Baseline separation results of 150 chiral 1°, 2°, and 3° amines.....	22
Chapter 2 Figure 3 The principle of complementary separations.....	23
Chapter 2 Figure 4. Chromatographic enantioseparation of 18 racemic controlled substance stimulant amines using liquid chromatography electrospray-mass spectrometry (LC-ESI-MS).....	24
Chapter 3 Figure 1. Structures of vancomycin and the vancomycin Edman degradation product.	34
Chapter 3 Figure 2. Percentage of racemic compounds separated by each macrocyclic glycopeptide-based chiral stationary phase.....	42
Chapter 3 Figure 3. Comparison of resolution obtained for macrocyclic glycopeptide-based selectors.....	43
Chapter 3 Figure 4. Highlighted applications of core-shell macrocyclic glycopeptide-based chiral stationary phases.....	44
Chapter 4 Figure 1. Optimized enantiomeric separation of nicotine standard.....	54
Chapter 4 Figure 2. Enantiomeric separation of nornicotine standard.....	55
Chapter 4 Figure 3. The enantiomeric separation of a nicotine standard and a TFN product, Coastline Stinson.	55
Chapter 5 Figure 1. Ultra-fast LC enantioseparation of nicotine.....	69
Chapter 5 Figure 2. Separation of ring-closed and ring-open equilibrating tobacco alkaloids.....	73
Chapter 5 Figure 3. Chromatographic separation and detection of 10 tobacco alkaloids and 7 nicotine metabolites.....	74
Chapter 5 Figure 4. The direct separation of tobacco-specific nitrosamines.....	75

Chapter 6 Figure 1. Optimized enantiomeric separations of pesticides.....	91
Chapter 6 Figure 2. Simultaneous enantiomeric separation of 14 racemic fungicides.....	93
Chapter 6 Figure 3. Enantiomeric separation trends of phenoxypropionate herbicides and their phenoxypropionic acid metabolites.....	95
Chapter 6 Figure 4. Iterative curve fitting of two pyrethroids.....	99
Chapter 7 Figure 1. Demonstration of the steps involved in the resolution enhancement process using even-derivatives.....	106
Chapter 7 Figure 2. Resolution of three pure overlapping Lorentzian peaks using the peak sharpening principle based on even-derivatives.....	110
Chapter 7 Figure 3. Recovery of peak areas of chiral separations using the even-derivative method.....	112
Chapter 7 Figure 4. Extraction of peak areas in the selected region using even-derivatives.....	115
Chapter 7 Figure 5. Clarifying peak shoulders using derivative sharpening.....	118
Chapter 7 Figure 6. Resolution and peak shape improvement using the first and second derivatives.....	120
Chapter 8 Figure 1. Normalized power law protocol for resolution enhancement.....	127
Chapter 8 Figure 2. Visualization and integration of trace enantiomers using normalized power law protocol.....	130
Chapter 8 Figure 3. Clarifying trace enantiomeric shoulders.....	133
Chapter 8 Figure 4. Visualization and quantitation of an embedded trace enantiomeric peak.....	136
Chapter 8 Figure 5. Utilizing a segmented normalized power law approach.....	138
Chapter 9 Figure 1. Removal of extra-column band broadening effects by Fourier transform deconvolution.....	147

Chapter 9 Figure 2. Iterative curve fitting of 7 simulated peaks with different peak heights, areas, and shapes.....	149
Chapter 9 Figure 3. Directly increasing resolution of two overlapping pairs by modified power law.....	153
Chapter 9 Figure 4. Sharpening peaks with even-derivatives.....	155
Chapter 9 Figure 5. Overview of each signal processing technique.	157
Chapter 10 Figure 1. The separation of 101 components in under 60 seconds.....	167
Chapter 10 Figure 2. Signal processing of the separation of 101 components in under 60 seconds	170
Chapter 10 Figure 3. The increased chromatographic resolution of the original chromatogram of 101 components ($n = 1$) when powered by $n = 3, 5,$ and 7	172

List of Tables

Chapter 2 Table 1. Optimized chiral separations of primary (1°) amines	13
Chapter 2 Table 2. Optimized chiral separations of secondary (2°) amines	16
Chapter 2 Table 3. Optimized chiral separations of tertiary (3°) amines	19
Chapter 3 Table 1. Chiral separation comparisons using core-shell macrocyclic glycopeptide-based CSPs.	36
Chapter 4 Table 1. Evaluation of enantiomeric ratio of nicotine in commercial tobacco products and TFN products.....	57
Chapter 5 Table 1. Structures of nicotine-related compounds	65
Chapter 5 Table 2. Optimized enantiomeric separations of nicotine-related compounds using macrocyclic glycopeptides.	70
Chapter 6 Table 1. Optimized enantiomeric separations of 100 chiral pesticides.	88
Chapter 6 Table 2. Area extraction of overlapped peaks using iterative curve fitting of 13 compounds. ...	97
Chapter 7 Table 1. Resolution enhancement using even-derivatives or first-second derivative combination.....	109
Chapter 7 Table 2. Comparison of errors in area recovery as a function of initial resolution of Gaussian peaks of equal area.....	113
Chapter 7 Table 3. Comparison of extracted areas by the proposed derivative method for the separation of deuterated benzenes.	115
Chapter 8 Table 1. Simulated R_s limitations for trace component analysis of peaks with an area ratio of <1:99.....	128
Chapter 9 Table 1. Overview of advanced signal processing techniques.	145
Chapter 10 Table 1. Signal processing protocols.....	165

Chapter 10 Table 2. Gain in chromatographic resolution and peak capacity using signal processing approaches.....	168
Chapter 10 Table 3. Representative quantitation evaluation of signal processing techniques.....	173

Chapter 1

Introduction

1.1 Resolution and the focus on selectivity in chiral separations

Recently, advances in chromatography technologies and instrumentation, like the use of sub-2 μm particles and ultra-high-pressure liquid chromatographs (UHPLCs), have provided a platform for extremely high-efficiency separations [1]. Even so, there are cases where one or two critical pairs of chromatographic peaks overlap and are not easily and accurately quantitated. Often, this is the case in chiral separations, where enantiomers require specific simultaneous interactions to separate. Chiral separations are typically done with a chiral stationary phase (CSP) that consists of a chiral selector bonded to a chromatographic support. Often, chiral separations are used to differentiate enantiomers and study their pharmacological properties. The FDA states that “the pharmacology and toxicology of the enantiomer should be characterized for the principal effects and any other pharmacological effect, with respect to potency, specificity, maximum effect, etc.” [2]. In some racemic mixtures, one of the enantiomers is inactive or contributes very little pharmacologically or in opposition compared to the other enantiomer [2]. Therefore, there is a need to analyze enantiomeric levels in new and untested drugs, food substances, natural products, etc. Generally, the main objective of analytical chromatographic analysis is to identify and quantitate an analyte or analytes subjected to a separation that is represented by their chromatographic peaks (retention time, peak area, etc.).

The fundamental resolution equation 1 provides three terms that represent chromatographic separations [3].

$$R_s = \left(\frac{\sqrt{N}}{4}\right) \left(\frac{\alpha-1}{\alpha}\right) \left(\frac{k_2}{1+k_2}\right) \quad (1)$$

Resolution, (R_s), is dependent on efficiency (N), selectivity (α), and the retention factor (k) of the analyte(s) subjected to separation. The goal of any chromatographic separation is to get baseline separation, $R_s = 1.5$, so each peak is clear to integrate. Usually, the integrated peak is then compared to a

calibration curve to quantify the components' concentration. With advanced chromatographic technologies, N may be high, but R_s only scales by \sqrt{N} . Also, fast separations are desired, which often results in low retention factors. Typically, chromatographers target α , which scales proportionally in relation to resolution. Selectivity is defined in equation 2.

$$\alpha = \frac{k_2}{k_1} \quad (2)$$

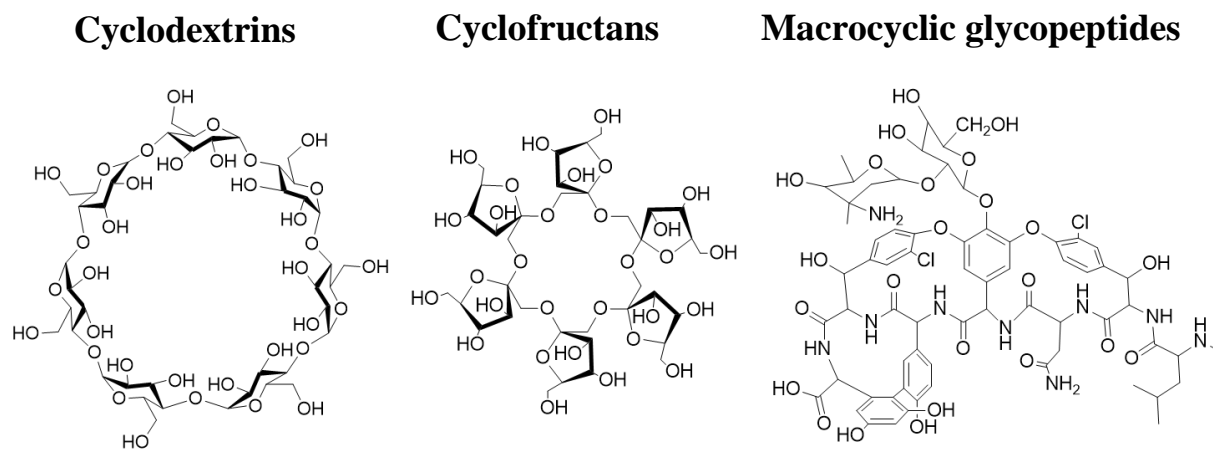
Selectivity is the ratio of the retention factors for two chromatographic peaks (k_2 and k_1). Another common definition is the “peak to peak” separation between adjacent chromatographic peaks. In chiral separations, the enantiomers are usually differentiated by their interactions with a CSP [4]. The analytes' enantiomers have different geometries that provide potential differences in interaction with the stationary phase, which results in enantiomeric separation. Common chiral selectors include cyclofructans, cyclodextrins, macrocyclic glycopeptides, polysaccharides, crown ethers, etc. [4]. Efforts are ongoing to discover/develop new classes of effective chiral selectors. Often, unique selectivity can be achieved by modifying the original selector. For example, native cyclofructans have very limited selectivity for any chiral molecule, but isopropyl derivatized cyclofructan-6 stationary phase is known to separate $\geq 90\%$ of all enantiomers that have a primary amine group [5].

1.2 Updating screening methodologies with new technologies

Derivatized chiral selectors, or selectors of the same class (i.e., vancomycin and teicoplanin of the macrocyclic glycopeptides) often show complementary effects. A separation not achieved with one selector may be obtained, even if the separation conditions are the same, just by switching from one chiral selector to the other [6]. Thus, these chiral selectors are complementary to one another. Chromatographic screening protocols often employ this principle [7]. Then, excessive time is spent in method development to choose optimal conditions for a specific separation (i.e., stationary phase type, length, and inner diameter, mobile phase additives and modifiers, temperature, etc.). Unfortunately, most industrial methodologies aren't updated to reflect the gains in resolution provided with advanced column and instrument technologies. Significant gains pertaining to the reduction of analytes time with similar

resolution (due to gains in N) have been reported with the use of chiral selectors bonded to smaller, 2.7 μm superficially porous particles (SPPs) as compared to conventional 5 μm fully porous particles (FPPs) [8].

In this work, screening protocols for 150 chiral amine-functionalized compounds, 100 pesticides, and 40 nicotine related compounds were developed using recently commercialized CSPs (using 2.7 μm SPPs) including the macrocyclic glycopeptides; vancomycin and teicoplanin, the derivatized cyclodextrin; hydroxypropyl beta cyclodextrin, and the derivatized cyclofructan; isopropyl cyclofructan-6 [9-10]. Representative structures of these chiral selectors are shown in Figure 1.



Chapter 1 Figure 1. Structures of chiral selectors (original work).

One key advantage of these chiral selectors compared to others are they have high chromatographic enantioselectivity when using electrospray ionization mass spectrometry compatible solvents. This is important for sensitive applications, including biological analysis, environmental testing, trace pharmaceutical impurity analysis, etc. One example is the use of teicoplanin to separation amino acid enantiomers in cancer cells to identify and quantitate trace levels of D-amino acids [11]. Recent efforts have focused on derivatizing and evaluating cyclofructan-based phases [12]. In this work, the efforts made to modify and evaluate macrocyclic glycopeptides for their selectivity differences are reported (see

Chapters 2-6) [9-10, 13-14]. Additional applications using these chiral selectors have been used to assign the absolute configuration of newly synthesized compounds [15].

1.3 Post-acquisition signal processing

Peak overlap can be commonly observed in many situations, despite advanced separation techniques. Baseline peak resolution is desired because peak integration becomes more challenging as chromatographic resolution decreases, especially with asymmetric peaks. Conventional practices as discussed in section 1.2, rely on method development to optimize chromatographic separations, which usually requires extensive time and cost. Also, since screening methods have become faster, even in under a second, other parameters like extra-column band broadening, noise, and frequency (response rate) have become increasingly important factors in chromatographic analysis and method development [1,8,16-17]. A recent direction to enhance chromatographic resolution is the use of post-acquisition signal processing, that is judicious treating of the data after collection. Post-acquisition signal processing is well established in optical and nuclear magnetic resonance spectroscopy. Recently, chromatographers have applied mathematical operations on raw chromatographic data to either extract peak areas of overlapping peaks or directly enhance the resolution of overlapping peaks, usually by reducing peak widths and enhancing the signal to noise [18-21]. Overlapped peaks ($R_s < 1.5$) can be baseline separated and accurately quantitated using simple mathematics [18-21]. This notion has the potential to increase throughput in screening or can be applied to difficult chiral separations in 2D-LC and many more applications. These principles have been explored using liquid chromatography but can be applied to all chromatographic and capillary electrophoresis analyses. A brief introduction to these principles is provided in this section and more details follow in Chapters 6-10.

Indirect methods, like curve fitting, estimate the position and shape of chromatographic peaks [18]. The estimation of peak position and shape is based on a model (i.e., iterative curve fitting uses least squares approximation and can be modeled using bidirectional exponentially modified Gaussians, exponentially modified Gaussians, etc.) [18]. Some curve fitting techniques are more complicated than others and

require multidimensional data (i.e., multivariate curve resolution) [22]. These indirect methods have been reported as useful for quick approximations of overlapping peak areas but can be inaccurate if an inappropriate model is utilized to estimate the peak position and shape [18].

Direct resolution enhancement methods typically focus on sharpening peaks to increase their resolution, and typically change peak shape and height. However, critical peak information like retention time and peak area can be maintained for compound identification and quantitation with the addition of some modifications. Operations like Fourier transform, and derivatives have been adapted from spectroscopy to directly enhance resolution in chromatography [17, 20, 23]. In chromatography, Fourier transform can be used to remove extra-column band broadening (i.e., from the volume of the injector, connecting tubing, and detector) [23]. The principle of even-derivatives has been shown to reduce peak widths, which results in resolution enhancement. After using the even-derivative peak sharpening protocol (discussed in Chapter 7), retention times are constant and peak areas can be recovered to within <1 % error if the chromatographic resolution before processing is ≥ 0.7 [20]. Another principle has been adapted from optical digital filtering, which is the use of power transforms to exponentially raise the signal intensity relative to background noise (power law) [24-25]. The fundamental principle of the recently proposed power law is that raising a given number to a power, n (where n is an integer > 1) increases the signal magnitude if it is >1 or decreases the signal magnitude if it is < 1 [24-25]. The power law reduces tailing, noise, maintains retention time, and increase resolution between overlapping chromatographic peaks, but the relative and absolute peak areas are not maintained [16, 24-25]. A modified power law approach normalizes the peak of interest for quantitation to a height value of 1 (and the rest of the chromatogram accordingly) before raising the chromatographic signal to a power (see Chapter 8) [19, 21]. Using a back-calculation, the peak area information is recovered with similar accuracy as the even-derivative sharpening method [19, 21]. The latest work in this field has focused on pushing the resolution limits of power law to accurately determine peak areas of overlapping peaks [26].

1.4 Organization of dissertation

This dissertation primarily focuses on how to increase chromatographic resolution by fundamental methodologies and novel signal processing protocols. Chapter 2 addresses methodology updates using superficially porous particle based chiral stationary phases. Chapters 3 and 4 describe the synthesis, development, and evaluation of two new chiral stationary phases. Chapter 4 also examines the use of a new chiral stationary phase for the enantiomeric nicotine in natural products like nicotine e-liquids and other tobacco products. Chapter 5 further examines the stationary phase described in Chapter 4 to other nicotine-related compounds. Chapter 6 begins the investigation of using signal processing techniques, specifically iterative curve fitting, to recover areas of overlapping pesticides, which is extremely useful for chiral pesticides that have up to 8 stereoisomers. Chapter 7 continues the investigation of signal processing techniques with the introduction of a derivative sharpening method that can recover areas of overlapping peaks with high accuracy. In Chapter 8, a second new processing technique called modified power law is described. Fundamental studies are described, and applications provided. Chapter 9 reviews and compares the derivative and power-based protocols to curve fitting and Fourier transform signal processing methods. Chapter 10 shows the applicability of these signal processing methods in combination with high-efficiency instrumentation, separating and accurately quantitating 101 compounds/peaks in under a minute. Chapter 11 concludes the manuscript with a summary and future outlook.

1.5 References

1. D.C. Patel, M.F. Wahab, D.W. Armstrong, Z.S. Breitbach, *J. Chromatogr. A* 1467 (2016) 2-18.
2. Food and Drug Administration, *Chirality* 4 (1992) 338–340.
3. P. Sandra, *J. High Res. Chromatogr.* 12 (1983) 82-86.
4. *Advances in Spectroscopy, Chromatography and Emerging Methods*, in: P.L. Polavarapu (Ed.), *Chiral Analysis*, 2nd ed., Elsevier, 2018, pp 507 – 564.
5. P. Sun, D.W. Armstrong, *J. Chromatogr. A* 1217 (2010) 4904-4918.
6. M.P. Gasper, A. Berthod, U.B. Nair, D.W. Armstrong, *Anal. Chem.* 68 (1996) 2501-2514.
7. C.L. Barhate, L.A. Joyce, A.A. Makarov, K. Zawatzky, F. Bernardoni, W.A. Schafer, D.W. Armstrong, C.J. Welch, E.L. Regalado, *Chem. Commun.* 53 (2016) 509-512.
8. D.C. Patel, Z.S. Breitbach, M.F. Wahab, C.L. Barhate, D.W. Armstrong, *Anal. Chem.* 87 (2015) 9137-9148.
9. G. Hellinghausen, D. Roy, Y. Wang, J.T. Lee, D.A. Lopez, C.A. Weatherly, D.W. Armstrong, *Talanta* 181 (2018) 132-141.

10. G. Hellinghausen, D. Roy, J.T. Lee, Y. Wang, C.A. Weatherly, D.A. Lopez, K.A. Nguyen, J.D. Armstrong, D.W. Armstrong, *J. Pharm. Biomed. Anal.* 155 (2018) 70-81.
11. S. Du, Y. Wang, C.A. Weatherly, K. Holden, D.W. Armstrong, *Anal. Bioanal. Chem.* 410 (2018) 2971 – 2979.
12. P. Sun, C. Wang, Z.S. Breitbach, Y. Zhang, D.W. Armstrong, *Anal. Chem.* 81 (2009) 10215-10226.
13. G. Hellinghausen, J.T. Lee, C.A. Weatherly, D.A. Lopez, D.W. Armstrong, *Drug Test. Anal.* 9 (2017) 944-948.
14. G. Hellinghausen, D.A. Lopez, J.T. Lee, Y. Wang, C.A. Weatherly, A.E. Portillo, A. Berthod, D.W. Armstrong, *Chirality* 30 (2018) 1067-1078.
15. H. Sato, M.A. Blemker, G. Hellinghausen, D.W. Armstrong, J.W. Nafie, S.T. Roberts, M.J. Krische, *Chem. Eur. J.* 25 (2019) 8719-8724.
16. M.F. Wahab, D.C. Patel, R.M. Wimalasinghe, D.W. Armstrong, *Anal. Chem.* 89 (2017) 8177-8191.
17. D.C. Patel, M.F. Wahab, T.C. O'Haver, D.W. Armstrong, *Anal. Chem.* 90 (2018) 3349-3356.
18. G. Hellinghausen, E.R. Readell, M.F. Wahab, J.T. Lee, D.A. Lopez, C.A. Weatherly, D.W. Armstrong, *Chromatographia* 82 (2018) 221-233.
19. G. Hellinghausen, M.F. Wahab, D.W. Armstrong, *J. Chromatogr. A*, 1574 (2018) 1-8.
20. M.F. Wahab, T.C. O'Haver, F. Gritti, G. Hellinghausen, D.W. Armstrong, *Talanta*, 192, 492-499 (2019).
21. M.F. Wahab, F. Gritti, T.C. O'Haver, G. Hellinghausen, D.W. Armstrong, *Chromatographia*, 82, (2019) 211-220.
22. D.W. Cook, S.C. Rutan, D.R. Stoll, C. Venkatramani, *LC GC N. Am.* 36 (2018) 248–255.
23. Y. Vanderheyden, K. Broeckhoven, G. Desmet, *J. Chromatogr. A*, 1465, (2016) 126-142.
24. R.A. Shalliker, P.G. Stevenson, D. Shock, M. Mnatsakanyan, P.K. Dasgupta, G. Guiochon, *J. Chromatogr. A* 1217 (2010) 5693-5699.
25. P.K. Dasgupta, Y. Chen, C.A. Serrano, G. Guiochon, H. Liu, J.N. Fairchild, R.A. Shalliker, *Anal. Chem.* 82 (2010) 10143-10150.
26. M.F. Wahab, A. Berthod, D.W. Armstrong, *J Sep Sci* (<https://doi.org/10.1002/jssc.201900799>).

Chapter 2

Effective methodologies for enantiomeric separations of 150 pharmacology and toxicology related 1°, 2°, and 3° amines with core-shell chiral stationary phases

2.1 Abstract

Core-shell particles (superficially porous particles, SPPs) have been proven to provide high-throughput and effective separations of a variety of chiral molecules. However, due to their limited commercialization, many separations have not been reported with these stationary phases. In this study, four SPP chiral stationary phases (CSPs) were utilized for the enantiomeric separation of 150 chiral amines. These amines encompass a variety of structural and drug classes, which are particularly important to the pharmaceutical industry and in forensics. This comprehensive evaluation demonstrates the power of these CSPs and the ease of method development and optimization. The CSPs used in this study included the macro-cyclic glycopeptide-based CSPs (VancoShell and NicoShell), the cyclodextrin-based CSP (CDSHell-RSP), and the cyclofructan-based CSP (LarihcShell-P). These CSPs offered versatility for a variety of applications and worked in a complementary fashion to baseline separate all 150 amines. The LarihcShell-P was highly effective for separating primary amines. VancoShell, NicoShell, and CDSHell-RSP were useful for separating all types of amines. These CSPs are multi-modal and can be utilized with mass spectrometry compatible solvents. Eighteen racemic controlled substances were simultaneously baseline separated in a single liquid chromatography–mass spectrometry (LC–MS) analysis. Details in high-performance liquid chromatography (HPLC) parameters will be discussed as well as the improved chromatographic performance afforded by the SPP CSPs.

2.2 Introduction

In 2017, the Food and Drug Administration (FDA) approved 22 small molecules as new molecular entities. In comparison to the last five years (2012-2016), the percentage of amines approved increased from 70% to 77%, and the percentage of chiral compounds and chiral amines remained constant at 59%

and 40%, respectively [1]. Since enantiomers may possess different biological activity, chiral separation methods of amines have become routine and important for chiral pharmaceutical analysis. The FDA states that “the pharmacology and toxicology of the enantiomer should be characterized for the principal effects and any other pharmacological effect, with respect to potency, specificity, maximum effect, etc.” In some racemic mixtures, one of the enantiomers is inactive or contributes very little pharmacologically or in opposition compared to the other enantiomer [2]. In the pharmaceutical industry from 1994 to 2011, 15 “chiral switches” were made due to the inactivity of one enantiomer [2]. Additionally, some compounds have more than one set of enantiomers, which further complicates their therapeutic use. One example is ephedrine, which has two chiral centers and is used as a vasopressor. However, its diastereomer, pseudoephedrine, acts oppositely and is used as a vasoconstrictor. Also, ephedrine and pseudoephedrine are both precursors to methamphetamine [3]. Depending on which diastereomer is used, different enantiomeric compositions of methamphetamine are obtained, which is used in forensics to trace the origin of the substance if it is under investigation for illicit use [3]. Of course, the isomeric ratio of ephedrine and pseudoephedrine cannot be determined by mass spectrometry (MS) unless they are chromatographically separated because they have the same m/z [3,4].

According to the 2017 DEA Orangebook, over 70% of scheduled controlled substances are amines, including catecholamines, cathinones, and substituted amphetamines [5]. Also, over 50% and 40% are chiral compounds and chiral amines, respectively [5]. According to the DEA Orangebook list I regulated chemicals, ~40% of the precursors to controlled substances are amines [5]. Also, 37% are chiral, and only one of the chiral chemicals is not an amine [5]. In addition, there are new designer drugs that have been derived from regulated substances to avert detection [3]. One of the most common techniques used by forensics is MS because it accurately provides sensitive identification and quantitation of target compounds in complex samples. Most reported analyses for designer drugs rely on gas chromatography (GC), which is not suited for biological analysis of nonvolatile or thermally labile samples. Liquid chromatography (LC) would be preferable for metabolic, pharmacokinetic, and pharmacodynamic

studies. Also, LC can be performed at preparative scales to obtain large amounts of individual enantiomers and assess their pharmacological properties. This approach might be particularly useful for the investigation of new chiral controlled substances and designer drugs and their metabolites.

Some commercial CSPs have solvent limitations, where the optimized mobile phase is not MS compatible. Recently, isopropyl cyclofructan-6 bonded to superficially porous particles (SPPs) was shown to provide faster and higher efficiency separations, while maintaining selectivity (α) at much higher flow rates in comparison to its analogous fully porous particles (FPPs) CSP [6]. The speed of chromatographic separation with SPP CSPs compared to FPP CSPs has advanced from minutes to seconds [7-8]. Merck researchers have demonstrated the power of a SPP teicoplanin CSP with high-throughput screening, estimating that over 1000 samples could be tested for enantiomeric excess within a single workday [9].

Macrocyclic glycopeptides, cyclodextrins, and cyclofructans have been investigated to achieve higher selectivities for difficult and important chiral separations [10-18]. However, few comprehensive studies, especially for controlled substances, have been performed using these chiral selectors bonded to SPPs [19-26]. The results of this study highlight new and highly improved separations of 150 chiral primary (1°), secondary (2°), and tertiary (3°) amines with three SPP-bonded derivatized chiral selectors (hydroxypropyl β -cyclodextrin, isopropyl cyclofructan-6-P, and a modified macrocyclic glycopeptide) and one native SPP-bonded chiral selector (vancomycin). Focus was paid to the “principle of complementary separations,” which states that a partial separation with one chiral selector can be brought to baseline with one of the other related selectors [27-28]. This characteristic provides a high likelihood of baseline separating any structure within a given class of compounds. In this study, the focus is on pharmaceuticals, stimulants, and related compounds. These chiral selectors are multi-modal, so they offer ease of optimization and perform well in MS compatible solvents, which would be useful for biological and forensic analyses.

2.3 Experimental

2.3.1 Chemicals and materials

Native vancomycin (VancoShell, VS), modified macrocyclic glycopeptide (NicoShell, NS), hydroxypropyl- β -cyclodextrin (CDShell-RSP, RSP), and isopropyl-cyclofructan (LarihcShell-P, LS-P) chiral selectors were bonded to 2.7 μ m SPP and obtained from AZYP, LLC. (Arlington, TX, USA) [18-20]. Analytes were purchased as racemic standards or individual enantiomer standards (then mixed to form racemates) from Cerilliant Corporation (Round Rock, TX, USA), Sigma-Aldrich (St. Louis, MO, USA), and LKT Laboratories Inc (Minneapolis, MN, USA). Racemic standards were prepared in methanol (MeOH) at 1 mg/mL for analysis. Solvents and additives including HPLC grade acetonitrile (ACN), ethanol (EtOH), MeOH, hexane (Hex), heptane (Hep), trifluoroacetic acid (TFA), acetic acid (AA), ammonium hydroxide (NH₄OH), trimethylamine (TEA), formic acid (FA), ammonium acetate (NH₄CH₃CO₂), ammonium formate (NH₄HCO₂), and ammonium trifluoroacetate (NH₄TFA) were obtained from Sigma-Aldrich (St. Louis, MO, USA). Water was purified by a Milli-Q water purification system (Millipore, Billerica, MA, USA).

2.3.2 Chromatographic conditions

An Agilent 1260 (Agilent Technologies, Palo Alto, CA, USA) HPLC was used. It consisted of a 1200 diode array detector, autosampler, and quaternary pump. The mass spectrometer used in this study was a Shimadzu triple quadrupole LC-MS instrument, LCMS-8040, (Shimadzu, Tokyo, Japan). All MS was operated in positive ion mode with an electron spray ionization source. The parameters were set as follows: nebulizer gas flow, 3 L/min; drying gas flow, 15 L/min; desolvation line temperature, 250 °C; heat block temperature, 400 °C. Multiple UV wavelengths of 220, 230, and 254 nm were utilized for detection and identification of enantiomers. All separations were carried out at room temperature, unless otherwise noted, using an isocratic method. Mobile phases were degassed by ultrasonication under vacuum for 5 minutes. Each analyte was screened and optimized as described in section 3.1.

When distinguishing the following mobile phases, the letters in parenthesis refer to the ratio changes in parenthesis. For example, 1(a,b): MeOH-NH₄TFA (100:(0.1,0.025), v/w) means 1a corresponds to MeOH-NH₄TFA (100:0.1, v/w) while 1b is MeOH-NH₄TFA (100:0.025, v/w). If the pH is given, it is the pH of the aqueous buffer prior to mixing with organic modifier. The optimized mobile phase conditions referring to Tables 1-3 were as follows: 1(a,b): MeOH-NH₄TFA (100:(0.1,0.025), v/w), 2(a,b,c): MeOH-NH₄HCO₂ (100:(0.2,0.5,0.1), v/w), 3(a,b): MeOH-AA-TEA (100:(0.2:0.1,0.1:0.05), v/v/v), 3(c,d,e): MeOH-AA-NH₄OH (100:(0.2:0.05,0.1:0.02,0.3:0.05), v/v/v), 4(a,b,c,d,e,f,g): ACN-MeOH-AA-TEA ((60:40,50:50,30:70,10:90,70:30,80:20,95:5):0.3:0.2, v/v/v/v), 4(g): ACN-MeOH-TFA-TEA (90:10:0.3:0.2, v/v/v/v), 5(a,b,c,d,e,f): ACN-NH₄HCO₂ (pH 3.6; 16 mM) ((30:70,25:75,20:80,15:85,10:90,5:95), v/v), 5(g,h,i,j): ACN-NH₄HCO₂ (pH 3.6; 48 mM) ((20:80,15:85,10:90,5:95), v/v), 5(k): ACN-NH₄HCO₂ (pH 3.6; 80 mM) (5:95, v/v), 6(a,b,c): MeOH-NH₄HCO₂ (pH 3.6; 16 mM) ((90:10,80:20,30:70), v/v), 6(d,e): MeOH-NH₄HCO₂ (pH 3.6; 48 mM) ((90:10,30:70), v/v), 6(f): MeOH-NH₄HCO₂ (pH 6.0; 16 mM) (35:65, v/v), 6(g): MeOH-NH₄HCO₂ (pH 5.0; 16 mM) (30:70, v/v), 7(a,b): EtOH-NH₄HCO₂ (pH 3.6; 16 mM) ((95:5,90:10), v/v), 8(a,b): Hex-EtOH-TFA-TEA ((70:30,80:20):0.3:0.2, v/v/v/v), 9(a,b): Hep-EtOH-TFA-TEA ((95:5,90:10):0.3:0.2, v/v/v/v).

2.3.3 Sample categorization

In Tables 1-3, the 150 amines are classified by their type; 1°, 2°, or 3°, then categorized into one of the following classes: pharmaceuticals, stimulants, reagents, or amino acids and derivatives (listed alphabetically). Pharmaceuticals were distinguished based on their pharmacological effects. Stimulants were defined as any amine that increases the functional activity of an organism, such as α - and β -adrenergic agonists (AAA, BAA), analgesics (ANA), antidepressants (AD), antiparasitics (AP), catecholamines (CAT), and tobacco-related compounds (TOB). Additionally, if stimulants were classified in the DEA Orangebook by a class scheduling action number (CSA #) or regulated chemical list number (RC #), they were labeled as such [5]. One non-stimulant (NS) was included with the stimulants due to its

similarity in structure to amphetamine. Pharmaceuticals included α -, β -, calcium channel, and sodium channel blockers (AB, BB, CCB, SCB), anesthetics (ANE), antibiotics (ABIO), antimuscarinics (AM), antipsychotics (APC), diuretics (DIU), and hormones (HOR).

Chapter 2 Table 1. Optimized chiral separations of primary (1°) amines.

a) Pharmaceuticals							
Name ¹	Class ²	CSP ³	MP ⁴	F(T) ⁵	k ₁ ^{6a}	α ^{6b}	R _s ^{6c}
Amlodipine	CCB	LS-P	4g	0.7	2.7	1.09	1.9
		NS	3c	1.0	7.7	1.09	1.7
		RSP*	5e	1.0	3.1	1.10	1.5
		VS	4a	1.0	7.6	1.11	2.0
Mexitilane	SCB	LS-P	4g	1.0	7.5	1.08	1.5
		VS**	3c	0.5	1.1	1.10	2.0
Thyroxine	HOR	LS-P	4g	1.0	2.3	1.21	2.8
b) Stimulants							
Name ¹	Class ²	CSP ³	MP ⁴	F(T) ⁵	k ₁ ^{6a}	α ^{6b}	R _s ^{6c}
3,4-methylenedioxyamphetamine (MDA)	CSA I	LS-P**	4g	1.0	3.1	1.06	1.7
		RSP*	5e	0.5	2.2	1.07	1.6
		VS**	7a	0.4	5.1	1.08	1.5
Amphetamine	CSA II	LS-P***	4g	0.3	5.5	1.05	1.5
		NS****	3c	0.3	2.9	1.05	1.5
		RSP*	5f	0.5(45)	2.4	1.08	1.5
		VS	1a	1.0	1.1	1.18	2.5
Aminorex	CSA I	NS	3c	0.5	4.6	1.06	1.5
		RSP*	5d	1.0	1.7	1.10	2.2
		VS	3c	0.7	2.6	1.10	2.0
Methoxamine	AAA	LS-P**	4e	0.5	3.7	1.06	1.5
		NS	4a	1.0	7.0	1.12	2.2
		RSP	5e	1.0	0.9	1.42	3.6
		VS	4a	0.5	3.2	1.10	1.5
Midodrine	AAA	LS-P*	4g	0.5	7.7	1.07	1.5
		NS	3c	1.0	5.2	1.23	2.9
Norepinephrine (Arterenol)	CAT	LS-P	4g	1.0(45)	3.7	1.13	2.4
Normetanephrine	CAT	LS-P	4a	1.0	3.5	1.14	2.9
		NS	3c	1.0	4.0	1.10	2.0
Norphenylephrine (3-octopamine)	CAT	LS-P	4a	1.0	3.3	1.14	2.8
		VS**	8a	0.5	11.5	1.05	1.5
Octopamine	CAT	LS-P	4a	1.0	3.2	1.13	2.1
		NS	3c	1.0	5.8	1.08	1.8
p-methoxyamphetamine (PMA)	CSA I	LS-P	4g	0.3	2.6	1.05	1.5
		RSP*	5d	0.5(45)	2.2	1.06	1.5
		VS	1a	0.6	1.0	1.17	2.5
p-chloroamphetamine (PCA)	NS	LS-P***	4g	0.3	2.7	1.05	1.5
		RSP*	5d	0.5	2.3	1.06	1.5
Phenylpropanolamine (Norephedrine)	RC I	LS-P	4a	0.8	2.4	1.10	2.0
		NS	4a	0.7	3.6	1.08	1.5
Tranilcypromine	AD	LS-P**	4g	1.0	5.5	1.06	1.5
		NS	3e	1.0(10)	5.0	1.12	2.0

		RSP*	5e	1.0	1.6	1.13	2.8
		VS	6a	0.5(30)	1.5	1.15	2.5
4-hydroxynorephedrine	CAT	LS-P	4a	0.5	2.4	1.09	1.9
		NS	8a	1.0	5.8	1.25	1.5
β -keto-amphetamine (Cathinone)	CSA I	LS-P	8b	1.0	6.0	1.12	2.3
		NS	2b	2.0(45)	1.4	1.44	4.5
		RSP*	5k	0.7	2.2	1.10	2.4
		VS	1a	1.0(15)	1.0	1.22	2.6
c) Reagents							
Name¹		CSP³	MP⁴	F(T)⁵	k₁^{6a}	α^{6b}	R_s^{6c}
1-(1,1-biphenyl-4-yl) ethanamine		LS-P	4g	1.0	2.4	1.14	2.6
		NS*	4a	1.0	7.4	1.12	2.5
		VS	1a	1.0	0.8	1.24	2.6
1-(1-naphthyl) ethylamine		LS-P	4a	1.0	1.6	1.18	3.3
		NS	2a	1.0	1.9	1.21	3.2
		VS	1a	1.0	1.1	1.21	2.8
1-(2-naphthyl) ethylamine		LS-P	4a	1.0	2.3	1.14	2.9
1-(4-chlorophenyl) ethylamine		LS-P	4g	1.0	2.9	1.13	2.6
		VS	3c	0.5	2.1	1.09	1.8
1-(4-methylphenyl)ethylamine		LS-P	4a	1.0	2.1	1.13	2.3
		NS*	4a	1.0	5.8	1.08	2.5
		VS	3c	1.0	1.4	1.15	2.4
1,1-diphenyl-2-amino-propane		LS-P	4g	1.0	0.8	1.14	2.0
		VS	1a	1.0	0.9	1.30	3.3
1,1-diphenyl-fluoro-2-aminopropane		LS-P**	9b	0.5	5.1	1.06	1.8
		RSP	5a	1.0	1.5	1.14	2.1
		VS	1a	1.0	0.5	1.39	3.2
1,2,2-triphenylethylamine		LS-P	4g	1.0	0.6	1.25	2.8
		NS***	3c	0.3	1.3	1.07	1.5
		VS	1a	1.0	0.6	1.45	3.9
1,2,3,4-tetrahydro-1-naphthylamine		LS-P	4a	1.0	1.8	1.17	2.8
		NS*	3c	0.5	2.9	1.08	1.9
		RSP***	5f	0.3(5)	1.1	1.05	1.5
		VS	1a	1.0	0.8	1.50	4.5
1,2-methoxyphenylethanamine		LS-P	4g	1.0	1.2	1.25	3.9
		NS	3c	1.0	1.9	1.13	2.3
		VS	3c	1.0	1.1	1.15	2.2
1-benzyl-2,2-diphenylethylamine		LS-P	9b	0.7	4.2	1.07	1.8
		RSP*	5a	1.0	0.5	1.25	3.5
		VS	1a	1.0	1.0	2.19	9.5
2-amino-1-(4-nitrophenyl)-1,3-propanediol		LS-P	4g	1.0	2.2	1.25	4.2
		NS	2a	1.0(45)	2.2	1.26	3.9
		RSP	5e	0.5	0.7	1.15	1.8
		VS*	8a	1.0	10.4	1.13	1.5
2-amino-1,1,3-triphenyl-1-propanol		RSP*	5e	1.0	2.7	1.14	3.0
		NS*	4f	0.5	0.6	1.17	1.5
		VS	1a	1.0	0.2	1.91	4.7
2-amino-1,1-diphenyl-1-propanol		NS	4a	1.0	3.2	1.11	2.0
		VS	6a	1.0	0.8	1.23	2.7
2-amino-1,2-diphenylethanol		LS-P	4a	1.0	1.0	1.23	2.8
		NS	3c	1.0	3.4	1.14	2.5
		VS	3c	0.5	1.3	1.13	2.0
2-amino-1-phenyl-1,3-propanediol		LS-P	4g	1.0	2.3	1.14	2.5

	RSP	5f	1.0	0.9	1.60	6.0
	NS	2a	1.0	1.4	1.27	3.7
2-amino-1-phenylethanol	LS-P	4g	1.0	3.8	1.20	4.0
	RSP*	5e	1.0	3.3	1.08	1.7
2-amino-3-phenyl-1-propanol	LS-P	4a	1.0	2.3	1.13	2.3
	NS***	3c	0.3	2.9	1.05	1.5
	VS	6a	1.0	1.3	1.15	2.0
2-amino-4-methyl-1,1-diphenylpentane	LS-P**	9a	0.5(5)	9.1	1.07	1.5
	NS***	3c	0.3	1.2	1.07	1.7
	VS	1a	2.0	0.4	1.94	4.5
2-chloro-indan-1-ylamine	LS-P	4g	2.0	2.0	1.60	7.2
	VS	6a	0.6	0.8	1.22	2.8
4-chlorobenzylhydramine	LS-P	4g	0.5	2.3	1.08	1.5
4-fluoro- α -methylbenzylamine	LS-P	4g	1.0	2.6	1.12	2.2
	NS**	4a	1.0	7.1	1.11	2.0
4-methoxy- α -methylbenzylamine	LS-P	4g	1.0	2.3	1.11	2.0
	NS**	4a	1.0	6.6	1.07	1.6
	VS	1a	1.0	0.8	1.52	5.6
6-methoxy-1,2,3,4-tetrahydro-1-naphthalenylamine	LS-P	4a	1.0	2.0	1.23	4.4
	NS	3c	0.5	3.5	1.07	1.5
	RSP*	5e	1.0	1.1	1.11	2.1
	VS	1a	2.3	0.7	1.70	5.2
<i>cis</i> -1-amino-2-indanol	LS-P	4g	1.0	2.1	1.19	3.1
	NS	3c	1.0	3.8	1.11	2.0
	VS	1a	1.0	0.6	1.28	2.8
N-p-tosyl-1,2-diphenylethylene diamine	LS-P	4g	1.0	0.9	1.15	2.0
	NS	3c	1.0	2.1	1.18	2.6
	VS	8a	1.0	4.4	1.83	3.9
<i>trans</i> -1-amino-2-indanol	LS-P	4a	1.0	1.9	1.28	4.4
	VS	1a	1.0	0.8	1.34	3.7
α -methyl-4-nitrobenzylamine	LS-P	4g	1.0	4.0	1.10	2.0
	NS	3c	1.0	7.1	1.08	1.7
	VS**	3c	0.5	3.1	1.07	1.5
α -methylbenzylamine	LS-P	4g	1.0	2.3	1.15	2.7
	NS*	4a	2.0(45)	4.8	1.13	1.5
	VS	6a	0.5	0.9	1.15	2.0
d) Amino acids & derivatives						
Name¹	CSP³	MP⁴	F(T)⁵	k₁^{6a}	α^{6b}	R_s^{6c}
3,4-dihydroxyphenylalanine	LS-P	4g	1.0	2.7	1.37	3.7
4-chlorophenylalaninol	LS-P	4a	1.0	2.3	1.12	2.3
	NS	4c	1.0	5.6	1.13	2.6
	RSP*	5c	0.5	1.0	1.08	1.5
4-nitrophenylalanine	LS-P	4g	1.0	2.7	1.23	3.2
Homocysteine thiolactone	LS-P	4g	1.0	4.2	1.13	2.2
	NS	3a	1.0	2.9	1.14	2.1
p-chlorophenylalanine	LS-P	4g	1.0	2.3	1.16	2.2
p-fluorophenylalanine	LS-P	4g	1.0	2.2	1.18	2.5
Phenylalanine	LS-P	4g	1.0	2.2	1.20	2.6
Tryptophan	LS-P	4g	1.0	2.0	1.25	3.1
Tryptophanamide	LS-P	4g	1.0	3.2	1.18	2.7
	VS	6a	1.0	1.2	1.22	2.7
Tryptophanol	LS-P	4a	1.0	2.4	1.15	2.9
Tyrosine methyl ester	LS-P**	4g	0.7	2.1	1.08	1.7

	NS	3c	0.3	1.9	1.10	1.7
Tyrosinol	LS-P	4a	1.0	2.4	1.13	2.5
	NS	4a	1.0	6.9	1.14	2.0

¹ See section 2.1 for all sample information.

² See section 2.3 for classification information.

³ All chiral stationary phases (CSP) were 100 x 4.6 mm (i.d.), unless indicated: *150 x 4.6 mm (i.d.), **200 x 4.6 mm (i.d.), ***250 x 4.6 mm (i.d.), ****300 x 4.6 mm (i.d.). See section 2.1 for more information.

⁴ See section 2.2 for mobile phase (MP) information.

⁵ All flow rates (F) are given in mL/min. All temperature (T) is 25 °C unless otherwise indicated (in °C).

^{6a,b,c} Chromatographic calculations: $k_1 = (t_{R1} - t_0) / (t_0)$; $\alpha = k_2 / k_1$; $R_s = 2(t_{R2} - t_{R1}) / (w_{0.5,1} + w_{0.5,2})$. See Supplemental data for abbreviations and more information.

Chapter 2 Table 2. Optimized chiral separations of secondary (2°) amines.

a) Pharmaceuticals							
Name ¹	Class ²	CSP ³	MP ⁴	F(T) ⁵	k_1 ^{6a}	α ^{6b}	R_s ^{6c}
Amlodipine	CCB	LS-P	4g	0.7	2.7	1.09	1.9
		NS	3c	1.0	7.7	1.09	1.7
		RSP*	5e	1.0	3.1	1.10	1.5
		VS	4a	1.0	7.6	1.11	2.0
Mexitilane	SCB	LS-P	4g	1.0	7.5	1.08	1.5
		VS**	3c	0.5	1.1	1.10	2.0
Thyroxine	HOR	LS-P	4g	1.0	2.3	1.21	2.8
b) Stimulants							
Name ¹	Class ²	CSP ³	MP ⁴	F(T) ⁵	k_1 ^{6a}	α ^{6b}	R_s ^{6c}
3,4-methylenedioxyamphetamine (MDA)	CSA I	LS-P**	4g	1.0	3.1	1.06	1.7
		RSP*	5e	0.5	2.2	1.07	1.6
		VS**	7a	0.4	5.1	1.08	1.5
Amphetamine	CSA II	LS-P***	4g	0.3	5.5	1.05	1.5
		NS****	3c	0.3	2.9	1.05	1.5
		RSP*	5f	0.5(45)	2.4	1.08	1.5
		VS	1a	1.0	1.1	1.18	2.5
Aminorex	CSA I	NS	3c	0.5	4.6	1.06	1.5
		RSP*	5d	1.0	1.7	1.10	2.2
		VS	3c	0.7	2.6	1.10	2.0
Methoxamine	AAA	LS-P**	4e	0.5	3.7	1.06	1.5
		NS	4a	1.0	7.0	1.12	2.2
		RSP	5e	1.0	0.9	1.42	3.6
		VS	4a	0.5	3.2	1.10	1.5
Midodrine	AAA	LS-P*	4g	0.5	7.7	1.07	1.5
		NS	3c	1.0	5.2	1.23	2.9
Norepinephrine (Arterenol)	CAT	LS-P	4g	1.0(45)	3.7	1.13	2.4
Normetanephrine	CAT	LS-P	4a	1.0	3.5	1.14	2.9
		NS	3c	1.0	4.0	1.10	2.0
Norphenylephrine (3-octopamine)	CAT	LS-P	4a	1.0	3.3	1.14	2.8
		VS**	8a	0.5	11.5	1.05	1.5
Octopamine	CAT	LS-P	4a	1.0	3.2	1.13	2.1
		NS	3c	1.0	5.8	1.08	1.8
p-methoxyamphetamine (PMA)	CSA I	LS-P	4g	0.3	2.6	1.05	1.5
		RSP*	5d	0.5(45)	2.2	1.06	1.5
		VS	1a	0.6	1.0	1.17	2.5
p-chloroamphetamine (PCA)	NS	LS-P***	4g	0.3	2.7	1.05	1.5

		RSP*	5d	0.5	2.3	1.06	1.5
Phenylpropanolamine (Norephedrine)	RC I	LS-P	4a	0.8	2.4	1.10	2.0
		NS	4a	0.7	3.6	1.08	1.5
		VS	4a	0.7	3.6	1.08	1.5
Tranlycypromine	AD	LS-P**	4g	1.0	5.5	1.06	1.5
		NS	3e	1.0(10)	5.0	1.12	2.0
		RSP*	5e	1.0	1.6	1.13	2.8
		VS	6a	0.5(30)	1.5	1.15	2.5
4-hydroxynorephedrine	CAT	LS-P	4a	0.5	2.4	1.09	1.9
		NS	8a	1.0	5.8	1.25	1.5
β -keto-amphetamine (Cathinone)	CSA I	LS-P	8b	1.0	6.0	1.12	2.3
		NS	2b	2.0(45)	1.4	1.44	4.5
		RSP*	5k	0.7	2.2	1.10	2.4
		VS	1a	1.0(15)	1.0	1.22	2.6
c) Reagents							
Name¹		CSP³	MP⁴	F(T)⁵	k₁^{6a}	α^{6b}	R_s^{6c}
1-(1,1-biphenyl-4-yl) ethanamine	LS-P	4g	1.0	2.4	1.14	2.6	
	NS*	4a	1.0	7.4	1.12	2.5	
	VS	1a	1.0	0.8	1.24	2.6	
1-(1-naphthyl) ethylamine	LS-P	4a	1.0	1.6	1.18	3.3	
	NS	2a	1.0	1.9	1.21	3.2	
	VS	1a	1.0	1.1	1.21	2.8	
1-(2-naphthyl) ethylamine	LS-P	4a	1.0	2.3	1.14	2.9	
1-(4-chlorophenyl) ethylamine	LS-P	4g	1.0	2.9	1.13	2.6	
	VS	3c	0.5	2.1	1.09	1.8	
1-(4-methylphenyl)ethylamine	LS-P	4a	1.0	2.1	1.13	2.3	
	NS*	4a	1.0	5.8	1.08	2.5	
	VS	3c	1.0	1.4	1.15	2.4	
1,1-diphenyl-2-amino-propane	LS-P	4g	1.0	0.8	1.14	2.0	
	VS	1a	1.0	0.9	1.30	3.3	
1,1-diphenyl-fluoro-2-aminopropane	LS-P**	9b	0.5	5.1	1.06	1.8	
	RSP	5a	1.0	1.5	1.14	2.1	
	VS	1a	1.0	0.5	1.39	3.2	
1,2,2-triphenylethylamine	LS-P	4g	1.0	0.6	1.25	2.8	
	NS***	3c	0.3	1.3	1.07	1.5	
	VS	1a	1.0	0.6	1.45	3.9	
1,2,3,4-tetrahydro-1-naphthylamine	LS-P	4a	1.0	1.8	1.17	2.8	
	NS*	3c	0.5	2.9	1.08	1.9	
	RSP***	5f	0.3(5)	1.1	1.05	1.5	
	VS	1a	1.0	0.8	1.50	4.5	
1,2-methoxyphenylethylamine	LS-P	4g	1.0	1.2	1.25	3.9	
	NS	3c	1.0	1.9	1.13	2.3	
	VS	3c	1.0	1.1	1.15	2.2	
1-benzyl-2,2-diphenylethylamine	LS-P	9b	0.7	4.2	1.07	1.8	
	RSP*	5a	1.0	0.5	1.25	3.5	
	VS	1a	1.0	1.0	2.19	9.5	
2-amino-1-(4-nitrophenyl)-1,3-propanediol	LS-P	4g	1.0	2.2	1.25	4.2	
	NS	2a	1.0(45)	2.2	1.26	3.9	
	RSP	5e	0.5	0.7	1.15	1.8	
	VS*	8a	1.0	10.4	1.13	1.5	
2-amino-1,1,3-triphenyl-1-propanol	RSP*	5e	1.0	2.7	1.14	3.0	
	NS*	4f	0.5	0.6	1.17	1.5	
	VS	1a	1.0	0.2	1.91	4.7	
2-amino-1,1-diphenyl-1-propanol	NS	4a	1.0	3.2	1.11	2.0	

	VS	6a	1.0	0.8	1.23	2.7
2-amino-1,2-diphenylethanol	LS-P	4a	1.0	1.0	1.23	2.8
	NS	3c	1.0	3.4	1.14	2.5
	VS	3c	0.5	1.3	1.13	2.0
2-amino-1-phenyl-1,3-propanediol	LS-P	4g	1.0	2.3	1.14	2.5
	RSP	5f	1.0	0.9	1.60	6.0
	NS	2a	1.0	1.4	1.27	3.7
2-amino-1-phenylethanol	LS-P	4g	1.0	3.8	1.20	4.0
	RSP*	5e	1.0	3.3	1.08	1.7
2-amino-3-phenyl-1-propanol	LS-P	4a	1.0	2.3	1.13	2.3
	NS***	3c	0.3	2.9	1.05	1.5
	VS	6a	1.0	1.3	1.15	2.0
2-amino-4-methyl-1,1-diphenylpentane	LS-P**	9a	0.5(5)	9.1	1.07	1.5
	NS***	3c	0.3	1.2	1.07	1.7
	VS	1a	2.0	0.4	1.94	4.5
2-chloro-indan-1-ylamine	LS-P	4g	2.0	2.0	1.60	7.2
	VS	6a	0.6	0.8	1.22	2.8
4-chlorobenzylhydramine	LS-P	4g	0.5	2.3	1.08	1.5
4-fluoro- α -methylbenzylamine	LS-P	4g	1.0	2.6	1.12	2.2
	NS**	4a	1.0	7.1	1.11	2.0
4-methoxy- α -methylbenzylamine	LS-P	4g	1.0	2.3	1.11	2.0
	NS**	4a	1.0	6.6	1.07	1.6
	VS	1a	1.0	0.8	1.52	5.6
6-methoxy-1,2,3,4-tetrahydro-1-naphthalenylamine	LS-P	4a	1.0	2.0	1.23	4.4
	NS	3c	0.5	3.5	1.07	1.5
	RSP*	5e	1.0	1.1	1.11	2.1
	VS	1a	2.3	0.7	1.70	5.2
<i>cis</i> -1-amino-2-indanol	LS-P	4g	1.0	2.1	1.19	3.1
	NS	3c	1.0	3.8	1.11	2.0
	VS	1a	1.0	0.6	1.28	2.8
N-p-tosyl-1,2-diphenylethylene diamine	LS-P	4g	1.0	0.9	1.15	2.0
	NS	3c	1.0	2.1	1.18	2.6
	VS	8a	1.0	4.4	1.83	3.9
<i>trans</i> -1-amino-2-indanol	LS-P	4a	1.0	1.9	1.28	4.4
	VS	1a	1.0	0.8	1.34	3.7
α -methyl-4-nitrobenzylamine	LS-P	4g	1.0	4.0	1.10	2.0
	NS	3c	1.0	7.1	1.08	1.7
	VS**	3c	0.5	3.1	1.07	1.5
α -methylbenzylamine	LS-P	4g	1.0	2.3	1.15	2.7
	NS*	4a	2.0(45)	4.8	1.13	1.5
	VS	6a	0.5	0.9	1.15	2.0
d) Amino acids & derivatives						
Name¹	CSP³	MP⁴	F(T)⁵	k₁^{6a}	α^{6b}	R_s^{6c}
3,4-dihydroxyphenylalanine	LS-P	4g	1.0	2.7	1.37	3.7
4-chlorophenylalaninol	LS-P	4a	1.0	2.3	1.12	2.3
	NS	4c	1.0	5.6	1.13	2.6
	RSP*	5c	0.5	1.0	1.08	1.5
4-nitrophenylalanine	LS-P	4g	1.0	2.7	1.23	3.2
Homocysteine thiolactone	LS-P	4g	1.0	4.2	1.13	2.2
	NS	3a	1.0	2.9	1.14	2.1
p-chlorophenylalanine	LS-P	4g	1.0	2.3	1.16	2.2
p-fluorophenylalanine	LS-P	4g	1.0	2.2	1.18	2.5
Phenylalanine	LS-P	4g	1.0	2.2	1.20	2.6

Tryptophan	LS-P	4g	1.0	2.0	1.25	3.1
Tryptophanamide	LS-P	4g	1.0	3.2	1.18	2.7
	VS	6a	1.0	1.2	1.22	2.7
Tryptophanol	LS-P	4a	1.0	2.4	1.15	2.9
Tyrosine methyl ester	LS-P **	4g	0.7	2.1	1.08	1.7
	NS	3c	0.3	1.9	1.10	1.7
Tyrosinol	LS-P	4a	1.0	2.4	1.13	2.5
	NS	4a	1.0	6.9	1.14	2.0

¹ See section 2.1 for all sample information.

² See section 2.3 for classification information.

³ All chiral stationary phases (CSP) were 100 x 4.6 mm (i.d.), unless indicated: *150 x 4.6 mm (i.d.), **200 x 4.6 mm (i.d.), ***250 x 4.6 mm (i.d.), ****300 x 4.6 mm (i.d.). See section 2.1 for more information.

⁴ See section 2.2 for mobile phase (MP) information.

⁵ All flow rates (F) are given in mL/min. All temperature (T) is 25 °C unless otherwise indicated (in °C).

^{6a,b,c} Chromatographic calculations: $k_1 = (t_{R1} - t_0) / (t_0)$; $\alpha = k_2 / k_1$; $R_s = 2(t_{R2} - t_{R1}) / (w_{0.5,1} + w_{0.5,2})$. See Supplemental data for abbreviations and more information.

Chapter 2 Table 3. Optimized chiral separations of tertiary (3°) amines.

a) Pharmaceuticals							
Name ¹	Class ²	CSP ³	MP ⁴	F(T) ⁵	k_1 ^{6a}	α ^{6b}	R_s ^{6c}
Atropine	AM	NS	2a	0.5	5.6	1.09	1.7
Brompheniramine	AH	VS	6a	0.7	2.5	1.13	2.0
Bupivacaine	ANE	NS	3c	1.0	1.9	1.21	2.5
		VS	1a	1.0	0.6	1.47	3.7
Carbinoxamine	AH	NS*	4f	0.5	2.2	1.08	1.5
		VS	3c	0.5	3.3	1.10	1.9
Cetirizine	AH	VS**	6a	0.3	1.3	1.08	1.5
Chlophedianol	AH	RSP*	5c	1.0	1.7	1.08	1.5
		VS	6a	0.6	1.6	1.14	2.5
Chlorpheniramine	AH	VS	6a	0.7	2.3	1.12	2.0
Diperodon	ABIO	NS	3c	1.0	5.8	1.13	1.7
		VS	3c	0.5	3.1	1.11	1.5
Disopyramide	SCB	NS***	3c	0.3	1.7	1.07	1.8
		VS	4a	1.0	2.9	1.13	2.1
Homatropine	AM	NS	2b	1.0(45)	2.4	1.19	3.1
		RSP*	5i	1.0	1.6	1.17	2.2
		VS**	9b	0.5	4.6	1.09	1.5
Indapamine	DIU	NS*	6c	0.3	11.0	1.13	1.5
		RSP	5h	0.3(10)	2.6	1.10	1.5
Mepivacaine	ANE	NS	4a	1.0	1.8	1.20	1.8
		VS	6a	0.5(30)	1.4	1.14	2.2
Methoxyverapamil	CCB	NS***	8a	0.5	3.6	1.08	1.5
		VS**	3c	0.5	3.0	1.10	1.5
Naftopidil	AB	NS	3c	0.5	3.2	1.12	1.5
Nicardipine	CCB	NS	3c	0.5	1.7	1.14	1.8
		VS	1a	2.0(45)	0.4	1.51	2.8
OctoclothePIN	APC	NS	3c	1.0	7.0	1.13	2.6
		RSP	5a	1.0	2.8	1.35	5.0
		VS*	6d	0.7(45)	0.8	1.17	2.2
Orphenadrine	AH	VS	6a	1.0	1.1	1.23	2.9
Piperoxan	AH	NS	3a	1.5	6.3	1.18	2.3

		VS	3a	0.7	2.3	1.12	2.2
Promethazine	AH	NS	2a	1.0	2.0	1.14	1.6
		VS	1a	2.0	3.0	1.72	7.5
Sulpiride	APC	NS	2b	1.0(45)	2.7	1.30	4.3
Thioridazine	APC	NS	2a	2.0(45)	2.8	1.38	5.0
Tolperisone	AM	NS	3c	0.5	5.2	1.07	1.5
		VS	1a	1.0	0.7	1.33	3.0
Trihexylphenidyl	AM	NS	3c	1.0	3.2	1.13	2.4
		VS	1a	1.0	0.7	1.29	2.7
Trimebutine	AM	NS	3c	0.5	1.5	1.13	1.7
		VS	1a	1.0	0.5	1.36	3.0
Verapamil	CCB	NS***	8a	0.5	4.1	1.09	1.5
		VS**	6a	0.3	1.9	1.08	1.5
b) Stimulants							
Name¹	Class²	CSP³	MP⁴	F(T)⁵	k₁^{6a}	α^{6b}	R_s^{6c}
Citalopram	AD	NS***	3c	0.3	4.8	1.05	1.6
		VS	3c	0.7	4.2	1.13	2.1
Methadone	CSA II	NS	3c	0.5	1.9	1.11	2.0
		RSP*	5g	0.7(45)	0.9	1.14	2.2
		VS	7b	0.5	2.5	1.12	2.1
Methorphan	CSA II	NS	2b	0.7(45)	3.6	1.09	1.6
		RSP*	5b	1.0	3.7	1.10	1.8
		VS	6b	1.0	1.2	1.27	3.3
Mianserin	AD	NS	3c	1.0	4.5	1.16	2.5
		RSP	5c	1.0	1.6	1.18	2.7
		VS	1a	2.0(45)	1.4	2.13	9.8
Nefopam	ANA	NS	2b	1.0(45)	2.0	1.19	2.6
		RSP	5e	1.0	1.7	1.23	3.5
		VS	1a	0.7(45)	1.5	1.12	2.1
Nicotine	TOB	NS	2b	1.5(45)	0.5	1.60	3.0
N-Methylephedrine	RC I	RSP*	5k	0.7	3.2	1.08	1.7
		VS	3b	1.0	2.7	1.10	1.9
Tetramisole	AP	NS	3c	0.7	3.5	1.12	2.5
Tramadol	CSA IV	VS*	6e	0.3(45)	0.5	1.21	1.5
Trimipramine	AD	VS	1a	1.0	1.0	1.33	3.4
Venlafaxine	AD	NS***	3c	0.3	2.0	1.06	1.6
		VS	3a	1.0	4.7	1.10	2.1
α-pyrrolidinopentiophenone (α-pvp)	CSA I	NS	4a	0.5	1.2	1.15	1.8
		RSP*	6d	0.3(10)	1.8	1.10	1.5
		VS	1a	1.0	0.6	1.44	4.3
c) Reagents							
Name¹		CSP³	MP⁴	F(T)⁵	k₁^{6a}	α^{6b}	R_s^{6c}
N,N-dimethyl-1-(1-naphthylethylamine)		NS	3c	1.0	4.7	1.11	2.3
		VS	8a	1.0	4.2	1.23	2.0
N,N-dimethyl-1-phenylethylamine		NS	3c	1.0	5.2	1.11	2.2
α-N,N-dimethylaminophenyl acetonitrile		RSP	5a	0.5	0.9	1.12	1.5

¹ See section 2.1 for all sample information.

² See section 2.3 for classification information.

³ All chiral stationary phases (CSP) were 100 x 4.6 mm (i.d.), unless indicated: *150 x 4.6 mm (i.d.), **200 x 4.6 mm (i.d.), ***250 x 4.6 mm (i.d.). See section 2.1 for more information.

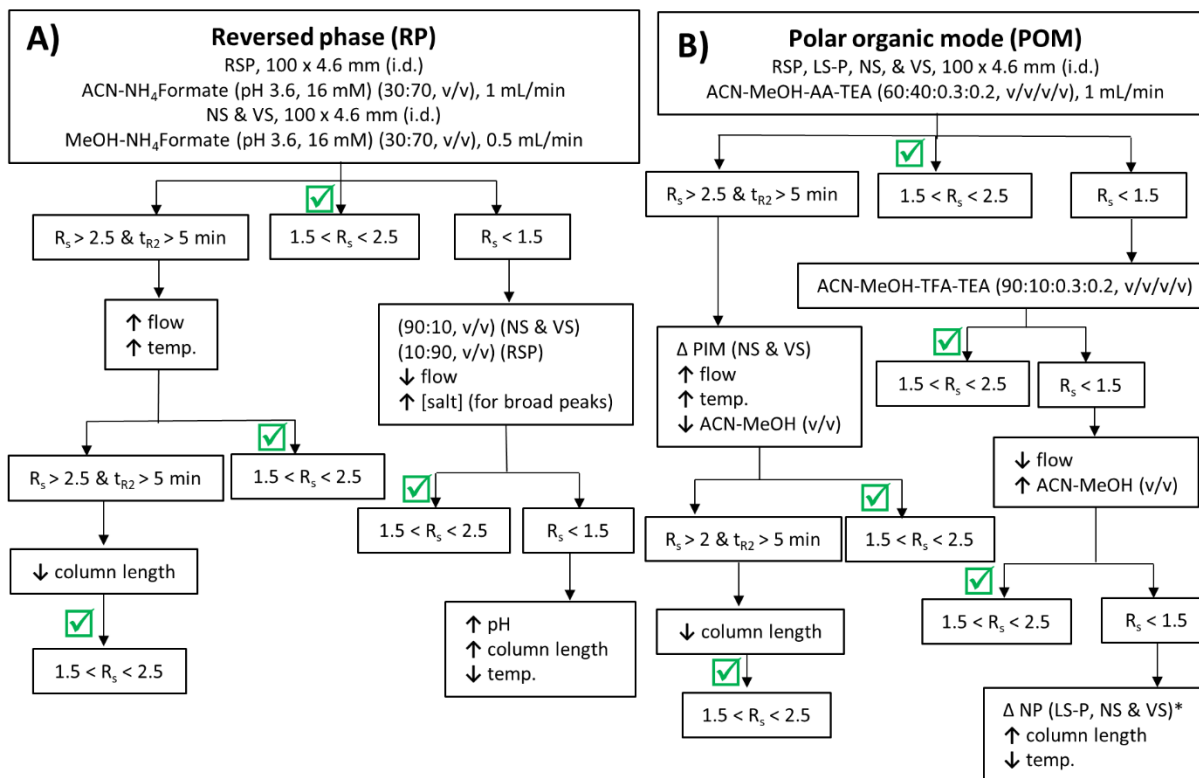
⁴ See section 2.2 for mobile phase (MP) information.

⁵ All flow rates (F) are given in mL/min. All temperature (T) is 25 °C unless otherwise indicated (in °C).

^{6a,b,c} Chromatographic calculations: $k_1 = (t_{R1} - t_0) / (t_0)$; $\alpha = k_2 / k_1$; $R_s = 2(t_{R2} - t_{R1}) / (W_{0.5,1} + W_{0.5,2})$. See Supplemental data for abbreviations and more information.

2.4 Results and discussion

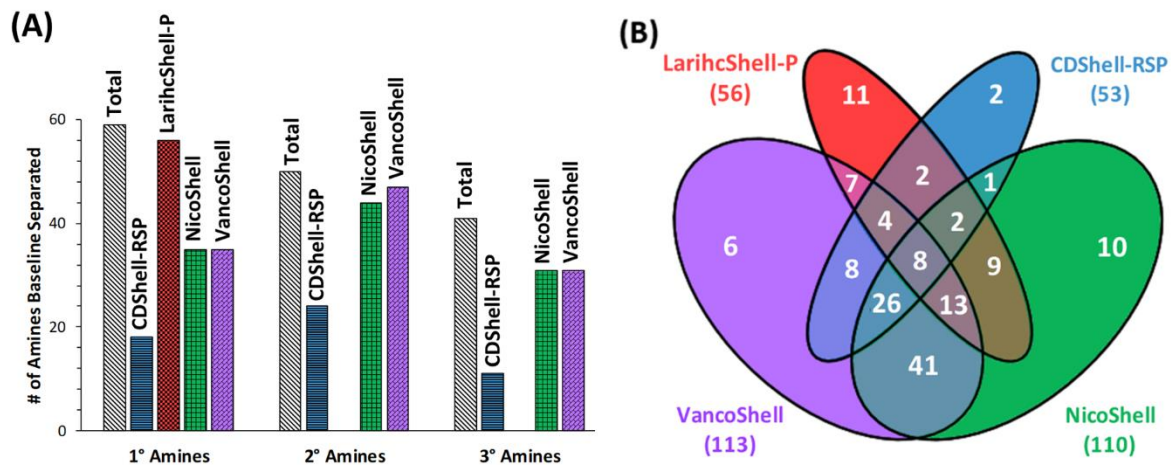
The following sections will discuss the method development of each CSP from screening to optimization for the chiral separation of amines (Fig. 1).



Chapter 2 Figure 1. Method development of chiral amines. Method development of chiral amines using SPP CSPs: CDShell-RSP (RSP), LarihcShell-P (LS-P), NicoShell (NS), and VancoShell (VS) in (A) reversed phase (RP) and (B) polar organic mode (POM). See Supplemental data for polar ionic mode (PIM) and normal phase (NP) method development and chromatographic parameter abbreviations (R_s , t_{R2}), and section 2.1 for all solvent abbreviations (ACN, MeOH, AA, TEA, NH₄HCO₂). Other abbreviations include temperature (temp.) and Δ , which represents “switch to.” See Fig. S1 and section S1 in Supplemental data for more information.

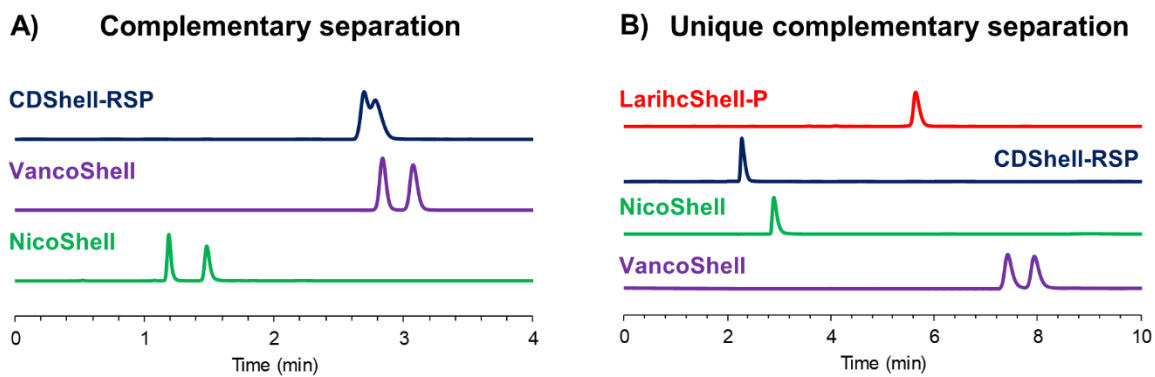
The goals for all separations were to result in a “hit” ($\alpha > 1.05$) from screening and get to baseline separation ($R_s \geq 1.5$) while operating at moderate pressure (<300 bar) and room temperature (25 °C). The optimized results of the 150 tested amines are tabulated in Tables 1-3. The number of baseline separations achieved with each CSP compared to the total possible separations according to the type of amine: 1°, 2°, or 3° is shown in Fig. 2A. All 150 amines were baseline separated by at least one CSP and often with

multiple CSPs. Fig. 2B illustrates, non-proportionally, the overlap of baseline separations between each CSP, and reports the total number of baseline separations for each CSP in parenthesis.



Chapter 2 Figure 2. Baseline separations results of 150 chiral 1°, 2°, and 3° amines with four superficially porous particle (SPP) chiral stationary phases (CSPs). **(A)** Number of baseline separations by each CSP compared to the total amines tested. **(B)** Number of amines baseline separation by each or more than one CSP. See Results and Discussion for further explanation.

The results show that 81% were baseline separated by two or more CSPs, 35% were baseline separated by three or more CSPs, and 5% were baseline separated by all four CSPs. These separations will be addressed according to the principle of complementary separations with the addition of the term, “unique,” which applies to complementary separations where the amine had no separation with any of the other CSPs (Fig. 3).

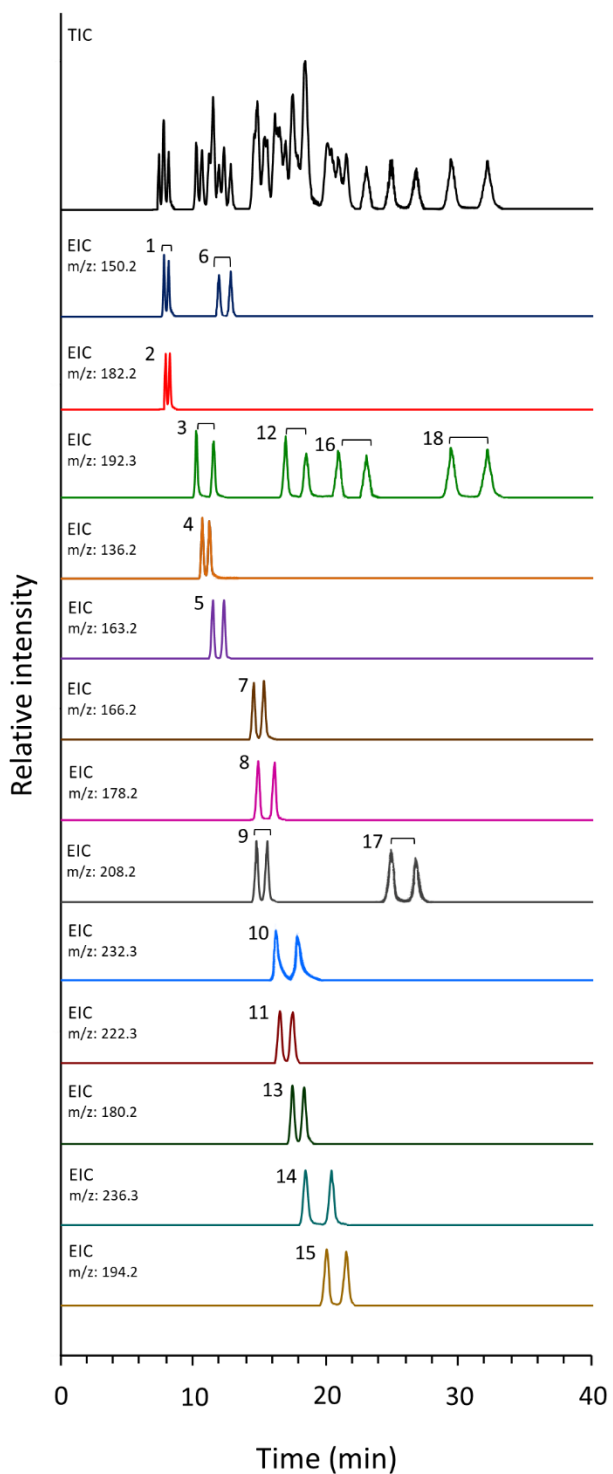


Chapter 2 Figure 3. The principle of complementary separations. **(A, B)**. The principle of complementary separations: the difference between **(A)** complementary and **(B)** unique complementary separations using **(A)** alprenolol and **(B)** tramadol. See Tables 1–3 for all chromatographic results. See Section Experimental for all chromatographic parameters and other information.

The numbers represented with just one CSP in Fig. 2B do not indicate “unique” complementary separations because a different CSP might have had $R_s < 1.5$ for that amine. Also, if the amine was separated by three CSPs, such as RSP, VS, and NS, it was not included in the overlap of two CSPs, like VS and NS (Fig. 2B).

Overall, LS-P (i.e., the isopropyl cyclofructan-6) was the most powerful CSP for separating 1° amines. LS-P achieved six “unique” complementary separations including phenylalanine, *p*-chlorophenylalanine, *p*-fluorophenylalanine, tryptophan, tryptophanol, and norepinephrine. Also, LS-P performed five other baseline separations that other CSPs could not, which included thyroxine, 1-(2-naphthylethylamine), 3,4-dihydroxyphenylalanine (DOPA), 4-chlorobenzylhydramine, and 4-nitrophenylalanine.

Most stimulants were best separated by RSP (i.e., hydroxypropyl β -cyclodextrin), which is shown in Fig. 4 with the baseline separation of 18 racemic controlled substances in a single LC-MS analysis. RSP had one “unique” complementary separation, 3,4-methylenedioxymethamphetamine (MDMA). Also, RSP baseline separated one other amine that was not by other CSPs: α -N,N-dimethylaminophenyl acetonitrile.



Chapter 2 Figure 4. Chromatographic enantioseparation of 18 racemic controlled substance stimulant amines using liquid chromatography electrospray-mass spectrometry (LC-ESI-MS). Total ion chromatogram (TIC) and extracted ion chromatograms (EIC) are shown. Conditions: CDShell-RSP, 150 x 4.6 mm (i.d.), ACN-NH₄HCO₂ (pH 3.6, 16 mM) (10:90), 0.4 mL/min, 25 °C. 1. rac-cathinone, 2. rac-3-

FMC, 3. rac-pentedrone, 4. rac-amphetamine, 5. rac-aminorex, 6. rac-methamphetamine, 7. rac-PMA, 8. rac-mephedrone, 9. rac-methylone, 10. rac- α -PVP, 11. rac-ethylone, 12. rac-4-MEC, 13. rac-MDA, 14. rac-pentylone, 15. rac-MDMA, 16. rac-3,4-DMMC, 17. rac-MDEA, 18. rac-4-EMC. See sections Experimental and Tables 1-3 for other acronyms and information.

NS and VS (i.e., both macrocyclic glycopeptides) dominated the separation of pharmaceuticals and demonstrated the most complementary behavior of any two CSPs. NS had two “unique” complementary separations: atropine and epinephrine, and eight other baseline separations not performed by other CSPs: ephedrine, fenfluramine, naftopidil, nicotine, N,N-dimethyl-1-phenylethylamine, sulpiride, tetramisole, and thioridazine. VS had four “unique” complementary separations including brompheniramine, cetirizine, chlorpheniramine, and tramadol. Also, VS baseline separated two amines, orphenadrine and trimipramine, that other CSPs could not.

2.4.1 Screening and optimization

Screening was performed with all 150 amines with reversed phase (RP) and polar organic mode (POM) (Fig. 1) The POM screening mobile phase comprised of ACN-MeOH-AA-TEA (60:40:0.3:0.2, v/v/v/v). LS-P utilized POM, and all other CSPs utilized both RP and POM. The RP screening mobile phase for NS and VS was MeOH-NH₄HCO₂ (pH 3.6, 16 mM) (30:70, v/v), while ACN-NH₄HCO₂ (pH 3.6, 16 mM) (30:70, v/v) was used for RSP. These screening solvents offered the best chance for a “hit” based on a thorough investigation of mobile phase additives, which are discussed in the Supplemental data (Section S1, Figs. S1-S6, Table 1). An optimized separation was targeted at a R_s between 1.5 and 2.5 with an analysis time < 5 min. For “hits,” optimizations were made according to each CSP. LS-P required the least optimization with most optimized separations performed using the screening mobile phase or ACN-MeOH-TFA-TEA (90:10:0.3:0.2, v/v/v/v) (Table 1, Fig. 1B). However, if $R_s > 1.5$ was not achieved sometimes a normal phase (NP) solvent, Hep-EtOH-TFA-TEA (60:40:0.3:0.2, v/v/v/v), was used. Since the back pressure was ~60-110 bar using a 100 x 4.6 mm (i.d.) column at 1.0 mL/min with these mobile phases, analysis time was often reduced by increasing the flow rate. RSP had the most separations in the reversed phase mode. If $R_s > 1.5$ was not achieved, the mobile phase was adjusted to ACN-NH₄HCO₂ (pH 3.6, 16 mM) (10:90, v/v) (Fig. 1A). For NS and VS optimization in the reversed phase mode, often

MeOH-NH₄HCO₂ (pH 3.6, 16 mM) (90:10, v/v) was used (Fig. 1A). However, most amines were best separated by NS and VS when using the polar organic mode. Frequently, the use of a polar ionic mode (PIM) solvent, MeOH-NH₄HCO₂ (100:1, v/w), was used for the amines that had enantiomeric selectivity in POM (Section S1.3, Figs. S1, S5). A variety of other optimization factors were investigated to improve R_s, especially for the non-optimal separations ($\alpha < 1.05$), which are not included in Tables 1-3 (Section S1, Figs.S1-S6, Table 1).

2.4.2 Cyclofructan-6-P (LS-P)

The derivatized cyclofructan, LS-P, baseline separated 95% of racemic chiral 1° amines, of which many were reagents used for organic synthesis (Fig. 2A, Table 1). Since LS-P had such high selectivities for almost all the racemates, it is best-suited to identify and quantify trace impurities of enantiomeric reagents in a synthetic therapeutic product. For example, rasagiline is used as a therapeutic for Parkinson's disease, and one of its chemical precursor, 2-chloro-indan-1-ylamine had a R_s of 7.2 with an analysis time under 2 min with LS-P (Table 1c). This large α also indicates a facile application for preparatory separations to isolate a single enantiomer in large quantities, especially since most analytes are soluble in these solvents used for LS-P [11]. Also, solvents used with the LS-P column are highly MS compatible compared to other CSPs, like crown ethers, which are commonly used to separate of 1° amines [11]. When a chiral 1° amine also had additional hydrogen bonding functionalities adjacent or connected to the chiral center, R_s increased - which was expected [11,16,29]. Difficult 1° amine separations included amphetamines and sterically hindered 1° amines, like 2-amino-1,1,3-triphenyl-1-propanol, 2-amino-1,1-diphenyl-1-propanol, and aminorex. It should also be noted that most amino acids and derivatives have 1° amine functionalities but have been shown to separate easily using other CSPs not included in this study, like TeicoShell [12,17].

2.4.3 Hydroxypropyl- β -cyclodextrin (RSP)

The RSP β -cyclodextrin CSP baseline separated 35% out of the 150 amines, 30% of the 1° amines, 48% of the 2° amines, and 27% of the 3° amines (Fig. 2A). It was best utilized for the stimulants, which included several controlled substances like amphetamines and cathinones, as well as alkaloids, opioids, and antidepressants (see Tables 1-3). Fig. 4 highlights the use of LC-MS with the baseline separation of 18 racemic controlled substances. Since the RSP primarily was used in the reversed phase mode, these methods had very high MS sensitivity, which enhances its applicability to forensic and toxicology studies. Separations included MDMA, and several synthetic cathinones, especially those that could interact through hydrogen bonding. Analytes that had two hydrogen bonding functionalities, such as pseudoephedrine, had larger R_s compared than those with only one, like methamphetamine, and those with none, like fenfluramine, which enantiomers coeluted, as expected (Table 2b) [30]. Interestingly, 4-fluoromethcathinone (4-FMC) could not be baseline separated by RSP, but 3-fluoromethcathinone (3-FMC) was. However, 4-FMC and all other stimulants not baseline separated by RSP were separated by a different CSP, which indicates the complementary behavior between all these macrocyclic CSPs.

2.4.4 Macrocyclic glycopeptides (VS & NS)

The native macrocyclic glycopeptide, VS, baseline separated 75% of all the amines: 59% of the 1° amines, 94% of the 2° amines, and 76% of the 3° amines (Fig. 2A). Overall, VS had the best performance, baseline separating more amines than the other tested CSPs. VS separated the most pharmaceutical amines, baseline separating all antihistamines, anesthetics, antidepressants, analgesics, antiarrhythmics, decongestants/bronchodilators, and antianginals. The modified macrocyclic glycopeptide, NS, baseline separated 73% of all the amines, 59% of the 1° amines, 88% of the 2° amines, and 76% of the 3° amines (Fig. 2A). NS has previously been shown to separate nicotine-related compounds, which was further demonstrated in this work [18-19]. Additionally, NS had higher R_s for all β -blockers compared to VS. Carbinoxamine, an antihistamine with a structure similar to chlorpheniramine, was baseline separated using NS, while chlorpheniramine was not. In general, antihistamines were better separated by VS than NS. One example was promethazine, an antihistamine

with a phenothiazine structure, which had an extremely high R_s of 7.5 within 3 min using VS (Table 2). However, another phenothiazine that is used as an antipsychotic, thioridazine, had low R_s using VS, but was baseline separated by NS. Thioridazine is currently under investigation as a treatment for schizophrenia, as is sulpiride and both were only baseline separated by NS. Another class of amines that NS dominantly separated were the catecholamines, except norepinephrine and N-methylephedrine. Since macrocyclic glycopeptides have complex separation mechanisms, it is difficult to predict why certain amines were or weren't separated. Thus, their highly complementary separation behavior contributes greatly to their ease of use and optimization.

2.5 Conclusions

Herein the broadest and most comprehensive separation strategies for chiral amine containing compounds is demonstrated. All 150 chiral amines were easily optimized to a R_s between 1.5 and 2.5, most within 5 min with at least one CSP, and several with more than one CSP. LS-P was shown to be best for 1° amines, while RSP, NS, and VS separated a variety of 1°, 2°, and 3° amines. RSP separated most chiral stimulants, which would provide sensitive forensic drug screening and testing. NS and VS best separated pharmaceuticals and provided the most complementary separations. Further investigation of these CSPs will lead to more information about their separation mechanisms and other novel applications.

2.6 References

1. Food and Drug Administration, New drugs at FDA: CDER's new molecular entities and new therapeutic biological products, <https://www.fda.gov/Drugs/DevelopmentApprovalProcess/DrugInnovation/default.htm>, 2017 (accessed 03 January 2018).
2. A. Calcaterra, I. D'Acquarica, The market of chiral drugs: Chiral switches versus *de novo* enantiomerically pure compounds, *J. Pharm. Biomed. Anal.* 147 (2018) 323-340.
3. J.-T. Liu, R.H. Liu, Enantiomeric composition of abused amine drugs: chromatographic methods of analysis and data interpretation, *J. Biochem. Biophys. Methods* 54 (2002) 115-146.
4. R.E. Boehm, D.E. Martire, D.W. Armstrong, Theoretical considerations concerning the separation of enantiomeric solutes by liquid chromatography, *Anal. Chem.* 60 (1988) 522-528.
5. Drug Enforcement Administration, Lists of scheduling actions, controlled substances, regulated chemicals, <https://www.deadiversion.usdoj.gov/schedules/orangebook/orangebook.pdf>, 2017 (accessed 03 January 2018).
6. D.A. Spudeit, M.D. Dolzan, Z.S. Breitbach, W.E. Barber, G.A. Micke, D.W. Armstrong, Superficially porous particles vs. fully porous particles for bonded high performance liquid

- chromatographic chiral stationary phases: Isopropyl cyclofructan 6, *J. Chromatogr. A* 1363 (2014) 89-95.
7. D.C. Patel, Z.S. Breitbach, M.F. Wahab, C.L. Barhate, D.W. Armstrong, Gone in seconds: praxis, performance, and peculiarities of ultrafast chiral liquid chromatography with superficially porous particles, *Anal. Chem.* 87 (2015) 9137-9148.
 8. D.C. Patel, M.F. Wahab, D.W. Armstrong, Z.S. Breitbach, Advances in high-throughput and high-efficiency chiral liquid chromatographic separations, *J. Chromatogr. A* 1467 (2016) 2-18.
 9. C.L. Barhate, L.A. Joyce, A.A. Makarov, K. Zawatzky, F. Bernardoni, W.A. Schafer, D.W. Armstrong, C.J. Welch, E.L. Regalado, Ultrafast chiral separations for high throughput enantiopurity analysis, *Chem. Commun.* 53 (2016) 509-512.
 10. D.W. Armstrong, Y. Tang, S. Chen, Y. Zhou, C. Bagwill, J.R. Chen, Macrocyclic antibiotics as a new class of chiral selectors for liquid chromatography, *Anal. Chem.* 66 (1994) 1473-1484.
 11. P. Sun, C. Wang, Z.S. Breitbach, Y. Zhang, D.W. Armstrong, Development of new HPLC chiral stationary phases based on native and derivatized cyclofructans, *Anal. Chem.* 81 (2009) 10215-10226.
 12. X. Zhang, Y. Bao, K. Huang, K. Barnett-Rundlett, D.W. Armstrong, Evaluation of dalbavancin as chiral selector for HPLC and comparison with teicoplanin-based chiral stationary phases, *Chirality*, 22 (2010) 495-513.
 13. T.L. Xiao, E. Tesarova, J.L. Anderson, M. Egger, D.W. Armstrong, Evaluation and comparison of a methylated teicoplanin aglycone to teicoplanin aglycone and natural teicoplanin chiral stationary phases, *J. Sep. Sci.* 29 (2006) 429-445.
 14. K.H. Ekborg-Ott, J.P. Kullman, X. Wang, K. Gahm, L. He, D.W. Armstrong, Evaluation of the macrocyclic antibiotic avoparcin as a new chiral selector for HPLC, *Chirality* 10 (1998) 627-660.
 15. A. Peter, E. Vêkes, D.W. Armstrong, Effects of temperature on retention of chiral compounds on a ristocetin A chiral stationary phase, *J. Chrom. A* 958 (2002) 89-107.
 16. D.W. Armstrong, R.M. Woods, Z.S. Breitbach, Z.S. Comparison of enantiomeric separations and screening protocols for chiral primary amines by SFC and HPLC, *LC-GC North America* 32 (2014) 742-752.
 17. D.W. Armstrong, Y. Liu, K.H. Ekborg-Ott, A covalently bonded teicoplanin chiral stationary phase for HPLC enantioseparations, *Chirality* 7 (1995) 474-497.
 18. G. Hellinghausen, J.T. Lee, C.A. Weatherly, D.A. Lopez, D.W. Armstrong, Evaluation of nicotine in tobacco-free-nicotine commercial products, *Drug Test. Anal.* 9 (2017) 944-948.
 19. G. Hellinghausen, D. Roy, Y. Wang, J.T. Lee, D.A. Lopez, C.A. Weatherly, D.W. Armstrong, A comprehensive methodology for the chiral separation of 40 tobacco alkaloids and their carcinogenic E/Z-(R,S)-tobacco specific nitrosamine metabolites, *Talanta* 181 (2017) 132-141.
 20. C.L. Barhate, D.A. Lopez, A.A. Makarov, X. Bu, W.J. Morris, A. Lekhal, R. Hartman, D.W. Armstrong, E.L. Regalado, Macrocyclic glycopeptide chiral selectors bonded to core-shell particles enables enantiopurity analysis of the entire verubecestat synthetic route, *J. Chrom. A* 1539 (2018) 87-92.
 21. D. Wolrab, P. Frühauf, A. Moulisová, M. Kuchař, C. Gerner, W. Lindner, M. Kohout, Chiral separation of new designer drugs (Cathinones) on chiral ion-exchange type stationary phases, *J. Pharm. Biomed. Anal.* 120 (2016) 306-315.
 22. N.L.T. Padivitage, E. Dodbiba, Z.S. Breitbach, D.W. Armstrong, Enantiomeric separations of illicit drugs and controlled substances using cyclofructan-based (LARIHC) and cyclobond I 2000 RSP HPLC chiral stationary phases, *Drug Test. Anal.* 6 (2014) 542-551.
 23. D.W. Armstrong, S.M. Han, Y.I. Han, Separation of optical isomers of scopolamine, cocaine, homatropine, and atropine, *Anal. Biochem.* 167 (1987) 261-264.
 24. M.D. Dolzan, Y. Shu, J.P. Smuts, H. Petersen, P. Ellegaard, G.A. Micke, D.W. Armstrong, Z.S. Breitbach, Enantiomeric separation of citalopram analogues by HPLC using macrocyclic glycopeptide and cyclodextrin based chiral stationary phases, *J. Liq. Chrom. & Rel. Tech.* 39 (2016) 154-160.

25. D. Albals, Y.V. Heyden, M.G. Schmid, B. Chankvetadze, D. Mangelings, Chiral separations of cathinone and amphetamine-derivatives: Comparative study between capillary electrochromatography, supercritical fluid chromatography and three liquid chromatographic modes, *J. Pharm. Biomed. Anal.* 121 (2015) 232-243.
26. B. Chankvetadze, L. Chankvetadze, Sh. Sidamonidze, E. Yashima, Y. Okamoto, High performance liquid chromatography enantioseparation of chiral pharmaceuticals using tris(chloro-methylphenylcarbamate)s of cellulose, *J. Pharm. Biomed. Anal.* 14 (1996) 1295-1303.
27. S. Chen, Y. Liu, D.W. Armstrong, J.I. Borrell, B. Martinez-Teipel & J.L. Matallana, Enantioresolution of substituted 2-methoxy-6-oxo-1,4,5,6-tetrahydropyridine-3-carbonitriles on macrocyclic antibiotic and cyclodextrin stationary phases, *J. Liq. Chrom. & Rel. Tech.* 18 (1995) 1495-1507.
28. M.P. Gasper, A. Berthod, U.B. Nair, D.W. Armstrong, Comparison and modeling study of vancomycin, ristocetin A, and teicoplanin for CE enantioseparations, *Anal. Chem.* 68 (1996) 2501-2514.
29. P. Sun, D.W. Armstrong, Effective enantiomeric separations of racemic primary amines by the isopropyl carbamate-cyclofructan6 chiral stationary phase, *J. Chromatogr. A* 1217 (2010) 4904-4918.
30. D.W. Armstrong, W. DeMond, Cyclodextrin bonded phases for the liquid chromatographic separation of optical, geometrical, and structural isomers, *J. Chromatogr. Sci.* 22 (1984) 411-415.

Chapter 3

Evaluation of the Edman degradation product of vancomycin bonded to core-shell particles as a new HPLC chiral stationary phase

3.1 Abstract

A modified macrocyclic glycopeptide-based chiral stationary phase (CSP), prepared via Edman degradation of vancomycin, was evaluated as a chiral selector for the first time. Its' applicability was compared to other macrocyclic glycopeptide-based CSPs: TeicoShell and VancoShell. In addition, another modified macrocyclic glycopeptide-based CSP, NicoShell, was further examined. Initial evaluation was focused on the complementary behavior with these glycopeptides. A screening procedure was utilized based on previous work for the enantiomeric separation of 50 chiral compounds including amino-acids, pesticides, stimulants, and a variety of pharmaceuticals. Fast and efficient chiral separations resulted by using superficially porous (core-shell) particle supports. Overall, the vancomycin edman degradation product (EDP) resembled TeicoShell with high enantioselectivity for acidic compounds in the polar ionic mode. The simultaneous enantiomeric separation of 5 racemic profens using liquid chromatography-mass spectrometry (LC-MS) with EDP was performed in ~3 min. Other highlights include simultaneous LC separations of rac-amphetamine and rac-methamphetamine with VancoShell, rac-pseudoephedrine and rac-ephedrine with NicoShell, and rac-dichlorprop and rac-haloxyfop with TeicoShell.

3.2 Introduction

Macrocyclic glycopeptide antibiotics were first introduced as chiral selectors for liquid chromatography by Armstrong in the early 1990s.¹ These natural products are produced by bacterial fermentation. Purified and bonded to silica particles, they make useful chiral stationary phases (CSPs) with a broad spectrum of interactions and therefore applicability.² The macrocyclic glycopeptide-based CSPs are multimodal, meaning they are stable and efficient in normal phase (NP), reversed phase (RP), polar organic mode

(POM), and polar ionic mode (PIM).^{3,4} The most distinctive feature of macrocyclic glycopeptides as chiral selectors is their ionic character. All macrocyclic glycopeptides are ionizable, bearing primary or secondary amines rendering them positively charged at neutral and acidic pH values.⁵⁻⁷ They also have a carboxylic acid bearing a negative charge at neutral and high pH values so that the net charge is adjustable according to the mobile phase pH. This is the foundation of PIM, which utilizes 100% methanol containing trace amounts of acid and base or a non-volatile salt to tune the charges on the chiral selector to effect ionizable enantiomers' retention and separation.⁶ Many ionizable compounds can be separated in PIM, but sometimes it is beneficial to adjust the hydrogen bonding interactions by switching to POM, which contains a mixture of acetonitrile and methanol with acid and base.³ Others favour RP, in which methanol is generally mixed with an ammonium salt with pH adjustment to enhance ionic interactions. In RP, a low pH is generally preferred for amines, which higher pH is favoured for acids. All these modes are compatible with mass spectrometry, and usually NP is not necessary for enantiomeric separations with macrocyclic glycopeptides, while other CSPs depend on it. This is especially important to biological analysis, which depends on mass spectrometry sensitivity for thermally labile and complex samples.

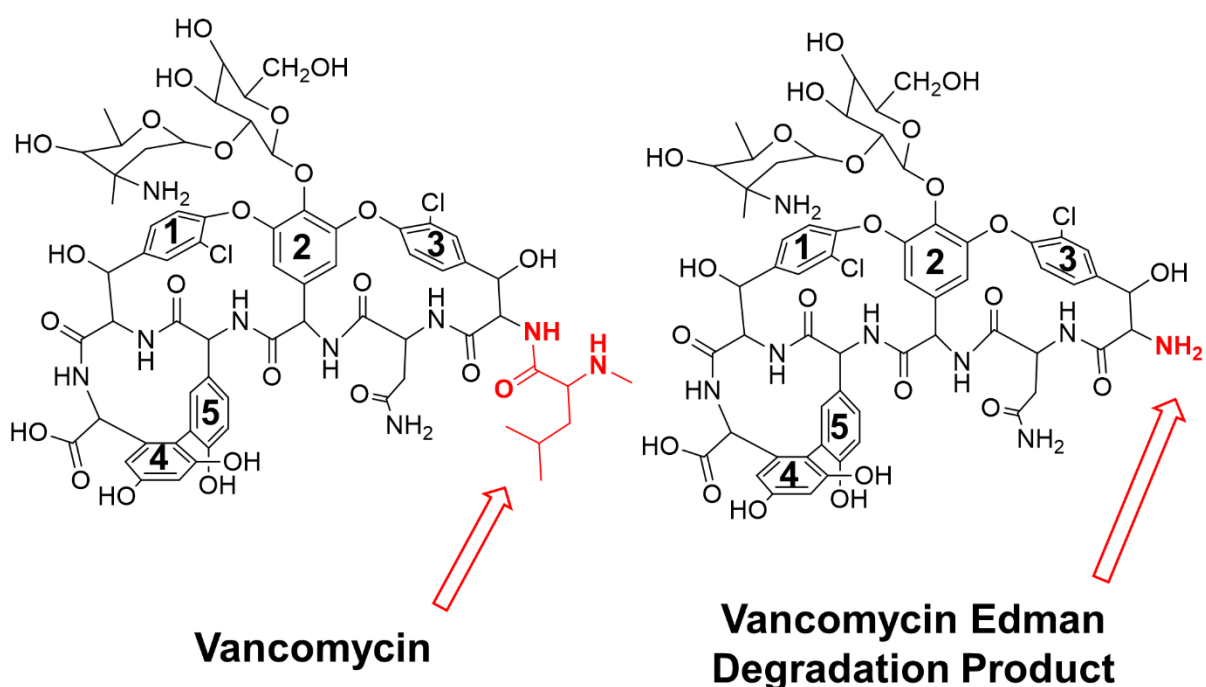
Another feature of the macrocyclic glycopeptide class of chiral selectors is their complementary behavior.^{5,9} If a separation of an enantiomeric pair is observed on a macrocyclic selector, say teicoplanin, chances are that a baseline separation of this pair will be observed on a different selector, say vancomycin. The large number of possible interactions and structural similarities between the different macrocyclic glycopeptides explain the observed complementary behaviour, which provides an ease of method development. A plethora of native macrocyclic glycopeptides have been explored for their use as chiral selectors, not only in liquid chromatography (LC), but also capillary electrophoresis and supercritical fluid chromatography.^{1,4,5,7-19} Of these, vancomycin, teicoplanin, and ristocetin A were commercialized as the CHIROBIOTICS as well as teicoplanin's aglycone.²⁰ Since the recent development of superficially porous particles or core-shell particles, which offer high-throughput and more effective

separations, several studies have been explored using core-shell macrocyclic glycopeptide-based CSPs (TeicoShell, VancoShell).²¹⁻²⁵ This has been particularly useful to ultrafast chiral separations needed in second dimension (2D) LC.²⁴⁻²⁹ However, many glycopeptides are costly, and have limited availability, which has led to a need to understand the applicability and limitations of more available glycopeptides so further exploration can be made concerning useful modifications.

Comprehensive studies have indicated that vancomycin is most useful for the separation of basic amines, while teicoplanin is most useful for the separation of acids, specifically amino acids.^{17,20,23} When exploring the structural interactions driving these separations, it is difficult to assess their separation mechanisms due to the diverse and complex interactions of each macrocyclic glycopeptide.⁶ However, it is thought that the carboxylic acid located in the vancomycin structure might play an important role for the interaction with amines, while the primary amine in teicoplanin might be important to chiral recognition for acids.⁶ Some studies have been done with modified macrocyclic glycopeptides, such as the crystalline degradation of vancomycin, which incorporates a second carboxylic acid moiety in the structure.³⁰⁻³² Recently, a modified macrocyclic glycopeptide-based CSP, NicoShell, was used for the novel LC enantiomeric separation of nicotine from tobacco e-liquids and several nicotine related compounds, including carcinogenic tobacco-specific nitrosamines.²¹⁻²² NicoShell was further utilized for the separation of several chiral amines.²³ An effective methodology was proposed for core-shell CSPs, and was used in this study to evaluate a new selector, the vancomycin Edman degradation product (EDP).²³ The EDP differs from native vancomycin by the loss the N-terminus leucine residue, leaving a primary amine (Fig.1).³⁴ A set of 50 biologically active chiral compounds including stimulants, non-steroidal anti-inflammatory drugs, pesticides, and a variety of acidic and basic pharmaceuticals were subjected to LC enantiomeric separation. EDP results were then compared to three other macrocyclic glycopeptide-based core-shell CSPs: TeicoShell, VancoShell, and NicoShell.

3.3 Materials and methods

Macrocytic glycopeptide-based core-shell CSPs (100 x 4.6 mm (i.d.)): vancomycin (VancoShell, VS), teicoplanin (TeicoShell, TS), NicoShell (NS), and the vancomycin Edman degradation product (EDP) were obtained from AZYP, LLC. (Arlington, TX, USA). The EDP selector was synthesized by reacting vancomycin with phenyl isothiocyanate in pyridine/water (50/50, v/v) followed by treatment with trifluoroacetic acid to selectively remove the N-terminal residue highlighted in red in Fig.1.³³ Thus, the hexapeptide derivative with a free primary amine (red arrow, Fig. 1) was produced. The hexapeptide selector was then bonded to 2.7 μm core-shell particles, like the other CSPs.



Chapter 3 Figure 1. Structures of vancomycin and the vancomycin Edman degradation product. The five-aromatic ring association in the peptidic aglycone “basket” is labeled 1-5. The red arrow indicates the structural modification leading to the vancomycin edman degradation product. See Materials and methods for information concerning preparation of macrocytic glycopeptide-based chiral stationary phases.

Analytes were purchased as racemic standards or individual enantiomer standards (then mixed to form racemates) from Cerilliant Corporation (Round Rock, TX, USA), Sigma-Aldrich (St. Louis, MO, USA), and LKT Laboratories Inc (Minneapolis, MN, USA). Racemic standards were prepared with methanol at 1 mg/mL for analysis. In the set of 50 selected analytes, 48 were ionizable compounds, mostly bases,

since only 10 acidic compounds did not contain a nitrogen atom. 26 analytes were amines or have an amine group in their structure. The remaining 14 nitrogen containing compounds were mostly amides (9 analytes) and a pyrrolizidine, pyran, benzoxazole, and two pyridine containing compounds.

Solvents and additives including HPLC grade acetonitrile (ACN), methanol (MeOH), ethanol (EtOH), hexane (Hex), acetic acid (AA), trifluoroacetic acid (TFA), trimethylamine (TEA), formic acid (FA), ammonium formate (NH₄HCO₂), and ammonium trifluoroacetate (NH₄TFA) were obtained from Sigma-Aldrich (St. Louis, MO, USA). Water was purified by a Milli-Q water purification system (Millipore, Billerica, MA, USA).

An Agilent 1260 (Agilent Technologies, Palo Alto, CA, USA) HPLC was used. It consisted of a 1200 diode array detector, autosampler, and quaternary pump. The mass spectrometer used in this study was a Shimadzu triple quadrupole liquid chromatography-mass spectrometry (LC-MS) instrument, LCMS-8040 (Shimadzu, Tokyo, Japan). All MS was operated in positive ion mode with an electron spray ionization source. The parameters were set as follows: nebulizer gas flow, 3 L/min; dryer gas flow, 15 L/min; desolvation line temperature, 250 °C; heat block temperature, 400 °C. Multiple UV wavelengths, 220, 230, and 254 nm were utilized for detection and identification of enantiomers. All separations were carried out at room temperature, unless otherwise noted, using an isocratic method. Mobile phases were degassed by ultrasonication under vacuum for 5 minutes. Each analyte was screened in PIM, POM, RP, and NP. The screening mobile phase conditions referring to Table 1 were as follows: PIM: MeOH-NH₄Formate (100:0.1, v/w), POM: ACN-MeOH-AA-TEA (60:40:0.3:0.2, v/v/v/v), RP: MeOH-NH₄Formate (pH 3.6; 16 mM) (30:70, v/v), NP: Hex-EtOH-TFA-TEA (70:30:0.3:0.2, v/v/v/v).

The dead time, t_0 , was determined by the peak of the refractive index change due to the unretained sample solvent. Retention factors (k) were calculated using $k = (t_R - t_0) / (t_0)$, where t_R is the retention time of the first peak and t_0 , the dead time of the column. Selectivity (α) was calculated using $\alpha = k_2 / k_1$, where k_1 and k_2 are retention factors of the first and second peaks, respectively. Resolution (R_s) was calculated using

the peak width at half peak height, $R_s = 2(t_{R2} - t_{R1}) / (w_1 + w_2)$. Two EDP columns were produced and had a relative standard deviation (%RSD) within 5.0% for all R_s factors obtained.

3.4 Results and discussion

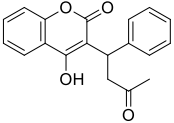
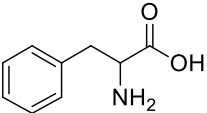
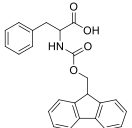
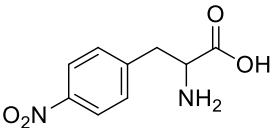
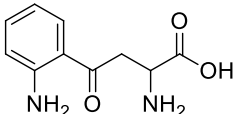
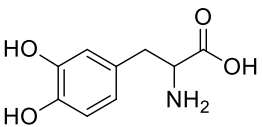
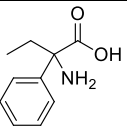
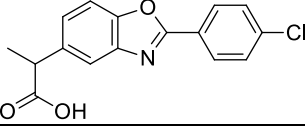
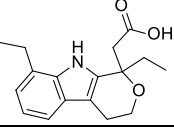
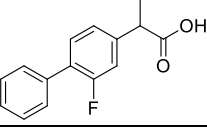
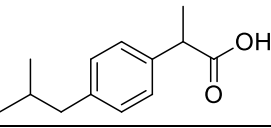
3.4.1 Screening Results

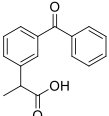
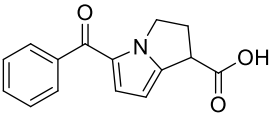
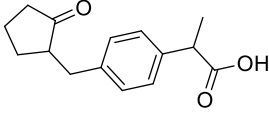
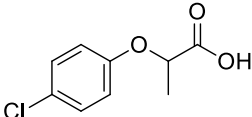
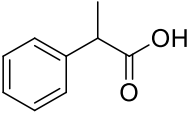
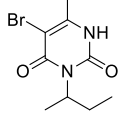
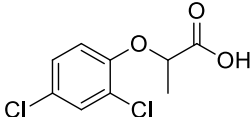
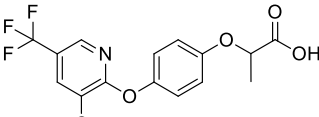
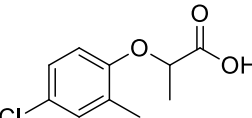
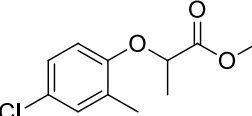
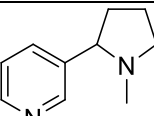
Preliminary screening with all 4 CSPs using 50 chiral compounds in each compatible chromatographic mode (PIM, POM, RP, and NP) was performed, making 200 analyses per CSP. When a partial separation of the enantiomers was obtained, this separation could be significantly improved by modulating the mobile phase as shown in previous studies but it should be noted that this was not the aim of this study.^{20,23} The best screening result (in terms of R_s) by each CSP are tabulated according to each compound in Table 1. In 46 cases (184 analyses), the compounds could not be separated on a CSP by all 4 mobile phases assayed. These are reported in Table 1 with $\alpha = 1.00$ and $R_s = 0.0$ in the Table 1. No k_1 was listed since 4 different values were obtained in the 4 modes tested, all four producing a single peak for the enantiomeric pair.

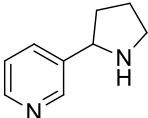
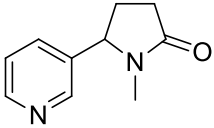
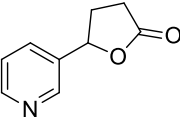
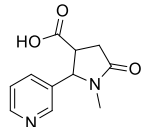
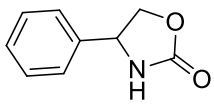
Chapter 3 Table 1. Chiral separation comparisons using core-shell macrocyclic glycopeptide-based CSPs.

a) Chemical amines						
Name¹	Structure¹	CSP²	MP³	k₁⁴	α⁴	R_s⁴
α-methylbenzylamine		VS	PIM	0.9	1.07	0.8
		NS	POM	5.8	1.17	2.4
		EDP	PIM	0.4	1.05	0.3
		TS	-	-	1.00	0.0
α,4-dimethylbenzylamine		VS	POM	3.0	1.12	1.4
		NS	POM	2.8	1.09	1.0
		EDP	POM	1.0	1.08	0.6
		TS	-	-	1.00	0.0
α-methyl-4-nitrobenzylamine		VS	PIM	1.5	1.07	0.9
		NS	PIM	4.3	1.06	1.2
		EDP	PIM	0.6	1.04	0.3
		TS	NP	7.0	1.02	0.4
4-methoxymethylbenzylamine		VS	PIM	1.0	1.45	5.1
		NS	PIM	2.2	1.08	1.6
		EDP	PIM	0.4	1.40	2.4
		TS	NP	4.6	1.03	0.5
N,N-α-trimethylbenzylamine		VS	RP	0.3	1.23	1.3
		NS	PIM	2.7	1.11	1.6
		EDP	-	-	1.00	0.0
		TS	NP	5.5	1.03	0.6
b) Stimulants						
Name¹	Structure¹	CSP²	MP³	k₁⁴	α⁴	R_s⁴
Amphetamine		VS	PIM	1.0	1.17	1.7
		NS	-	-	1.00	0.0
		EDP	NP	2.0	1.12	1.6
		TS	-	-	1.00	0.0
Methamphetamine		VS	PIM	1.3	1.11	1.6
		NS	PIM	4.0	1.02	0.4
		EDP	NP	1.8	1.14	1.8
		TS	-	-	1.00	0.0
β-ketoamphetamine (cathinone)		VS	PIM	0.9	1.18	1.6
		NS	PIM	2.3	1.80	8.3
		EDP	PIM	0.4	1.12	0.6
		TS	NP	5.4	1.11	1.1
(1 RS; 2 SR)-Ephedrine		VS	POM	2.5	1.02	0.4
		NS	POM	6.2	1.13	2.0
		EDP	NP	1.9	1.01	0.2
		TS	POM	4.8	1.03	0.6
(1 RS; 2 RS)-Pseudoephedrine		VS	POM	2.5	1.08	1.4
		NS	POM	4.7	1.38	5.0
		EDP	NP	2.5	1.12	1.6
		TS	POM	5.4	1.09	1.4
Norephedrine		VS	NP	3.2	1.03	0.4
		NS	PIM	2.4	1.07	1.3
		EDP	NP	2.3	1.04	0.6
		TS	PIM	2	1.02	0.4

Epinephrine		VS	-	-	1.00	0.0
		NS	POM	1.7	1.06	1.0
		EDP	-	-	1.00	0.0
		TS	POM	8.7	1.04	0.5
Citalopram		VS	PIM	1.8	1.13	1.4
		NS	PIM	3.4	1.05	0.9
		EDP	NP	4.2	1.13	2.0
		TS	-	-	1.00	0.0
Fluoxetine		VS	PIM	1.2	1.26	2.5
		NS	POM	3.3	1.05	1.1
		EDP	RP	2.0	1.32	1.8
		TS	-	-	1.00	0.0
Methylphenidate		VS	PIM	0.9	1.48	3.3
		NS	POM	2.6	1.10	1.6
		EDP	PIM	0.4	1.36	1.7
		TS	PIM	2.5	1.12	1.7
Mianserin		VS	PIM	0.6	2.07	3.6
		NS	PIM	0.9	1.21	1.8
		EDP	PIM	0.4	1.38	1.6
		TS	PIM	1.7	1.09	1.0
Lorazepam		VS	RP	11.1	1.03	0.5
		NS	-	-	1.00	0.0
		EDP	PIM	0.3	1.10	0.6
		TS	PIM	0.4	3.60	6.3
Temazepam		VS	RP	7.4	1.12	1.0
		NS	RP	6.7	1.04	0.5
		EDP	PIM	0.3	1.13	0.6
		TS	NP	2.8	1.12	1.0
c) Pharmaceuticals						
Name¹	Structure¹	CSP²	MP³	k₁⁴	α⁴	R_s⁴
Carboxamine		VS	PIM	1.3	1.08	0.8
		NS	PIM	2.3	1.06	1.0
		EDP	NP	5.0	1.14	2.1
		TS	-	-	1.00	0.0
Propranolol		VS	POM	2.2	1.13	1.7
		NS	POM	5.3	1.59	5.0
		EDP	POM	1.2	1.07	0.6
		TS	POM	3.1	1.15	2.3
Phensuximide		VS	RP	1.3	1.11	1.4
		NS	RP	1.2	1.05	0.6
		EDP	NP	0.5	1.10	0.9
		TS	RP	1.3	1.16	1.9
Proglumide		VS	RP	4.1	2.10	3.5
		NS	RP	3.9	2.10	3.9
		EDP	PIM	0.4	1.16	0.7
		TS	RP	2.9	1.16	1.9
Hexobarbital		VS	RP	2.0	1.18	1.8
		NS	RP	1.6	1.11	1.4
		EDP	RP	2.5	1.14	1.2
		TS	RP	1.3	1.14	1.4

Warfarin		VS	RP	8.5	1.10	1.5
		NS	RP	9.5	1.04	1.4
		EDP	NP	0.8	1.05	0.5
		TS	RP	3.0	1.32	3.5
d) Amino acids and derivatives						
Name ¹	Structure ¹	CSP ²	MP ³	k ₁ ⁴	α ⁴	R _s ⁴
Phenylalanine		VS	NP	5.1	1.08	0.6
		NS	-	-	1.00	0.0
		EDP	PIM	0.5	1.20	0.8
		TS	RP	0.7	1.40	2.3
FMOC Phenylalanine		VS	RP	0.9	1.07	0.5
		NS	-	-	1.00	0.0
		EDP	PIM	1.0	1.27	1.7
		TS	PIM	0.2	2.33	2.5
4-nitrophenylalanine		VS	RP	0.6	1.11	1.0
		NS	RP	1.0	1.07	0.6
		EDP	RP	0.8	1.13	0.7
		TS	RP	1.3	1.19	1.4
Kynurenine		VS	RP	0.8	1.98	3.2
		NS	-	-	1.00	0.0
		EDP	RP	1.3	1.40	1.9
		TS	RP	1.0	3.67	8.5
DOPA		VS	-	-	1.00	0.0
		NS	-	-	1.00	0.0
		EDP	RP	0.4	1.50	1.7
		TS	RP	0.5	1.75	2.4
2-amino-2-phenylbutyric acid		VS	RP	0.3	1.14	0.7
		NS	POM	1.6	1.12	0.6
		EDP	PIM	0.5	1.57	2.7
		TS	RP	0.7	2.12	3.6
e) Non-steroidal anti-inflammatory drugs (NSAIDs)						
Name ¹	Structure ¹	CSP ²	MP ³	k ₁ ⁴	α ⁴	R _s ⁴
Benoxaprofen		VS	-	-	1.00	0.0
		NS	-	-	1.00	0.0
		EDP	PIM	0.9	1.35	2.0
		TS	-	-	1.00	0.0
Etodolac		VS	-	-	1.00	0.0
		NS	-	-	1.00	0.0
		EDP	PIM	0.7	1.17	1.1
		TS	RP	0.8	1.08	0.9
Flurbiprofen		VS	-	-	1.00	0.0
		NS	-	-	1.00	0.0
		EDP	PIM	0.9	1.37	2.1
		TS	RP	3.3	1.12	1.4
Ibuprofen		VS	-	-	1.00	0.0
		NS	-	-	1.00	0.0
		EDP	PIM	0.6	1.26	1.4
		TS	RP	3.2	1.15	1.4

Ketoprofen		VS	-	-	1.00	0.0
		NS	-	-	1.00	0.0
		EDP	PIM	0.9	1.31	1.8
		TS	RP	1.7	1.06	0.7
Ketorolac		VS	-	-	1.00	0.0
		NS	-	-	1.00	0.0
		EDP	PIM	1.1	1.10	0.9
		TS	PIM	0.4	2.40	3.5
Loxoprofen		VS	-	-	1.00	0.0
		NS	-	-	1.00	0.0
		EDP	PIM	0.5	1.17	1.5
		TS	RP	2.6	1.19	1.8
f) Pesticides						
Name¹	Structure¹	CSP²	MP³	k₁⁴	α⁴	R_s⁴
2-(4-chlorophenoxy)propionic acid		VS	-	-	1.00	0.0
		NS	NP	0.3	1.08	0.5
		EDP	PIM	0.9	1.36	2.1
		TS	PIM	0.1	3.64	3.5
2-phenylpropionic acid		VS	-	-	1.00	0.0
		NS	-	-	1.00	0.0
		EDP	PIM	0.8	1.18	1.2
		TS	RP	0.8	1.11	1.1
Bromacil		VS	RP	2.9	1.14	1.6
		NS	RP	2.7	1.04	0.6
		EDP	RP	1.7	1.05	0.6
		TS	RP	2.2	1.18	2.1
Dichlorprop		VS	-	-	1.00	0.0
		NS	-	-	1.00	0.0
		EDP	PIM	0.9	1.37	2.1
		TS	PIM	0.1	1.70	3.5
Haloxypop		VS	RP	9.6	1.05	0.7
		NS	-	-	1.00	0.0
		EDP	PIM	0.5	1.26	1.4
		TS	PIM	0.1	1.70	3.6
Mecoprop		VS	-	-	-	0.0
		NS	-	-	-	0.0
		EDP	PIM	0.7	1.36	2.1
		TS	PIM	0.1	1.70	2.9
Mecoprop methyl ester		VS	RP	6.6	1.10	1.4
		NS	RP	6.8	1.17	2.0
		EDP	-	-	-	0.0
		TS	-	-	-	0.0
g) Nicotine and metabolites						
Name¹	Structure¹	CSP²	MP³	k₁⁴	α⁴	R_s⁴
Nicotine		VS	NP	15.1	1.06	0.6
		NS	PIM	0.8	1.81	3.5
		EDP	NP	4.0	1.05	0.6
		TS	PIM	1.6	1.04	0.4

Nornicotine		VS	PIM	2.6	1.08	1.1
		NS	PIM	10.7	1.19	3.1
		EDP	-	-	1.00	0.0
		TS	-	-	1.00	0.0
Cotinine		VS	PIM	0.3	1.11	0.6
		NS	-	-	1.00	0.0
		EDP	NP	2.4	1.02	0.3
		TS	PIM	0.8	1.12	1.1
5-(3-pyridyl)tetrahydrofuran-2-one		VS	NP	12.2	1.13	1.4
		NS	NP	7.1	1.14	1.5
		EDP	NP	3.0	1.01	0.2
		TS	RP	3.4	1.10	1.6
Rac-(*,*)-4-trans-cotinine carboxylic acid		VS	PIM	1.0	1.12	0.9
		NS	NP	5.9	1.33	1.8
		EDP	PIM	1.3	1.39	2.1
		TS	RP	1.0	1.2	1.4
h) Oxazolidinone						
Name¹	Structure¹	CSP²	MP³	k₁⁴	α⁴	R_s⁴
4-phenyl-2-oxazolidinone		VS	NP	2.3	1.26	2.5
		NS	-	-	1.00	0.0
		EDP	NP	1.1	1.12	1.4
		TS	RP	3.2	1.79	4.2

¹See Materials and methods for sample information.

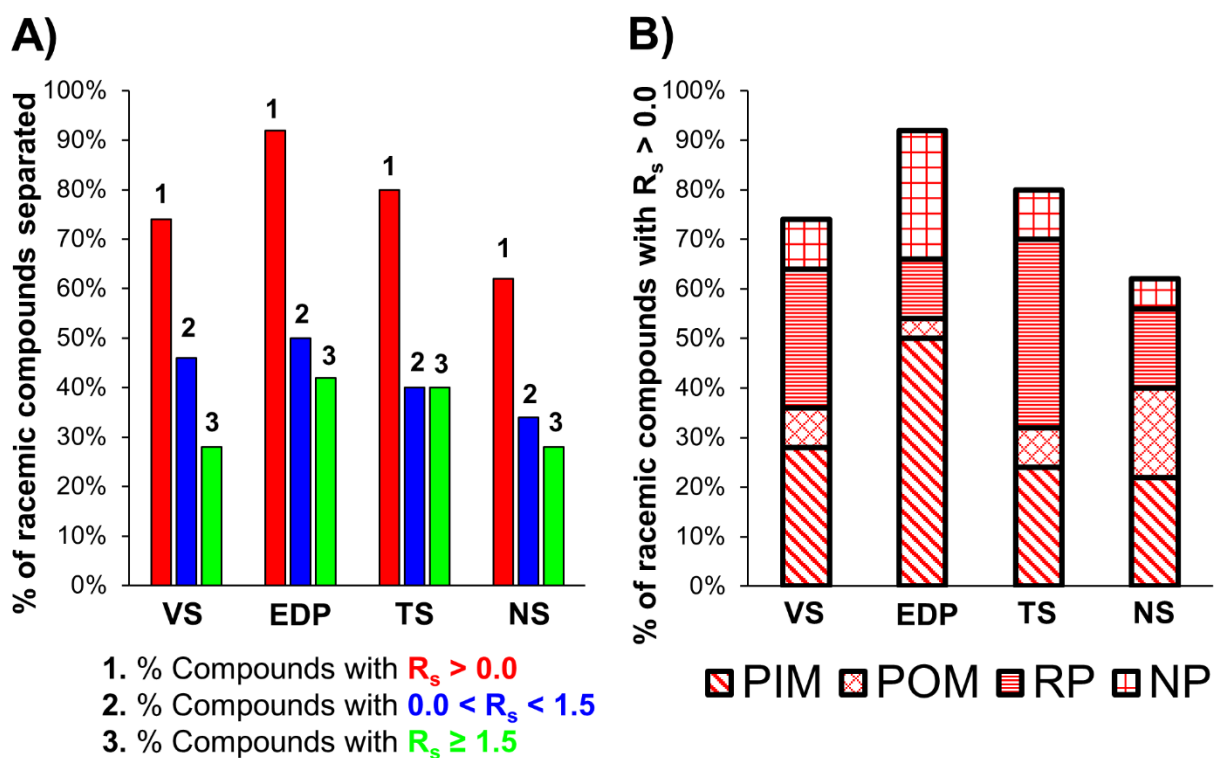
²Core-shell chiral stationary phases (CSPs) were all 100 x 4.6 mm (i.d.); VancoShell (VS), NicoShell (NS), Vancomycin edman degradation product (EDP), and TeicoShell (TS). See Materials and methods for more information.

³See Materials and methods for mobile phase (MP) conditions: polar ionic mode (PIM), polar organic mode (POM), reversed phase (RP), and normal phase (NP).

⁴See Materials and methods for chromatographic calculations of retention factor of the first peak (k_1), selectivity (α), and resolution (R_s).

Overall, the screening procedure resulted in 40 racemic compounds (80%) baseline separated ($R_s \geq 1.5$) (Table 1). Several had $R_s \geq 1.5$ with more than one CSP; one compound (methylphenidate) separated on all four CSPs, five compounds on three of the CSPs, 17 compounds with two CSPs, and 17 compounds with only one CSP (Table 1). Of the remaining 10 compounds, all had a partial separation ($R_s > 0.0$) with at least one CSP (Table 1). The data from Table 1 is illustrated in Fig. 2A. Fig. 2A depicts the number of separations in terms of $R_s > 0.0$ (bar 1, red), $0.0 > R_s > 1.5$ (bar 2, blue), and $R_s \geq 1.5$ (bar 3, green) for each CSP. Each macrocyclic glycopeptide-based core-shell CSP was able to separate ($R_s > 0.0$) at least 60% of the 50 chiral compounds (Fig. 2A). EDP had the highest efficacy of the 4 CSPs, separating 46 out of 50 (92%) of the set ($R_s > 0.0$) with only 4 chiral compounds with $R_s = 0.0$; the 3 basic amines: trimethylbenzylamine, epinephrine, and nornicotine as well as the non-ionizable methyl ester of mecoprop (Fig. 2A, Table 1). In

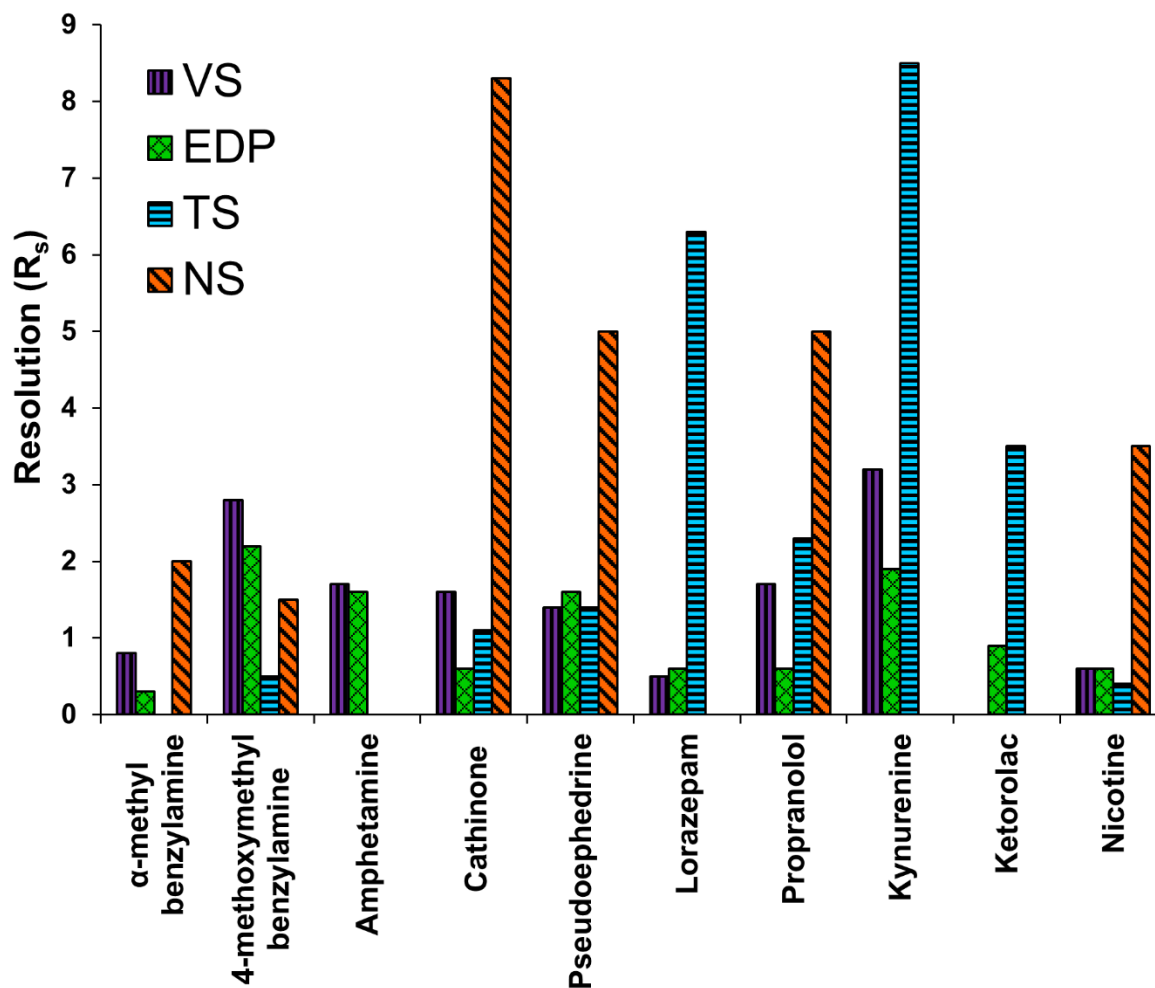
Fig. 2B, the number of separations with $R_s > 0.0$ (bar 1, red) were distinguished by which chromatographic mode was utilized. PIM was the most successful chromatographic mode, utilized overall to perform 40% the best separations and for each respective CSP: EDP, TeicoShell, VancoShell, and NicoShell, 54%, 30%, 38%, and 35% (Table 1, Fig. 2B). RP was the next most efficient mode, utilized for 31% of the best separations, dominantly for VancoShell and TeicoShell, 38% and 48%. RP was less useful for NicoShell and EDP, 26% and 13%, respectively (Table 1, Fig. 2B). NP and POM were less utilized as the best mobile phases, only used for 17% and 12% of all the best separations obtained by the 4 CSPs (Table 1, Fig. 2B).



Chapter 3 Figure 2. Percentage of racemic compounds separated by each macrocyclic glycopeptide-based chiral stationary phase (CSP): VancoShell (VS), Vancomycin edman degradation product (EDP), TeicoShell (TS), and NicoShell (NS). **(A)** The highest resolution (R_s) for all 50 compounds obtained during screening (from Table 1) by each CSP is indicated by each bar. Bar 1 (red) represents the number of racemic compounds with $R_s > 0.0$, while bar 2 (blue) indicates the number of racemic compounds with $0.0 < R_s < 1.5$, and bar 3 (green) shows the number of baseline separations obtained ($R_s \geq 1.5$). **(B)** Bar 1 ($R_s > 0.0$ during screening from Table 1) from Fig. 2A for each CSP is distinguished into the chromatographic modes utilized. From the bottom to the top of each bar, it is divided into polar ionic mode (diagonal lines), polar organic mode (crisscross), reversed phase (horizontal lines), and normal phase (grid), respectively. See Materials and methods for chromatographic parameters and information.

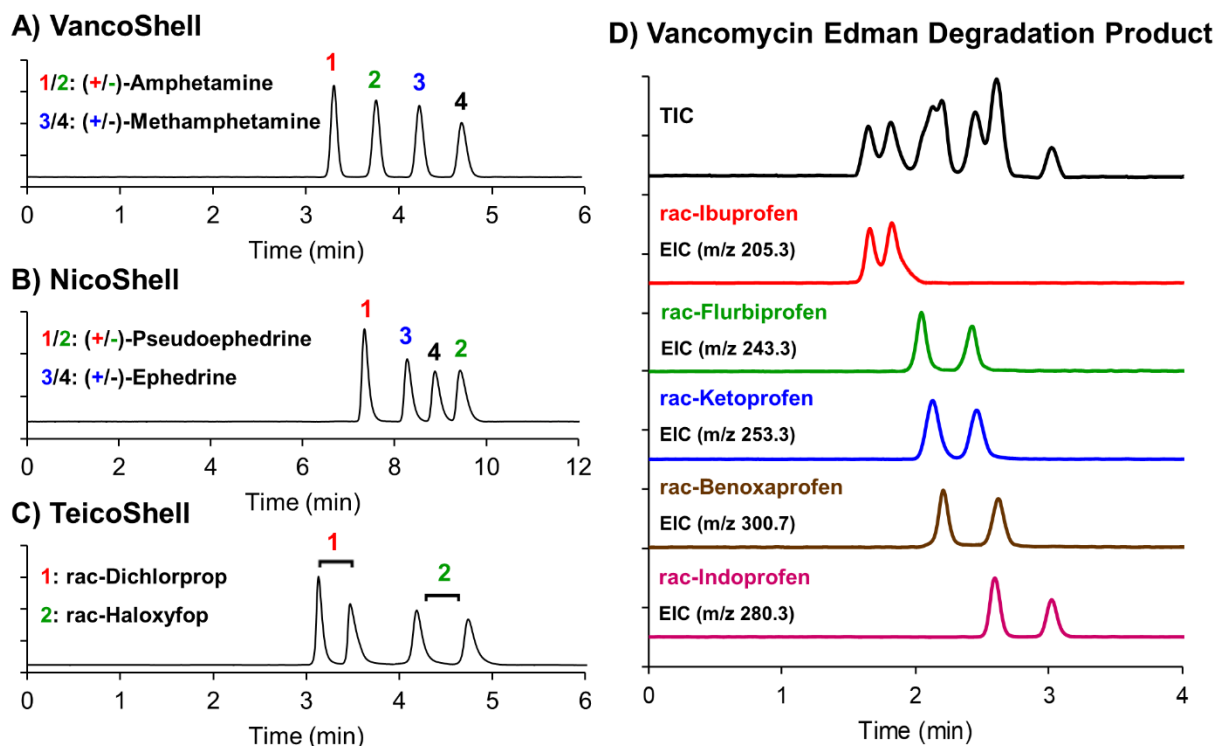
3.4.2 Complementary behavior and best applications

As expected, VancoShell and NicoShell were highly effective for separating basic amines, while TeicoShell was more effective for separating acidic compounds, which highlights their complementary behavior. EDP was most like the teicoplanin chiral selector as it separated most chiral acids, like the amino acids, herbicides, non-steroidal anti-inflammatory drugs, etc. (Table 1). To illustrate this, Fig. 3 compares the R_s obtained from a selection of 10 chiral compounds between each CSP. EDP was able to differentiate all 10 compounds, exhibiting the broadest spectrum of the 4 CSPs.



Chapter 3 Figure 3. Comparison of resolution obtained for macrocyclic glycopeptide-based selectors: VancoShell (VS, purple and vertical lines), the vancomycin edman degradation product (EDP, green and crisscross), TeicoShell (TS, light blue and horizontal lines), and NicoShell (NS, orange and diagonal lines) to emphasize the broad-spectrum recognition of VS and EDP compared to the high chiral selectivity obtained from TS and NS for 10 selected chiral compounds (full data in Table 1). See Materials and methods for chromatographic parameters and information.

However, the most effective selector was not EDP for each of the 10 compounds. TeicoShell was more selective than EDP and had the highest R_s for 19 of the 50 compounds (Table 1). As shown in Fig. 3, the R_s was 3-10 times higher for TeicoShell compared to the other CSPs for the neutral lorazepam, and the two acids, kyurenine and ketorolac. Clearly, the acidic enantiomers are most easily recognized by TeicoShell. Similarly, when examining the results of VancoShell, it was clearly the most applicable CSP for basic enantiomers. However, certain compounds were more selective to NicoShell and EDP. For example, EDP was the only CSP to separate the non-steroidal anti-inflammatory benoxaprofen (Table 1). Also, NicoShell was by far the best CSP for cathinone, pseudoephedrine, propranolol, and nicotine with R_s factors 3-10 higher than the other CSPs (Fig. 3). Overall, the screening procedure showed that 19, 13, 10, and 8 compounds were best separated by TeicoShell, NicoShell, EDP, and VancoShell, respectively (Table 1). Specific applications of these CSPs based on their complementary behavior are shown in Fig. 4.



Chapter 3 Figure 4 Highlighted applications of core-shell macrocyclic glycopeptide-based chiral stationary phases. **A)** Separation of rac-Amphetamine and rac-Methamphetamine using VancoShell (100 x 4.6 mm (i.d.)) with MeOH-AA-TEA (100:0.2:0.1, v/v/v) at 0.5 mL/min, 25 °C, UV 254 nm. [1]: (+)-

Amphetamine, [2]: (-)-Amphetamine, [3]: (+)-Methamphetamine, [4]: (-)-Methamphetamine. **B)** Separation of rac-Pseudoephedrine and rac-Ephedrine using NicoShell (100 x 4.6 mm (i.d.)) with MeOH-AA-NH₄OH (100:0.2:0.05, v/v/v) at 0.5 mL/min, 25 °C, UV 220 nm. [1]: (+)-Pseudoephedrine, [2]: (-)-Pseudoephedrine, [3]: (+)-Ephedrine, [4]: (-)-Ephedrine. **C)** Separation of rac-Dichlorprop and rac-Haloxypof using TeicoShell (100 x 4.6 mm (i.d.)) with MeOH-NH₄Formate (pH 3.6; 16 mM) (30:70, v/v) at 0.8 mL/min, 45 °C, UV 230 nm. **D)** Simultaneous LC-MS separation of rac-Ibuprofen (red), rac-Flurbiprofen (green), rac-Ketoprofen (blue), rac-Benoxaprofen (brown), and rac-Indoprofen (pink) using the vancomycin edman degradation product (100 x 4.6 mm (i.d.)) with MeOH-NH₄Formate (100:0.1, v/w) at 1.0 mL/min, 25 °C, UV 230 nm. The total ion chromatogram (TIC) is shown in black, and each profen is shown according to their m/z in the extracted ion chromatograms (EICs). See Materials and methods for more information.

The simultaneous separations of rac-amphetamine and rac-methamphetamine in 5 min, rac-pseudoephedrine and rac-ephedrine in 10 min, and rac-dichlorprop and rac-haloxypof in 5 min, are shown using VancoShell, NicoShell, and TeicoShell, respectively (Fig. 4A, 4B, 4C). EDP was the most effective CSP for the separation of racemic profens (non-steroidal anti-inflammatory drugs) with fast analysis times using PIM, which is shown in Fig. 4D. The simultaneous LC-MS separation of 5 profens was performed within ~3 minutes, which is shown in the total ion chromatogram (TIC), then each profen's m/z extracted in the subsequent extracted ion chromatograms (EICs) (Fig. 4D). This instrument was not optimized for its extra column band broadening, explaining the lower efficiency observed compared to the screening results, such as for rac-ibuprofen.

3.5 Conclusions

The screening procedure used to evaluate the new vancomycin edman degradation product as a chiral selector demonstrated its ability to discriminate the enantiomers of 46 chiral compounds out of a set of 50. The other recent modified macrocyclic glycopeptide-based core-shell CSP, NicoShell, was shown to separate some non-ionizable and acidic compounds, but was most useful for amines, like beta blockers and stimulants. These modified macrocyclic glycopeptides provide examples of complementary behavior with their native analogs, indicating the value and need for investigation of new macrocyclic glycopeptide chiral selectors.

3.6 References

1. Armstrong DW, Tang Y, Chen S, Zhou Y, Bagwill C, Chen JR. Macrocyclic antibiotics as a new class of chiral selectors for liquid chromatography. *Anal Chem* **1994**; 66:1473-1484.
2. Boehm RE, Martire DE, Armstrong DW. Theoretical considerations concerning the separation of enantiomeric solutes by liquid chromatography. *Anal Chem* **1988**; 60:522-528.
3. Beesley TE. Description and evaluation of chiral interactive sites on bonded chiral stationary phases for liquid chromatography. In: Berthod A, editor. *Chiral recognition in separation methods*, Heidelberg, Germany: Springer; **2010**, p 53-76.
4. Xiao TL, Rozhtov RV, Larock RC, Armstrong DW. Separation of the enantiomers of substituted dihydrofurocoumarins by HPLC using macrocyclic glycopeptides CSPs. *Anal Bioanal Chem* **2003**; 377:639-654.
5. Gasper MP, Berthod A, Nair UB, Armstrong DW. Comparison and modeling study of vancomycin, ristocetin A, and teicoplanin for CE enantioseparations. *Anal Chem* **1996**; 68:2501-2514.
6. Berthod A, Qiu HX, Staroverov SM, Kuznestov MA, Armstrong DW. Chiral recognition with macrocyclic glycopeptides: mechanisms and applications. In: Berthod A, editor. *Chiral recognition in separation methods*, Heidelberg, Germany: Springer; **2010**, p 203-222.
7. Ekborg-Ott KH, Kullman JP, Wang X, Gahm K, He L, Armstrong DW. Evaluation of the macrocyclic antibiotic avoparcin as a new chiral selector for HPLC. *Chirality* **1998**; 10:627-660.
8. Peter A, Vèkes E, Armstrong DW. Effects of temperature on retention of chiral compounds on a ristocetin A chiral stationary phase. *J Chrom A* **2002**; 958:89-107.
9. Chen S, Liu Y, Armstrong DW, Borell JI, Martinez-Terpel B, Matallama JL. Enantioresolution of substituted 2-methoxy-6-oxo-tetrahydropyridine-3-carbonitriles on macrocyclic antibiotic and cyclodextrin stationary phases. *J Liq Chromatog Rel Technol* **1995**; 18:1495-1507.
10. Karlsson C, Karlsson, L, Armstrong DW, Owens PK. Evaluation of a vancomycin chiral stationary phase in capillary electrochromatography using polar organic and reversed-phase modes. *Anal Chem* **2000**; 72:4394-4401.
11. Rundlett KL, Gasper MP, Zhou EY, Armstrong DW. Capillary electrophoretic enantiomeric separations using the glycopeptide antibiotic, teicoplanin. *Chirality* **1996**; 8:88-107.
12. Maier V, Ranc V, Švidnoch M, Petr J, Ševčík J, Tesařová E, Armstrong DW. Study on the use of boromycin as a chiral selector in capillary electrophoresis. *J Chromatogr A* **2012**; 1237:128-132.
13. Berthod A, Yu T, Kullman JP, Armstrong DW. Evaluation of the macrocyclic glycopeptide A-40,926 as a high-performance liquid chromatographic chiral selector and comparison with teicoplanin chiral stationary phase. *J Chromatogr A* **2000**; 897:113-129.
14. Berthod A, Nair UB, Bagwill C, Armstrong DW. Derivatized vancomycin stationary phases for LC chiral separations. *Talanta* **1996**; 43:1767-1782.
15. Xiao TL, Tesarova E, Anderson JL, Egger M, Armstrong DW. Evaluation and comparison of a methylated teicoplanin aglycone to teicoplanin aglycone and natural teicoplanin chiral stationary phases. *J Sep Sci* **2006**; 29:429-445.
16. Zhang X, Bao Y, Huang K, Barnett-Rundlett K, Armstrong DW. Evaluation of dalbavancin as chiral selector for HPLC and comparison with teicoplanin-based chiral stationary phases. *Chirality* **2010**; 22:495-513.
17. Armstrong DW, Liu Y, Ekborg-Ott KH. A covalently bonded teicoplanin chiral stationary phase for HPLC enantioseparations. *Chirality* **1995**; 7:474-497.
18. Dolzan MD, Shu Y, Smuts JP, Petersen H, Ellegaard P, Micke GA, Armstrong DW, Breitbach ZS. Enantiomeric separation of citalopram analogues by HPLC using macrocyclic glycopeptide and cyclodextrin based chiral stationary phases. *J Liq Chromatog Rel Technol* **2016**; 39:154-160.
19. Liu Y, Berthod A., Mitchell CR, Xiao TL, Zhang B, Armstrong DW. Super/subcritical fluid chromatography chiral separations with macrocyclic glycopeptide stationary phases. *J Chromatogr A* **2002**; 978:185-204.
20. Beesley TE, Lee JT. Method development strategy and applications update for CHIROBIOTIC chiral stationary phases. *J Liq Chromatog Rel Technol* **2009**; 32:1733-1767.

21. Hellinghausen G, Lee JT, Weatherly CA, Lopez DA, Armstrong DW. Evaluation of nicotine in tobacco-free-nicotine commercial products. *Drug Test Anal* **2017**; 9:944-948.
22. Hellinghausen G, Roy D, Wang Y, Lee JT, Lopez DA, Weatherly CA, Armstrong DW. A comprehensive methodology for the chiral separation of 40 tobacco alkaloids and their carcinogenic E/Z-(R,S)-tobacco specific nitrosamine metabolites. *Talanta* **2018**; 181:132-141.
23. Hellinghausen G, Roy D, Lee JT, Wang Y, Weatherly CA, Lopez DA, Nguyen KA, Armstrong JD, Armstrong DW. Effective methodologies for enantiomeric separations of 150 pharmacology and toxicology related 1°, 2°, and 3° amines with core-shell chiral stationary phases. *J Pharm Biomed Anal* **2018**; 155:70-81.
24. Barhate CL, Breitbach ZS, Costa Pinto E, Regalado EL, Welch CJ, Armstrong DW. Ultrafast separation of fluorinated and desfluorinated pharmaceuticals using chiral selectors bonded to superficially porous particles. *J Chromatogr A* **2015**; 1426:241-247.
25. Barhate CL, Wahab MF, Breitbach ZS, Bell DS, Armstrong DW. High efficiency, narrow particle size distribution, sub-2 µm based macrocyclic glycopeptide chiral stationary phases in HPLC and SFC. *Anal Chim Acta* **2015**; 898:128-137.
26. Patel DC, Breitbach ZS, Wahab MF, Barhate CL, Armstrong DW. Gone in seconds: praxis, performance, and peculiarities of ultrafast chiral liquid chromatography with superficially porous particles. *Anal Chem* **2015**; 87:9137-9148.
27. Patel DC, Wahab MF, Armstrong DW, Breitbach ZS. Advances in high-throughput and high-efficiency chiral liquid chromatographic separations. *J Chromatogr A* **2016**; 1467:2-18.
28. Barhate CL, Joyce LA, Makarov AA, Zawatzky K, Bernardoni F, Schafer WA, Armstrong DW, Welch CJ, Regalado EL. Ultrafast chiral separations for high throughput enantiopurity analysis. *Chem Commun* **2016**; 53:509-512.
29. Spudeit DA, Dolzan MD, Breitbach ZS, Barber WE, Micke GA, Armstrong DW. Superficially porous particles vs. fully porous particles for bonded high performance liquid chromatographic chiral stationary phases: Isopropyl cyclofructan 6. *J Chromatogr A* **2014**; 1363:89-95.
30. Ghassempour A, Aboul-Enein HY. Vancomycin degradation products as potential chiral selectors in enantiomeric separation of racemic compounds. *J Chromatogr A* **2008**; 1191:182-187.
31. Ghassempour A, Abdollahpour A, Tabar-Heydar K, Nabid MR, Mansouri S, Aboul-Enein HY. Crystalline degradation products of vancomycin as a new chiral stationary for liquid chromatography. *Chromatographia* **2005**; 61:151-155.
32. Mojtahedi MM, Chalavi S, Ghassempour A, Tabar-Heydar K, Sharif SJG, Malekzadeh M, Aboul-Enein HY. Chiral separation of three agrochemical toxins enantiomers by high-performance liquid chromatography on a vancomycin crystalline degradation products-chiral stationary phase. *Biomed Chromatogr* **2007**; 21:234-240.
34. Booth PM, Stone DJM, Williams DH. The Edman degradation of vancomycin: Preparation of vancomycin hexapeptide. *J Chem Soc. Chem Commun* **1987**; 709:1694-1695.

Chapter 4

Evaluation of Nicotine in Tobacco Free Nicotine Commercial Products: Nicotine Enantiomers in Tobacco Free Nicotine

4.1 Abstract

Recently, a variety of new tobacco free nicotine, TFN, products were commercialized as e-liquids. Tobacco derived nicotine contains predominantly (S)-(-)-nicotine, whereas TFN products may not. The TFN products are said to be cleaner, purer substances, devoid of toxic components that come from the tobacco extraction process. A variety of commercial tobacco and TFN products were analyzed to identify the presence and composition of each nicotine enantiomer. A rapid and effective enantiomeric separation of nicotine has been developed using a modified macrocyclic glycopeptide bonded to superficially porous particles. The enantiomeric assay can be completed in < 2 minutes with high resolution and accuracy using high performance liquid chromatography with electrospray ionization mass spectrometry. The results of this study suggest the need for pharmacological studies of (R)-(+)-nicotine, which is present in much greater quantities in commercial TFN products compared to commercial tobacco-derived products. Such studies are required by the FDA for new enantiomeric pharmacological products.

4.2 Introduction

Nicotine has been extensively studied due to its presence in tobacco products. Nicotine makes up about 95% of all the alkaloids in tobacco, while minor alkaloids, such as nornicotine, anatabine, and anabasine individually make up about 0.3 to 3% of the alkaloids in tobacco.^[1] Nicotine is chiral and the tobacco plant produces predominantly the (S)-(-) enantiomer. This characteristic of nicotine is not surprising as enantioselectivity is a common trait for biological systems.^[2] The percent (R)-(+)-nicotine in tobacco, and medicinal products derived from tobacco was reported to be in the 0.1 to 1.2% range.^[1] Therefore, tobacco derived nicotine, TDN, mainly consists of (S)-(-)-nicotine. The LD₅₀ for (R)-(+)-nicotine was reported as 2.75 mg/kg, while (S)-(-)-nicotine was measured at 0.38 mg/kg.^[3] Armstrong and coworkers

reported that (R)-(+)-nicotine produced different levels of oxidative stress than (S)-(-)-nicotine.^[4] Pogoeki et al. reviewed studies done on the effects and potency of (R)-(+)-nicotine versus S(-)-nicotine, concluding that (R)-(+)-nicotine had potential as a therapeutic target for neurodegenerative disease and tobacco smoking addiction.^[5] Therefore, both enantiomers could be therapeutic agents for smoking cessation.^[5] During nicotine metabolism nicotine enantiomers reorient their structure forming carcinogenic metabolites.^[6] Jones et al. measured the rate of metabolism of both nicotine enantiomers in cytochrome P450cam. The metabolic rate was found to be 1.4 times faster for (R)-(+)-nicotine than (S)-(-)-nicotine.^[6] Zhang et al. indicated that (R)-(+)-nicotine did not affect body weight in rats, as did (S)-(-)-nicotine, which caused a loss of body weight.^[7] Ikushima et al. investigated the sympathomimetic effects of each nicotine enantiomer, discovering (R)-(+)-nicotine did not release norepinephrine as did (S)-(-)-nicotine.^[8] Because of the different binding mechanisms of the nicotine enantiomers to nicotinic acetylcholine receptors, it has been suggested that there is a need to further investigate the desensitization of these receptors, specifically in the dopaminergic system.^[5,8] However, (R)-(+)-nicotine is not absent of risk, being similar to (S)-(-)-nicotine in that it might increase the risk of cardiovascular diseases due to its inhibitory effect on thromboxane.^[9]

Clearly the effects of (R)-(+)-nicotine differ from the dominant (S)-(-) enantiomer and have not been adequately studied. The pharmacology of (R)-(+)-nicotine has not been extensively studied due the lack of an effective purification procedure for the (R)-(+)-antipode, which is time extensive and not sufficient to collect enough (R)-(+)-nicotine for an extensive pharmacology study. Also there is no effective asymmetric synthesis for this enantiomer.^[5] This has not been an area of great concern, most likely because human exposure and intake of (R)-(+)-nicotine is minimal. (S)-(-)-nicotine is commonly found in commercial tobacco-derived products, including nicotine gum, lozenges, and the transdermal patches that are used as nicotine therapy replacements to reduce the withdrawal symptoms of smoking cessation.^[10] Also, vaporizing “e-liquids” may be used as a nicotine therapy replacement, which also mimics the act of smoking.^[10]

Tobacco free nicotine, TFN, which is trademarked by Pharmanic, is synthesized by Next Generations Labs, and commercialized in electronic cigarette liquid products (commonly called e-liquids) by several companies.^[11] It is uncertain if TFN will be subjected to the Tobacco Control Act, which is regulated by the Food and Drug Administration, FDA.^[12] This is due to the fact that TFN is not derived from the tobacco plant.^[11] The Tobacco Control Act (August 8, 2016) warrants FDA regulation over commercial affiliated tobacco products such as e-cigarettes, and e-liquids.^[12] After this date the FDA will not allow affiliated tobacco-derived products to be commercialized without regulation.^[12] Currently it is not clear whether TFN products will be considered affiliated tobacco products since totally synthetic nicotine is not derived from tobacco and had not been commercialized until recently.

TFN is the first synthetic nicotine process that is considered economically feasible compared to the readily available tobacco extraction processes for TDN products.^[11] A stated feature of TFN products is the lack of “impurities” associated with the tobacco extraction processes of TDN products.^[11] The total nicotine content in the commercial TFN e-liquids ranges from 0 to 6 mg per 30 mL.^[13] TFN products are not predominantly (S)-(-)-nicotine and may contain substantial amounts of the (R)-(+)-enantiomer, which is not indicated by the container label. TFN products may be subject to an earlier FDA policy statement that was established for the development of new stereoisomeric drugs.^[14] Because of the possibility of different physiological effects, the FDA stated: ...“the pharmacology and toxicology of the enantiomer should be characterized for the principal pharmacological effect and any other important pharmacological effect, with respect to potency, specificity, maximum effect, etc.”.^[14] Currently it is unclear if the FDA will or can regulate TFN products.

The enantiomeric separation of nicotine has been reported, but not with an effective method.^[15,16,17] Early methods have long retention times and are not mass spectrometry compatible.^[15,16,17] To perform a more rapid and effective enantiomeric separation of nicotine a synthetically modified macrocyclic glycopeptide was bonded to superficially porous particles.^[18] Nicotine enantiomers were separated in approximately

two minutes using solvent systems that are compatible with electrospray ionization mass spectrometry, which is beneficial for the sensitive identification of nicotine.

4.3 Experimental

4.3.1 Materials

A modified macrocyclic glycopeptide chiral stationary phase was bonded to superficially porous particles (100 x 4.6 mm i.d.), which were produced by AZYP, LLC. (Arlington, TX, USA).^[18] Analytic standards were purchased as racemates from Cerilliant Corporation (Round Rock, TX, USA) and Sigma-Aldrich (St. Louis, MO, USA). TFN e-liquids were selected from different manufacturers to evaluate a variety of TFN products. TFN e-liquids were labeled similarly with 0.6% by volume nicotine (6 mg/mL in 30 mL bottle), $\leq 75\%$ vegetable glycerin, $\leq 25\%$ propylene glycol, and $\leq 10\%$ natural and artificial flavors. The 4 TFN e-liquid products used in this study were NKTR Guava and Melt by SQN (Cerritos, CA, USA), Coastline Stinson by Spotlight Vapors, LLC (Camarillo, CA, USA), and Peel Apple by CRFT INC (Irvine, CA, USA). A variety of tobacco derived nicotine products were selected for this study to highlight the differences between TFN and TDN products. A tobacco-derived-nicotine e-liquid included in this study was 24 mg/mL nicotine vanilla french e-liquid (Smokefree Vapor, Oklahoma, OK, USA). Four other TDN products used in this study were 4 mg/piece nicotine gum (Walgreen Co., Deerfield, IL, USA), 21 mg nicotine/day NicoDerm transdermal nicotine patch (GlaxoSmithKline Consumer Healthcare, L.P., Zebulon, NC, USA), 4 mg/piece nicotine lozenges (CVS Pharmacy Inc., Woonsocket, RI, USA), and 1.5 mg nicotine/piece dissolvable smokeless tobacco tablets. (Rock Creek Pharmaceuticals Inc., Sarasota, FL, USA). High performance liquid chromatography grade methanol was obtained from Sigma-Aldrich (St. Louis, MO, USA) as well as triethylamine, and ammonium trifluoroacetate. Water was purified by a Milli-Q water purification system (Millipore, Billerica, MA, USA). DSC-18 solid phase extraction tubes with 10 grams C18 were obtained for the extraction of solid TDN products (SUPELCO, Bellefonte, PA, USA).

4.3.2 Sample preparation

TFN and TDN e-liquids were diluted, filtered and injected directly into the HPLC. They were quantitated using liquid chromatography with ultraviolet detection (LC-UV) by comparing their peak areas to the racemic nicotine standard. The solid TDN products, which included the gum, lozenge, patch and smokeless tobacco tablet, were crushed and or placed in 50 mL of Milli-Q water containing 0.1% (v/v) triethylamine. Solid phase extraction was used with DSC-18 cartridges, which were conditioned with methanol then water. Cartridges were flushed with 25 mL of methanol and then sonicated for 2 hours, and the methanol was evaporated at 35° C under gentle air. The remaining sample was diluted in methanol and then filtered for LC-UV analysis. To ensure that the level of racemization was insignificant during the extraction procedure, a standard of (S)-(-)-nicotine was subjected to the extraction procedure then compared to a neat standard with LC-UV (see Table 1).

4.3.3 Chromatographic conditions

An Agilent 1200 high performance liquid chromatography instrument (Agilent Technologies, Palo Alto, CA, USA) was used in this study. It consisted of a 1200 diode array detector, autosampler, and quaternary pump. A Jasco CD-2095 (JASCO, Easton, MD, USA) circular dichroism chiral detector was also utilized with manual injection through a Rheodyne Model 7225 injector and a Shimadzu LC-6A pump. Extra column band broadening was not optimized for the Jasco CD-2095, which resulted in slightly longer retention times. A Shimadzu LCMS-8040 (Shimadzu Scientific Instruments, Inc., Columbia, MD) that had a triple quadrupole was used with electrospray ionization. All separations were carried out at room temperature using an isocratic method. The mobile phase used was 100/0.1 wt%: methanol/ammonium trifluoroacetate with a flow rate of 1 mL/min. The mobile phase was degassed by ultrasonication under vacuum for 5 minutes. The UV wavelength 263 nm was employed for detection. All analytes were dissolved in methanol. All the TFN e-liquids, tobacco-nicotine e-liquid and TDN products were compared to the pure racemic nicotine standard using CD and MS-MS with the LCMS-8040 at a m/z of 163.00 (see Figure 3 and Supplemental Figure 1S). A m/z of 163.00 was chosen for selective ion monitoring of

nicotine because this is the molecular weight of protonated nicotine. Also, to distinguish nicotine from the complex matrices of the samples, multiple reaction monitoring was utilized to monitor major fragments at 117.00 and 129.95 m/z (see Figure 2S in Supplemental).

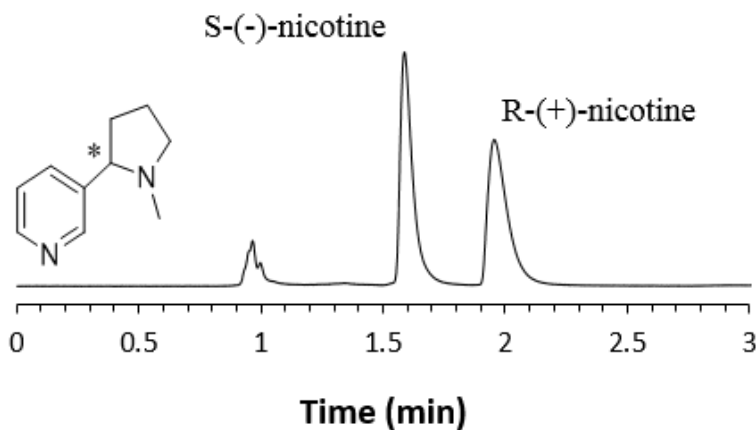
The dead time, t_0 , was determined by the peak of the refractive index change due to the unretained sample solvent. Retention factors (k) were calculated using $k = (t_r - t_0)/t_0$, where t_r is the retention time of the first peak and t_0 the dead time of the column. Selectivity was calculated using $\alpha = k_2/k_1$, where k_2 and k_1 are retention factors of the first and second peaks, respectively. Resolution was calculated using the peak width at half peak height, $R_s = (t_{R2} - t_{R1})/(0.5*(w_{0.5,1} + w_{0.5,2}))$. Each sample was analyzed in triplicate. Peak areas were determined both instrumentally (Chem Station) and manually (expand chromatograph, cut and weigh). Both approaches produced identical results within experimental error. The enantiomeric ratio was then determined by dividing the peak area of each enantiomer by the total peak area of both enantiomers (see Table 1). The nicotine content was determined by comparing the average peak area of each sample to the nicotine standard (see Table 1). The confidence limit using a confidence level of 95% was determined to be within ± 0.05 mg for the nicotine content for all samples. The relative standard deviation (%RSD) was determined to be within $\pm 0.2\%$ for the enantiomeric ratios for all samples.

A calibration curve was established using the nicotine standard to determine the LOD and LOQ of each nicotine enantiomer. A series of 5 μ L injections of the nicotine standard at enantiomeric concentrations of 0.15, 0.75, 1.25, 2, 3.25 and 6.5 ng/mL were performed in triplicate. The average integrated peak area of each enantiomer was plotted against the enantiomeric concentration. The LOD was calculated using $LOD = 3.3(S_y/S)$ and the LOQ was calculated using $LOQ = 10(S_y/S)$, where S_y is the standard deviation of the intensity response, and S is the slope of the calibration plot. Nicotine was found to have a LOD of 0.7 ng/mL and LOQ of 2.2 ng/mL (see Fig. 3S in Supplemental). The sensitivity of this analysis compares well to the reported LOD and LOQ of below 3 ng/mL and from 0.4 to 8.5 ng/mL.^[19]

4.4 Results and discussion

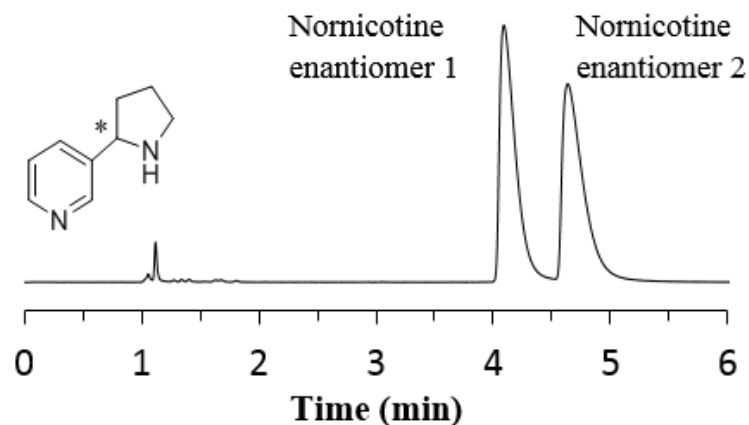
There are few reports on the analysis of nicotine in personal vaporizers or e-cigarettes. In one case the total nicotine was measured and found to vary widely from the labeled amounts.^[20] However the enantiomeric composition of this nicotine was not considered. Apparently, the enantiomeric content of nicotine has been determined only in tobacco derived products including smokeless tobacco and medicinal products.^[1]

A rapid enantiomeric separation of nicotine in under two minutes with a resolution (R_s) of 3.0 was achieved and utilized to determine the presence and composition of nicotine in TFN and TDN products (see Fig.1).



Chapter 4 Figure 1 Optimized enantiomeric separation of nicotine standard. See Experimental for method parameters. Results: $k_1 = 0.586$, $\alpha = 1.63$, $R_s = 3.0$.

The racemic nicotine analogue, nor nicotine, also was baseline separated indicating that this method might be useful for further analysis of other nicotine analogues (see Fig.2).^[21]



Chapter 4 Figure 2. Enantiomeric separation of nornicotine standard. See Experimental for method parameters. Results: $k_1 = 3.090$, $\alpha = 1.18$, $R_s = 1.8$.

Another advantage of this method was that it is electrospray ionization mass spectrometry compatible.

The enantioseparation of (S)-(-)-nicotine and (R)-(+)-nicotine was confirmed utilizing circular dichroism (CD) and mass spectrometry (see Fig. 3 and Figures 1S and 2S in Supplemental).^[22]

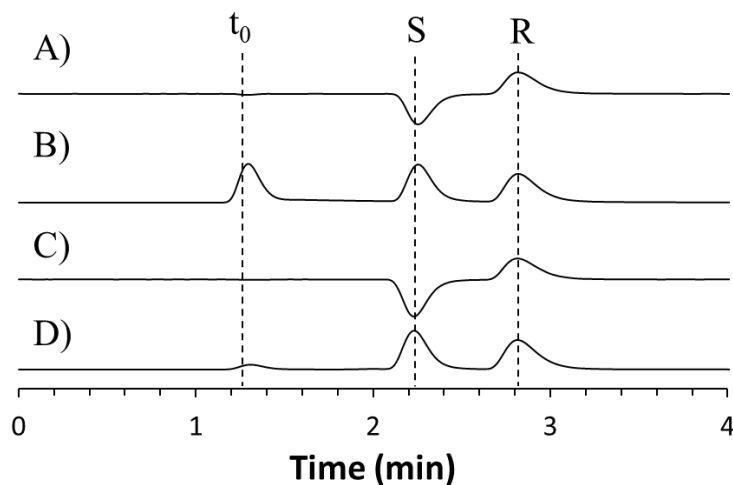


Figure 4.3 The enantiomeric separation of a nicotine standard and a TFN product, Coastline Stinson. The nicotine standard was analyzed as a pure standard, while the TFN product was diluted and directly injected as described in the Experimental section. Circular dichroism detection was utilized coupled with UV absorption at 263 nm. See Experimental for method parameters. A) Chiral detection of Coastline Stinson extraction. B) UV detection of Coastline Stinson extraction. C) Chiral detection of (+/-) nicotine

standard. D) UV detection of (+/-) nicotine standard. At t_0 (dead volume) impurities in B and D can be seen (S: (S)-(-)-nicotine; R: (R)-(+)-nicotine).

The first eluted peak was confirmed with the standard (S)-(-)-nicotine. To confirm the presence of both enantiomers of nicotine in the standard, selective ion monitoring and multiple reaction monitoring were utilized, which is shown in Fig. 1S and 2S in the Supplemental. The racemic nicotine standard was compared to the TFN product, Coastline Stinson, which confirms the presence of each nicotine enantiomer in equal amounts (see Fig. 3).

All the TFN e-liquids and tobacco-derived nicotine e-liquids showed the presence of other components coming out near the dead volume, which are possibly impurities, excipients and/or flavor additives (see Fig. 3). The extraction procedure for TFN and TDN e-liquids was not necessary because these samples could be diluted and injected directly, while solid TDN products required extraction. The TDN products gum and lozenge were not effectively extracted using the same process as other solid TDN products like the patch and tablet. Perhaps there is a matrix effect with nicotine polacrilex that might require an ion exchange with acid/base to perform complete extraction. As the focus of this study was to evaluate TFN products, the TDN extraction procedure was not further optimized. The level of racemization of the (S)-(-)-nicotine standard before and after each extraction was compared and the enantiomeric ratio of the (S)-(-)-nicotine standard remained constant (see Table 1 and Experimental). The ratio of each nicotine enantiomer found in all the TFN e-liquids, tobacco-nicotine e-liquids, and TDN products is also shown in Table 1. The ratio of (R)-(+)-nicotine in tobacco commercial products was determined to be 0.4% to 1.1% of the total enantiomeric nicotine content. The amount of each enantiomer in TFN products was determined to be equal, therefore they are racemic. This evaluation shows that the enantiomer excess of TFN products is much lower than that of TDN products.^[3] The amount of (R)-(+)-nicotine in TFN compared to commercial tobacco products is much greater.

Evaluation of the nicotine content was performed to determine whether the nicotine determined experimentally matched the labeled amount (see Table 1).

Chapter 4 Table 1. Evaluation of enantiomeric ratio of nicotine in commercial tobacco products and TFN products.

Sample ^a	Type ^b	Nicotine Content ^c	Experimental Nicotine Content ^d	Enantiomeric Ratio ^e
(+/-)-Nicotine Std.	TDN	1 mg/mL	1.00 mg/mL	50.0/50.0
(S)-(-)-Nicotine Std.	TDN	1mg/mL	1.00 mg/mL	99.6/0.4
(S)-(-)-Nicotine Extraction Std.	TDN	1 mg/mL	1.00 mg/mL	99.6/0.4
Transdermal Nicotine Patch	TDN	21 mg/day	26.78 mg/piece	99.2/0.8
Dissolvable Smokeless Tobacco	TDN	1.5 mg/piece	1.48 mg/piece	99.2/0.8
Nicotine Gum	TDN	4 mg/piece	2.41 mg/piece ^f	98.9/1.1
Nicotine Lozenge	TDN	4 mg/piece	1.43 mg/piece ^f	98.9/1.1
Vanilla e-liquid	TDN	24 mg/mL	24.04 mg/mL	99.6/0.4
Coastline e-liquid	TFN	6 mg/mL	6.04 mg/mL	50.0/50.0
Peel e-liquid	TFN	6 mg/mL	5.97 mg/mL	50.0/50.0
NKTR e-liquid	TFN	6 mg/mL	12.04 mg/mL	50.0/50.0
Melt e-liquid	TFN	6 mg/mL	6.04 mg/mL	50.0/50.0

^a See Experimental section for sample preparation and information. Std.: standard

^b TFN: tobacco free nicotine; TDN: tobacco derived nicotine

^c Nicotine content as indicated on the label by individual manufacturers.

^d Experimental nicotine content determined by LC-UV, all with a confidence limit within ± 0.05 mg (see Experimental).

^e The enantiomeric ratio = [average peak area of (S)-(-)-nicotine/average peak area of (R)-(+)-nicotine]. All samples were determined to have a %RSD within $\pm 0.2\%$ (see Experimental).

^f Extraction was not optimized, see Experimental.

In the TFN product, NKTR, the amount of total nicotine (the sum of both enantiomers) determined by LC-UV was twice that of the labeled amount (i.e. 6 mg nicotine on label, but 12 mg total present). This was interesting as the other TFN products contained 6 mg of total nicotine. Since all of these TFN products were racemic, only half of the “total nicotine” was the natural (S)-(-) enantiomer. Therefore, the NKTR e-liquid contained 6 mg (S)-(-)-nicotine and the other e-liquids contained 3 mg (S)-(-)-nicotine (Table 1). Clearly their potency is different even though the stated amount of their “active ingredient” is the same. It is not clear what the term “nicotine” on the label refers to in terms of stereochemistry or amounts of total vs. active stereoisomers.

4.5 Conclusions

An effective method for the fast enantioseparation of nicotine and the nicotine analogue, normnicotine, was developed. This method is electrospray ionization mass spectrometry compatible. The approach could be used in preparative scale chromatography for the purification of individual nicotine enantiomers for pharmacological studies and possibly for other nicotine metabolites. Using this method was it was shown

that all TFN products contain racemic nicotine while TDN products contain only small amounts of (R)-(+)-nicotine. The labeled amount of nicotine on TFN e-liquid products was found to not always correspond to the total nicotine amount, or the amount of the natural (S)-(-)-nicotine enantiomer. All TFN products contain much greater amounts of the (R)-(+)-nicotine than commercial tobacco-derived (TDN) products. Due to the likely differences in pharmacological effects of nicotine enantiomers and given current FDA guidelines for development of new stereoisomeric drugs, it is suggested that further pharmacological studies of (R)-(+)-nicotine are undertaken to assess the properties and safety of TFN products.

4.6 References

- [1] D.W. Armstrong, X. Wang, N. Ercal. Enantiomeric composition of nicotine in smokeless tobacco, medicinal products, and commercial reagents. *Chirality*. **1998**, *10*, 587-591.
- [2] J. Gal. The discovery of biological enantioselectivity: Louis Pasteur and the fermentation of tartaric acid, 1857-A review and analysis 150 yr later. *Chirality*. **2008**, *20*, 5-19.
- [3] M.D. Aceto, B.R. Martin, I.M. Uwaudah, E.L. May, L.S. Harris, C. Izazole-Conde, W.L. Dewey, T.J. Bradshaw, W.C. Vincek. Optically pure (+)-nicotine from (+/-)-nicotine and biological comparisons with (-)-nicotine. *J. Med. Chem.* **1979**, *22*, 174-177.
- [4] D. Yildiz, N. Ercal, D.W. Armstrong. Nicotine enantiomers and oxidative stress. *J. Toxicol.* **1998**, *130*, 155-165.
- [5] D. Pogocki, T. Ruman, M. Danilczuk, M. Danilczuk, M. Celuch, E. Walajtys-Rode. Application of nicotine enantiomers, derivatives and analogues in therapy of neurodegenerative disorders. *Eur. J. Pharmacol.* **2007**, *563*, 18-39.
- [6] J.P. Jones, W.F. Trager, T.J. Carlson. The binding and regioselectivity of reaction of (R)- and (S)-nicotine with cytochrome P-450cam: parallel experimental and theoretical studies. *J. Amer. Chem. Soc.* **1993**, *115*, 381-387.
- [7] X. Zhang, Ze-Hui Gong, A. Nordberg. Effects of chronic treatment with (+)- and (-)-nicotine on nicotinic acetylcholine receptor and *N*-methyl-D-aspartate receptors in rat brain. *Brain Research*. **1994**: *644(1)*, 32-39.
- [8] S. Ikushima, I. Muramatsu, Y. Sakakibara, K. Yokotani, M. Fujiwara. The effects of d-nicotine and l-isomer on nicotinic receptors. *J. Pharmacol. Exp. Ther.* **1982**, *222*, 463-470.
- [9] V. Saareks, I. Mucha, E. Sievi, H. Vapaatalo, A. Riutta. Nicotine stereoisomers and cotinine stimulate prostaglandin E2 but inhibit thromboxane B₂ and leukotriene E₄ synthesis in whole blood. *Eur. J. Pharmacol.* **1998**, *353*, 87-92.
- [10] C. Bullen, C. Howe, M. Lugesen, H. McRobbie, V. Parag, J. Williman, N. Walker. Electronic cigarettes for smoking cessation: a randomized controlled trial. *Lancet*. **2013**, *382(9905)*, 16-22.
- [11] Arnold, M. Process for the preparation of (R,S)-nicotine. US 20160115150 A1, April 28, 2016.
- [12] Food and Drug Administration. Deeming tobacco products to be subject to the federal food, drug and cosmetic act, as amended by the family smoking prevention and tobacco control act; regulations on the sale and distribution of tobacco products and required warning statements for tobacco products. *Federal Register*. **2016**, *79*, 28973-29106.

- [13] Hartley-Barnes, T.; McBride, T.; Hartley-Barnes, K.; Little, J. SUA Vapors – A TFN eLiquid Review. *Spinfuel eMagazine*, Aug 16, 2016.
- [14] Food and Drug Administration. FDA's policy statement for the development of new stereoisomeric drugs. *Chirality*. **1992**, *4*: 338–340.
- [15] D.W. Armstrong, L.A. Spino, S.M. Han, J.I. Seeman, H.V. Secor. Enantiomeric resolution of racemic nicotine and nicotine analogues by microcolumn liquid chromatography with β -cyclodextrin inclusion complexes. *J. Chromatogr.* **1987**, *411*, 490-493.
- [16] D. Demetriou, K. Rustemeier, P. Voncken, G. Schepers. HPLC separation of the enantiomers of nicotine and nicotine like compounds. *Chirality*. **1993**, *5*, 300-302.
- [17] Y. Tang, W.L. Zielinski, H.M. Bigott. Separation of nicotine and nornicotine enantiomers via normal phase HPLC on derivatized cellulose chiral stationary phases. *Chirality*. **1998**, *10*, 364-369.
- [18] D.W. Armstrong, Y. Tang, S. Chen, Y. Zhou, C. Bagwill J.R. Chen. Macrocyclic antibiotics as a new class of chiral selectors for liquid chromatography. *Anal. Chem.* **1994**, *66* (9), 1473-1484.
- [19] Z. Fan, F. Xie, Q. Xia, S. Wang, L. Ding, H. Liu. Simultaneous determination of nicotine and its nine metabolites in human urine by LC-MS-MS. *Chromatographia*. **2008**, *68*, 623-627.
- [20] M.R. Peace, T.R. Baird, N. Smith, C.E. Wolf, J.L. Poklis, A. Poklis. Concentration of nicotine and glycols in 27 electronic cigarette formulations. *J. Anal. Toxicol.* **2016**, *40*, 403-407.
- [21] D.W. Armstrong, X. Wang, Jauh-Tzuoh Lee, Yan-Song Liu. Enantiomeric concentration of nornicotine, anatabine, and anabasine in tobacco. *Chirality*. **1999**, *11*, 82-84.
- [22] P.M. Clayton, C.A. Vas, T.T.T. Bui, A.F. Drake, K. McAdam. Spectroscopic studies on nicotine and nornicotine in the UV region. *Chirality*. **2013**, *25*, 288-293.

Chapter 5

A comprehensive methodology for the chiral separation of 40 tobacco alkaloids and their carcinogenic E/Z-(R,S)-tobacco-specific nitrosamine metabolites

5.1 Abstract

The predominant enantiomer of nicotine found in nature is (S)-nicotine and its pharmacology has been widely established. However, pharmacologic information concerning individual enantiomers of nicotine-related compounds is limited. Recently, a modified macrocyclic glycopeptide chiral selector was found to be highly stereoselective for most tobacco alkaloids and metabolites. This study examines the semi-synthetic and native known macrocyclic glycopeptides for chiral recognition, separation, and characterization of the largest group of nicotine-related compounds ever reported (tobacco alkaloids, nicotine metabolites and derivatives, and tobacco-specific nitrosamines). The enantioseparation of nicotine is accomplished in less than 20 seconds for example. All liquid chromatography separations are mass spectrometry compatible for the tobacco alkaloids, as well as their metabolites. Ring-closed, cyclized structures were identified and separated from their ring-open, straight chain equilibrium structures. Also, E/Z-tobacco-specific nitrosamines and their enantiomers were directly separated. E/Z isomers also are known to have different physical and chemical properties and biological activity. This study provides optimal separation conditions for the analysis of nicotine-related isomers, which in the past have been reported to be ineffectively separated which can result in inaccurate results. The methodology of this study could be applied to cancer studies, and lead to more information about the role of these isomers in other diseases and as treatment for diseases.

5.2 Introduction

Tobacco smoke has been reported to contain at least 60 carcinogens and several have been directly related to cancer [1]. Tobacco and its derived products constitute a leading preventable cause of death in the United States (US) [2]. The Food and Drug Administration (FDA) regulates all commercial tobacco

products via the Family Smoking Prevention and Tobacco Control Act and the extension, the Deeming Rule [3-4]. Recently, the FDA also announced a comprehensive plan for lowering the nicotine (NIC) content in cigarettes to make them less or non-addictive [5]. To facilitate dependence, the reduced amount has been estimated to be 0.05 mg NIC compared to the current range of 0.5-1.5 mg NIC yield in one cigarette [1,6]. One challenge might be that smokers turn to other tobacco products for the higher NIC content compared to reduced NIC content cigarettes, such as smokeless tobacco products, which are connected to oral and esophageal cancers [7]. Smokeless tobacco products, like moist snuff, have been determined to contain tobacco-specific nitrosamines (TSNAs), which have been shown to be responsible for oral cavity cancer from smokeless tobacco [7]. The most prevalent and toxic TSNAs have been reported as *N*'-nitrosornicotine (NNN) and 4-(methylnitrosamino)-1-(3-pyridyl)-1-butanone (NNK) [1]. The other main TSNAs, *N*'-nitrosoanatabine (NAT) and *N*'-nitrosoanabasine (NAB), haven't shown as potent carcinogenicity in laboratory animals [7-8]. In one study, 12 rats were treated with racemic NNN and 96 oral cavity tumors and 153 esophageal tumors were observed [8]. Also, the (S)-NNN enantiomer was determined to be more tumorigenic than (R)-NNN indicating that the stereochemistry of this compound is highly important [8].

In 2017, the FDA proposed, "The mean level of *N*'-nitrosornicotine in any batch of finished smokeless tobacco product not exceed 1 microgram per gram ($\mu\text{g/g}$) of tobacco (on a dry weight basis) at any time through the product's labelled expiration date as determined by specified product testing." [9]. Current commercial US smokeless tobacco products contain NNN levels ranging from 1 to 10 $\mu\text{g/g}$ dry weight [10]. NNN is formed by the nitrosation of NIC and nornicotine (NNIC), which is a tobacco alkaloid native to tobacco, as well as a nicotine metabolite [7]. The level of NNIC is dependent on the leaf senescence and curing process [7,11]. Tobacco strains with less (S)-NNIC have been reported to contain less (S)-NNN [11]. Therefore, genetic engineering efforts have been focused on reducing the inherent amount of NNIC [11]. Also, NNN can be formed endogenously, which was shown when NNN was found in saliva after using NIC replacement therapies [12]. Furthermore, NNN metabolizes to another TSNA,

N'-nitrosornicotine-1-*N*-oxide (NNNO), which has been shown to be less carcinogenic than NNN in F344 rats and Syrian golden hamsters [13].

The other major carcinogen found in unburnt tobacco and tobacco smoke is NNK, an achiral TSNA, which is formed from NIC during the curing and processing of tobacco [7]. NNK was found to be the only potent lung carcinogen that formed tumors in rats, mice, and hamsters [14]. Metabolites of NNK and other TSNAs are known to bind to DNA once activated, forming adducts that can cause oncogene activation leading to tumor development if they persist [7]. Long-term exposure to these mutation events can lead to cancer and death [7]. NNK is known to metabolize mainly to 4-(methylnitrosamino)-1-(3-pyridyl)-1-butanol, NNAL, and its glucuronides [15]. Since NNK and NNAL are only found in tobacco and not from any other source, they can be used as highly specific biomarkers of carcinogen exposure, especially second-hand smoke exposure [16]. Also, the ratio of NNAL-glucuronide to NNAL has been used as a biomarker of susceptibility to lung cancer [16].

NNAL has been reported to have similar toxicity as NNK, with a higher tumorigenicity of the R-NNAL enantiomer than (S)-NNAL, due to preferential metabolic activation [17]. NNK, NNAL, and NNN were reported to form E/Z isomers [18-20]. The relative level of E isomers was higher than Z isomers [18-20]. Some previous reports have shown the separation of a few TSNAs, but most do not report the separation of both their enantiomers and E/Z isomers [20-23]. Thus, some researchers have expressed confusion because the tops of their TSNA chromatographic peaks show splitting [24]. However, TSNAs are known to interconvert between E/Z isomers [18-20]. Chiral capillary electrophoresis has been used to separate E/Z-NNK and (R,S)-(E/Z)-NNAL [20]. Also, achiral nitrosamines, other than TSNAs, have been separated by LC into their E/Z isomers. For example, fish toxicants like 6',7'-acetylenic nitrosamines were efficiently resolved with an achiral LC method [25]. Using a similar LC method, but with the addition of chiral derivatizing agents, the indirect separation of (R)-(E/Z) and (S)-(E/Z)-TSNA isomers were performed [18-19]. The approach described in this work provides a direct and efficient separation of both E/Z isomers and their enantiomers as well as indicating if isomeric interconversions occur under

“ordinary” conditions. In jaundice phototherapy, toxic, unconjugated bilirubin is isomerized to several E/Z configurations [26]. This isomerization makes bilirubin become more soluble in plasma so it can be excreted by the liver [26]. Therefore, E/Z isomers have different physical and biological properties and should be further studied with TSNAs.

TSNAs are nitrosated metabolites of chiral tobacco alkaloids, which have similar structures as NIC [7]. NIC is predominantly found as the (S)-(-) enantiomer in tobacco plants [27]. The percent (R)-(+)-NIC in tobacco, and medicinal products derived from tobacco was reported to be in the 0.1 to 1.2% range [27]. The pharmacology of (R)-(+)-NIC has not been an area of great concern, most likely because human exposure and intake of (R)-(+)-NIC is minimal. However, the individual enantiomers have been examined for their use as therapies for neurodegenerative diseases. These studies have reported that NIC enantiomers have different pharmacological effects, such as oxidative stress, weight loss, and binding mechanisms [28-30]. (R)-NIC has been reported as eighty times less cytotoxic than (S)-NIC, when considering their metabolites [30]. A recent study determined new smoking products (e-liquids), which have synthetic NIC (tobacco-free nicotine, TFN), contained 50% of (R)-(+)-NIC [31]. Since new products contain higher (R)-NIC levels than in tobacco-derived products, it was suggested that the pharmacology of (R)-NIC should be more extensively studied [31]. The binding affinity of (R)-NIC to nicotine acetylcholine receptors was estimated to be 10 times lower than (S)-NIC, which might result with a less stimulating dopaminergic response [30]. New TFN products with higher (R)-NIC might be analogous to commercial products with less addictive NIC levels.

While (S)-NIC is the main alkaloid in tobacco products, minor chiral alkaloids also are present including NNIC, anatabine (AT), and anabasine (AB) [32]. The R-enantiomers of minor tobacco alkaloids have been reported to be present at higher relative levels than (R)-(+)-NIC [32]. Most biomarker strategies utilize tobacco alkaloids or their metabolites, such as the major chiral metabolite, cotinine (COT). COT is used to measure NIC uptake, due to its long half-life, such as in smoking cessation trials and tobacco exposure tests [33]. However, tobacco alkaloids are useful to differentiate the use of tobacco while using

NIC replacement therapies [34]. Also, chiral alkaloids have been reported to be useful as therapies for neurodegenerative diseases by mimicking NIC's neuropharmacological and neuroprotective effects [30,35]. Enantiomers are well known to have different pharmacological effects, e.g. (R)-AB was reported to be more toxic and cause more birth defects than (S)-AB [36]. So, if these alkaloids were developed into medicinal products, the FDA would require, in their words, "the pharmacology and toxicology of the enantiomer should be characterized for the principal effects and any other pharmacological effect, with respect to potency, specificity, maximum effect, etc." [37]. However, most analytical methods do not have the capability to analyze the individual enantiomers of these alkaloids and metabolites, so new more effective methods are needed. To quantitate and perform biological studies, it would be useful if such "chiral methods" were compatible with mass spectrometry (MS).

Some separation approaches for chiral nicotine-related compounds, more importantly the carcinogenic compounds, have been reported, but most have disadvantages that limit the analysis. Most analyses are similar to those of achiral nitrosamine analysis and do not have the capability of separating enantiomers, such as a study which determined the amount of TSNAs in replacement liquids for electronic cigarettes [38]. One chiral approach reported the separation of NIC and several alkaloids using a packed liquid chromatography (LC) microcolumn with a β -cyclodextrin mobile phase, but required three hours [39]. Other previous approaches mainly utilized chiral gas chromatography (GC) or chiral derivatization LC [18,23,32]. GC isn't best suited for the biological analysis of these compounds due to the thermal liability of the sample. Chiral derivatization LC methods increase cost and analysis times and rely on the purity of the chiral derivatization agent. The best approach for chiral separations of nicotine-related compounds is using LC chiral stationary phases (CSPs). Enantioseparations of three tobacco alkaloids using LC CSPs have been reported, but they used normal phase solvents, which are not compatible with MS [36,40]. These alkaloids might be possible targets for neurodegenerative therapies, but these methods won't be compatible for biological analysis [30].

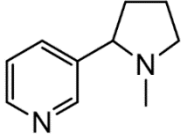
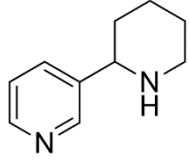
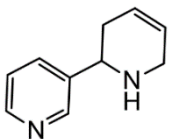
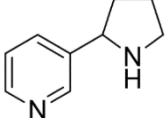
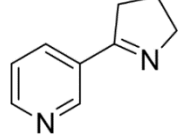
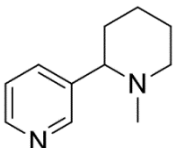
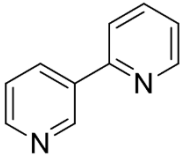
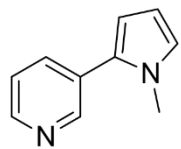
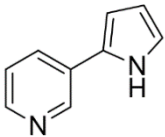
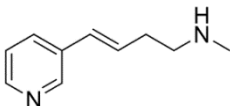
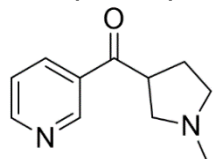
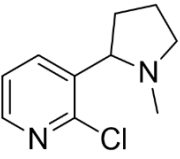
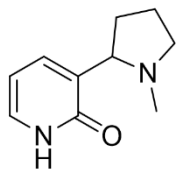
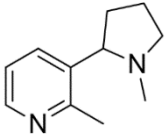
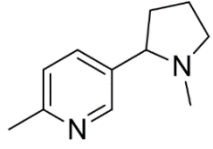
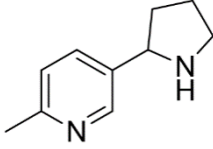
Recently, a fast, high efficiency, mass spectrometry compatible, chiral LC approach was developed to analyze NIC in TFN commercial e-liquids [31]. Herein we examine this approach for applicability for the sensitive identification and enantiomeric quantification of most nicotine-related compounds and metabolites in commercial tobacco products and biological samples. Focus is paid to the LC separation of carcinogenic compounds, like NNN or NNK, and other complex isomeric mixtures that have not been reported to separate previously. This study examines the effectiveness of new and known macrocyclic glycopeptide chiral selectors in resolving the most comprehensive set of chiral nicotine-related compounds yet investigated, including minor tobacco alkaloids, metabolites, synthetic related compounds, and E/Z-TSNAs [31,41-44]. Further, only LC-MS compatible formats were considered.

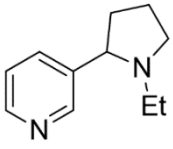
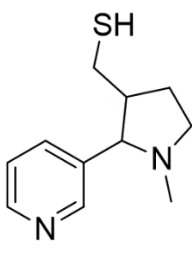
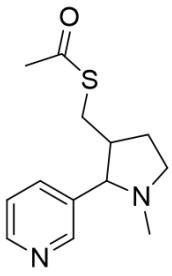
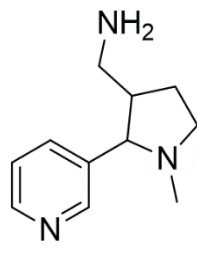
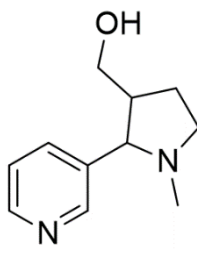
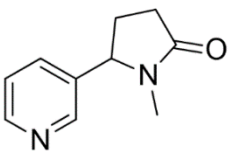
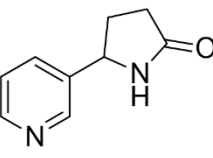
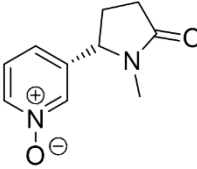
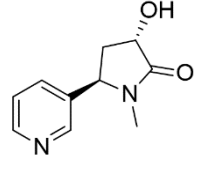
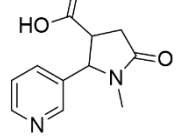
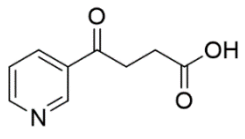
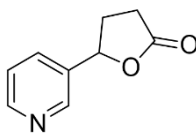
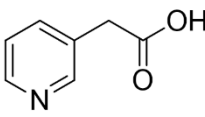
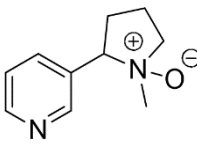
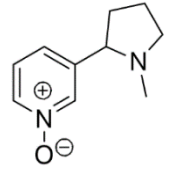
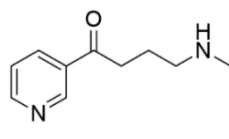
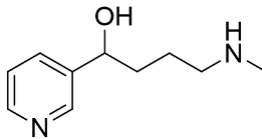
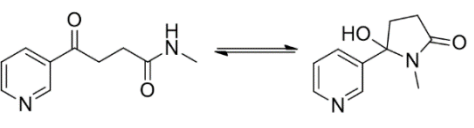
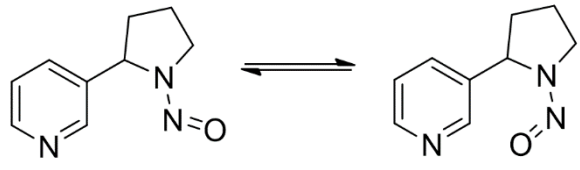
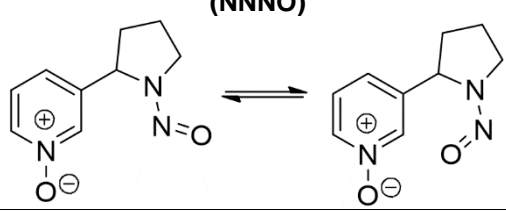
5.3 Materials and methods

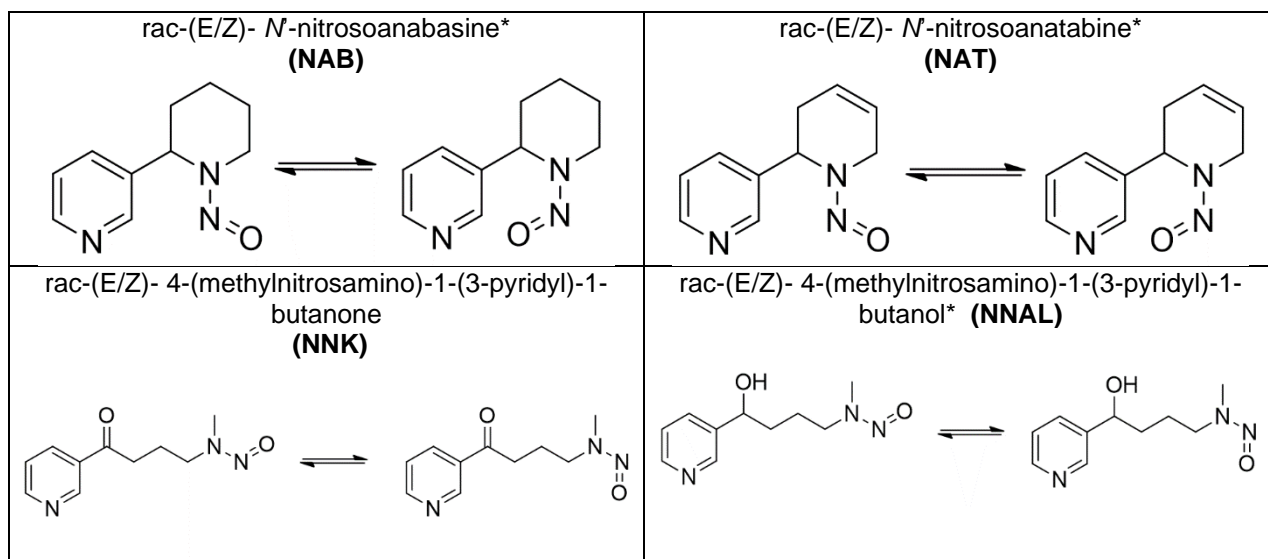
Native vancomycin (VancoShell, V, 100 x 4.6 mm inner diameter (i.d.)) and teicoplanin (TeicoShell, T, 100 x 4.6 mm i.d.), hydroxypropyl- β -cyclodextrin (CDShell-RSP, 100 x 4.6 mm i.d.), quinine (Q-Shell, 100 x 4.6 mm i.d.) and modified macrocyclic glycopeptide (NicoShell, N, 100 x 4.6 mm i.d.) CSPs were bonded to superficially porous particles (SPP), and obtained from AZYP, LLC. (Arlington, TX, USA). An Eclipse XDB-C18 (C18), 5 μ m, 150 x 4.6 mm i.d. column was obtained from Agilent Technologies (Palo Alto, CA, USA). A broad set of nicotine-related compounds were selected (see Table 1 for structures drawn as manufacturer label and acronyms, * denotes chiral compounds) and all chiral compounds were obtained as racemic analytical standards from Toronto Research Chemicals (Toronto, Canada) except cotinine-N-oxide (CNO) and *trans*-3'-hydroxycotinine (T3HC). Also, individual enantiomers of AT, AB, NIC, NNIC, COT, NNN, NAT, and NAB were obtained. An achiral compound, metanicotine (MET) was obtained as an E isomer. TSNAs were obtained as racemates, but these compounds are also known to exist as a mix of E/Z isomers and were not labelled accordingly. The standards were diluted with methanol to concentrations of 1 mg/mL and stored 24 hours before analysis.

Chapter 5 Table 1. Structures of nicotine-related compounds (all chiral compounds denoted by *).

a) Tobacco alkaloids

<p>Nicotine* (NIC)</p> 	<p>Anabasine* (AB)</p> 	<p>Anatabine* (AT)</p> 	<p>Nornicotine* (NNIC)</p> 	<p>Myosmine (MYS)</p> 
<p>N-methylanabasine* (MAB)</p> 	<p>2,3'-bipyridyl (BPY)</p> 	<p>β-nicotyrine (β-NT)</p> 	<p>β-nornicotyrine (β-NNT)</p> 	<p>Metanicotine (E) (MET)</p> 
b) Synthetic derivatives				
<p>1-methyl-3-nicotinoylpyrrolidine* (1M3NP)</p> 	<p>2-chloronicotine* (2CN)</p> 	<p>2-hydroxynicotine* (2HN)</p> 	<p>2-methylnicotine* (2MN)</p> 	<p>6-methylnicotine* (6MN)</p> 
<p>6-methylnornicotine* (6MNN)</p> 	<p>rac-(2S,3S & 2R,3R)-<i>trans</i>-3'-thiomethyl nicotine* (T3TMN)</p>	<p>rac-(2S,3S & 2R,3R)-<i>trans</i>-3'-acetylthiomethyl nicotine* (T3ATMN)</p>	<p>rac-(2S,3R & 2R,3S)-<i>trans</i>-3'-aminomethyl nicotine* (T3AMN)</p>	<p>rac-(2S,3S & 2R,3R)-<i>trans</i>-3'-hydroxymethyl nicotine* (T3HMN)</p>

<p>N-ethyl-nornicotine* (NENN)</p> 				
c) Metabolites				
<p>Cotinine* (COT)</p> 	<p>Norcotinine* (NCOT)</p> 	<p>(5S)-Cotinine-N-oxide (CNO)</p> 	<p><i>trans</i>-(3S,5R)-3'-hydroxy-cotinine (T3HC)</p> 	<p><i>rac-trans</i>-(2S,3R & 2R,3S)-cotinine carboxylic acid* (4TCCA)</p> 
<p>γ-oxo-3-pyridinebutyric acid (OPBA)</p> 	<p>5-(3-pyridyl) tetrahydro-2-furanone* (5THF)</p> 	<p>3-pyridylacetic acid (LAC)</p> 	<p><i>rac</i>-Nicotine-1'-N-oxide* (S,S & R,R) (NNO)</p> 	<p>Nicotine-1-oxide* (NO)</p> 
<p>4-(methylamino)-1-(3-pyridyl)-1-butanone (NAN)</p> 	<p><i>rac</i>-4-(methylamino)-1-(3-pyridyl)-1-butanol* (NAL)</p> 		<p>N-methyl-γ-oxo-pyridinebutanamine (OPBN) to 5'-hydroxycotinine* (5HCOT)</p> 	
d) (E/Z)-Tobacco-specific nitrosamines				
<p><i>rac</i>-(E/Z)-N-nitrosornornicotine* (NENN)</p> 		<p><i>rac</i>-(E/Z)-N-nitrosornornicotine-1-N-oxide* (NENNO)</p> 		



High performance LC grade methanol (MeOH) was obtained from Sigma-Aldrich (St. Louis, MO, USA) as well as acetonitrile (ACN), acetic acid (HOAc), ethanol (EtOH), triethylamine (TEA), ammonium hydroxide (NH₄OH), ammonium formate (NH₄Formate), and ammonium trifluoroacetate (NH₄TFA). Water was purified by a Milli-Q water purification system (Millipore, Billerica, MA, USA).

A 1260 high performance LC instrument (Agilent Technologies, Palo Alto, CA, USA) was used in this study. It consisted of a 1200 diode array detector, autosampler, column oven, and quaternary pump. Also, a Shimadzu triple quadrupole LC-MS instrument, LCMS-8040, (Shimadzu, Tokoyo, Japan) was used. All MS was operated in positive ion mode with an electron spray ionization source. The parameters were set as follows: nebulizer gas flow, 3 L/min; drying gas flow, 15 L/min; desolvation line temperature, 250 °C; heat block temperature, 400 °C. All separations were carried out at room temperature, unless otherwise noted, using an isocratic method. All analytes were screened, then optimized using a variety of mobile phases in the polar ionic mode (PIM), polar organic mode (POM), and reversed phase (RP) with all stationary phases. The mobile phases were degassed by ultrasonication under vacuum for 5 minutes. The UV wavelengths 220 and 263 nm were utilized for detection. Chiral separations were optimized (as shown in Table 2) with the following mobile phases: PIM1: 100/0.1wt%: MeOH/NH₄TFA; PIM2: 100/0.025wt%: MeOH/NH₄Formate; PIM3: 100/0.5wt%: MeOH/NH₄Formate; PIM4: 100/0.2wt%:

MeOH/NH₄Formate; PIM5: 100/0.2/0.05: MeOH/HOAc/NH₄OH; POM1: 60/40/0.3/0.2:

ACN/MeOH/HOAc/NH₄OH; POM2: 50/50/0.3/0.2: ACN/MeOH/HOAc/NH₄OH; POM3: 100: MeOH;

RP1: 90/10: MeOH/16 mM NH₄Formate pH 3.6; RP2: 90/10: EtOH/16 mM NH₄Formate pH 3.6; RP3:

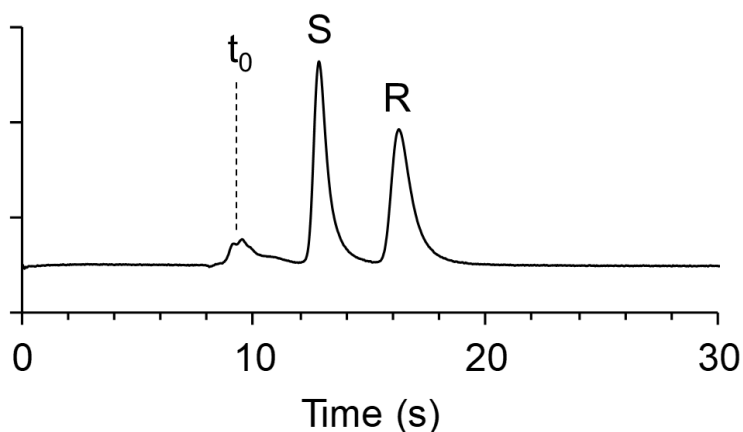
30/70: MeOH/16 mM NH₄Formate pH 3.6; RP4: 30/70: ACN/16 mM NH₄Formate pH 3.6; RP5: 10/90:

ACN/16 mM NH₄Formate pH 3.6.

The dead time, t_0 , was determined by the peak of the refractive index change due to the unretained sample solvent. Retention factors (k) were calculated using $k = (t_R - t_0) / (t_0)$, where t_R is the retention time of the first peak. Selectivity (α) was calculated using $\alpha = k_2 / k_1$, where k_1 and k_2 are retention factors of the first and second peaks, respectively. Resolution (R_s) was calculated using the peak width at half peak height, $R_s = 2(t_{R2} - t_{R1}) / (w_{0.5,1} + w_{0.5,2})$. Each sample was analyzed in triplicate. The relative standard deviation (%RSD) was determined to be within $\pm 1.0\%$ for the resolution of all analytes. Peak area calculations were determined by peak deconvolution according to a previous report [45]. The relative standard deviation (%RSD) was determined to be within $\pm 3.0\%$ for the area ratios reported.

5.4 Results

The enantioseparation of NIC can be obtained in 18 seconds with a $R_s = 2.6$ (Fig. 1).



Chapter 5 Figure 1. Ultra-fast LC enantioseparation of nicotine (NIC) using NicoShell, 50 x 4.6 mm (i.d.), PIM4 at 4 mL/min. S: S-NIC; R: R-NIC; t_0 : impurities at dead time. See Materials and methods for other acronyms and calculations ($k_1 = 0.7$, $\alpha = 1.64$, $R_s = 2.6$).

Table 1 provides the structures and names of 40 nicotine-related compounds analyzed in this study. The optimized, baseline separation conditions for all chiral nicotine-related compounds using macrocyclic glycopeptides are given in Table 2.

Chapter 5 Table 2. Optimized enantiomeric separations of nicotine-related compounds using macrocyclic glycopeptides.

Class ^{1a}	Name ^{1b}	CSP ²	MP ³	T ⁴	F ⁵	k ₁ ^{6a}	α ^{6b}	R _s ^{6c}
Tobacco alkaloids	NIC	N	PIM4	45	1.5	0.5	1.60	3.0
	AB	V	POM1	45	1.0	3.2	1.21	2.6
		N	PIM4	45	1.0	3.0	1.16	2.8
	AT	V	RP1	25	1.0	2.0	1.18	2.9
		N	PIM3	45	1.0	1.1	1.45	5.2
	NNIC	V	PIM2	45	0.7	4.1	1.10	1.5
		N	PIM3	45	1.0	2.7	1.14	2.3
	MAB	V	PIM4	25	0.5	1.3	1.38	3.2
N		PIM5	25	1.0	1.9	1.24	2.5	
Synthetic derivatives	1M3NP	N	PIM3	45	1.0	1.7	1.17	2.6
	2CN	V**	RP2	25	0.5	3.4	1.08	1.5
		N	PIM5	45	1.0	0.6	1.55	5.4
	2HN	N	PIM3	30	1.0	2.0	1.30	3.5
	2MN	V	RP1	30	0.7	2.3	1.11	1.7
		N	PIM4	45	1.5	1.1	1.17	2.2
	6MN	V**	PIM5	25	0.3	2.3	1.09	1.5
		N	PIM4	45	1.5	0.6	1.42	3.1
	6MNN	V	PIM1	25	1.0	2.3	1.20	2.7
		N	PIM4	45	2.0	3.7	1.26	3.6
	NENN	V	PIM5	25	1.0	2.3	1.19	2.5
		N	PIM4	45	2.0	0.5	1.76	4.6
	T3ATMN	V**	PIM2	25	0.5	1.3	1.06	1.5
		N	RP1	45	1.0	0.8	1.58	5.7
	T3AMN	V	RP1	45	0.5	5.0	1.15	1.5
		N	PIM4	45	0.5	4	1.21	1.5
	T3HMN	V	RP2	25	0.5	3.9	1.14	1.9
		N	PIM4	25	1.0	0.5	1.42	2.7
	T3TMN	V	RP2	25	0.5	2.7	1.15	1.7
		N	PIM4	25	1.0	0.4	1.72	3.5
Nicotine metabolites	COT	T**	POM3	25	0.5	0.7	1.12	1.5
	NCOT	T	POM3	25	1.0	0.9	2.64	9.3
	4TCCA	T*	RP3	45	0.5	0.9	1.18	2.0
	5THF	T	POM3	25	0.3	0.7	1.15	1.5
	NNO	N	POM2	25	0.7	1.4	1.21	2.2
	NO	V	RP1	45	0.5	1.4	1.12	1.6
		N	PIM3	45	1.0	0.4	2.18	3.0
	NAL	N	PIM4	25	0.5	5.9	1.09	1.8
5HCOT	V	POM1	25	1.0	0.4	1.58	3.5	

^{1a,b} See Table 1 and Materials and methods.

² Refer to Materials and methods for information concerning chiral stationary phases (CSP). * denotes 150 x 4.6 mm (i.d.), ** denotes 2 columns coupled, 200 x 4.6 mm (i.d.).

³ Refer to Materials and methods for information concerning mobile phase conditions.

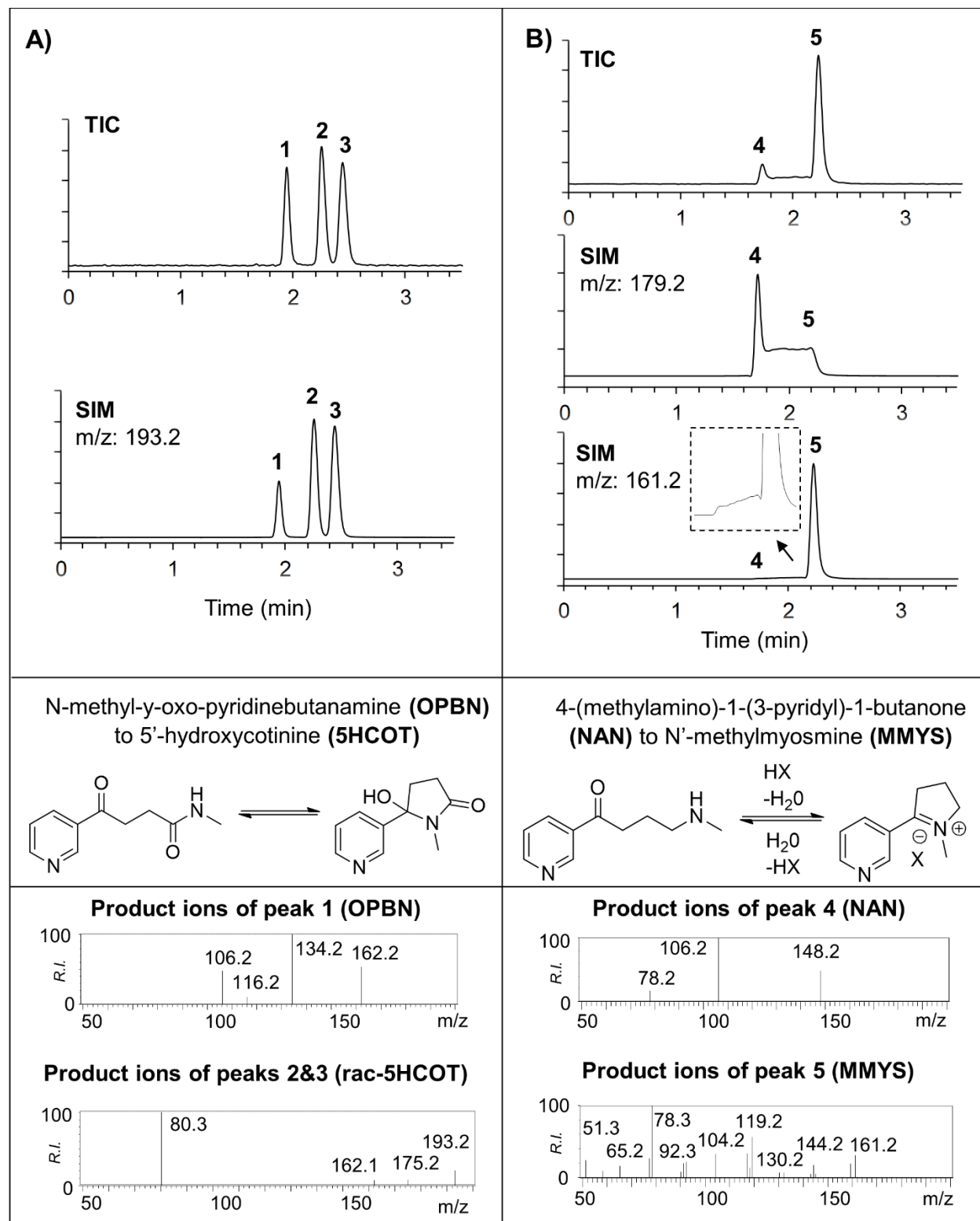
⁴ T: column temperature (° C)

⁵ F: flow rate (mL/min)

^{6a,b,c} Chromatographic parameters calculated according to Materials and methods.

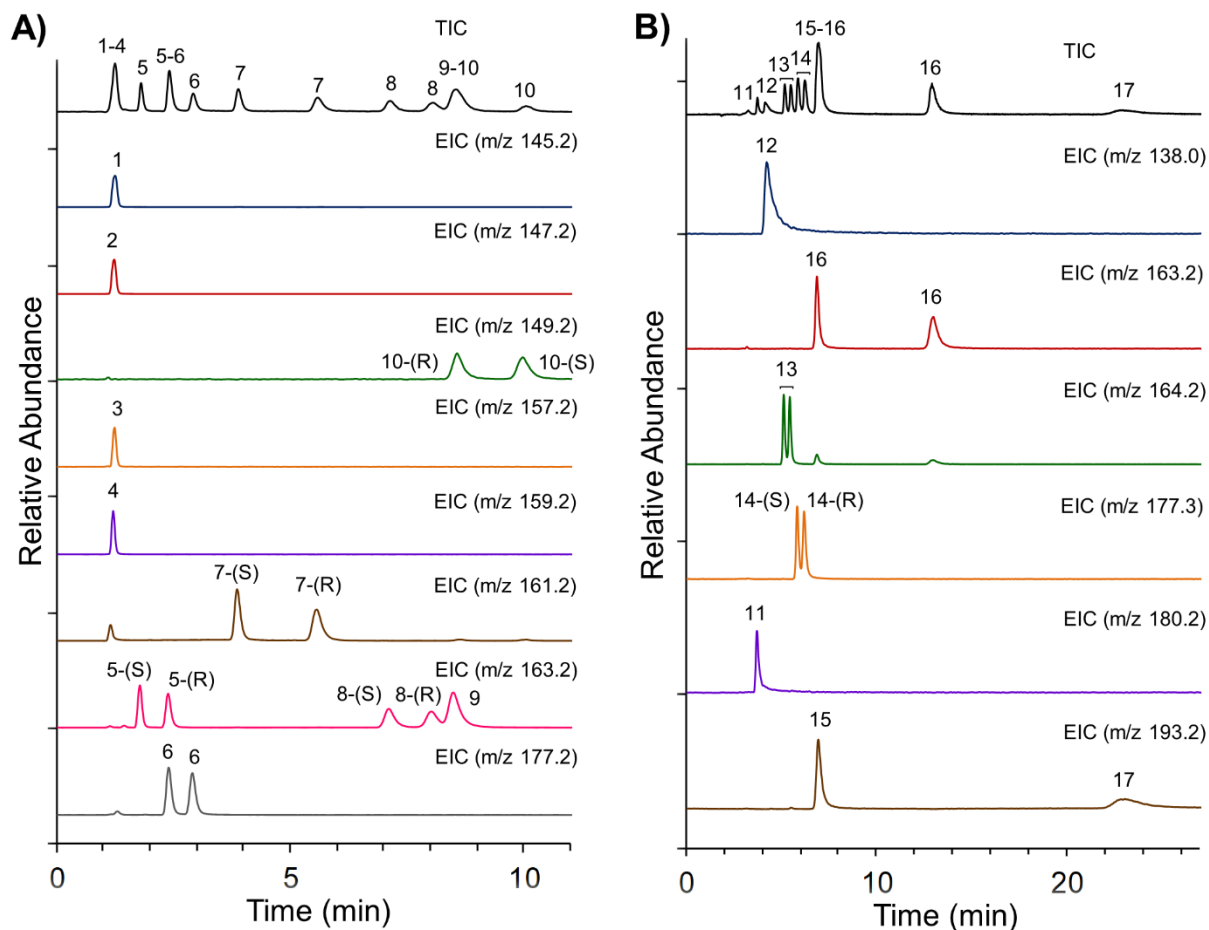
NicoShell separated 19 compounds, VancoShell separated 15 compounds, and TeicoShell separated 4 compounds. Racemic AT, AB, and NNIC had higher resolution with NicoShell compared to VancoShell, but were baseline separated with VancoShell. NIC could not be baseline separated with VancoShell and TeicoShell. Addition of methyl groups to either adjacent carbons of the pyridine nitrogen, 2-methylnicotine (2MN) and 6-methylnicotine (6MN), increased resolution with VancoShell in comparison to NicoShell. 2MN and 6MN, in comparison to NIC, decreased selectivity with NicoShell, but increased selectivity with VancoShell. Addition of chlorine groups to NIC, 2-chloronicotine (2CN), increased resolution using NicoShell and VancoShell. Addition of oxygen functionalities to the pyridinium nitrogen, nicotine-1-oxide (NO), compared to NIC, increased selectivity with NicoShell and VancoShell. However, oxygen functionalities added to the pyrrolidinium group, nicotine-1'-oxide (NNO), resulted in less than a baseline separation with VancoShell. Also, NNO had decreased selectivity and longer retention than NIC and NO with NicoShell. Addition of alkyl groups to AB or NNIC, N-methylanabasine (MAB) or N-ethyl-nornicotine (NENN), had different effects depending on the CSP. In comparison to AB, MAB had increased resolution using NicoShell, but similar resolution with VancoShell. When comparing to NNIC, NENN had increased resolution for both NicoShell and VancoShell. Synthetic *rac-trans* nicotine-related compounds were also compared, which differed by peripheral functional groups. All *rac-trans* enantiomers were baseline separated by NicoShell and VancoShell. COT, norcotinine (NCOT), 4-*trans*-cotinine-carboxylic acid (4TCCA), and 5-(3-pyridyl)-tetrahydro-2-furanone (5THF) were only baseline separated by TeicoShell, while 1-methyl-3-nicotinoylpyrrolidine (1M3NP), 2-hydroxynicotine (2HN), 4-(methylamino)-1-(3-pyridyl)-1-butanol (NAL), NIC, and NNO were only baseline separated by NicoShell.

The only macrocyclic glycopeptide that separated 5'-hydroxycotinine, 5HCOT, was VancoShell, but 5HCOT was also separated by CDSHell-RSP, which is shown in Fig. 2A.



Chapter 5 Figure 2. Separation of ring-closed and ring-open equilibrating tobacco alkaloids. (A) OPBN (peak 1) to 5HCOT (peaks 2,3) (TIC scan from 110 to 220 m/z and product ion scan from 50 – 200 m/z) (B) NAN (peak 4) to MMYS (peak 5) (TIC scan from 150 – 220 m/z and product ion scan from 50 - 200 m/z) Conditions: CDShell-RSP, 100 x 4.6 mm (i.d.), RP5, 1.0 mL/min, 25 °C. R.I.: Relative intensity, TIC: total ion chromatogram, SIM: selective ion monitoring. See Materials and methods for other acronyms and information.

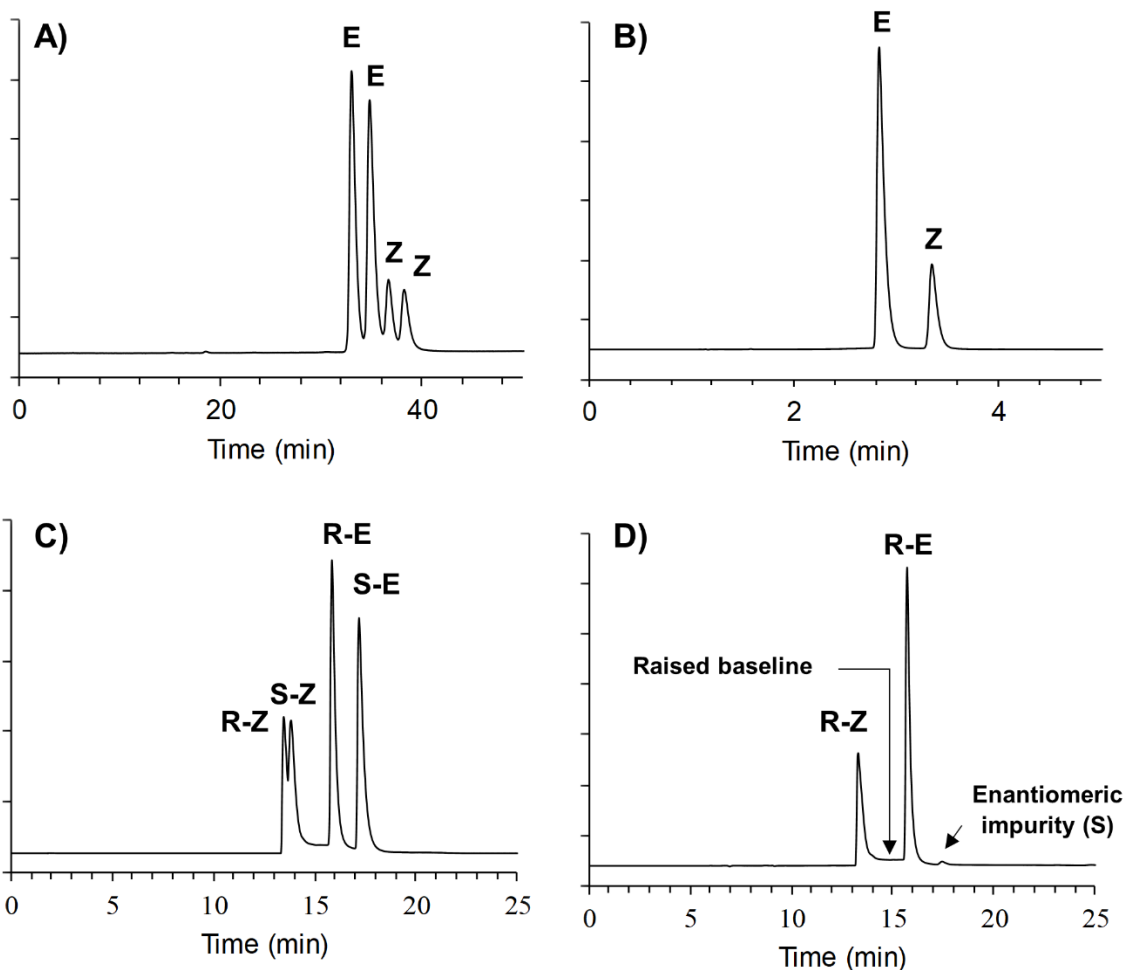
Fig. 2A also depicts a third component in the total ion chromatogram and selective ion monitoring chromatogram, which was identified as *N*-methyl-*y*-oxo-pyridinebutanamine, OPBN, based on the manufacturer label and mass spectra obtained. The manufacturer label marks 5HCOT and OPBN as equilibrating structures with the same mass, forming ring-open and ring-closed structures. The product ion scans for the two compounds were similar for peaks 2 and 3, but different for peak 1. Peaks 2 and 3 were identified as the chiral compound, 5HCOT, and peak 1 was identified as OPBN. The ratio of racemic HCOT to OPBN was 85:15 at 263 nm. 4-(methylamino)-1-(3-pyridyl)-1-butanone (NAN) was analyzed using CDShell-RSP, but wasn't expected to result in multiple peaks because it isn't chiral (Fig. 2B). There were two chromatographic peaks (peaks 4 and 5) at a ratio of 90:10 at 263 nm, and a raised baseline between the two peaks. A raised baseline between two related peaks indicates that there is an interconversion on the chromatographic time scale (see Discussion). The additional peak was identified as *N'*-methylmyosmine (MMYS) based on the mass spectra obtained. The product ion scans had different fragmentation patterns for each peak. The raised baseline was present in the selective ion monitoring of each peak. Fig. 3 shows the separation of 10 tobacco alkaloids and 7 nicotine metabolites.



Chapter 5 Figure 3. Chromatographic separation and detection of 10 tobacco alkaloids (**A**) and 7 nicotine metabolites (**B**). Total ion chromatograms (TIC) and extracted ion chromatograms (EIC) are shown. (**A**) Conditions: NicoShell, 100 x 4.6 mm (i.d.), PIM4, 1 mL/min. Tobacco alkaloids: 1. β -NNT, 2. MYS, 3. BPY, 4. β -NT, 5. (S,R)-NIC, 6. MANB, 7. (S,R)-ANT, 8. (S,R)-ANB, 9. MET, 10. (R,S)-NNIC. (**B**) Conditions: TeicoShell, 150 x 4.6 mm (i.d.), POM3, 0.5 mL/min. Nicotine metabolites: 11. OPBA, 12. LAC, 13. rac-5THF, 14. (S,R)-COT, 15. T3HC, 16. rac-NCOT, 17. (S)-CNO.

NicoShell enantioseparated 5 chiral tobacco alkaloids in 10 minutes (Fig. 3A). Also, 3 enantioseparations of chiral nicotine metabolites were obtained with TeicoShell in 14 minutes (Fig. 3B). For identification, the appropriate m/z value was selected, and the ion chromatogram of interest extracted. The components that had the same m/z were identified by spiking the sample with a standard.

The separation of NNAL is shown in Fig. 4A, and resulted in two pairs of chromatographic peaks that had similar areas.



Chapter 5 Figure 4. The direct separation of tobacco-specific nitrosamines. R = R-NNN, S = S-NNN, E = E isomer, Z = Z isomer based on previous reports (see Discussion), see Materials and methods and Table 1 for other acronyms used. **(A)** rac-NNAL, TeicoShell, 100 x 4.6 mm (i.d.), RP3, 0.3 mL/min, 25 °C. **(B)** NNK, CDShell-RSP, 100 x 4.6 mm (i.d.), RP4, 1.0 mL/min, 25 °C. **(C)** rac-NNN, Q-Shell, 250 x 4.6 mm (i.d.), RP3, 0.3 mL/min, 25 °C. **(D)** R-NNN, Q-Shell, 250 x 4.6 mm (i.d.), RP3, 0.3 mL/min, 25 °C.

The ratio of each pair was 75:25 at 263 nm. The separation of NNK is shown in Fig. 4B, with two chromatographic peaks at a ratio of 75:25 at 263 nm. Fig. 4C shows 4 distinct peaks from the separation of racemic NNN with the Q-Shell column. When pure enantiomers were injected, (R)-NNN in Fig. 4D,

each enantiomer showed two peaks at a ratio of 65:35 at 263 nm with a raised baseline between them (Fig. 4C and 4D). Single enantiomers were spiked into the original sample to identify each enantiomeric peak. An enantiomeric impurity was observed in the (R)-NNN sample, and identified as (S)-NNN (Fig. 4D). The elution order of NNN and NNIC enantiomers were different than the other tobacco alkaloids and metabolites (Fig. 3A, 3B, and 4D). Additionally, a reversal of elution for AB was observed when switching between PIM and POM solvents (Fig. S1A and S1B). Racemic NAB was separated into 2 peaks of equal area, while (S)-NAB was separated into 2 peaks at a ratio of 80:20 at 263 nm (Fig. S2A and S2B). NAT was separated into 2 peaks that each had a peak shoulder at a ratio of 80:20 at 263 nm (Fig. S2C). NNNO was separated into 4 peaks with similar ratios at 263 nm with a raised baseline using NicoShell coupled to TeicoShell (Fig. S2D). The separation of each TSNA resulted with similar MS fragmentation patterns for each respective peak.

5.5 Discussion

The chiral selectors examined in this study were shown to have both broader and higher selectivity for tobacco alkaloids and their metabolites than other approaches (Table 2) [27,39-40]. Higher selectivities and efficiencies allows the use of shorter columns and higher flow rates, which produces faster analysis times, and often sharper peaks, and better detection (Fig. 1) [32,39-40]. In turn, this can be useful in high throughput screening, and studying biotransformations and the biokinetics and dynamics of low levels of tobacco alkaloid metabolites [46]. For such studies, it is essential for the stereoselective separation methods to be compatible with ESI-MS detection as were all methods herein (Table 2). Separations that didn't work well for one macrocyclic glycopeptide separated with a different related one, which is known as complementary behaviour (Table 2). The "principle of complementary separations" states that a partial separation with one chiral selector can be brought to baseline with one of the other related selectors [47]. Complementary separations were seen with NIC and several derivatives (2HN, 1M3NP, NNO), which had poor resolution using VancoShell, but worked well with NicoShell. Also, TeicoShell baseline separated the metabolites that VancoShell and NicoShell didn't. Usually within a class of structures

several functionalities differ, which might enhance the separation using one macrocyclic glycopeptide, but inhibit another. It is unclear why some compounds had poor resolution using NicoShell and VancoShell due to the complex interaction mechanisms of macrocyclic glycopeptides. However, complementary separations offer an effective solution for difficult separations, which has been exploited for high-throughput screening [46]. This significant characteristic provides a high likelihood of baseline separating any structure within a certain class, as in the case of the tobacco alkaloids and their metabolites (Fig. 3A and 3B). Utilizing multiple chiral selectors and chromatographic solvents also gave rise to a reversal of elution order. So, this method could also be applied to situations that require a certain elution profile of enantiomers, such as in determining enantiomeric purity or in preparative separations.

Additional chromatographic peaks were observed in the separation of some tobacco alkaloids (Fig. 2 and 4). Fig. 2 shows the separation of 5HCOT, which has been reported as the chiral cyclized, ring-closed form of the straight-chain structure, OPBN [33,48-49]. 5HCOT was previously reported to be quickly and favourably formed in water, which agrees with our results [49]. Some chromatographic separations have been challenging as indicated in previous reports [50]. The separation approach of this study provides two methods (Table 2 and Fig. 2A). A raised baseline was not observed, but in the separation of NAN a raised baseline was seen between the NAN chromatographic peak and the additional peak, MMYS, indicating interconversions on the chromatographic time scale (Fig. 2B). NAN was previously reported to equilibrate with MMYS by a dehydration/hydration reaction, but little was found in the literature about their roles in metabolism [33,48-49,51]. NAN and MMYS might have faster interconversion rates than the other ring-closed and straight-chain equilibrating structures, in Fig. 2A, due to the observed raised baseline at ordinary conditions. The reproducibility of a separation was highly dependent on the time between sample preparation and analysis. It was observed that differences in this time and temperature would change the ratio between the chromatographic peaks. Also, if another solvent was used to dissolve the analyte for analysis, the equilibration time was much different. Furthermore, other equilibrating

structures have been reported to exist between these structures [48]. Detection and separation of these components has not been reported in the literature, but with this procedure, it is now possible.

A single enantiomer of NNN was separated into 2 chromatographic peaks at ratio of 70/30, which agrees with a previous report of NNN's E and Z isomeric ratio in tobacco and were labelled accordingly (Fig. 4D) [19]. E/Z isomers in TSNAs have not been extensively studied. Reports of some have been performed, such as NNN, NNK, and NNAL, concluding there is generally a higher concentration of the E isomer than the Z isomer [18-20]. Our results indicate that this also is true for NAB and NAT (Fig. 4B, and S2). Upon further inspection, a raised baseline was observed between the peaks. This indicates the diastereomeric interconversion of E and Z isomers on the chromatographic time scale (Fig. 4D). In general, decreasing the temperature of the column lowered the baseline between the converting peaks. On the other hand, higher column temperatures increased the rate of conversion, such that no peak separation was observed. Perhaps, this explains why previous reports that use GC at high temperatures didn't observe E/Z isomers during TSNA analysis [23]. The interconversion rate between E/Z isomers was different because some TSNAs had distinct raised baselines, like NNN, while others like NNK didn't (Fig. 4B and 4D). However, a raised baseline was observed at higher temperatures for NNK, so it does interconvert, but slowly at ordinary conditions. Previous reports of some pharmacokinetics of racemic TSNAs have been investigated, such as their half-lives. An observed trend was that a short half-life correlated to the carcinogenicity of the TSNA, so more potent TSNAs were eliminated faster [52]. However, the half-lives and interconversion rates of single enantiomers have not been reported, which may be different, especially since they contain equilibrating isomers. This equilibration was observed to be stable under room temperature conditions as shown in previous literature, but due to the raised chromatographic baseline, there is difficulty in isolating pure E or Z isomer [18-19]. Since E/Z isomers were observed for all TSNAs, further investigation of the enantiomers and their respective isomers as well as other TSNA metabolites, such as their half-lives, might be useful to determine their stereoselective roles and routes in metabolism.

Since the FDA has issued the mandatory regulation of NNN levels in smokeless tobacco products, manufacturers will have to quantify the amount of NNN in their finished products [9]. This may lead to confusion, as some manufacturers might use achiral LC methods, which might broaden or split their chromatographic peaks [24]. Since these splits are most likely E/Z isomers of the TSNAs, it is important that they be included in the quantification required by the FDA. However, E/Z isomers are known to have different physical and biological properties, so studies might be needed to evaluate whether these E/Z isomers contribute differently to cancer and other diseases [26]. The methodology of this study can be applied, as the results of this study clearly demonstrate a comprehensive approach for the analysis and enantioseparation of these nicotine-related compounds. Further investigation is ongoing, but with the methods presented in this study, more pharmacological information concerning individual enantiomers and other isomers of nicotine-related compounds can effectively and quickly be obtained. These studies would lead to a more complete knowledge about tobacco alkaloids and their metabolites and their roles or therapeutic use for cancer and other diseases.

5.6 References

1. S.S. Hecht, Tobacco carcinogens, their biomarkers, and tobacco-induced cancer, *J. Nat. Rev. Cancer* 3 (2003) 733-744.
2. U.S. Department of Health and Human Services, The health consequences of smoking—50 years of progress: A report of the Surgeon General. Atlanta, GA: U.S. Department of Health and Human Services, Centers for Disease Control and Prevention, National Center for Chronic Disease Prevention and Health Promotion, Office on Smoking and Health, 2014.
3. Food and Drug Administration. Family smoking prevention and tobacco control and federal retirement reform. Public law 111–31—June 22, 2009.
4. Food and Drug Administration, Deeming tobacco products to be subject to the federal food, drug and cosmetic act, as amended by the family smoking prevention and tobacco control act; regulations on the sale and distribution of tobacco products and required warning statements for tobacco products, *Fed. Regist.* 79 (2016) 28973.
5. Food and Drug Administration, Protecting American families: comprehensive approach to nicotine and tobacco. <https://www.fda.gov/NewsEvents/Speeches/ucm569024.htm>, 2017 (accessed August 17, 2017).
6. D.K. Hatsukami, M. Kotlyar, L.A. Hertsgaard, Y. Zhang, S.G. Carmella, J.A. Jensen, S.S. Allen, P.G. Shields, S.E. Murphy, I. Stepanov, S.S. Hecht., Reduced nicotine content cigarettes: effects on toxicant exposure, dependence and cessation, *Addiction* 105 (2010) 343-355.
7. D. Hoffmann, S.S. Hecht, Nicotine-derived *N*-nitrosamines and tobacco related cancer: current status and future directions, *Cancer Research* 45 (1985) 935-944.

8. S. Balvo, S. James-Yi, C.S. Johnson, M.G. O'Sullivan, I. Stepanov, M. Wang, D. Bandyopadhyay, F. Kassie, S. Carmella, P. Upadhyaya, S.S. Hecht, (S)-*N'*-nitrosornicotine, a constituent of smokeless tobacco, is a powerful oral cavity carcinogen in rats, *Carcinogenesis* 34 (2013) 2178-2183.
9. Food and Drug Administration, Tobacco product standard for *N'*-nitrosornicotine level in finished smokeless tobacco products, Fed. Regist. Proposed Rules 82 (2017) 8004-8053.
10. S.S. Hecht, I. Stepanov, D.K. Hatsukami, Major tobacco companies have technology to reduce carcinogen levels but do not apply it to popular smokeless tobacco products, *Tob. Control* 6 (2011) 443.
11. R.S. Lewis, A.M. Jack, J.W. Morris, V.J.M. Robert, L.B. Gavilano, B. Siminszky, L.P. Bush, A.J. Hayes, R.E. Dewey, RNA interference (RNAi)-induced suppression of nicotine demethylase activity reduces levels of a key carcinogen in cured tobacco leaves, *Plant Biotech. J.* 6 (2008) 346-354.
12. A. Knezevich, J. Muzic, D.K. Hatsukami, S.S. Hecht, I. Stepanov, Nicotinic nitrosation in saliva and its relation to endogenous synthesis of *N'*-nitrosornicotine in humans, *Nicotine Tob. Res.* 15 (2013) 591-595.
13. S.S. Hecht, R. Young, Y. Maeura, Comparative carcinogenicity in F344 rats and Syrian golden hamsters of *N'*-nitrosornicotine and *N'*-nitrosornicotine-1-*N*-oxide, *Cancer Lett.* 20 (1983) 333-340.
14. S.S. Hecht, Biochemistry, biology, and carcinogenicity of tobacco-specific N-nitrosamines, *Chem. Res. Toxicol.* 11 (1998) 559-603.
15. S.G. Carmella, S. Akerkar, S.S. Hecht, Metabolites of the tobacco-specific nitrosamine 4-(methylnitrosamino)-1-(3-pyridyl)-1-butanone in smokers' urine, *Cancer Res.* 53 (1993) 721-724.
16. S.S. Hecht, Human urinary carcinogen metabolites: biomarkers for investigating tobacco and cancer, *Carcinogenesis* 23 (2002) 907-922
17. P. Upadhyaya, P.M.J. Kenney, J.B. Hochalter, M. Wang, S.S. Hecht, Tumorigenicity and metabolism of 4-(methylnitrosamino)-1-(3-pyridyl)-1-butanol enantiomers and metabolites in the A/J mouse, *Carcinogenesis* 20 (1999) 157-1582.
18. S.S. Hecht, T.E. Spratt, N. Trushin, Absolute configuration of 4-(methylnitrosamino)-1-(3-pyridyl)-1-butanol formed metabolically from 4-(methylnitrosamino)-1-(3-pyridyl)-1-butanone, *Carcinogenesis* 18 (1997) 1851-1854.
19. S.S. Hecht, C.B. Chen, M. Dong, R.M. Orna, D. Hoffman, T.C. Tso, Chemical studies on tobacco smoke L1: studies on non-volatile nitrosamines in tobacco, *Beitrag zur Tabakforschung* 9 (1977) 1-6.
20. Y. Yang, C. Yu, M. Zhou, N. Pang, N. Li, H. Nie, J. Liao, Y. Bai, H. Liu, Metabolic study of 4-(methylnitrosamino)-1-(3-pyridyl)-1-butanone to the enantiomers of 4-(methylnitrosamino)-1-(3-pyridyl)-1-butanol in vitro in human bronchial epithelial cells using chiral capillary electrophoresis, *J. Chrom. A* 1218 (2011) 6505-6510.
21. S.G. Carmella, S.S. Hecht, High-performance liquid chromatographic analysis of metabolites of the nicotine-derived nitrosamines, *N'*-nitrosornicotine and 4-(methylnitrosamino)-1-(3-pyridyl)-1-butanone, *Anal. Biochem.* 145 (1985) 239-244.
22. J. Yang, S.G. Carmella, S.S. Hecht, Analysis of *N'*-nitrosornicotine enantiomers in human urine by chiral stationary phase liquid chromatography-nanoelectrospray ionization-high resolution tandem mass spectrometry, *J. Chrom. B* 1044-1055 (2017) 127-131.
23. S.G. Carmella, E.J. McIntee, M. Chen, S.S. Hecht, Enantiomeric composition of *N'*-nitrosornicotine and *N'*-nitrosoanatabine in tobacco, *Carcinogenesis* 21 (2000) 839-843.
24. J. Jiang, L. Li, M. Wang, J. Xia, W. Wang, X. Xie, Theoretical explanation of the peak splitting of tobacco-specific N-nitrosamines in HPLC, *Bull. Korean Chem. Soc.* 33 (2012) 1722-1728.
25. S.L. Abidi, Chromatographic investigations of the configurational and geometrical isomerism of allylic N-terpenyl-N-hydroxyethylnitrosamines, *J. Chrom. A* 288 (1984) 277-292.
26. D.A. Lightner, T.A. Wooldridge, A.F. McDonagh, Configurational isomerization of bilirubin and the mechanism of jaundice phototherapy, *Biochem. Biophys. Res. Commun.* 86 (1979) 235-43.
27. D.W. Armstrong, X. Wang, N. Ercal, Enantiomeric composition of nicotine in smokeless tobacco, medicinal products, and commercial reagents, *Chirality* 10 (1998) 587-591.

28. M.D. Aceto, B.R. Martin, I.M. Uwaydah, E.L. May, L.S. Harris, C. Izzola-Conde, W.L. Dewey, T.J. Bradshaw, W.C. Vincek, Optically pure (+)-nicotine from (+/-)-nicotine and biological comparisons with (-)-nicotine, *J. Med. Chem.* 22 (1979) 174-177.
29. D. Yildiz, N. Ercal, D.W. Armstrong, Nicotine enantiomers and oxidative stress, *J. Toxicol.* 130 (1998) 155-165.
30. D. Pogocki, T. Ruman, M. Danilczuk, M. Celuch, E. Walajtys-Rode, Application of nicotine enantiomers, derivatives and analogues in therapy of neurodegenerative disorders, *Eur. J. Pharmacol.* 563 (2007) 18-39.
31. G. Hellinghausen, J.T. Lee, C.A. Weatherly, D.A. Lopez, D.W. Armstrong, Evaluation of nicotine in tobacco-free-nicotine commercial products, *Drug Test. Analysis* 9 (2017) 944-948.
32. D.W. Armstrong, X. Wang, J.T. Lee, Y.S. Liu, Enantiomeric composition of nornicotine, anatabine, and anabasine in tobacco, *Chirality* 11 (1999) 82-84.
33. J. Hukkanen, P. Jacob, N.L. Benowitz, Metabolism and disposition kinetics of nicotine, *Pharm. Reviews.* 57 (2005) 79-115.
34. P. Jacob III, L. Yu, A.T. Shulgin, N.L. Benowitz, Minor tobacco alkaloids as biomarkers for tobacco use: comparison of users of cigarettes, smokeless tobacco, cigars, and pipes, *Am. J. Public Health* 89 (1999) 731-736.
35. L.P. Dwoskin, L. Teng, S.T. Buxton, A. Ravard, N. Deo, P.A. Crooks, Minor alkaloids of tobacco release [³H]dopamine from superfused rat striatal slices, *Euro. J. Pharm.* 276 (1995) 195-199.
36. S.T. Lee, K. Wildeboer, K.E. Panter, W.R. Kern, D.R. Gardner, R.J. Molyneux, C.W. Chang, F. Soti, J.A. Pfister, Relative toxicities and neuromuscular nicotinic receptor agonistic potencies of anabasine enantiomers and anabaseine, *Neurotoxicol. and Teratol.* 28 (2006) 220-228.
37. Food and Drug Administration, FDA's policy statement for the development of new stereoisomeric drugs, *Chirality* 4 (1992) 338-340.
38. H.-J. Kim, H.-S. Shin, Determination of tobacco-specific nitrosamines in replacement liquids of electronic cigarettes by liquid chromatography-tandem mass spectrometry, *J. Chrom. A* 1291 (2013) 48-55.
39. D.W. Armstrong, L.A. Spino, S.M. Han, J.I. Seeman, H.V. Secor, Enantiomeric resolution of racemic nicotine and nicotine analogues by microcolumn liquid chromatography with β -cyclodextrin inclusion complexes, *J. Chromatogr.* 411 (1987) 490.
40. Y. Tang, W.L. Zielinski, H.M. Bigott, Separation of nicotine and nornicotine enantiomers via normal phase HPLC on derivatized cellulose chiral stationary phases, *Chirality* 10 (1998) 364.
41. D.W. Armstrong, Y. Tang, S. Chen, Y. Zhou, C. Bagwill, J.R. Chen, Macrocyclic antibiotics as a new class of chiral selectors for liquid chromatography, *Anal. Chem.* 66 (1994) 1473-1484.
42. D.W. Armstrong, Y. Liu, K.H. Ekborgott, A covalently bonded teicoplanin chiral stationary phase for HPLC enantioseparations, *Chirality*, 7 (1995) 474-497.
43. K.H. Ekborg-Ott, J.P. Kullman, X. Wang, K. Gahm, L. He, D.W. Armstrong, Evaluation of the macrocyclic antibiotic avoparcin as a new chiral selector for HPLC, *Chirality* 10 (1998) 627-660.
44. A. Peter, E. Vekes, D.W. Armstrong, Effect of temperature on retention of chiral compounds on a ristocetin A chiral stationary phase, *J. Chrom. A*, 958, (2002) 89-107.
45. A. Feurcova, M. Vancova, J. Mydlova, J. Lehotay, J. Krupcik, D.W. Armstrong, Interconversion of oxazepam enantiomers during HPLC separation. Determination of thermodynamic parameters, *J. Liq. Chromatogr. Relat. Technol.* 29 (2006) 2889-2900.
46. C.L. Barhate, L.A. Joyce, A.A. Makarov, K. Zawatzky, F. Bernardoni, W.A. Schafer, D.W. Armstrong, C.J. Welch, E.L. Regalado, Ultrafast chiral separations for high throughput enantiopurity analysis, *Chem. Commun.* 53 (2016) 509-512.
47. M.P. Gasper, A. Berthod, U.B. Nair, D.W. Armstrong, Comparison and modeling study of vancomycin, ristocetin A, and teicoplanin for CE enantioseparations, *Anal. Chem.* 68 (1996) 2501-2514.
48. Neurath, G.B. Aspects of the oxidative metabolism of nicotine, *Clin. Investig.* 72 (1994) 190-195.
49. T.L. Nguyen, E. Dagne, L. Gruenke, H. Bhargava, N. Castagnoli Jr., The tautomeric structures of 5-hydroxycotinine, a secondary mammalian metabolite of nicotine, *J. Org. Chem.* 46 (1981) 758-760.

50. G.B. Neurath, M. Dunger, D. Orth, Detection and determination of tautomers of 5'-hydroxynicotine and 2-hydroxynicotine in smoker's urine, *Med. Sci. Res.* 20 (1992) 853-858
51. P.G. Haines, A. Eisner, Identification of pseudo-oxynicotine and its conversion to N-methylmyosmine, *J. Am. Chem. Soc.* 72 (1950) 1719-1721.
52. J.D. Adams, E.J. LaVoie, D. Hoffman, On the pharmacokinetics of tobacco-specific N-nitrosamines in Fischer rats, *Carcinogenesis* 6 (1985) 509-511.

Chapter 6

Mass Spectrometry-Compatible Enantiomeric Separations of 100 Pesticides Using Core–Shell Chiral Stationary Phases and Evaluation of Iterative Curve Fitting Models for Overlapping Peaks

6.1 Abstract

Pesticides are often chiral, and their isomers have different activity, toxicity, metabolism, and degradation properties. Perhaps, the most complex pesticides are the synthetic pyrethroid insecticides that have up to 8 stereoisomers, but not all are active. Pyrethroids are toxic to aquatic invertebrates and non-targeted species like honey bees since they persist in the environment. Extensive biological studies of the pyrethroid enantiomers are limited. Possibly, this is because liquid chromatography enantiomeric methods for these studies often have limitations with mass spectrometry (MS) compatibility. In this study, an effective methodology was developed with MS compatible solvents to evaluate several core-shell (superficially porous particle, SPP) chiral stationary phases (CSPs) for the enantiomeric separation of several classes of chiral pesticides. The CSP with the broadest selectivity or spectrum amongst all pesticide classes was the β -hydroxypropyl cyclodextrin (CDShell-RSP). The other CSPs (LarihcShell-P, NicoShell, Q-Shell, and TeicoShell) had more selective applications including separations of the pesticides with amine or acid functionalities. Overall, 74 of 100 pesticides were baseline separated. Most of the remaining, partially had multiple stereogenic centers and had only one overlapping pair. Several were evaluated with a convenient new peak area extraction protocol by iterative curve fitting. Most likely, this approach will lead to more significant enantiomeric analysis where MS is needed to overcome complex matrices and reduce extensive method optimization.

6.2 Introduction

Pesticides are substances used for controlling, preventing, or destroying animal, microbiological or plant pests [1]. Most commercial pesticides are synthetic and can be categorized by their activity as insecticides, rodenticides, fungicides, herbicides, etc. They are also commonly categorized by their

structures, including pyrethroids, organophosphates, acylanilides, triazole-related fungicides, imidazolidinones, and phenoxypropionic acid herbicides. Many are chiral and commercialized as racemic mixtures. However, their isomers have differences in terms of metabolism, toxicity, carcinogenicity, activity, etc. In the 1950s, R enantiomers of phenoxypropionic herbicides like dichlorprop and mecoprop were found to be more active than their respective S antipodes [2]. Their enantiomers also biodegrade differently [3]. One of the four isomers of the fungicide, triadimenol, was found to be 1000-fold more active than the other three [4]. These enantiomeric studies have led to more effective commercial pesticides with selected active isomers, a procedure analogous to a “chiral switch” in the pharmaceutical industry [5]. Also, it limits unnecessary pollution found in foods, beverages, and the environment [6-7]. While metabolism and risk to the environment have sometimes been assessed for individual pesticide enantiomers, less is known those with multiple chiral centers [8-10].

Perhaps, the most complex chiral pesticides are the pyrethroid insecticides, which commonly have two to eight stereoisomers [11]. Pyrethroids are popular due to their high specificity, activity, low toxicity to mammals, and UV-resistance compared to other insecticides such as organophosphates and natural pyrethrins (from *Chrysanthemum cinerariaefolium*) [11]. However, they persist, polluting the environment, specifically crops and small aquatic reservoirs [11]. Most are deadly to aquatic species, especially bottom-feeder scavenger fish and other non-target organisms like honey bees and butterflies [12-15]. Their enantiomers are likely to have different effects on non-target organisms. In general, the *cis*-isomers of pyrethroids are more toxic than the *trans*-isomers [11]. However, trends are not as general for the pyrethroid's various S and R configurations. For example, 1R-*cis*-permethrin and 1S-*cis*-fenvalerate have the highest acute toxicity compared to their other three respective stereoisomers [12-13]. These studies might be important to the continual prevention of insecticidal diseases, like malaria [16]. Recently, pyrethroid resistance has increased, which has led to new pyrethroid-based interventions [16]. Therefore, with adequate enantiomeric analysis new pyrethroid stereochemical properties could be thoroughly understood so the applications could be more effective and environmentally friendly.

Enantiomeric pesticide analysis is commonly performed by LC for high sensitivity and GC, but GC might not be best to study enantiomeric properties since pesticide enantiomers are susceptible to isomerization and epimerization at elevated temperatures [17-18]. With LC, the most commonly reported enantiomeric pesticide separations utilized π -complex-type, cellulose and/or amylose-based chiral stationary phases (CSPs), while some are performed by cyclodextrin-based CSPs [19-26]. Some approaches used reversed phase solvents, which has led to enantiomeric studies of some triazole fungicides with two to four stereoisomers [23-24]. However, for other pesticides (up to 8 stereoisomers) normal phase solvents and multiple CSPs coupled in tandem usually were required [19-22]. Recently, improved methodologies utilize core-shell or superficially porous particle (SPP) CSPs to increase efficiency and shorten analysis times [27-32]. Also, they are compatible with mass spectrometry (MS) detection, which is especially significant when sensitive pesticide analysis is needed, using new MS techniques like paired-ion electrospray ionization (PIESI) [33]. We effectively utilized screening and optimization methodologies for 100 chiral pesticides with 6 SPP CSPs; hydroxypropyl- β -cyclodextrin (CDShell-RSP), isopropyl-cyclofructan 6 (LarihcShell-P), a quinine-based CSP (Q-Shell), and three macrocyclic glycopeptides (NicoShell, TeicoShell, and VancoShell) [27-32, 34-36].

Since some complex chiral pesticides required extensive method optimization for baseline separation of all isomers, and usually just had one overlapped pair, iterative curve fitting was found to recover the overlapping peak areas. Deconvolution techniques are usually utilized to remove band broadening and other distortions but can be used to determine areas of overlapped peaks with errors less than or comparable to other peak integration methods [37-40]. Commercial software is available for curve fitting, but it can now be performed using ubiquitous Excel [41]. Often, these methods are used for separations from complex matrices, as in omics-related fields [40-41]. More recently, they have been utilized in ultra-fast chiral chromatography and highly accurate enantiomeric fraction analysis of pesticides [42-44]. The protocol utilized in this study is thoroughly described.

6.3 Experimental

6.3.1 Chemicals and materials

(R,S)-hydroxypropyl- β -cyclodextrin (CDShell-RSP, RSP), teicoplanin (TeicoShell, TS), modified macrocyclic glycopeptide (NicoShell, NS), vancomycin (VancoShell, VS), quinine-based (Q-Shell, QS), isopropyl-cyclofructan 6 (LarihcShell-P, LSP) were obtained as 2.7 μ m core-shell (superficially porous particles) 100 x 4.6 mm (i.d.) and 150 x 4.6 mm (i.d.) columns from AZYP, LLC. (Arlington, TX, USA). The packing procedure of the 150 x 4.6 mm (i.d.) CDShell-RSP column was slightly modified, especially for the pyrethroids with multiple stereogenic centers. Analytes were purchased as racemic standards from Sigma-Aldrich (St. Louis, MO, USA), Toronto Research Chemicals (Toronto, CN), and LKT Laboratories Inc (Minneapolis, MN, USA). Racemic standards were prepared with methanol at 1 mg/mL for analysis. Solvents and additives including HPLC grade acetonitrile (ACN), methanol (MeOH), ethanol (EtOH), isopropyl alcohol (IPA), tetrahydrofuran (THF), hexane (Hex), *tert*-butyl methyl ether (MTBE), acetic acid (HOAc), trifluoroacetic acid (TFA), trimethylamine (TEA), formic acid (FA), and ammonium formate (NH₄HCO₂) were obtained from Sigma-Aldrich (St. Louis, MO, USA). Water was purified by a Milli-Q water purification system (Millipore, Billerica, MA, USA).

6.3.2 Chromatographic conditions

An Agilent 1260 (Agilent Technologies, Palo Alto, CA, USA) HPLC was used for all studies. It consisted of a 1200 diode array detector, autosampler, and quaternary pump. The mass spectrometer used in this study was a Shimadzu triple quadrupole liquid chromatography-mass spectrometry (LC-MS) instrument, LCMS-8040, (Shimadzu, Tokyo, Japan). All MS was operated in positive ion mode with an electron spray ionization source. The parameters were set as follows: nebulizer gas flow, 3 L/min; drying gas flow, 15 L/min; desolvation line temperature, 250 °C; heat block temperature, 400 °C. Multiple UV wavelengths, 220, 230, and 254 nm were utilized for detection and identification of enantiomers. Most separations were carried out at 25 °C, unless otherwise noted, using an isocratic method. Mobile phases were degassed by ultrasonication under vacuum for 5 minutes. Each analyte was screened in polar ionic mode (PIM), polar organic mode (POM), reversed phase (RP), and normal phase (NP) following previous

protocols [26-30,32-34]. The optimized conditions as labeled in Table 1 were: PIM1(a,b,c,d): 100:(0.5,0.2,0.1,0.025) MeOH:NH₄HCO₂ (v/w), PIM2: 100:0.2:0.05, MeOH:HOAc:NH₄OH (v/v/v), POM1: 60:40:0.3:0.2, ACN:MeOH:HOAc:TEA (v/v/v/v), RP1(a,b,c,d): (90:10,60:40,40:60,30:70), MeOH:16 mM NH₄HCO₂ pH 3.6 (v/v), RP1(e): 30:70, MeOH:48 mM NH₄HCO₂ pH 3.6 (v/v), RP2(a,b,c,d,e,f): (30:70,25:75,20:80,15:85,10:90,5:95), ACN:16 mM NH₄HCO₂ pH 3.6 (v/v), RP2(g): 20:80, ACN:48 mM NH₄HCO₂ pH 3.6 (v/v), RP2(h): 20:80:0.005, ACN:16 mM NH₄HCO₂ pH 3.6: MTBE (v/v/v), RP2(i): 15:85, ACN:48 mM NH₄HCO₂ pH 3.6 (v/v), RP3(a,b,c): (40:60,35:65,20:80), EtOH:16 mM NH₄HCO₂ pH 3.6 (v/v), RP4(a,b): (30:70,20:80) IPA:16 mM NH₄HCO₂ pH 3.6 (v/v), RP5: 10:90, THF:16 mM NH₄HCO₂ pH 3.6 (v/v), NP1: 95:5, Hex:IPA (v/v), NP2: 90:10, Hep:EtOH (v/v), NP3: 90:10:0.3:0.2, Hep:IPA:TFA:TEA (v/v/v/v), NP4: 70:30:0.3:0.2, Hex:EtOH:TFA:TEA (v/v/v/v).

6.3.3 Data processing

The dead time, t_0 , was determined by the peak of the refractive index change due to the unretained sample solvent. Retention factors (k) were calculated using $k = (t_R - t_0) / (t_0)$, where t_R is the retention time of the first peak and t_0 , the dead time of the column. Selectivity (α) was calculated using $\alpha = k_2 / k_1$, where k_1 and k_2 are retention factors of the first and second peaks, respectively. Resolution (R_s) was calculated using the peak width at half peak height, $R_s = 2(t_{R2} - t_{R1}) / (w_1 + w_2)$. Iterative curve fitting was performed with PeakFit version 4.12 (SeaSolv Software Inc. 1999-2003). See Results and Discussion and Supplemental material for the curve fitting protocol.

6.4 Results and discussion

Core-shell CSPs were clearly applicable for the enantiomeric separation of chiral pesticides, as shown with all isomers of 74 pesticides baseline separated ($R_s > 1.5$) with at least one CSP (Table 1).

Chapter 6 Table 1. Optimized enantiomeric separations 100 chiral pesticides.

Name ¹	# Isomers ¹	CSP ²	Mobile Phase ³	F,T ⁴	k _i ^{5a}	α ^{5b}	R _s ^{5c}
2-(2-Chlorophenoxy)propionic acid	2	QS ¹⁰	PIM2	0.5, 25	2.1	1.15	2.4
		TS ¹⁰	PIM1b	1.0, 25	0.2	2.49	2.2
2-(3-Chlorophenoxy)propionic acid	2	QS ¹⁰	PIM2	0.5, 25	1.5	1.15	2.1
		TS ¹⁰	PIM1b	1.0, 25	0.2	1.76	1.8
		RSP ¹⁰	RP2e	0.5, 25	2.2	1.09	1.5
2-(4-Chlorophenoxy)propionic acid	2	QS ¹⁰	PIM2	0.5, 25	1.6	1.13	1.9
		TS ¹⁰	PIM1b	1.0, 25	0.2	3.13	2.5
		RSP ¹⁵	RP2f	0.8, 25	9.6	1.06	1.5
2-Phenoxypropionic acid	2	QS ¹⁰	PIM2	0.5, 25	1.6	1.13	2.0
		TS ¹⁰	PIM1b	1.0, 25	0.2	2.39	2.1
Allethrin	8	RSP ¹⁵	RP2a	0.8, 25	1.9	1.04	0.7
					2.2	1.16	2.8
					2.8	1.18	3.0
					4.4	1.52	9.0
Anabasine	2	NS ¹⁰	PIM1b	1.0, 45	3.0	1.16	2.8
		VS ¹⁰	POM1	1.0, 45	3.2	1.21	2.6
Anatabine	2	NS ¹⁰	PIM1a	1.0, 45	1.1	1.45	5.2
		VS ¹⁰	RP1	1.0, 25	2.0	1.18	2.9
Ancymidol	2	RSP ¹⁰	RP2b	0.5, 25	2.1	1.12	1.5
Benalaxyl	2	RSP ¹⁰	RP2a	1.0, 25	0.6	1.36	2.4
Benoxacor	2	RSP ¹⁵	RP2a	0.8, 25	0.6	1.31	2.8
Bifonazole	2	RSP ¹⁵	RP1b	0.5, 25	7.1	1.08	1.4
Brodifacoum	4	QS ¹⁰	PIM2	0.5, 25	2.2	1.17	2.5
					4.2	1.78	9.0
Bromacil	2	VS ¹⁰	RP1d	0.5, 25	2.8	1.15	1.9
		TS ¹⁰	RP1d	0.5, 25	2.0	1.20	2.5
Bromuconazole	4	RSP ¹⁵	RP2a	0.8, 25	2.1	1.65	9.0
					2.8	1.07	1.5
Butoconazole	2	RSP ¹⁵	RP2c	0.5, 25	8.6	1.06	1.5
Carfentrazone	2	QS ¹⁰	PIM2	0.5, 25	2.3	1.15	2.5
Carfentrazone-ethyl	2	QS ¹⁰	RP1d	0.5, 25	1.4	1.33	2.0
		RSP ¹⁵	RP2a	0.8, 25	0.5	1.16	1.5
Chlorfenprop-methyl	2	RSP ¹⁵	RP2a	0.8, 25	1.6	1.05	1.0
Chlorflurenol-methyl	2	RSP ¹⁵	RP3c	0.5, 25	2.5	1.31	4.0
Cloquintocet-mexyl	2	RSP ¹⁵	RP2	0.5, 25	0.9	1.21	2.0
Closantel	2	LSP ¹⁰	NP3	0.8, 25	2.1	1.18	2.0
Coumachlor	2	NS ¹⁰	NP4	1.0, 25	0.8	1.42	1.8
		TS ¹⁰	RP2a	1.0, 25	1.5	1.32	2.4
Coumatetralyl	2	QS ¹⁰	PIM1c	1.0, 25	0.8	1.28	2.3
Cycloprothrin	4	RSP ¹⁵	RP1b	0.8, 25	1.7	1.07	1.4
					2.1	1.13	2.0
Cyfluthrin	8	RSP ¹⁵	RP1b	0.5, 25	1.5	1.05	0.9
					1.5	1.14	2.4
					1.9	1.12	3.3
					2.0	1.04	1.0
Cypermethrin	8	RSP ¹⁵	RP1b	0.5, 25	3.2	1.02	0.3
					3.2	1.29	1.9
					3.6	1.07	0.7
					4.2	1.07	0.9
Cyproconazole	4	RSP ¹⁵	RP2c	0.5, 10	3.4	1.19	3.0
					3.8	1.46	6.7
Dichlorprop	2	QS ¹⁰	PIM1c	1.0, 25	0.3	1.35	2.3
		TS ¹⁰	PIM1b	1.0, 25	0.2	3.17	3.3
Diclofop	2	QS ¹⁰	PIM2	0.5, 25	2.0	1.18	2.8
		TS ¹⁰	PIM1b	1.0, 25	0.2	2.93	4.0
Diclofop-methyl	2	RSP ¹⁰	RP2a	0.7, 25	2.6	1.09	1.5
Diniconazole	2	QS ¹⁰	RP1d	0.5, 25	2.5	1.14	1.5
		RSP ¹⁰	RP2b	0.5, 25	2.8	1.09	1.5
Dinoseb	2	RSP ¹⁵	RP2d	0.8, 25	5.3	1.07	1.5
Dinotefuran	2	TS ¹⁰	PIM1c	1.0, 25	0.6	1.13	1.0
Dyfonate	2	RSP ¹⁵	RP2a	0.8, 25	2.7	1.04	0.9
Econazole	2	RSP ¹⁰	RP2a	0.7, 25	0.9	1.17	1.6
Enilconazole	2	RSP ¹⁰	RP2a	1.0, 25	0.5	1.26	1.9

EPN	2	RSP ¹⁵	RP2a	1.0, 25	3.6	1.09	2.1
<i>cis</i> -Epoxiconazole	2	RSP ¹⁰	RP2a	1.0, 25	0.9	1.19	1.8
Etaconazole	4	RSP ¹⁵	RP1b	0.5, 25	1.6 2.0	1.21 1.15	4.7 2.8
Ethofumesate	2	RSP ¹⁵	RP2e	1.0, 25	11.6	1.07	1.5
Etoazole	2	RSP ¹⁵	RP1b	0.5, 25	6.4	1.31	1.5
Famoxadone	2	LSP ¹⁰	NP1	1.0, 25	7.0	1.39	4.5
Fenamiphos	2	RSP ¹⁵	RP2a	1.0, 25	2.6	1.10	1.9
Fenarimol	2	TS ¹⁰	NP2	0.8, 25	1.7	1.14	2.0
Fenarimol	2	RSP ¹⁵	RP2a	0.8, 25	2.5	1.04	0.9
Fenbuconazole	2	RSP ¹⁵	RP4b	0.5, 25	6.9	1.04	0.8
Fenobucarb	2	RSP ¹⁵	RP2d	0.8, 25	6.5	1.07	1.5
Fenoprop	2	TS ¹⁰	RP1d	0.5, 45	1.0	1.29	1.9
Fenoxanil	4	RSP ¹⁵	RP3c	0.8, 25	2.9 3.2	1.08 1.04	1.3 0.7
Fenoxaprop	2	QS ¹⁰	PIM2	0.5, 25	2.0	1.12	2.0
Fenoxaprop	2	TS ¹⁰	PIM1b	1.0, 25	0.2	3.16	2.9
Fenoxaprop ethyl	2	RSP ¹⁵	RP1b	0.5, 25	1.6	1.03	0.5
Fenpropathrin	2	RSP ¹⁵	RP4a	0.5, 25	1.2	1.08	1.0
Fenvalerate	4	RSP ¹⁵	RP1b	0.5, 25	2.0 2.2	1.04 1.12	0.9 2.5
Fipronil	2	LSP ¹⁰	NP1	1.0, 25	5.3	1.24	3.7
Flucythrinate	4	RSP ¹⁵	RP1b	0.5, 25	1.7 1.9	1.07 1.10	1.3 1.5
Fluroxypyr-1-methylheptyl ester	2	RSP ¹⁰	RP2b	0.5, 25	1.6	1.15	1.5
Flurprimidol	2	RSP ¹⁵	RP2a	1.0, 25	1.6	1.10	1.5
Flutriafol	2	RSP ¹⁰	RP2a	0.5, 25	0.7	1.17	1.5
Furalaxyl	2	VS ¹⁰	RP1d	0.5, 25	5.1	1.08	0.8
Haloxypop	2	TS ¹⁰	PIM1b	1.0, 25	0.1	4.03	2.4
Haloxypop-methyl	2	RSP ¹⁵	RP1b	0.5, 25	1.3	1.06	0.7
Hexaconazole	2	RSP ¹⁰	RP2a	1.0, 25	1.1	1.34	2.3
Imazaquin	2	TS ¹⁰	RP1e	0.5, 25	3.7	1.07	0.7
Isocarbofos	2	RSP ¹⁵	RP3c	0.5, 25	1.9	1.11	1.6
Isofenfos-methyl	2	RSP ¹⁵	RP2f	0.5, 25	3.9	1.06	0.9
<i>cis</i> -Ketoconazole	2	RSP ¹⁵	RP2h	0.8, 25	2.5	1.11	1.5
Mandipropamid	2	TS ¹⁰	RP1e	0.5, 45	2.8	1.10	1.7
Mecoprop	2	QS ¹⁰	PIM2	0.5, 25	1.4	1.20	2.8
Mecoprop	2	TS ¹⁰	PIM1b	1.0, 25	0.1	2.88	2.4
Mecoprop methyl ester	2	NS ¹⁰	RP1d	0.5, 25	6.8	1.17	2.2
Mecoprop methyl ester	2	VS ¹⁵	RP1e	0.5, 45	3.2	1.07	1.5
Metconazole	4	RSP ¹⁵	RP2h	0.8, 25	3.3 3.8	1.09 1.16	1.9 3.5
Miconazole	2	RSP ¹⁰	RP2a	0.7, 25	0.9	1.17	1.7
Mitotane	2	RSP ¹⁵	RP2a	0.8, 25	2.1	1.04	0.6
Myclobutanil	2	RSP ¹⁵	RP1c	0.5, 25	2.2	1.06	1.2
Napropamide	2	VS ¹⁰	RP1a	0.3, 25	0.1	1.86	1.5
Napropamide	2	TS ¹⁰	RP1e	1.0, 45	2.4	1.14	1.8
Nicotine	2	NS ¹⁰	PIM1b	1.5, 45	0.5	1.60	3.0
N-methylanabasine	2	NS ¹⁰	PIM2	1.0, 25	1.9	1.24	2.5
N-methylanabasine	2	VS ¹⁰	PIM1b	0.5, 25	1.3	1.38	3.2
Nornicotine	2	NS ¹⁰	PIM1a	1.0, 45	2.7	1.14	2.3
Nornicotine	2	VS ¹⁰	PIM1d	0.7, 45	4.1	1.10	1.5
<i>rac</i> -(2R,3R)-Paclobutrazol	2	RSP ¹⁵	RP2g	1.0, 25	3.2	1.09	1.8
Penconazole	2	RSP ¹⁵	RP2b	0.8, 25	2.6	1.07	1.5
Pentachlor	2	RSP ¹⁵	RP3c	0.5, 25	8.1	1.04	0.6
Penthiopyrad	2	RSP ¹⁵	RP3c	0.5, 25	4.4	1.13	2.1
Permethrin	4	RSP ¹⁵	RP3a	0.4, 25	4.2 5.6	1.14 1.02	2.0 0.5
d-Phenothrin	2	RSP ¹⁵	RP2a	0.8, 25	4.7	1.53	5.6
Phenthoate	2	RSP ¹⁰	RP2b	0.5, 25	1.5	1.14	1.7
(1 <i>R</i> ;cis;trans;S)-Prallethrin	2	RSP ¹⁵	RP2a	0.8, 25	2.2	1.57	9.0
Praziquantel	2	RSP ¹⁵	RP2g	0.7, 45	2.3	1.11	1.5
Praziquantel	2	TS ¹⁰	RP5	0.8, 25	12.3	1.15	2.0
Propiconazole	4	RSP ¹⁵	RP3b	0.5, 25	1.8 2.6	1.19 1.13	2.0 1.5
Prothioconazole	2	RSP ¹⁰	RP2a	1.0, 25	1.5	1.18	2.2

Quizalofop ethyl	2	RSP ¹⁵	RP2i	1.0, 25	7.4	1.05	0.9
Resmethrin	4	RSP ¹⁵	RP4a	0.5, 25	2.4	1.04	0.7
					3.1	1.31	4.5
Ruelene (Cruformate)	2	NS ¹⁰	RP2b	1.0, 25	3.6	1.09	1.6
rac-(2R)-Spiroxamine	2	QS ¹⁰	NP1	1.0, 25	0.3	1.54	1.5
Sulprofos	2	RSP ¹⁵	RP1b	0.5, 25	2.3	1.08	1.8
Tebuconazole	2	RSP ²⁵	RP5	0.5, 25	4.4	1.07	1.5
Tetramethrin	4	RSP ¹⁵	RP4a	0.5, 25	0.9	1.08	0.8
					1.8	1.33	3.0
Tetramisole	2	NS ¹⁰	PIM2	0.7, 25	3.5	1.13	2.1
Triadimefon	2	RSP ¹⁵	RP2a	0.8, 25	1.4	1.09	1.5
Triadimenol	4	RSP ¹⁵	RP2c	0.5, 25	1.5	1.44	5.7
					2.3	1.06	1.6
Triticonazole	2	RSP ¹⁵	RP2b	0.8, 25	4.3	1.09	1.5
<i>E</i> -Uniconazole	2	RSP ¹⁵	RP2a	1.0, 25	2.2	1.08	1.5
Warfarin	2	NS ¹⁰	RP2a	1.0, 25	4.4	1.11	1.7
		TS ¹⁰	RP2a	1.0, 25	1.1	1.29	2.3
		VS ¹⁰	RP2a	1.0, 25	4.3	1.19	2.0

¹ Pesticide name and number of isomers, see Experimental for more information.

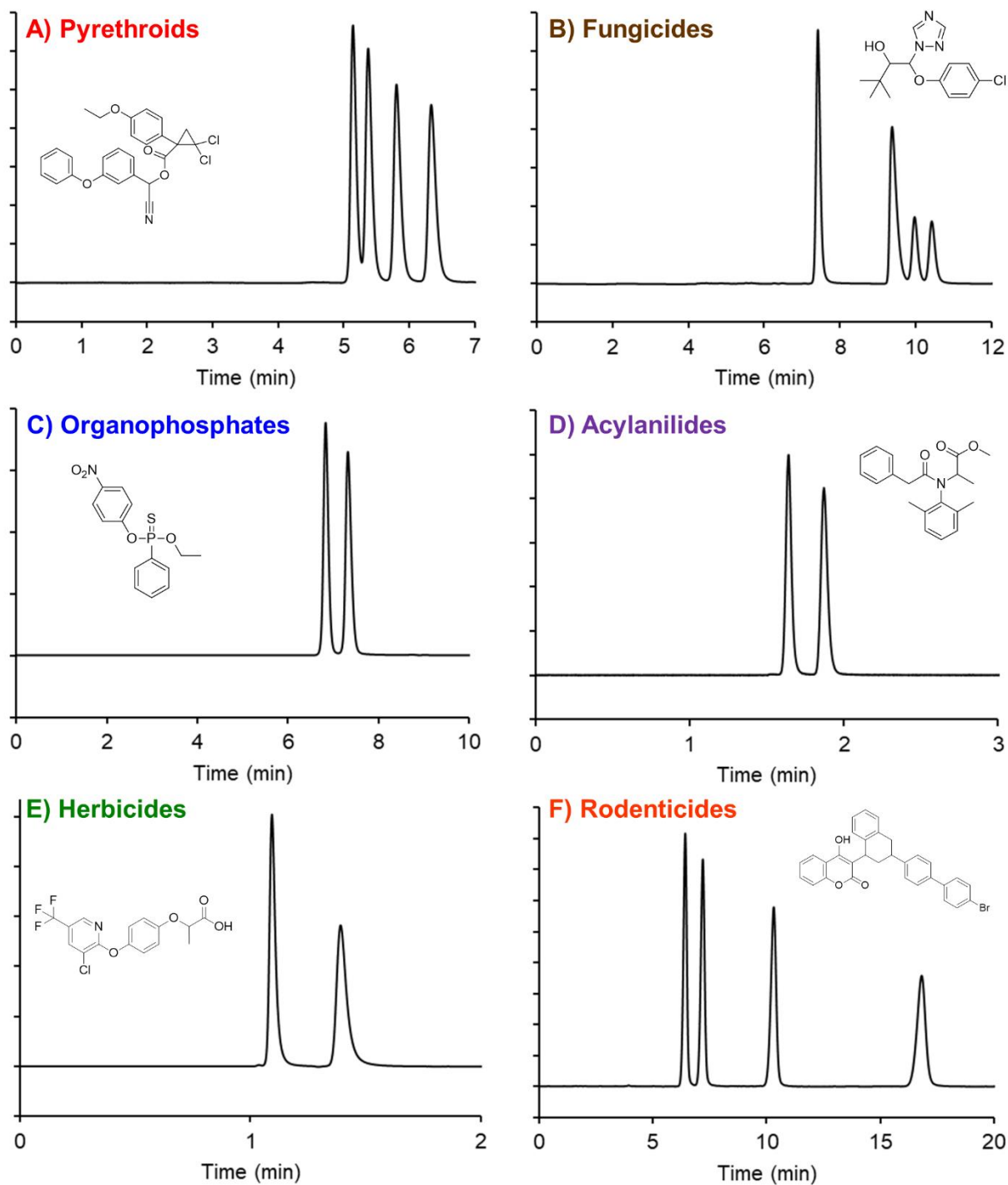
² Chiral stationary phase (CSP) with length in cm denoted in superscript (all 0.46 cm (i.d.)), ¹⁰: 10 cm x 0.46 cm (id), ¹⁵: 15 cm x 0.46 cm (id), ²⁵: 10 x 0.46 cm (id) coupled to 15 x 0.46 cm (id). These include CDShell-RSP (RSP), NicoShell (NS), TeicoShell (TS), VancoShell (VS), LarihcShell-P (LSP) and Q-Shell (QS). See Experimental for more information.

³ See experimental for optimized mobile phases and acronyms.

⁴ Flow (F) in mL/min / Temperature (T) in ° C.

^{5a,b,c} Calculated chromatographic parameters of retention factor of the first peak (k_1), selectivity (α), and resolution (R_s). See Experimental for more information.

Further, 18 compounds were baseline separated with two or more CSPs, and three compounds with 3 CSPs. Most pesticides required little optimization to provide $R_s > 1.5$, but different alcohols and salt concentrations were used to improve efficiency and/or selectivity. Most separations were performed in under ten minutes, and many compounds contained more than two stereoisomers. In Table 1, the selectivity and resolution are reported for each enantiomeric pair. The partial separations that could not be optimized to baseline without extensive optimization are not shown in Table 1. However, a partial separation with one chiral selector was often brought to baseline with one of the other related selectors, demonstrating the principle of complementary separations [31]. If there were one or more critical pairs that could not be baseline separated without extensive optimization the iterative curve fitting procedure was utilized. Overall, 69 pesticides were separated by CDShell-RSP, 19 by TeicoShell, 14 by Q-Shell, ten by NicoShell, nine by VancoShell, and three by LarihcShell-P. Representative chromatograms of each pesticide class separated by different CSPs are shown in Fig. 1, which will be discussed in subsequent sections.

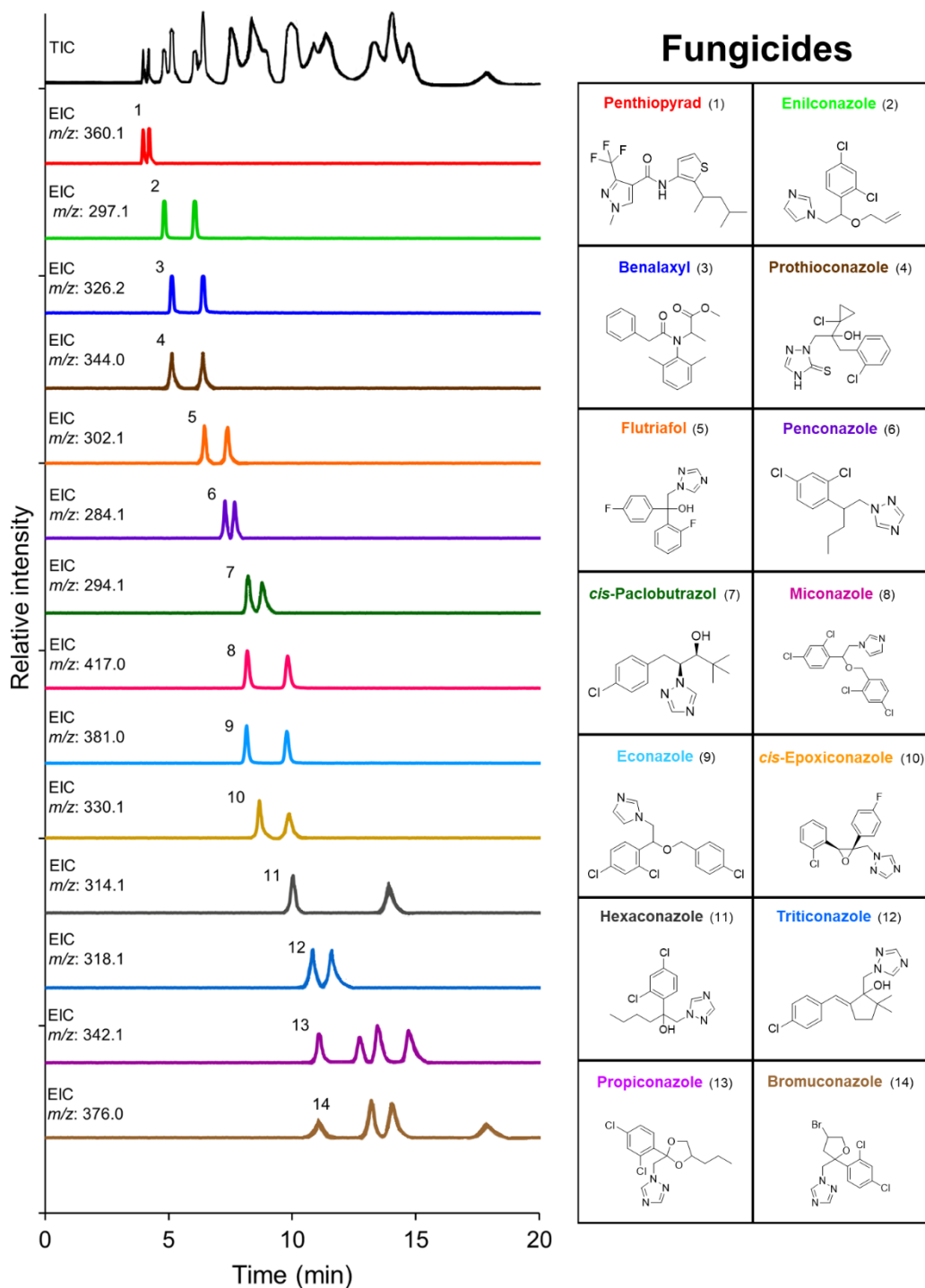


Chapter 6 Figure 1. Optimized enantiomeric separations of pesticides from Table 1 indicative of their class. Enantiomeric separations of **A)** cycloprothrin, **B)** triadimenol, **C)** EPN, **D)** benalaxyl, **E)** haloxyfop, **F)** brodifacoum by **A-D)** CDShell-RSP, **E)** TeicoShell, **F)** Q-Shell. All conditions are listed in Table 1.

6.4.1 Broad spectrum of enantioselectivity by CDShell-RSP

CDSHELL-RSP had the broadest selectivity, enough to achieve $R_s > 1.5$, for all pesticide classes and in the reversed phase mode. A representative chromatogram of the pyrethroid class of compounds is shown in Fig. 1A for cycloprothrin, which has four stereoisomers. Most pyrethroids, including permethrin, resmethrin, and tetramethrin produced similar results. Allethrin, which has eight stereoisomers, provided the best example of a critical overlapping pair, in which all other 6 isomers were easily baseline separated. In the past, β -cyclodextrin has been used for the separation of allethrin but had much less resolution, which shows the power of the current core-shell CSPs [24]. Other pyrethroids with eight stereoisomers, like cyfluthrin and cypermethrin, were less resolved than allethrin, with more than one overlapping pair. The area extraction of these overlapped peaks will be discussed in a subsequent section and reported in Table 2.

The most powerful application of CDSHELL-RSP was for chiral fungicides (Fig. 1B). In Figure 2, the universal nature of the CDSHELL-RSP for chiral fungicides was highlighted with the simultaneous LC-MS enantiomeric separation of 14 chiral fungicides in 20 minutes.



Chapter 6 Figure 2. Simultaneous enantiomeric separation of 14 racemic fungicides using liquid chromatography electrospray ionization mass spectrometry (LC-ESI-MS). Total ion chromatogram (TIC) and extracted ion chromatograms (EICs) are shown. Conditions: CDSshell-RSP, 150 x 4.6 mm (i.d.), ACN-NH₄HCO₂ (pH 3.6, 16 mM) (25:75), 0.8 mL/min, 25 °C. See Experimental for more information.

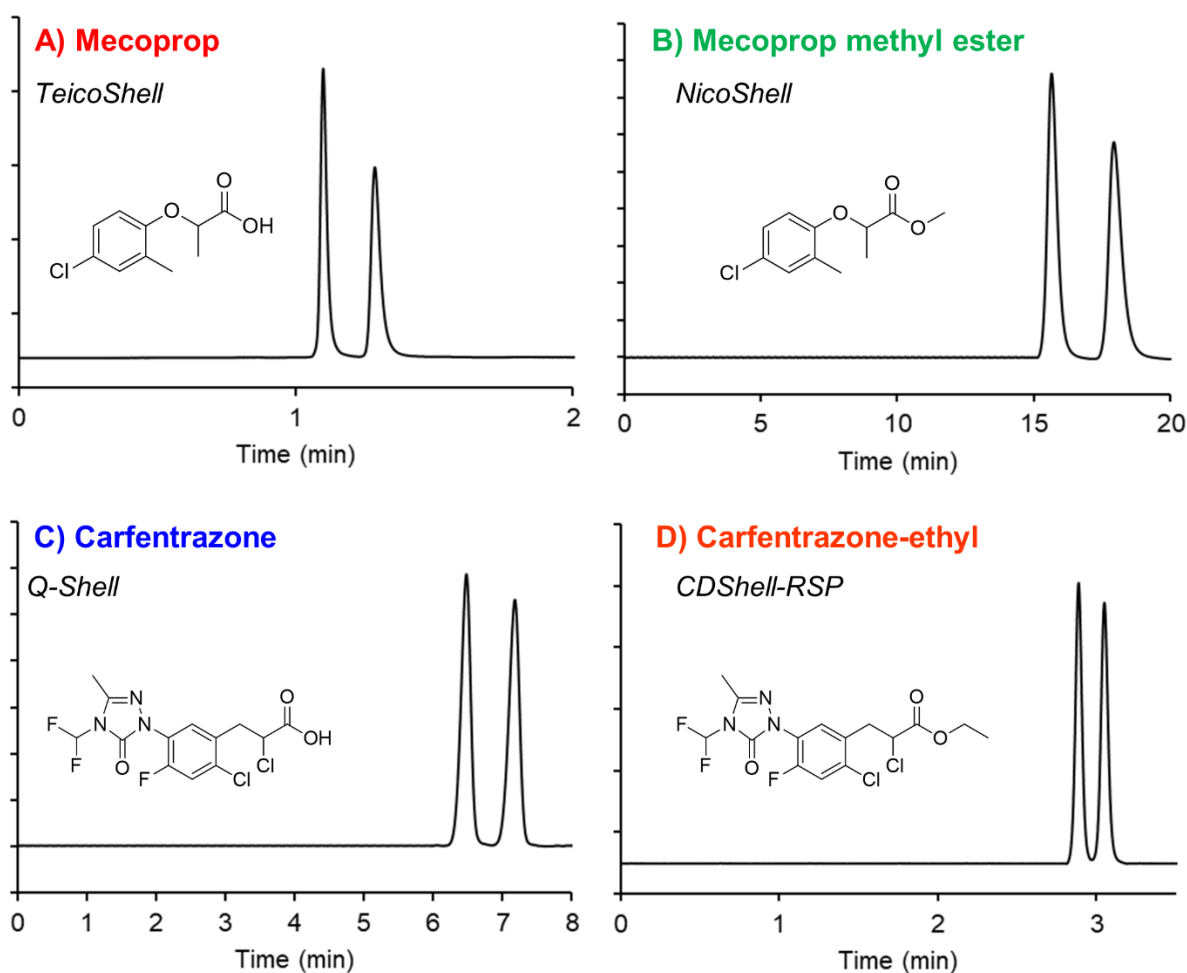
This LC-MS approach would allow the simultaneous investigation of 32 fungicide enantiomers in foods, beverages, and any number of biological systems. Many of these are triazole fungicides that have up to 4 isomers, including bromuconazole and propiconazole (Fig. 2). Others with four stereoisomers which required different mobile phase compositions included cyproconazole and triadimenol (Table 1). Etaconazole and metconazole were baseline separated, except for one overlapping pair, which will be discussed in sec. 3.3 (Table 2). CDShell-RSP also had high selectivity for the topical anti-fungal pesticides like miconazole and econazole (Fig. 2 and Table 1). Other baseline separated fungicides included the recently commercialized carboxamide, penthiopyrad, and the dicarboximide, famoxadone (Table 1).

CDShell-RSP also had selectivity for most organophosphates that had phosphorous stereogenic centers as shown in Fig. 1C. Some partially resolved organophosphates were ruelene (crufomate) and fenamiphos, which were baseline separated by other core-shell CSPs (Table 1). Also, the acylanilide, benalaxyl was easily baseline separated by CDShell-RSP (Fig. 1D), but others like mandipropamid and napropamide were best separated by other core-shell CSPs. An acaricide, etoxazole, and an imidazolidinone, bifonazole, were separated by CDShell-RSP (Table 1). Herbicides and their associated safeners [45], as well as other plant growth regulators without acidic functionalities, such as benoxacor, chlorfenprop-methyl, chlorflurenol-methyl, cloquintocet-mexyl, diclofop-methyl, and flupiridimol were baseline separated by CDShell-RSP. Herbicide metabolites, like the phenoxypropionic acid herbicides, were better separated by other core-shell CSPs, like TeicoShell and Q-Shell. Overall, these results indicate that CDShell-RSP had the broadest selectivity amongst the tested pesticide classes. Complementary separations of a chiral herbicide and a rodenticide with two stereogenic centers by other core-shell CSPs are shown in Figs. 1E and 1F.

6.4.2 Specific enantioselectivity by other core-shell CSPs

Some SPP CSPs had more specific enantioselectivity amongst the pesticide classes compared to CDShell-RSP. TeicoShell and Q-Shell had the highest selectivity for the phenoxypropionic acid herbicides, like

haloxyfop (Fig. 1E). This is not surprising as teicoplanin and quinine have amine groups, which can interact with acidic moieties of the analytes [32,34]. Usually, these separations were performed in polar ionic mode, with methanol and a volatile salt. Phenoxypropionic acid herbicides were almost always separated with $1.5 < R_s < 4.0$ within 1-2 min using TeicoShell. Under environmental conditions, these herbicides are formed as metabolites via hydrolysis from phenoxypropionate herbicide derivatives [10]. The phenoxypropionate herbicides, like mecoprop methyl ester and carfentrazone-ethyl, were found to separate better by other CSPs, including NicoShell and CDSHell-RSP (Fig. 3).



Chapter 6 Figure 3. Enantiomeric separation trends of phenoxypropionate herbicides and their phenoxypropionic acid metabolites **A)** Enantiomeric separations of mecoprop, a phenoxypropionic metabolite of **B)** mecoprop methyl ester using TeicoShell and NicoShell. **C)** Enantiomeric separations of carfentrazone, a triazolone herbicide metabolite of **D)** carfentrazone-ethyl, using Q-Shell and CDSHell-RSP. See Table 1 for conditions.

Another class of pesticides with high selectivity using TeicoShell or Q-Shell were the rodenticides (Fig. 1E). First-generation anticoagulants, coumachlor and warfarin, were best separated using macrocyclic glycopeptide-based CSPs like TeicoShell, as expected (Table 1) [23,34-35]. Brodifacoum, a newer anticoagulant meant for larger rodents is a much larger molecule than older generation rodenticides and has 4 stereoisomers. Brodifacoum had no selectivity with TeicoShell and was partially separated by CDShell-RSP. It was best separated by Q-Shell as shown in Fig. 1E. Q-Shell was also the only CSP to baseline separate coumatetralyl (Table 1). However, Q-Shell had no selectivity for coumachlor and warfarin. Extensive enantiomeric methods have not been published with Q-Shell, but it seems that it has high selectivity for phenoxypropionic acids, and complementary behavior with TeicoShell for larger rodenticides.

The other macrocyclic glycopeptide-based CSPs, VancoShell and NicoShell, were most useful to separate chiral pesticides with amine functionalities, like the tobacco-based insecticides (Table 1). NicoShell was the only CSP that baseline separated the anti-fungal tetramisole and the organophosphate ruelene (crufomate) (Table 1). VancoShell was the only CSP that had selectivity for the acylanilide furalaxyl. A partial separation, which was only achieved by TeicoShell, was the neonicotinoid dinotefuran (Table 1). Since neonicotinoids have extreme toxicity towards honey bees, perhaps TeicoShell should be further evaluated for other chiral neonicotinoid separations, especially those with undetermined enantiomeric properties [14].

Perhaps, the most interesting pesticide separations were those by the isopropyl-cyclofructan 6, LarihcShell-P. This derivatized cyclofructan is best known for separating primary amines, which explains the separation of fipronil [31,36]. However, it has also been reported to separate other non-primary amines, like Tröger's base [36]. Further evidence of non-primary amine enantiomeric selectivity was observed with the separations of closantel and famoxadone (Table 1). These separations were only achieved in normal phase solvents, but no other CSP could baseline separate closantel (Table 1). This

shows that this chiral selector has broader enantioselectivity, not just for primary amines but also for neutral compounds.

6.4.3 Area extraction of overlapped peaks using iterative curve fitting

Out of the 100 pesticides, 26 were partially resolved, but many like cycloprothrin (Fig. 2A) had multiple enantiomers that were all baseline separated except for one pair of overlapping peaks. Instead of spending extensive time working on method development, iterative curve fitting was used to determine their overlapped peak areas (see Table 2). The subsequent protocol was followed and is illustrated with two examples, then used for 11 other pesticides to evaluate its applicability (see Fig. 4 and Table 2).

Chapter 6 Table 2. Area extraction of overlapped peaks using iterative curve fitting of 13 compounds.

Name	# Stereo.	# Overlap ₁	Model _{2a}	% Area _{2b}	Std. Error _{2c}	R ² _{2d}
Allethrin	8	2	EMG	Peak ₁ = 5.8	0.774	0.9983
				Peak ₂ = 5.6		
Cyfluthrin	8	8	EMG	Peak ₁ = 11.4	1.913	0.9933
				Peak ₂ = 18.2		
				Peak ₃ = 10.7		
				Peak ₄ = 17.9		
				Peak ₅ = 9.8		
				Peak ₆ = 10.9		
				Peak ₇ = 11.6		
				Peak ₈ = 9.5		
Cypermethrin	8	8	EMG	Peak ₁ = 7.8	0.4748	0.9996
				Peak ₂ = 18.3		
				Peak ₃ = 9.0		
				Peak ₄ = 12.1		
				Peak ₅ = 14.4		
				Peak ₆ = 18.0		
				Peak ₇ = 9.4		
				Peak ₈ = 10.9		
Cycloprothrin	4	2	EMG	Peak ₁ = 25.8	0.122	0.9995
				Peak ₂ = 26.0		
Etaconazole	4	2	GMG	Peak ₂ = 21.6	0.276	0.9985
				Peak ₃ = 28.5		
Fenoxalil	4	4	EMG	Peak ₁ = 26.3	0.024	0.9993
				Peak ₂ = 26.1		
				Peak ₃ = 25.0		
				Peak ₄ = 22.6		
Fenpropathrin	2	2	EMG	Peak ₁ = 49.6	0.108	0.9994
				Peak ₂ = 50.4		
Fenvalerate	4	3	EMG	Peak ₁ = 26.1	0.338	0.9986
				Peak ₂ = 23.2		
				Peak ₃ = 25.7		

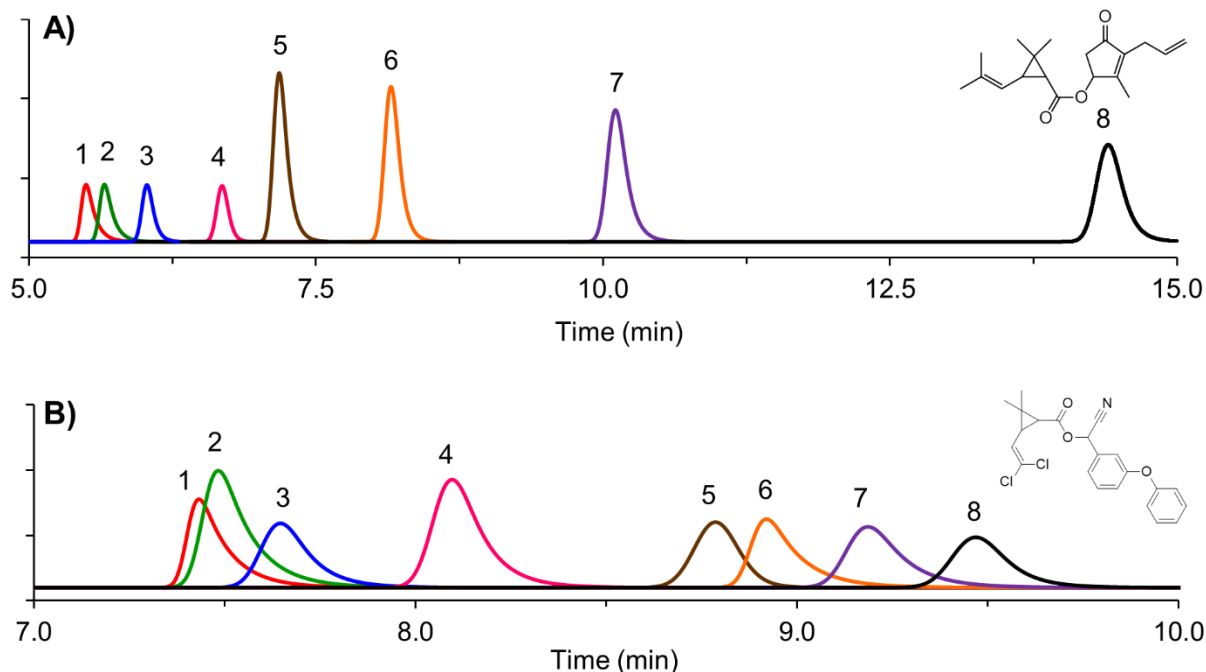
Flucythrinate	4	3	GMG	Peak ₁ = 26.1	1.514	0.9996
				Peak ₂ = 24.8		
				Peak ₃ = 25.4		
Metconazole	4	2	GMG	Peak ₂ = 41.9	0.069	0.9992
				Peak ₃ = 9.1		
Permethrin	4	2	GMG	Peak ₃ = 19.2	0.351	0.9980
				Peak ₄ = 19.5		
Resmethrin	4	2	GMG	Peak ₁ = 15.0	0.295	0.9967
				Peak ₂ = 14.3		
Tetramethrin	4	2	EMG	Peak ₁ = 11.1	0.250	0.9991
				Peak ₂ = 11.3		

¹ Number of overlapped pairs from the chromatographic conditions in Table 1.

^{2a,b,c,d} See Results and Discussion and Supplemental Material for protocol using iterative curve fitting with the exponentially modified Gaussian model (EMG), Gaussian modified Gaussian (GMG) and a linear background using PeakFit software (2a). Extracted area percentages of overlapped peaks were determined from this protocol and numbered by their elution order in original chromatograms (see Table 1 for data) (2b). The standard error (Std. Error) and coefficient of determination (R^2) of the fit were also obtained from PeakFit and reported (2c,2d).

First, the raw data of the best separation possible was obtained. The data was then imported to PeakFit software and smoothed with a Savitsky-Golay weighted filter. Next, the model was chosen to fit the number of peaks involved with the chromatogram. Last, the curve fitting program simulated the fit and provided the areas of each peak.

Using this simple four-step protocol, worked examples are shown for a simple case of one overlapping pair, and a more complex case with several overlapping peaks (Fig. 4, Fig. S1 in supplemental material).



Chapter 6 Figure 4. Iterative curve fitting of two pyrethroids. **A)** Enantiomeric separation of allethrin with CDShell-RSP resulting in one overlapped enantiomeric pair. **B)** Enantiomeric separation of cyfluthrin with CDShell-RSP resulting in several overlapping peaks. Areas of the overlapped peaks were extracted according to the protocol discussed in the Results and Discussion and Supplemental material. See Table 1 for chromatographic information, and Table 2 for extracted areas and other results.

The eight isomers of the pyrethroid, allethrin, were all baseline separated by CDShell-RSP except the first two peaks, which was representative of most pyrethroid enantiomeric separations (Fig. 4A). After using the protocol above, the extracted area percentages of peak 1 and peak 2 were determined after 68 iterations as 5.77% and 5.61%, respectively (Fig. 4A and Table 2). The number of peaks is chosen by the user, which might be erroneous with complex samples and complete overlap ($R_s = 0.0$), but with the MS-compatible methods reported in this study, quick MS peak purity checks can be performed. Hidden peaks with the same m/z values, like enantiomers, must be separated or their retention times determined separately as they cannot be differentiated by MS [46]. However, all enantiomers were visible for the standard compounds used in this study. Overall, this approach provided a better estimation of the two allethrin peak areas compared to simple integration methods, which reported the incorrect area percentages as 4.87% and 6.43%.

More difficult situations, as in the case of cyfluthrin, which had seven out of eight overlapping isomers on the CDShell-RSP, were also assessed by the iterative curve fitting protocol (Fig. 4B and Tables 1 and 2). Since all the peaks were less resolved in comparison to allethrin, the curve fitting was more challenging, but with the exponentially modified Gaussian (EMG) model and seven iterations, the recovered areas were estimated (following elution order of peak 1 to peak 8) as 11.4%, 18.2%, 10.7%, 17.9%, 9.8%, 10.9%, 11.6%, and 9.5%. With ideal peak shapes and in the absence of noise, iterative curve fitting error has been reported as < 1% error [42]. The extensive overlap between these peaks makes simple integration very difficult, especially to determine which peaks are racemic, enantiomeric pairs. However, from this approach, the enantiomeric pairs can be better estimated as peaks 1 and 3, 2 and 4, 5 and 8, and 6 and 7. Further confirmation was provided with the separation of β -cyfluthrin, which only contains 4 of the 8 stereoisomers of cyfluthrin. These 2 enantiomeric pairs were aligned with peaks 1 and 3, and 5 and 8.

As seen in Figs. 4A and 4B, the area ratios between all the peaks were not equal, which might lead to errors if the peaks overlap when using conventional integration methods [37]. Iterative curve fitting is very flexible as even asymmetric peak shapes can also be modeled with high accuracy [40]. However, it is subjective to the user and which model is chosen. In the 12 separations assessed, the best models with least error seemed to be the exponentially modified Gaussian (EMG) and the Gaussian modified Gaussian (GMG) (Table 2). Overall, the peak areas were conveniently extracted from partially resolved chromatograms, even the pyrethroids with up to 8 stereoisomers. Undoubtedly, this procedure applies to all complex enantiomeric separations that require extensive chromatographic method development. It could provide quantitative information from overlapping signals, which might be useful for complex biological enantiomeric studies, especially those of pesticides.

6.5 Concluding remarks

Effective methods with core-shell (superficially porous particles) CSPs and mass spectrometry-compatible mobile phases were established for 100 chiral pesticides, many with more than one chiral

center. In past studies, cyclodextrins have had success in separating pesticides, but never has such a comprehensive study, with the evaluation of several chiral selectors towards chiral pesticides been reported. The hydroxypropyl- β -cyclodextrin CSP (CDShell-RSP) provided the broadest enantiomeric selectivity for chiral pesticide separations. High enantiomeric selectivity for pesticides with acidic functionalities were dominantly provided by the macrocyclic glycopeptide and quinine-based CSPs (TeicoShell and Q-Shell). Pesticides with amine functionalities and a few unique cases were better suited towards the other macrocyclic glycopeptides and derivatized cyclofructan (NicoShell, VancoShell, and LarihcShell-P). A convenient protocol using iterative curve fitting was developed and can be applied to any partially separated pesticides, which would provide the necessary information needed for biological and/or environmental enantiomeric studies.

6.6 References

1. IUPAC. Compendium of Chemical Terminology, 2nd ed. (the "Gold Book"). Blackwell Scientific Publications, Oxford (1997).
2. Matell M (1953) *Ark Kemi* 6:365–373
3. Schneiderheinze JM, Armstrong DW, Berthod A (1999) *Chirality* 11:330-337
4. Burden RS, Carter GA, Clark T, Cooke DT, Croker SJ, Deas AHB, Hedden P, James CS, Lenton JR (1987) *Pestic Sci* 21:253-267
5. Calcaterra A, D'Acquarica I (2018) *J Pharm Biomed Anal* 147:323–340.
6. Armstrong DW, Chang CD, Li WY (1990) *J Agric Food Chem* 38:1674-1677
7. Armstrong DW, Reid III GL, Hilton ML, Chang CD (1993) *Environ Pollut* 79:51-58
8. Liu W, Gan J, Schlenk D, Jury WA (2005) *Proc. Natl. Acad. Sci. USA* 102:701-706
9. Ye J, Zhao M, Liu J, Liu W (2010) *Environ Pollut* 158:2371-2383
10. Perez de Albuquerque NC, Carrão DB, Habenschus MD, Moraes de Oliveira AR (2018) *J Pharm Biomed Anal* 147:89-109
11. Schleier III JJ, Peterson RKD (2011) Pyrethrins and pyrethroid insecticides. In: Lopez Ó, Fernández-Bolaños JG (eds) *Green Trends in Insect Control*, RSC Green Chemistry, No. 11, RSC Publishing, Cambridge (UK), pp 94-131
12. Miyamoto J (1976) *Environ Health Perspect* 14:15-28
13. Ma Y, Chen L, Lu X, Chu H, Xu C, Liu W (2009) *Ecotoxicol Environ Saf* 72:1913-1918
14. Oberhauser KS, Brinda SJ, Weaver S, Moon RD, Manweiler SA, Read N (2006) *Environ Entomol* 35:1626-1634
15. Johnson RM, Ellis MD, Mullin CA, Frazier M (2010) *Apidologie* 441:312-331
16. Vontas J, Grigoraki L, Morgan J, Tsakireli D, Fuseini G, Segura L, Niemczura de Carvalho J, Nguema R, Weetman D, Slotman MA, Hemingway J (2018) *Proc Natl Acad Sci U S A* 115 (18):4619-4624
17. Chen ZM, Wang YH (1996) *J Chromatogr A* 754:367-395

18. Alder L, Greulich K, Kempe G, Vieth B (2006) *Mass Spectrom Rev* 25:838-865
19. Ye J, Wu J, Liu W (2009) *Trends Anal Chem* 28:1148-1163
20. Okamoto M (2012) Direct chiral separation of pyrethroid isomers by HPLC with chiral stationary phases In: Knaak JB, Timchalk C, Tornero-Velez R (eds) *Parameters for Pesticide QSAR and PBPK/PD Models for Human Risk Assessment*, ACS Symposium Series, vol 1099, pp 31-40
21. Ôi N, Kitahara H, Kira R (1990) *J Chromatogr A* 515: 441-450.
22. Lisseter SG, Hambling SG (1991) *J Chromatogr A* 539:207-210
23. Armstrong DW, Chang CD, Lee SH (1991) *J Chromatogr A* 539:83-90
24. Kutter JP, Class TJ (1992) *Chromatographia* 33:103-112
25. Zhang H, Qian M, Wang X, Wang X, Xu H, Wang Q, Wang M (2012) *J Sep Sci* 35:773-781
26. Li Y, Dong F, Liu X, Xu J, Li J, Kong Z, Chen X, Liang X, Zheng Y (2012) *J Chrom A* 1224:51-60
27. Patel DC, Wahab MF, Armstrong DW, Breitbach ZS (2016) *J Chromatogr A* 1467:2–18
28. Hellinghausen G, Lee JT, Weatherly CA, Lopez DA, Armstrong DW (2017) *Drug Test Anal* 9:944–948
29. Hellinghausen G, Roy D, Wang Y, Lee JT, Lopez DA, Weatherly CA, Armstrong DW (2017) *Talanta* 181:132-141
30. Barhate CL, Lopez DA, Makarov AA, Bu X, Morris WJ, Lekhal A, Hartman R, Armstrong DW, Regalado EL (2018) *J Chrom A* 1539:87-92
31. Hellinghausen G, Roy D, Lee JT, Wang Y, Weatherly CA, Lopez DA, Nguyen KA, Armstrong JD, Armstrong DW (2018) *J Pharm Biomed Anal* 155:70-81
32. Patel DC, Breitbach ZS, Yu J, Nguyen KA, Armstrong DW (2017) *Anal Chim Acta* 963:164-174
33. Xu C, Armstrong DW (2013) *Anal Chim Acta* 792:1-9
34. Armstrong DW, Liu Y, Ekborg-Ott KH (1995) *Chirality* 7:474–497
35. Armstrong DW, Tang Y, Chen S, Zhou Y, Bagwill C, Chen JR (1994) *Anal Chem* 66:1473–1484
36. Sun P, Wang C, Breitbach ZS, Zhang Y, Armstrong DW (2009) *Anal Chem* 81:10215–10226
37. Bicking MKL (2006) *LC GC N Am* 24:605-616
38. Chesler SN, Cram SP (1973) *Anal Chem* 45:1354-1359
39. Anderson AH, Gibb TC, Littlewood AB (1970) *Anal Chem* 42:434-440
40. Amigo JM, Skov T, Bro R (2010) *Chem Rev* 110:4582-4605
41. Kemmer G, Keller S (2010) *Nat Protoc* 5:267-281
42. Asher BJ, D'Agostino LA, Way JD, Wong CS, Harynuk JJ (2009) *Chemosphere* 75:1042-1048
43. Wahab MF, Wimalasinghe RM, Wang Y, Barhate CL, Patel DC, Armstrong DW (2016) *Anal Chem* 88:8821-8826
44. Patel DC, Wahab MF, O'Haver TC, Armstrong DW (2018) *Anal Chem* 90:3349-3356
45. Kraehmer H, Laber B, Rosinger C, Schulz A (2014) *Plant Physiol* 166:1119-1131
46. Boehm RE, Martire DE, Armstrong DW (1988) *Anal Chem* 60:522-528

Chapter 7

Increasing chromatographic resolution of analytical signals using derivative enhancement approach

7.1 Abstract

A few decades ago, Giddings made a bleak statistical prediction stating that when using a chromatographic column with a peak capacity of n , one “has no real hope” of separating n compounds because of peak overlap. This statement holds true for today’s far more complex separations including chiral, achiral or isotopic separations. Co-eluting chiral and isotopically labeled positional isomers pose a mass spectrometric challenge as isobaric analytes. Several advanced mathematical approaches exist to resolve and extract areas from overlapping data, such as Fourier self-deconvolution, wavelets, multivariate curve resolution, and iterative curve fitting. In this work, we develop a very straightforward approach to mathematically enhance signal resolution using the properties of even-derivative while conserving peak area and its position. This technique is based on the fact that the area under an even-derivative of a distribution is equal to zero. Consequently, by alternately subtracting and adding multiples of even-derivatives (second, fourth, sixth, and so on) from the original peak, the area under a peak is conserved, and the bandwidth is reduced. Unlike multivariate curve resolution and iterative curve fitting approaches, this approach does not require prior knowledge of the number of peaks. The concept is theoretically discussed for Gaussian and Lorentzian peaks. Several challenging chromatographic applications using deuterated benzenes, chiral separations, and biological applications are shown using twin-column recycling and conventional chromatography. The proposed protocol for a pair of overlapping peaks is currently limited to a R_s of 0.7 or greater with error <1 % under ideal conditions. Furthermore, tuning of peak shape by the first derivative is also described which can remove the exponential convolution of tailing peaks.

7.2 Introduction

The maximum number of peaks separable by a given column, at a fixed resolution, is given by its peak capacity [1, 2]. Gidding's theory predicts for a case where the number of components in a mixture is equal to the peak capacity of a separation column, only 18% of the analytes will be single component peaks in a randomly spaced chromatogram; the rest will appear as partially or entirely overlapped peaks [3]. In experimental separations, the picture may not be that dismal because the columns are rarely operated above their peak capacity [4]. However, critical pairs invariably exist throughout in a given separation time-window. The problem becomes worse when the analytes are enantiomers, isotopic positional isomers, or similar-shaped molecules. Even liquid chromatography-mass spectrometry fails under such scenarios. Today, peak overlap in separation science and spectroscopy is one of the significant challenges faced by analytical chemists [5-7].

Several sophisticated solutions exist to solve these problems, e.g., two-dimensional (2D) chromatography such as 2D gas or liquid chromatography (2D-GC or 2D-LC) [8-10], where columns of orthogonal selectivity are chosen, and an "impure" peak is resolved in the second dimension. For instance, a challenging chiral mixture of eight diastereomers/enantiomers of a hepatitis-C protease inhibitor was separated using 2D-LC using two chiral columns, but the separation required 2.16 h. The potential of twin-column recycling HPLC has been shown as a powerful approach to achieve ultrahigh resolution separations, which are not possible under ordinary circumstances [11-13]. Recently, we demonstrated baseline sub-second liquid chromatography separations of multiple analytes using short, 0.5 or 1 cm, columns [14, 15]. The sensor-like speed of short columns is the future direction in separation sciences. The chromatographic-sensor technology is generally limited by the relatively low efficiency of short columns (~2500 plates/cm) even with sub-2 μm core-shell particles under optimum conditions. Peak overlap is commonly observed with fast separations [14, 15]. Consequently, simple mathematical techniques are desirable to accurately recover information from partially resolved

signals. However, many resolution enhancing approaches, such as wavelet transform and Fourier self-deconvolution are quite challenging to implement for routine analysis, similarly multivariate curve resolution needs multidimensional data [16-18]. In this work, we report a simple resolution enhancing protocol by utilizing the fundamental properties of even-derivatives of a distribution, which can be easily carried out in Excel or MATLAB. The fundamental property is that the area under the even-derivatives of a symmetric distribution is equal to zero. Real peaks are rarely symmetric, but it can be readily shown that the area under the derivatives of tailing/fronting peaks also is practically negligible (on the order of 10^{-11} units). In the following section, we briefly outline the theory followed by some challenging cases and applications.

7.3 Theory

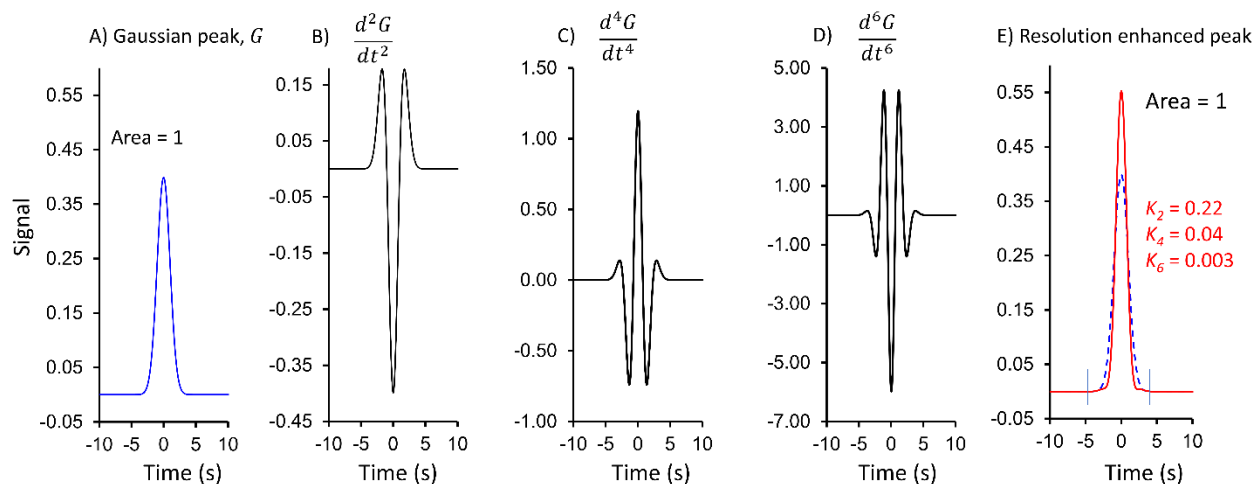
Consider an area normalized Gaussian peak as a function of time t , which is centered at zero, i.e., $t_R = 0$,

$$G(t, \sigma) = \frac{1}{\sigma\sqrt{2\pi}} \exp\left(-\frac{t^2}{2\sigma^2}\right) \quad (1)$$

It can be shown that the general n^{th} derivative of Gaussian is a polynomial multiplied by the original Gaussian function. Considering Equation (2), it can be shown that the n^{th} derivative of Gaussian is a polynomial multiplied by the original Gaussian function,

$$\frac{d^n G(\sigma, t)}{dt^n} = (-1)^n \frac{1}{(\sigma\sqrt{2})^n} H_n\left(\frac{t}{\sigma\sqrt{2}}\right) G(\sigma, t) \quad (2)$$

where H_n is a Hermite polynomial consisting of various powers t and standard deviation σ [19]. If we subtract a multiple of the second derivative and add a multiple of the fourth derivative, the “width” of the peak G is reduced, and the area is maintained (Fig. 1).



Chapter 7 Figure 1. Demonstration of the steps involved in the resolution enhancement process using even-derivative: A) shows a Gaussian function with a unit area B) the second derivative of the peak C) fourth derivative of the peak and (D) the sixth derivative, and E) resolution enhanced peak obtained by subtracting the second and adding the fourth and subtracting the sixth derivative from the original peak with appropriate K_2 , K_4 and K_6 values as shown in part E. The area after numerical integration is conserved.

We describe the resolution enhanced peak (R.E.P) as:

$$R.E.P = G \left(1 - K_2 \frac{(-1)^2}{(\sigma\sqrt{2})^2} H_2 + K_4 \frac{(-1)^4 1}{(\sigma\sqrt{2})^4} H_4 - K_6 \frac{(-1)^6 1}{(\sigma\sqrt{2})^6} H_6 + \dots \right) \quad (3)$$

Here the constants, K_i , ($i=2,4,6\dots$) are “adjustable” numerical multipliers of the second, fourth and sixth derivatives to ensure consistent dimensions and decrease the peak width. The area of the original peak G is maintained because the second, fourth, sixth, etc. derivatives are symmetric at zero (even functions) and the net area under these even functions is given by the difference of their primitives (odd functions) at $t=+\infty$ and $t=-\infty$, which are both zero. Thus, subtracting and adding constant multiples of even-numbered derivatives from the original function does not alter the peak area because any function will remain unaltered by ± 0 . This concept is illustrated in Fig.

1. The values of K_2 , K_4 and K_6 in Fig. 1, were empirically set to 0.22, 0.04 and 0.003

respectively, to enhance the resolution. A criterion for choosing the K_i values is given in Table 1.

The same idea can be extended to a Lorentzian distribution which is the natural line shape of spectroscopic peaks. The equations (1) to (3) were analytical versions. Since most instruments use

analog-to-digital convertors, the even derivatives can be calculated from the first principles as a numerical finite difference approximation of analytical derivatives [20]. In general, if the n^{th} derivative is to be calculated from digitized data, then:

$$\frac{d^n G}{dt^n} \approx \frac{\delta_h^n [G](t)}{h^n} \quad (4)$$

where the approximation sign shows that there will be a small truncation error, and $\delta_h^n [G](t)$ is the general central finite difference given in Eq (5) [21].

$$\delta_h^n [G](t) = \sum_{i=0}^n (-1)^i \binom{n}{i} G\left(t + \left(\frac{n}{2} - i\right) h\right) \quad (5)$$

and h is the equal spacing of the data points, and i is the index of the data point being considered. Any higher order derivative can be directly calculated from the raw data using Equation (5). The advantages of equations (4) and (5) is that no prior analytical expression for the peak function is required for differentiation. This can be contrasted with iterative curve method [22]. Another useful property of derivatives is that the n^{th} order derivative of an m^{th} derivative is equivalent to an $(n+m)^{\text{th}}$ order derivative. This property is utilized in the Microsoft Excel Template i.e. first a second derivative is calculated and the second derivative of the second derivative gives the fourth derivative. The template also smooths the derivative before subtraction.

7.4 Materials and methods

7.4.1 Software for data processing

All the resolution enhancing procedures were carried out in Microsoft Excel 2016 template (available in the Supporting Information). MATLAB R2017b (Windows 64 bit) was used for simulations of Gaussians or Lorentzians using the following functions. For Gaussian curves, the “normpdf” function of MATLAB with various multipliers to alter peak areas whereas the Lorentzian was modelled as follows, where y is the signal, A represents the area, w is the width parameter and a_1 is the center of the Lorentzian peak.

$$y = \frac{A}{\pi w \left(1 + \left(\frac{x - a_1}{w}\right)^2\right)} \quad (6)$$

The iterative curve resolution method was done on PeakFit version 4.12 (SeaSolv Software Inc. 1999-2003) moreover, OriginPro 2015 (OriginLab Corporation, MA, USA) was employed for numerical integration. This peak fitting method is based on the minimization of residuals on curve fitting. A moment-based expression for the 4σ resolution factor is then proposed as a general case. The resolution equation can be written in terms of second moments for any peak shape *i.e.*, any distribution.

$$R_s = \frac{t_{Ref} - t_A}{2(\sqrt{m_{2Ref}} + \sqrt{m_{2A}})} \quad (7)$$

where, t_{Ref} is the retention time of the reference peak, t_A is the retention time of the analyte of interest (from the first moment), and the m_2 is the second moment which is the variance of the distribution of the reference peak and the analyte. Note that equation (7) may deliver a resolution factor < 1.0 when the first peak is fronting and the second peak is tailing, even though the valley touches the baseline. This calculation is offered by Chromeleon in Vanquish UHPLC (Thermo Fisher Scientific 2009–2016) whereas PeakFit version 4.12 employs a base-width resolution formula.

7.4.2 Chromatographic conditions and hardware

All HPLC grade solvents, reagents, and analytes were purchased from Sigma-Aldrich (St. Louis, MO, USA). Distilled deionized water (18.2 MΩ.cm) was produced by the Milli-Q purification system (EMD Millipore, Billerica, MA, U.S.A.). The 2.7 μm superficially porous particles (SPP) were received from Agilent Technologies (Santa Clara, CA, U.S.A.). The SPP particles were modified with (R, S)-hydroxypropyl modified β-cyclodextrin (Cyclodextrin-RSP), and macrocyclic glycopeptides (NicoShell or TeicoShell) by AZYP LLC (TX, USA). The columns were slurry packed using a non-aggregating solvent into stainless steel columns (5 or 10x0.46 cm i.d.). The detailed packing hardware design to produce high-efficiency columns is already described in our previous work [23, 24]. Vanquish UHPLC

instrument (Thermo Fisher Scientific, Waltham, MA) was used for collecting chromatograms. The column oven was by-passed, and the column was connected to the injector and the 2.5 μL UV-Vis detector. The data was sampled at 250 or 200 Hz on the UHPLC. The UHPLC is controlled using Chromeleon 7.2 SR4 software (Thermo Fisher Scientific 2009–2016).

7.4.3 Recycling HPLC experiments and LC isotopic separations

The experimental design of the custom-made recycling HPLC system by Waters has been given along with photographs [11, 12]. Deuterated isotopes of benzene, 1,3,5-benzene- d_3 , and benzene- d_6 were separated on an HPLC in recycling mode. One isotope mixture was analyzed consisting of benzene/1,3,5-benzene- d_3 /benzene- d_6 . The mobile phase was a mixture of acetonitrile and water (55/45, v/v). The sample was prepared by dissolving 10 μL of each compound in 2.0 mL of eluent. The sample concentration was close to 4.4 g/L. 2.0 μL was injected into the 15x0.3 cm columns packed with 2.7 μm Cortecs-C-18 particles. The flow rate was set at 0.4 mL/min. The detection wavelength was 210 nm for a sampling rate fixed at 20 Hz. The identification of benzene, 1,3,5-benzene- d_3 , and benzene- d_6 was achieved by injecting each compound separately. Similarly, the analytes benzo[a]anthracene and chrysene ($\geq 97\%$ purity) purchased from Sigma–Aldrich. The twin column recycling HPLC of these two compounds was performed on XBridge BEH-C18 columns (3.0 mm \times 150 mm, 3.5 μm particles).

7.5 Results and discussion

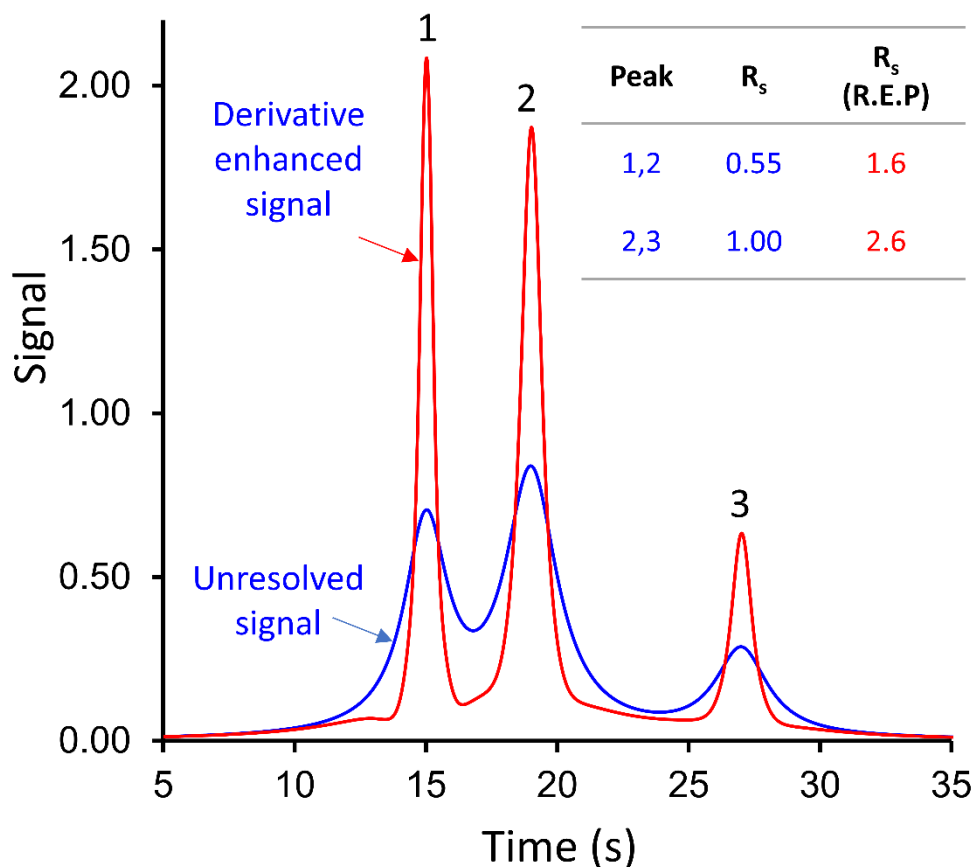
Table 1 summarizes the five steps outlined in the Theory section to mathematically enhance the experimental resolution using even derivatives.

Chapter 7 Table 1. Resolution enhancement using even-derivatives or first-second derivative combination.

- a. Choose a critical pair with low-resolution on the order of $R_s \geq 0.7$ using a data acquisition software. Export the time vs. instrument signal data.
- b. Calculate the second derivative and the fourth derivative. The sixth derivative is rarely needed.

- c. Remove noise from derivatives by using a centered moving average. Apply any centered moving average until the second, the fourth and the sixth derivatives have low noise levels.
 - d. Subtract the second and add the fourth derivative with appropriate coefficients K_2 and K_4 from the raw data. Approximately, $K_4=K_2/F$ with $F > 0$ (10-10000).
 - e. Calculate resolved peak areas by numerical integration.
-

Later we show how a combination of odd-even can be applied for deconvolution purposes. This approach is generic, and it can be applied to chromatograms or non-Gaussian peak models. Fig. 2 shows the generality of the even-derivative method on three simulated overlapping Lorentzians (sum of three Lorentzians, Equation 6).

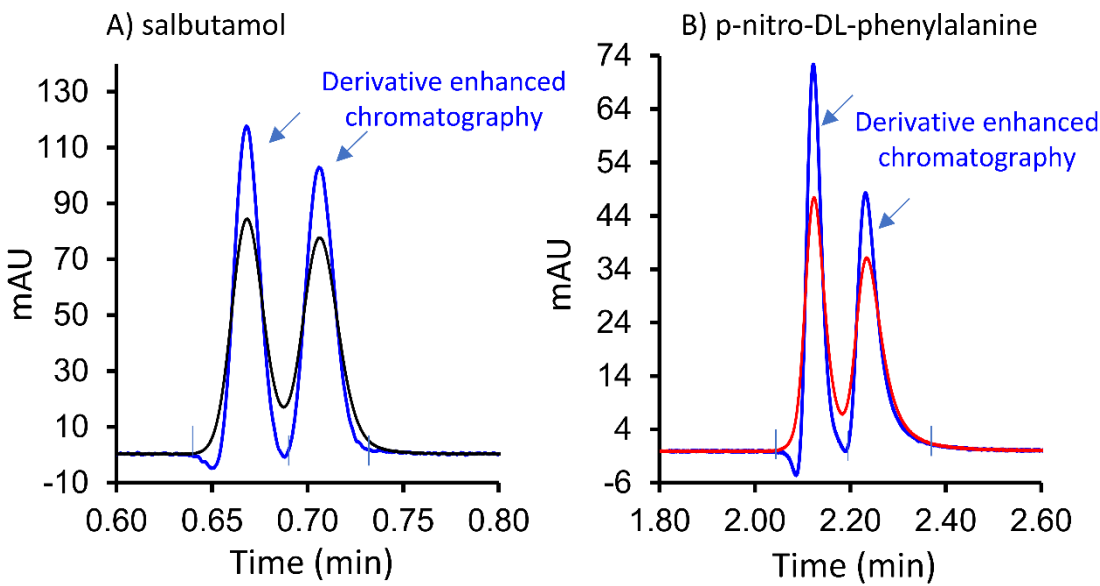


Chapter 7 Figure 2. Resolution of three pure overlapping Lorentzian peaks using the peak sharpening principle based on even-derivatives. The K_i factors for the second, fourth and sixth derivatives are 0.8, 0.0008, and 0.0008 respectively.

This method can then be used for detecting hidden spectroscopic peaks and their position for qualitative purposes. In the following experimental chromatographic examples, we examine various difficult situations, which can pose significant challenges to chromatographers. In the provided template (Supporting Information) we have to choose K_i values. Empirically, the values of K_i are chosen in such a way that a resolution > 1.5 is obtained. To begin, $K_2 \gg K_4 \gg K_6$ is a good starting point. In fact, the sixth derivative is not needed, in general. The second derivative multiplier is $K_4 = K_2/F$; the third one is $K_6 = K_4/F$, and so on. The value of F can be chosen from 10-10000 as a starting point. See additional details for starting in Table 1. A good place to start for Gaussian peaks is $\sigma^2/30$ for the second derivative and $(\sigma^4)/200$ for the fourth derivative factor, where sigma is the standard deviation of the Gaussian. One can adjust these factors give the narrowest peaks without significant negative dips. Adjust these factors give the narrowest peaks without significant negative dips. The best-optimized value of K_2 is that which enhances the resolution to baseline without degrading the signal to noise ratio along with small negative dips (to be discussed later).

7.5.1 Even-derivative method for single critical pairs

When the column selectivity, i.e., the ratio of retention factors is very close to unity, the given critical pair appears as a set of partially overlapping peaks with an $R_s < 1.5$. This situation is often seen in enantiomeric separations which are often complicated by asymmetric peak shapes of enantiomers [25]. Other powerful mathematical techniques such as Fourier transform self-deconvolution [16] can change peak positions while reducing their width and power-transforms change areas and heights while the peak position remains constant [26]. Fig. 3 shows an interesting application of the even-derivative method on partially resolved racemic peaks of salbutamol.



Chapter 7 Figure 3. Recovery of peak areas of chiral separations in case of symmetrical and highly tailing peaks using the even-derivative method. A) salbutamol isomers, Chromatographic conditions: NicoShell, 10 cm x 0.46 cm i.d, 2.7 μ m SPP, 100% MeOH with 0.2 wt % ammonium formate at 3.00 mL/min, detection using UV: 220 nm 250 Hz 0.00 s. B) p-nitro-DL-phenylalanine isomers, Chromatographic conditions, TeicoShell, 10x0.46cm, 2.7 μ m SPP, 1.0 mL/min, 93% H₂O containing 0.05% formic acid and 7% acetonitrile.

Both peaks tail very slightly with an asymmetry of ~ 1.21 and 1.23 at 10% height, as is typical of any compound with slow mass-transfer kinetics of adsorption and desorption. The Gaussian efficiency is moderate (~ 6000 plates) for both peaks. In the chiral analysis, the area ratio of enantiomers is also of prime importance. Before applying the protocol, the resolution was determined as 0.89 (full base-width resolution). In Fig. 3A, the salbutamol separation was resolved using the derivative method. The second and fourth derivative were subtracted and added from the raw data as per equation 3. The value of coefficients K_2 and K_4 were varied empirically until a baseline separation was obtained. The value of $K_2 = 2.7 \times 10^{-5}$ units and $K_4 = 0$ was sufficient to make the separation baseline. The area of the peaks was calculated by numerical integration, which assumes no peak shape beforehand. The comparative areas of the first and second enantiomer are shown in Fig. 3A are 1.79 and 1.81 mAU.min with a % RSD ($n=3$) of 0.17 and 0.35 respectively. This gives an area ratio of 49.6% to 50.4% . As a benchmark, iterative curve using exponentially modified peaks gave an area of 1.78 and 1.79 for the first and the second peak

with nine iterations. The same salbutamol enantiomers when chromatographically resolved gives an area ratio of $49.6 \pm 0.09\%$ and $50.4 \pm 0.09\%$. Therefore, the even-derivative methodology is a straightforward resolution enhancing tool with good precision.

Chiral separations are often afflicted with tailing or “Eiffel tower” peaks [27]. Such peaks appear to have concurrent fronting and tailing element. We show a separation of p-nitro-DL-phenylalanine on a superficially porous teicoplanin column (TeicoShell, $2.7 \mu\text{m}$, $10 \times 0.46 \text{ cm}$) in Fig. 3B. The mobile phase of ACN and H_2O (containing formic acid) is chosen so that it shows a partial resolution with significant tailing of the second peak. The Gaussian efficiency of the first peak is very high with 10,600 plates and a 10% asymmetry of 1.50; however, the second peak has an efficiency of 6900 with a 10% asymmetry factor of 1.94. However the moment analysis shows a plate count of 7200 and 3560 for the first and the second peak respectively, confirming that the peaks are no longer Gaussian. In general, an asymmetry of 2.0 is recommended as an upper limit for quantification purposes [28]. Using the same procedure as described above, the areas of both can be recovered successfully with the derivative sharpening method as 2.52 and 2.63 mAU.min units with $K_2 = 2.10 \times 10^{-4}$ and $K_4 = 1.50 \times 10^{-9}$ units. These numerically calculated areas match very well with the numerical area under exponentially modified Gaussian as 2.55 and 2.59 mAU.min units. It should be noted that the derivative sharpening may produce small disturbances dips near the baseline. The peaks should be numerically integrated as shown by including the dip. Note as in this case, the classical perpendicular drop method systematically produces a larger area for the second peak $2.73 \pm 0.04 \text{ mAU.min}$ ($n=4$) because of tailing problems. In Table 2 we show the slight systematic error in the area of recovery as a function of resolution.

Chapter 7 Table 2. Comparison of errors in area recovery as a function of initial resolution of Gaussian peaks of equal area.

Initial Resolution	Peak 1	Peak 2	% Error in Peak 1	% Error in Peak 2
1.26	250.130	250.031	0.05	0.01

1.15	250.134	249.915	0.05	-0.03
0.97	250.362	249.648	0.14	-0.14
0.84	250.761	249.309	0.30	-0.28
0.74	251.037	248.957	0.41	-0.42
<0.6	Significant peak distortion in the baseline			

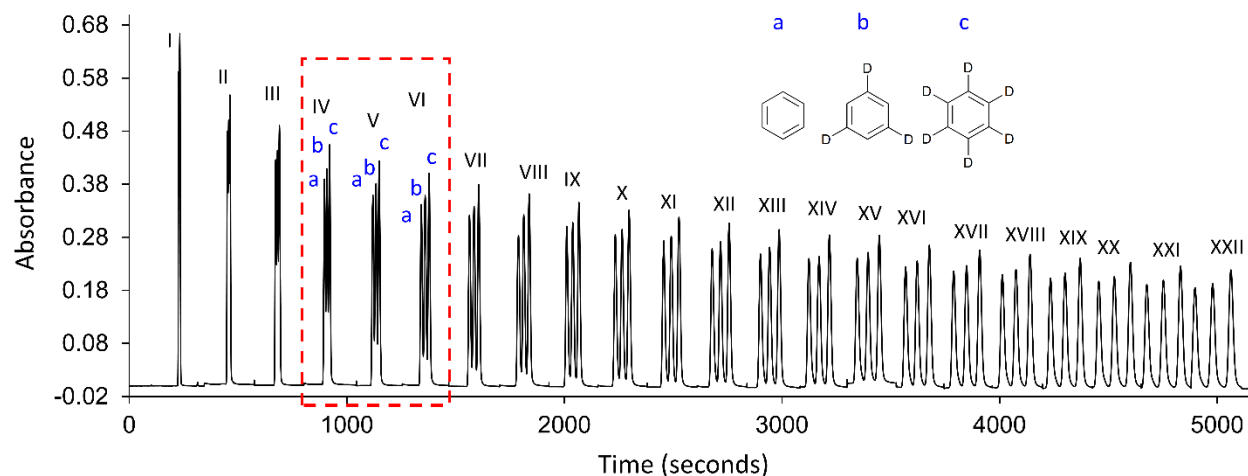
^aCalculated resolution (R_s) of the simulated chromatogram (area ratio of 50:50) using the PeakFit software. Different K value were applied to make separation baseline. % error = $100[\text{area (recovered)} - \text{area (true)}] / [\text{area (true)}]$. The area of both peaks was set to 250.0000 units, and the standard deviation was varied to alter resolution while retention times were held constant.

Table 2 shows that with simulated peaks with a resolution of less than R_s than 0.6 will lead to a significant baseline distortion. Therefore, we recommend this method for critical pairs with a $R_s \geq 0.7$. In Table 3, we will compare the extracted areas from real data.

If the resolution is lower than 0.7, one can still resolve the peaks for qualitative purposes. Under such experimental situations, the chromatographer should continue to improve the separation by adjusting the mobile phase or temperature until a resolution of 0.7 to 0.8 can be obtained with the same column. Additionally, it is not necessary that the peaks be of equal height or area for this even-derivative sharpening method.

7.5.2 Twin-column recycling HPLC for ultrahigh resolution separations

Twin-column recycling chromatography has recently emerged as a potent approach to deal with complex mixtures [11, 12, 29]. Fig. 4 shows a challenging liquid chromatographic separation of isotopes under analytical conditions.



Chapter 7 Figure 4. Extraction of peak areas in the selected region using the even-derivatives. Separation of the benzene/1,3,5-benzene-d3/benzene-d6 isotope mixture. 2.7 μm Cortecs-C-18 stationary phase. The average retention factor is = 1.6. The selectivity factors of for ba and cb are both 1.02. The average incremental system efficiency is= 7000 for the three isotopes. See the experimental section for more details. The recovered areas are shown for the selected set from IV to VI in Table 3.

Traditional LC is unable to separate such deuterated homologs in routine run times. For the sake of comparison, it took as much as 10 h to obtain a low resolution of ~ 1 with these three compounds using with two 25 cm long columns packed with 5 μm silica C18 particles or with two 45 cm \times 0.10 mm i.d. monolith silica-C-18 capillary columns. Recycling HPLC can provide the power needed to separate three deuterated benzenes. Indeed, for isolation or preparative purposes, full physical separation of all three peak is desirable. However, for semi- or fully quantitative information, the area can be easily extracted using higher order even-derivatives. In the recycling HPLC mode, it takes about 1.5 h to separate deuterated benzenes completely. However, even in the fourth “recycle” the resolution ~ 0.78 (peaks b and c). From this point onwards, one can conveniently apply the derivative sharpening method to get an accurate estimate of the area of each peak even before the physical separation begins. In each cycle, one can choose an independent set of coefficients K_2 and K_4 to bring peaks to the baseline. For instance, the (K_2 , K_4) pairs for the IV, V and VI chromatograms are (2.55, 4×10^{-3}), (2.70, 1×10^{-2}), and (2.80, 1×10^{-4}) respectively. The values of these coefficients were chosen empirically. This sectional approach for derivative sharpening is far more convenient than the conventional power transforms which are available in one commercial instrument’s software (Chromeleon) [14]. In such cases, area information is easily lost until additional steps of area recovery are applied. The comparison of numerically integrated data of resolution enhanced peak is also shown in Table 3, where it can be seen that iterative curve fitting areas match very well the results obtained by derivative sharpening method.

Chapter 7 Table 3. Comparison of extracted areas by the proposed derivative method for the separation of deuterated benzenes.

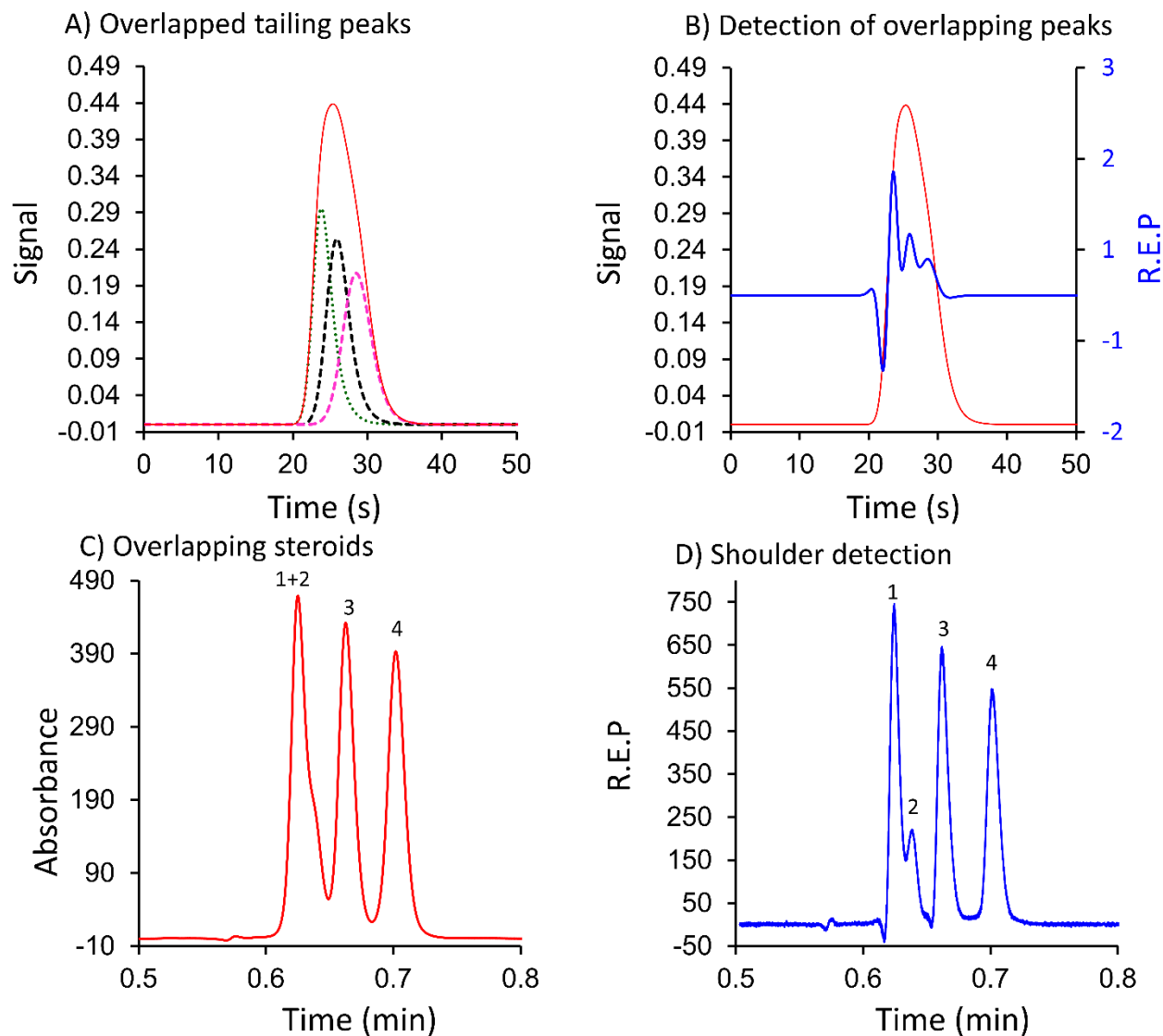
Valve switch	Resolution in Critical Pairs	Area by Even-Derivative Method			Area by Iterative Curve Fitting Method		
#	Peaks (a,b), (b,c)	Peak a	Peak b	Peak c	Peak a	Peak b	Peak c
IV	0.79, 0.78	3.08	3.28	3.83	3.10	3.16	3.85
V	0.86, 0.86	3.24	3.48	4.01	3.25	3.47	4.04
VI	0.94, 0.94	3.41	3.65	4.18	3.44	3.63	4.20

The bidirectional exponentially modified Gaussian model was chosen as a model (see equation the Supplementary Material), but the model fit shows a correlation coefficient of R^2 of 0.998 with a progressive linear background. Note that the recovered areas match quite well with the equal volumes of the three benzenes added to the injected sample (within experimental error of pipetting 10 μ L benzenes and assuming the the molar absorptivities of benzene and deuterated benzene are comparable).

7.5.3 Detection of hidden peaks and shoulders by even derivatives

The previous sections dealt with resolving a critical pair for area recovery. Often, the analyst is concerned with peak purity. The established methods of peak purity usually include mass spectrometry or photodiode array detection, using a column of orthogonal selectivity and two-dimensional liquid chromatography [30, 31]. These approaches can be expensive and suffer from some limitations. For example, the mass spectrometer is not a universal detector, since it only measures m/z values, it cannot "differentiate" isobaric impurities such as enantiomers. More importantly, closely related m/z analytes may not be differentiated by more economical, low-resolution mass spectrometers. Secondly, many analytes do not ionize well [32]. Area extraction approaches such as iterative curve fitting [22] or multivariate curve resolution will be ambiguous because we do not know the number of components contributing to the peak if there is a complete overlap [33].

The first and the second derivatives have been utilized to assess the peak structure, especially in spectroscopy often with a severe compromise on the signal to noise ratio. An entire spectroscopic field (derivative spectroscopy) is devoted to the application of derivatives [34, 35]. However, in the following examples, we utilize the digital version of equation (3) for qualitative resolution enhancement of the chromatograms and to assess the number of components. Although derivatives also are being used here for chromatographic data, the approach is visually more powerful. Peak pairs with $R_s > 0.2$ can be easily detected by using equation (3). Similarly, for detecting peak shoulders by the method of even-derivative, very low resolution or even complete overlapping peaks may be detectable. To test these limiting cases, three exponentially modified Gaussians (see Supplementary Material for the equation) were simulated with a width of 0.95, 1.2, and 1.6 s and a retention time difference of 2 s between the first two peaks and a 2.5 s difference between the second and third peaks (Fig. 5A). The overall envelope is *deceptively* a single peak (Fig. 5A). The individual simulated peaks contributing to the peak profile are shown (Fig. 5A). After applying equation (3) with appropriate K_i values of 3 and 1.5 respectively; the even-derivative method detects three hidden peaks under this envelope (Fig. 5B). This is precisely where the power law and the iterative curve fitting method will not be successful. The power law would merely reduce the width of the entire envelope, and the iterative curve fitting method has a fundamental requirement of knowing the number of peaks along with a choice of model. One can fit as many peaks as desired under this peak in Fig. 5A. The same approach is applied to detect the presence of shoulders in a separation of steroids, prednisone, cortisone, prednisolone, and hydrocortisone (Figs. 5C and 5D).



Chapter 7 Figure 5. (A) Simulation of highly overlapping peaks under a single envelope, (B) applying the derivative sharpening method reveals three hidden peaks (C) Detection of shoulders in real data of steroids. Peaks 1. prednisone, 2. cortisone, 3. prednisolone and 4. hydrocortisone. Column: RSP, 10 x 0.46 cm (i.d.), SPP 2.7 μm Mobile Phase: 60/40: ACN/16 mM ammonium formate pH 3.6, Flow: 2.0 mL/min, sample concentrations ~ 1.25 mg/mL of prednisone, prednisolone and hydrocortisone each, and ~ 0.25 mg/mL of cortisone, UV detection at 230 nm, injection volume: 0.5 μL (D) Detection of hidden shoulder in peak of cortisone.

The molar masses of the co-eluting peak of prednisone and cortisone (358.428 g/mol and 360.45 g/mol) are very close. Herein very small K_i values were employed ($K_2 = 9.9 \times 10^{-6}$, and $K_4 = 1 \times 10^{-11}$).

The shoulder detection methods will alert the chromatographer to further improve the method in

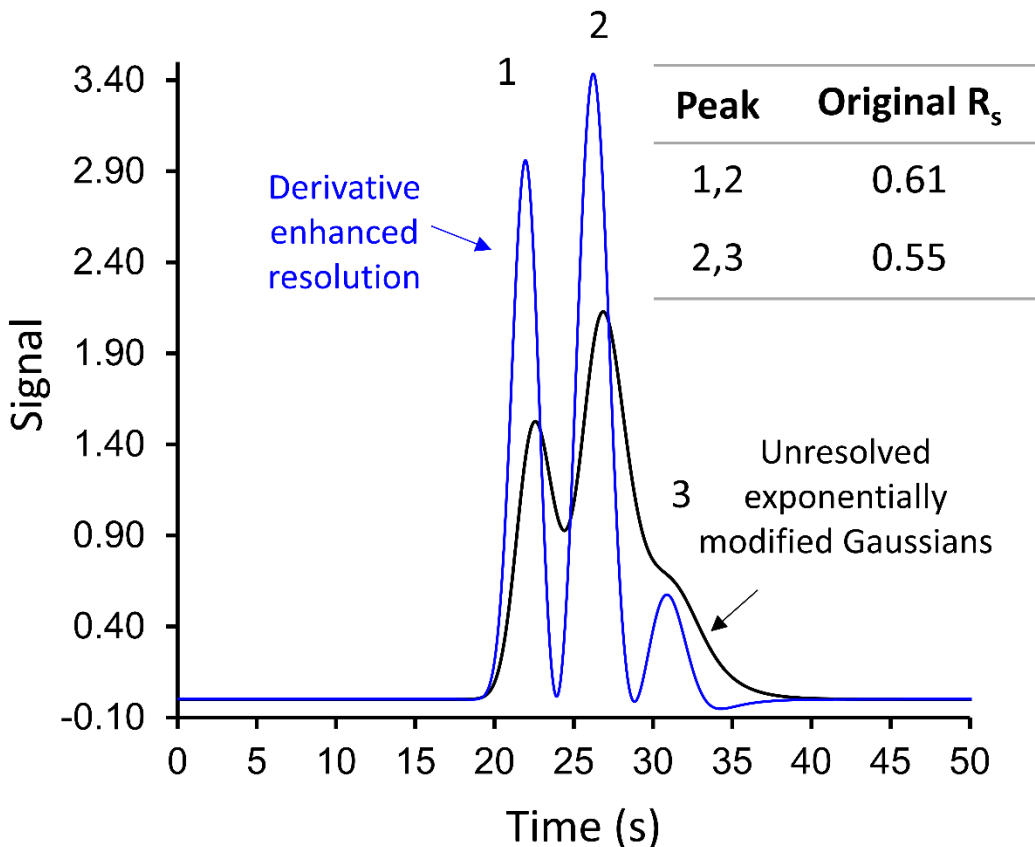
such a way that either the peaks are fully resolved or partially resolved to the extent where the derivative method can be applied with confidence.

7.5.4 Qualitative resolution enhancements of highly asymmetric peaks with the odd-even derivative method

As alluded to earlier, depending on the fluid mechanics of the bed and detector settings real peaks can have concurrent fronting and tailing, or excessive tailing or fronting [24, 27, 36]. Columns which produce visually fronting or tailing peaks are discarded by the manufacturers, whereas slight fronting or tailing is generally acceptable in C18 columns (tailing at 5% ranges from 0.98-1.2) whereas acceptable chiral columns have a larger tailing window (USP tailing of 1.7). The previous example showed resolution enhancement of wholly overlapped peaks. In this section, we show how peak tailing or fronting can be reduced by adding or subtracting the first derivative term in Equation (3).

$$\mathbf{R.E.P} = \mathbf{Signal} - (K_1)\mathbf{first\ derivative} - (K_2)\mathbf{second\ derivative} \quad (8)$$

where K_2 is another non-zero constant factor like the even derivative method. The value of K_1 is positive for a tailing peak and negative if the peak is fronting. Three low-efficiency tailing peaks neatly demonstrate this idea in Fig. 6.



Chapter 7 Figure 6. Resolution and peak shape improvement of three severely tailing peaks using the first and the second derivative. See text for details.

The peaks have the following efficiency by moment analysis and 10% asymmetry: (225, 1.54), (218, 1.60) and (242, 1.51). These figures of merit are typical of very short columns such as 0.5-1 cm and narrow bore diameters under ultrafast conditions. Applying the equation (8) with a K_1 and K_2 value of 1.78 and 0.65 separates the peaks to the baseline. Note that Equation (8) behaves similarly to deconvolution of exponentially modified Gaussians, i.e., the tailing effect is removed. This approach is practically shown in the Supplementary Data Figure S1 on fully resolved but tailing peaks. Using 5-methyl-5-phenylhydantoin as an example, the equation (8) can be used to deconvolve the response time of the detector. The first and second derivative combination can also be used to make tailing peaks into Gaussian peaks while conserving the area (Figure S1). This approach is a powerful tool for qualitative resolution enhancement and determining the number of components in a given chromatogram when the peaks tail or front severely, mainly due

to chemical reasons. The actual areas of the three peaks are precisely 5.00, 8.00 and 2.00 units. After the sharpening protocol, the recovered areas were 5.97, 7.80 and 1.19 units respectively. Since the resolution of the small peak is very poor, the error in area recovery is large. As suggested earlier, this resolution enhancement tool should be applied with a resolution larger than 0.7. However, the first derivative also works very well for qualitative resolution enhancement or to determine any hidden peaks or shoulders very well.

7.6 Conclusions

A straightforward but powerful approach is proposed with the theoretical basis to resolve overlapping peaks which may be experimentally difficult to separate. The peak areas, retention time and hence selectivity remain the same. These approaches will be helpful when a critical pair is present in an otherwise fully resolved chromatogram. The proposed derivative sharpening protocol for a pair of overlapping peaks is limited to a R_s of 0.7 or greater with error < 1% when the peaks purely Gaussian. The even-derivative method does not depend on the peak model or prior knowledge of the number of peaks which is needed in iterative curve fitting approach and multivariate curve resolution method. Additionally, the first derivative method is beneficial for tailing or fronting peaks, with the power of resolving shoulders to the baseline. Its effect is similar to deconvolution. These simple approaches will be helpful in multidimensional chromatography, spectroscopy and other analytical sciences where signals are acquired as peaks, and there is a chance of peak overlap.

7.7 References

- [1] E.J. Hsieh, M.S. Bereman, S. Durand, G.A. Valaskovic, M.J. MacCoss, Effects of Column and Gradient Lengths on Peak Capacity and Peptide Identification in Nanoflow LC-MS/MS of Complex Proteomic Samples, *J. Am. Soc. Mass. Spectrom.* 24(1) (2013) 148-153.
- [2] C.G. Horvath, S.R. Lipsky, Peak capacity in chromatography, *Anal. Chem.* 39(14) (1967) 1893-1893.
- [3] J.M. Davis, J.C. Giddings, Statistical theory of component overlap in multicomponent chromatograms, *Anal. Chem.* 55(3) (1983) 418-424.
- [4] M. Gilar, A.E. Daly, M. Kele, U.D. Neue, J.C. Gebler, Implications of column peak capacity on the separation of complex peptide mixtures in single- and two-dimensional high-performance liquid chromatography, *J. Chromatogr. A* 1061(2) (2004) 183-192.

- [5] B. Wouters, E. Davydova, S. Wouters, G. Vivo-Truyols, P.J. Schoenmakers, S. Eeltink, Towards ultra-high peak capacities and peak-production rates using spatial three-dimensional liquid chromatography, *Lab on a Chip* 15(23) (2015) 4415-4422.
- [6] A. Cristobal, M.L. Hennrich, P. Giansanti, S.S. Goerdalay, A.J.R. Heck, S. Mohammed, In-house construction of a UHPLC system enabling the identification of over 4000 protein groups in a single analysis, *Analyst* 137(15) (2012) 3541-3548.
- [7] D.K. Pinkerton, K.M. Pierce, R.E. Synovec, Chapter 10 - Chemometric Resolution of Complex Higher Order Chromatographic Data with Spectral Detection, Elsevier 2016.
- [8] D.R. Stoll, P.W. Carr, Two-Dimensional Liquid Chromatography: A State of the Art Tutorial, *Anal. Chem.* 89(1) (2017) 519-531.
- [9] D.R. Stoll, X. Wang, P.W. Carr, Comparison of the Practical Resolving Power of One- and Two-Dimensional High-Performance Liquid Chromatography Analysis of Metabolomic Samples, *Anal. Chem.* 80(1) (2008) 268-278.
- [10] H.P. Bailey, S.C. Rutan, Chemometric resolution and quantification of four-way data arising from comprehensive 2D-LC-DAD analysis of human urine, *Chemometrics and Intelligent Laboratory Systems* 106(1) (2011) 131-141.
- [11] F. Gritti, S. Besner, S. Cormier, M. Gilar, Applications of high-resolution recycling liquid chromatography: From small to large molecules, *J. Chromatogr. A* 1524 (2017) 108-120.
- [12] F. Gritti, M. Leal, T. McDonald, M. Gilar, Ideal versus real automated twin column recycling chromatography process, *J. Chromatogr. A* 1508 (2017) 81-94.
- [13] Q. Liu, J. Xiao, J. Yu, Y. Xie, X. Chen, H. Yang, Improved enantioseparation via the twin-column based recycling high performance liquid chromatography, *J. Chromatogr. A* 1363 (2014) 236-241.
- [14] M.F. Wahab, R.M. Wimalasinghe, Y. Wang, C.L. Barhate, D.C. Patel, D.W. Armstrong, Salient Sub-Second Separations, *Anal. Chem.* 88(17) (2016) 8821-8826.
- [15] D.C. Patel, M.F. Wahab, T.C. O'Haver, D.W. Armstrong, Separations at the Speed of Sensors, *Anal. Chem.* 90(5) (2018) 3349-3356.
- [16] J.K. Kauppinen, D.J. Moffatt, H.H. Mantsch, D.G. Cameron, Fourier self-deconvolution: a method for resolving intrinsically overlapped bands, *Appl. Spectrosc.* 35(3) (1981) 271-276.
- [17] X.-G. Shao, A.K.-M. Leung, F.-T. Chau, Wavelet: a new trend in chemistry, *Acc. Chem. Res.* 36(4) (2003) 276-283.
- [18] C. Ruckebusch, L. Blanchet, Multivariate curve resolution: A review of advanced and tailored applications and challenges, *Anal. Chim. Acta* 765 (2013) 28-36.
- [19] B.M.t.H. Romeny, *Front-End Vision and Multi-Scale Image Analysis Multi-Scale Computer Vision Theory and Applications*, written in Mathematica Springer Science and Business Media B.V. 2008.
- [20] D.Z. (Ed.), *CRC Standard Mathematical Tables and Formulas*, CRC Taylor and Francis, Boca Raton, FL, 2017.
- [21] A.C. Faul, *A Concise Introduction to Numerical Analysis*, Taylor and Francis, Boca Raton, FL, 2016.
- [22] S.N. Chesler, S.P. Cram, Iterative curve fitting of chromatographic peaks, *Anal. Chem.* 45(8) (1973) 1354-1359.
- [23] F. Gritti, M.F. Wahab, Understanding the Science Behind Packing High-Efficiency Columns and Capillaries: Facts, Fundamentals, Challenges, and Future Directions, *LCGC North America* 36(2) (2018) 82-98.
- [24] M.F. Wahab, D.C. Patel, R.M. Wimalasinghe, D.W. Armstrong, Fundamental and Practical Insights on the Packing of Modern High-Efficiency Analytical and Capillary Columns, *Anal. Chem.* 89(16) (2017) 8177-8191.
- [25] T. Fornstedt, G. Zhong, G. Guiochon, Peak tailing and mass transfer kinetics in linear chromatography, *J. Chromatogr. A* 741(1) (1996) 1-12.

- [26] P.K. Dasgupta, Y. Chen, C.A. Serrano, G. Guiochon, H. Liu, J.N. Fairchild, R.A. Shalliker, Black box linearization for greater linear dynamic range: the effect of power transforms on the representation of data, *Anal. Chem.* 82(24) (2010) 10143-10150.
- [27] M.F. Wahab, D.C. Patel, D.W. Armstrong, Total peak shape analysis: detection and quantitation of concurrent fronting, tailing, and their effect on asymmetry measurements, *J. Chromatogr. A* 1509 (2017) 163-170.
- [28] U.G. Chapter, 621> Chromatography, 2012.
- [29] F. Gritti, S. Cormier, Performance optimization of ultra high-resolution recycling liquid chromatography, *J. Chromatogr. A* 1532 (2018) 74-88.
- [30] K. Wiberg, M. Andersson, A. Hagman, S.P. Jacobsson, Peak purity determination with principal component analysis of high-performance liquid chromatography–diode array detection data, *J. Chromatogr. A* 1029(1-2) (2004) 13-20.
- [31] J.A. Navarro-Huerta, T. Alvarez-Segura, J.R. Torres-Lapasió, M.C. García-Alvarez-Coque, Study of the performance of a resolution criterion to characterise complex chromatograms with unknowns or without standards, *Analytical Methods* 9(29) (2017) 4293-4303.
- [32] F.S. Pullen, G.L. Perkins, K.I. Burton, R.S. Ware, M.S. Teague, J.P. Kiplinger, Putting mass spectrometry in the hands of the end user, *J. Am. Soc. Mass. Spectrom.* 6(5) (1995) 394-399.
- [33] R. Tauler, D. Barceló, Multivariate curve resolution applied to liquid chromatography—diode array, *TrAC: Trends in Analytical Chemistry* 12(8) (2013) 319.
- [34] T.C. O'Haver, An introduction to signal processing in chemical measurement, *J. Chem. Educ.* 68(6) (1991) A147.
- [35] T.C. O'Haver, Derivative spectroscopy and its applications in analysis (Plenary Lecture), *Analytical Proceedings* 19(1) (1982) 22-46.
- [36] M.F. Wahab, P.K. Dasgupta, A.F. Kadjo, D.W. Armstrong, Sampling frequency, response times and embedded signal filtration in fast, high efficiency liquid chromatography: A tutorial, *Anal. Chim. Acta* 907 (2016) 31-44.

Chapter 8

Improving visualization of trace components for quantification using a power law based integration approach

8.1 Abstract

In some cases, trace component analysis only requires a sensitive and high-resolution mass spectrometer. However, enantiomers must be completely separated to be differentiated with a mass spectrometer, which is highly dependent on the stationary-mobile phase composition. In case of a challenging chiral separation, instead of trying new columns for screening purpose, resolution enhancement techniques could be used to resolve partially overlapping peaks. A well-known enhancement method is the power law, which increases the linear dynamic range of each analyte and reduces excessive noise. In many cases, the peak noise can decrease significantly by applying the power law. However, the main drawback is that this approach changes relative peak areas and heights of each peak in a non-linear fashion which limits its use for quantitative purposes. In this study, a normalized power law was utilized for extracting correct area information. It is a simple (5 step) protocol that only required Microsoft Excel, and results in enhanced visualization of trace components, especially in low signal/noise environments, and makes integration convenient and reproducible. Several difficult chiral trace component analyses were investigated, including applications pertaining to ultrafast high-throughput chromatography, enantiopurity, and peak purity analysis. For complicated cases with multiple overlapped peaks of different resolutions, a segmented normalized power law was utilized. A trace component coeluting near a dead volume peak and a trace enantiomeric component in the tail of the corresponding enantiomeric peak were virtually enhanced. As an additional tool, first and second derivatives were utilized to identify if an enantiomeric impurity is coeluting with the dominant enantiomer under overload conditions. Idiosyncrasies of the derivative test are discussed. This study shows how these simple approaches can be used for accurate quantitation, specifically for trace enantiomeric components.

8.2 Introduction

A trace component typically ranges in the concentration of parts per million to parts per trillion [1]. Liquid chromatography (LC) tandem mass spectrometry (MS), LC-MS, often is utilized to provide selectivity and sensitivity for trace components, including pesticides, pharmaceuticals, and other pollutants [2]. Often, chromatographic peaks of these analytes are overlapping, especially with high-throughput methods, and/or near the dead time of a column which can make visualization and quantification difficult and/or inaccurate. Also, there can be problems in peak purity analysis, especially when MS cannot differentiate components like enantiomers or epimers [3-8]. Further, purity analyses might be performed under overload conditions, where peaks are distorted, and retention times can shift due to displacement or tag-along effects [8-10]. Typically, resolution enhancement of overlapping peaks in chiral LC involves changing the stationary-mobile phase composition, which requires extensive time and testing [11-12]. Sometimes an efficiency increase is enough to separate overlapping peaks by using smaller particle sizes, longer columns, and superficially porous particles [13-17]. However, under ultrafast or high-throughput conditions, shorter columns are needed, which usually results in less efficient chromatographic peaks [14-17]. Also, the presence of noise and nearby eluting system peaks make visualization difficult [18-19].

Resolution enhancement techniques, developed or utilized for ultrafast chromatography, have become popular, including power law, curve fitting by non-linear regression, deconvolution, and derivative based methods [14, 17, 20-21]. Some of these approaches are available with modern instrument software to directly modify the collected chromatographic data, but most require additional sophisticated software and several idiosyncrasies exist, making them only appropriate for specific applications. For example, the power law approach is useful to remove excessive noise, and increase the linear dynamic range, but is not the best for accurate quantitation because it results in a change of chromatographic peak areas and heights [14, 20-21]. Other ways to reduce noise include the use of a smoothing digital filter, which some instruments intrinsically use, and can result in severe peak distortion [18-19]. The Gaussian weighted centered moving average filter might be most favorable because it maintains the retention time of the peak [19].

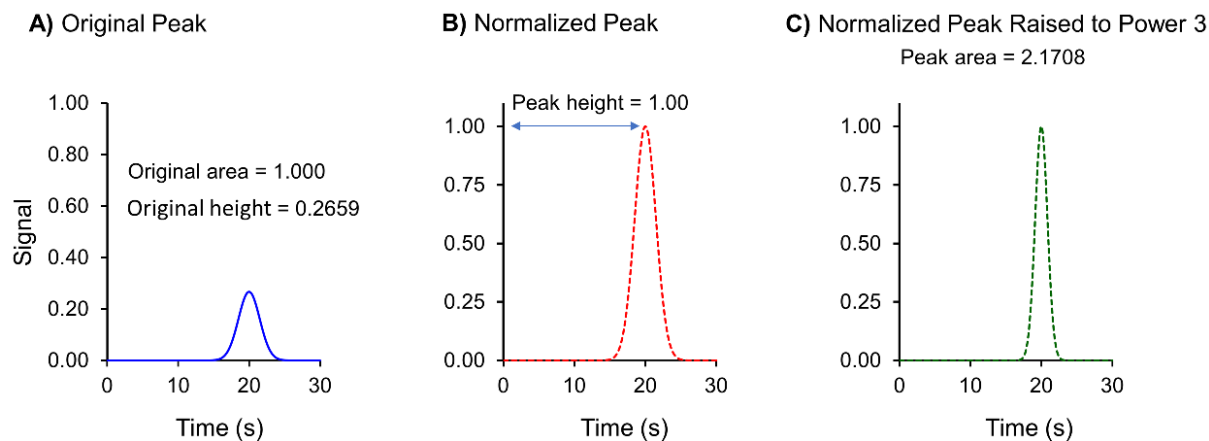
Deconvolution techniques are appropriate when a known distortion is present, such as with Fourier transform deconvolution, which has been used to detect and remove instrument system peaks [17, 19]. Fourier transform deconvolution coupled with a derivative-based method led to the resolution of 10 unresolved chromatographic peaks in a second [17]. Derivatives have also been used to identify underlying compounds in overlapped peaks and the presence of asymmetry on peak shape [22-26]. Iterative curve fitting was utilized to model peak asymmetry for sub-second separations [16]. In this study, we will use first and the second derivatives to visualize hidden trace components under overload conditions, which could then be quantitated by a new normalized power law protocol. This approach enhances visualization of trace components while maintaining essential peak characteristics. It provides a route for accurate quantification and only requires use of ubiquitous Microsoft Excel. The protocols for each method are thoroughly outlined with an illustrative stepwise simulation of the new normalized power law.

8.2.1 Derivative test

The derivative test was utilized only to qualitatively detect the presence of hidden peaks in the chromatogram before using the resolution enhancement by normalized power law (see Section 1.2). The first step was taking the derivative of the raw chromatographic data, i.e., the first derivative means taking the difference between two consecutive signal values and dividing it by the time interval [22]. The result of this first derivative, if the peak is purely Gaussian, is the numerically equal values of the maximum and minimum [23]. Therefore, if a hidden trace component were present, then these values would not be equal, and a shoulder would be viewable along the slope rise or fall. If necessary, a second step could be taken to further enhance the changes seen in the first derivative by taking the second derivative, i.e., the second derivative means taking the derivative of the first derivative [22, 27-28]. The derivatives should be smoothed using standard digital filtering techniques such as using centered moving average procedure. The idiosyncrasies of the derivative test will be discussed in the Results and Discussion.

8.2.2 Normalized power law

The normalized power law was utilized for resolution enhancement and area recovery of trace components. This protocol works for one peak at a time and must be repeated for each peak of interest in the original chromatogram (i.e., 2 trace components requires that the protocol be followed twice). The following steps describe the protocol and were simulated in Fig.1.



Chapter 8 Figure 1. Simulation of the normalized power law technique, proving peak area remains constant when following the protocol described in Section 1.2. **A)** The original simulated peak was set to have an original area of 1.000 and had a corresponding height of 0.2659. **B)** The original height of 0.2659 was normalized to 1. **C)** The normalized peak was then raised to a power ($n = 3$), and the peak area was found to be 2.1708. When using the equation from Section 1.2, the area of the original peak can be back-calculated, resulting in the original area of 1.000.

The first step is to smooth the raw data *via* a Gaussian-weighted centered moving average to minimize the peak noise (Fig. 1A). Then, if necessary, baseline correction was performed based on previous literature (see Results and Discussion) [29]. Next, the trace peak of interest for integration was identified, and the peak height was normalized to equal one (Fig.1B). The peak height normalization is the critical step, which allows area recovery. After normalization, the discrete time series data was raised to a power, n ($n > 1$ and an integer) [16,20-21]. The power law is based on the simple mathematical fact that $(1)^n$ equals 1 and is unchanged with any value of n . If the signal, S , is < 1 , it will decrease when raised to the power, n . If $S > 1$ it will be magnified after applying the power, n . Additionally, since the background noise is usually small, the noise is also decreased by the power law. Note that the change in area will be different in subsequent cases (depending on the original peak area) even if the power, n is the same. A suitable power was chosen until the peak became an easily integrable peak (Fig.1C). The peak area could be determined by simple

numerical integration or other curve fitting methods depending on the separation environment (see Results and Discussion). The last step is to recover the area using the equation: Original Area = Height (original peak) x Area (normalized powered peak) x \sqrt{n} . In Fig.1, the expected original area calculated would be 1.000 after multiplying the height of the original peak (1.00) by the area of the normalized powered peak (2.1708) then multiplied by the sqrt (3). Thus, this protocol overcame the loss of peak area and height due to the normalization step. Also, for accurate peak area recovery a resolution on the order of 1.0, depending on the peak area ratios, should be acquired before enhancement (see Table 1).

Chapter 8 Table 1. Simulated R_s limitations for trace component analysis of peaks with an area ratio of <1:99.

Trace component R_s ¹	Power n for baseline separation ²	% Error in trace peak area ³
1.5 ^{1a}	2	-0.19
1.4	3	-0.15
1.3	4	+0.12
1.2	8	+1.3
1.08	19	+11.8
0.88 ^{1b}	400	+66.7

¹ Calculated resolution (R_s) of the trace component and the adjacent larger peak (with a simulated % area ratio of 0.756: 99.244) using PeakFit software. The actual areas were set at 0.02255 units and 2.96211 units.

^{1a} The R_s of 1.5 usually means a baseline resolution, but when the peak heights are not equal, this R_s does not represent a baseline separation.

^{1b} When $R_s < 0.88$, the peaks merged, so the trace peak's maximum was barely visible.

² See protocol in Section 1.2.

³ % error = 100[Area (recovered) – Area (true)] / [Area(true)].

At resolution < 0.88, a trace component commonly merges with adjacent peaks, making the trace peak maximum ambiguous to recognize.

8.3 Materials and methods

8.3.1 Chromatographic conditions

The macrocyclic glycopeptide, teicoplanin, and hydroxypropyl- β -cyclodextrin were bonded to 2.7 μ m superficially porous particles as 100 x 4.6 mm (i.d.) columns (TeicoShell and CDShell-RSP), and obtained from AZYP, LLC (Arlington, TX, USA). CHIROBIOTIC T (100 x 4.6 mm (i.d.), 5 μ m fully porous particles) was obtained from Supelco (Bellefonte, PA, USA). The analyte, 5-methyl-5-phenylhydantoin,

was obtained as a racemate, while individual enantiomers of 4-phenyl-2-oxazolidinone were obtained from Sigma-Aldrich (St. Louis, MO, USA). All hormone analytes (17 α -ethynylestradiol, estrone, estriol, estradiol, androstadienone (androsta-4,16-dien-3-one), progesterone, and testosterone) were also obtained from Sigma-Aldrich (St. Louis, MO, USA). HPLC grade methanol and acetonitrile, formic acid, and ammonium formate were purchased from Sigma-Aldrich (St. Louis, MO, USA). Water was purified by a Milli-Q water purification system (Millipore, Billerica, MA, USA). The Vanquish UHPLC instrument (Thermo Fisher Scientific, Waltham, MA) was utilized for all HPLC experiments. This instrument is custom configured to by-pass column oven to minimize extra-column effects. The column was connected to the injector and the 2.5 μ L UV-Vis detector.

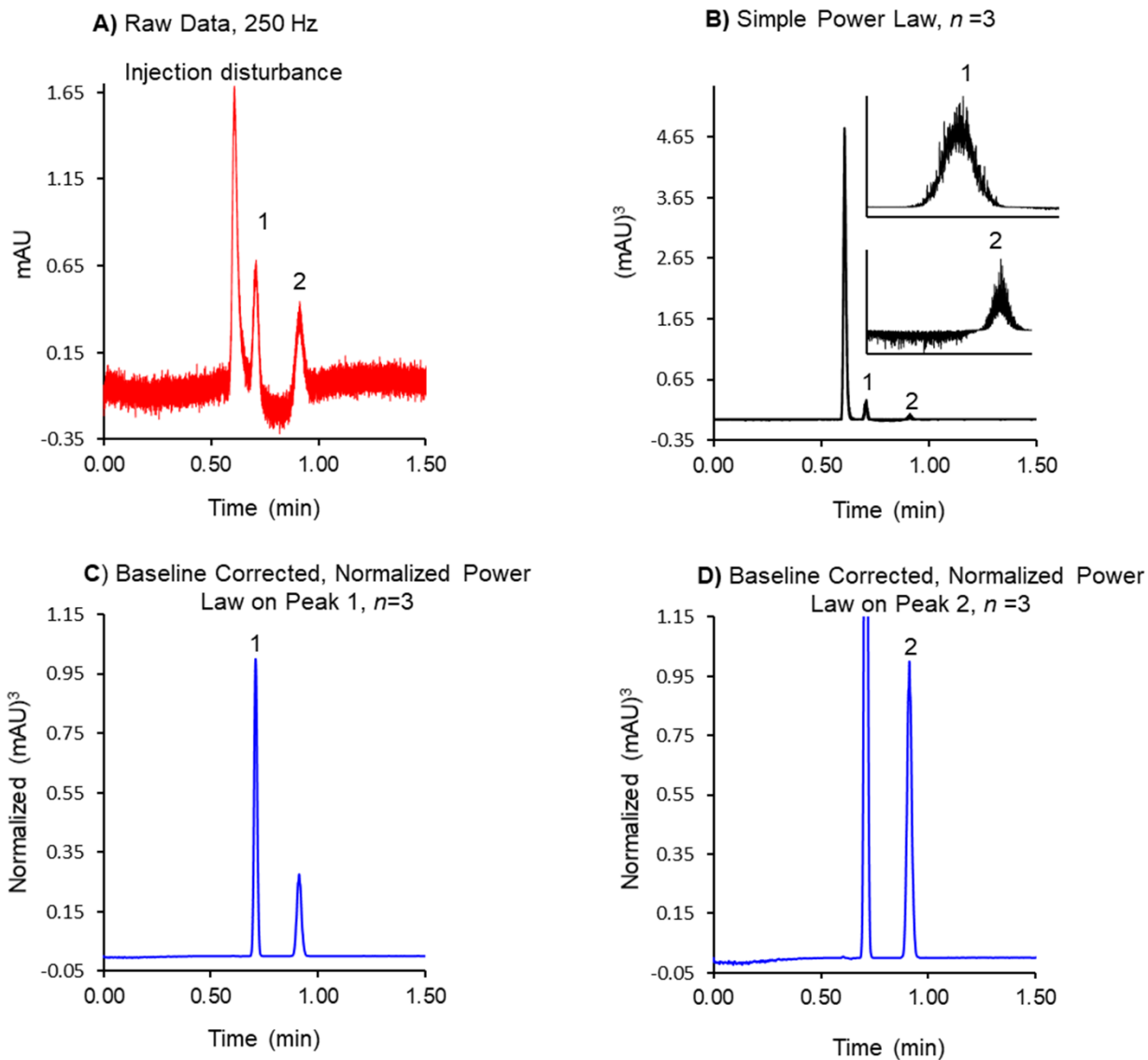
8.3.2 Theory/calculation

The data was sampled at 250 Hz with a response time of 0.00 s (instrument setting) and collected at 220 nm. Chromeleon 7.2 ST4 software (Thermo Fisher Scientific 2009-2016) controlled the Vanquish system. Smoothing was performed in Chromeleon with a Gaussian filter using a centered moving average value of 101 points. The smoothed data was then subjected to a resolution enhancement protocol (the normalized power law or the derivative test, see Section 1.1 and 1.2). The peak areas were either recovered with PeakFit version 4.12 (SeaSolv Software Inc. 1999-2003) and OriginPro 2018 (OriginLab Corporation, MA, USA). The former requires a peak model, and the latter can integrate peak areas by numerical integration. Preliminary results showed no significant difference between the areas calculated by the two different softwares. Each area calculation was performed with triplicate injections and had a %RSD < 3.5%.

8.4 Results and discussion

8.4.1 Recovering peak areas from noisy and drifting baselines

Using the protocol outlined in Section 1.2 and illustrated in Fig. 1, several instances of difficult integration for trace components were investigated. The first case, shown in Fig. 2, was the enantiomeric separation of rac-5-methyl-5-phenylhydantoin using a Chirobiotic-T HPLC column.



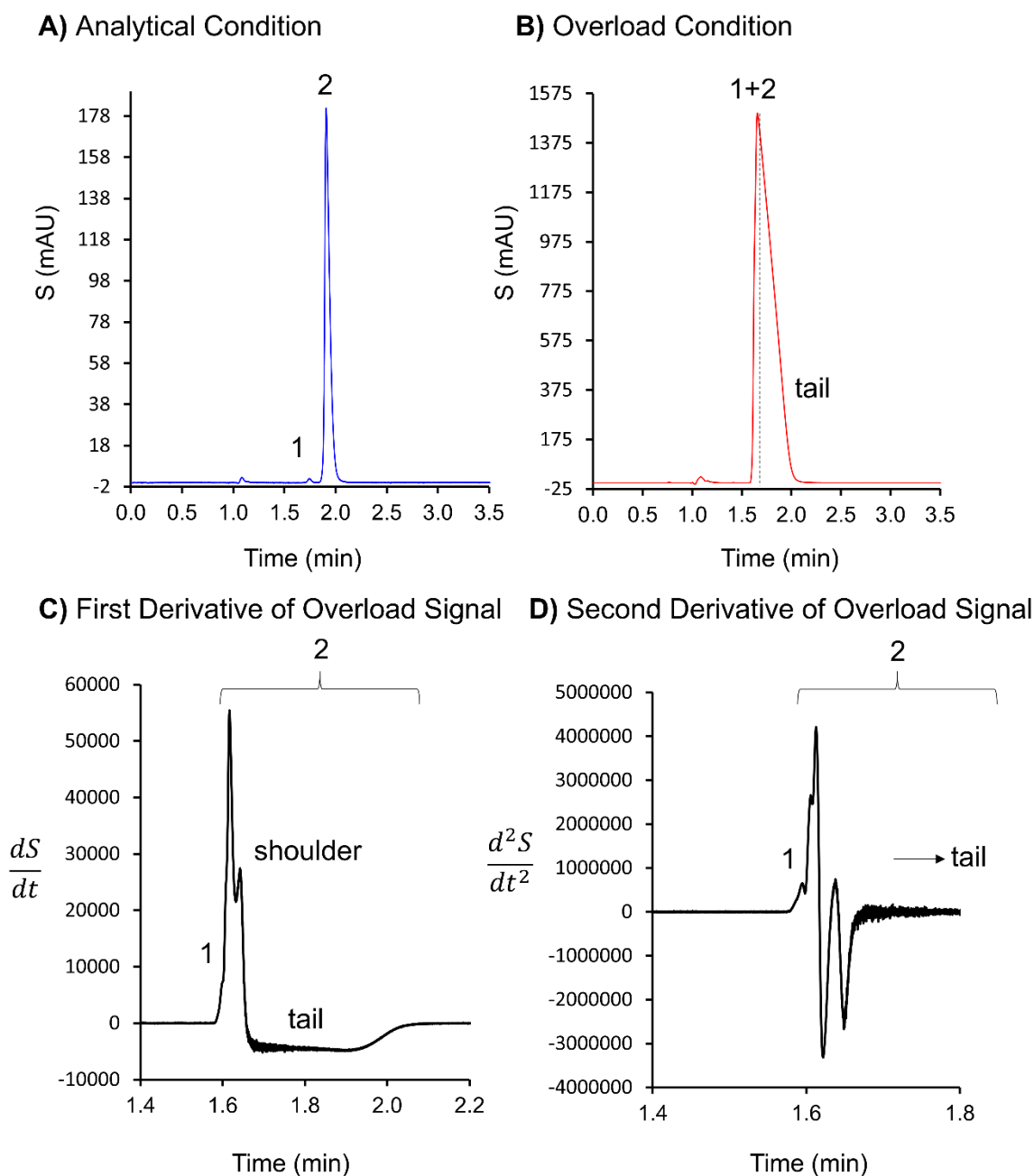
Chapter 8 Figure 2. Visualization and integration of trace enantiomers (peaks 1 and 2: rac-5-methyl-5-phenylhydantoin) near injection disturbance peak. **A)** Raw chromatographic data of 5-methyl-5-phenylhydantoin. **B)** Traditional power law ($n=3$) of raw data without smoothing, with rac-5-methyl-5-phenylhydantoin peaks, expanded. **C)** Peak 1 for area recovery after normalization power law procedure. **D)** Peak 2 for area recovery after normalization power law procedure. Chromatographic conditions: Chirobiotic-T, 5 μm particle size, 100 x 4.6 mm (i.d.), 100% methanol, 2.0 mL/min. Sample conditions: 0.05 mg/mL (*R/S*)-5-methyl-5-phenylhydantoin, injection volume: 0.2 μL . See Section 1.2 for normalized power law protocol.

Known from previous work, these enantiomers are baseline separated in 100% methanol but elute near the dead time [30]. Therefore, the goal was to improve their visualization, specifically the enantiomer (peak 1) that eluted near the dead volume peak (Fig. 2A). The concentration of rac-5-methyl-5-phenylhydantoin was

intentionally prepared at low levels and the flow pumped at 2.0 mL/min to produce an ultrafast enantiomeric separation, which increased the noise to 0.27 mAU (E1657-98 ASTM standard). Also, a dip in the baseline was observed between peak 1 and peak 2 (enantiomers of 5-methyl-5-phenylhydantoin) (Fig. 2A) probably from valve switching at high pressure. Such injection-related baselines disturbances in ultrafast LC have been documented in our previous works [15-16]. Considering the noise and a sloping baseline (drift value of 0.047 mAU/min) as shown in Fig. 2A, consistent and unambiguous integration can be difficult. The noise was still significant when a simple power law ($n = 3$) was used, especially in the apices of the chromatographic signals (Fig. 2B). As expected, the power law also changed the areas and heights of each peak making accurate quantitation impossible. According to the protocol outlined in Section 1.2, Gaussian smoothing and baseline subtraction was performed on the raw data. The baseline data was collected by injecting the sample solvent. After these operations, peak 1 of 5-methyl-5-phenylhydantoin was first selected for the normalized power law and produced an area of 0.01720 maU·min (Fig. 2C). Similarly, this was performed for peak 2 of 5-methyl-5-phenylhydantoin, providing an area of 0.02533 maU·min (Fig. 2D). When using the equation outlined in the protocol of Section 1.2, the original areas were determined for peak 1 and peak 2 as 0.02083 maU·min and 0.01996 maU·min, respectively. As noted in the protocol, even though $n = 3$, as in Fig. 1, the percent area change is different based on the original peak area. From several runs, the average enantiomeric percentage was determined as 50.9:49.1 with an error $\pm 0.2\%$. Note that it was difficult to correctly integrate the raw data (Fig. 2A) in Chromeleon as well by iterative curve fitting because of the noisy and drifting baseline. These results were compared with an enantiomeric separation of rac-5-methyl-5-phenylhydantoin at high signal to noise ratio using a 1.0 mg/mL concentration and 1.0 mL/min flow rate. By simple numerical integration an enantiomeric percentage of 50.0:50.0 was determined. Compared to the power law approach, a 1.8% error was observed. Overall, the normalized power law protocol enhanced visualization which provided accurate quantitation under ultrafast and noisy conditions.

8.4.2 Derivative testing of overload peaks to visualize hidden peaks

In the second case, the derivative test outlined in Section 1.1 was used to identify a hidden, trace enantiomeric component (S enantiomer) in its corresponding enantiomeric peak (R enantiomer) (Fig. 3). Figs. 3A and 3B show the enantiomeric separations of (*S,R*)-4-phenyl-2-oxazolidinone at a enantiomeric ratio of 1.00/99.00 in the analytical (Fig. 3A) and overload (Fig. 3B) conditions by the superficially porous particle bonded teicoplanin column.



Chapter 8 Figure 3. Visualization of the trace enantiomeric impurity, peak 1: (*S*)-4-phenyl-2-oxazolidinone, eluting before the other enantiomer, peak 2: (*R*)-4-phenyl-2-oxazolidinone. **A)** Enantiomeric separation of 1:99 (*S/R*)-4-phenyl-2-oxazolidinone under analytical conditions. **B)** Enantiomeric separation of 1:99 (*S/R*)-4-phenyl-2-oxazolidinone under overload conditions with retention shift. **C)** Identification of (*S*)-4-phenyl-2-oxazolidinone of the overload signal using the first derivative test. **D)** Identification of (*S*)-4-phenyl-2-oxazolidinone of the overload signal using the second derivative test. A third structure was visualized with the second derivative labeled peak 3. Chromatographic conditions: TeicoShell, 2.7 μm particle size, 100 x 4.6 mm (i.d.), 90:10, methanol:16 mm ammonium formate pH 3.6, 1.0 mL/min. Sample conditions: 0.1 mg/mL (*S*)-4-phenyl-2-oxazolidinone mixed with 10

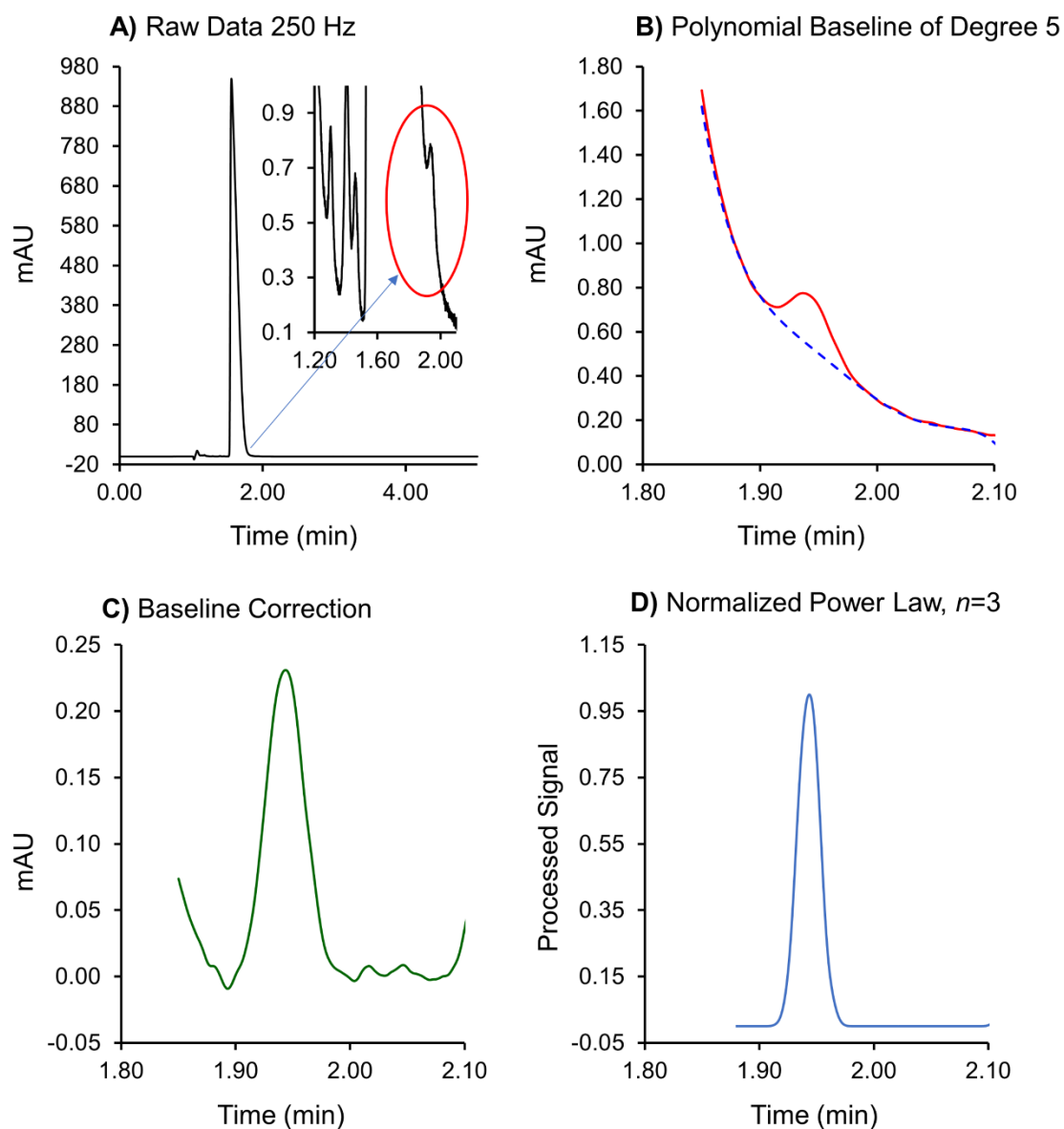
mg/mL (*R*)-4-phenyl-2-oxazolidinone, injection volume: **A**) 0.3 μ L, **B**) 10 μ L. The derivatives were calculated manually with Microsoft Excel. See Section 1.1 for derivative test protocol.

(*S*)-4-phenyl-2-oxazolidinone (peak 1) eluted before (*R*)-4-phenyl-2-oxazolidinone (peak 2). The retention time of peak 2, compared to the analytical conditions, dramatically shifted in the overload conditions, overlapping peak 1. This displacement behavior has been reported with high-concentration bands due to non-linear adsorption isotherms [9-10]. If integration of the trace peak 1 component was needed, then the analytical separation would suffice (Fig. 3A). However, a peak purity check of the overloaded condition might be needed to discern that a trace component was present, thus necessary to integrate (Fig. 3B). By taking the derivative of the overload signal, the peak purity could be determined (Fig. 3C). If the peak were pure Gaussian, with no asymmetry, then the maximum and minimum would have the same magnitude [22]. Usually, smoothing is necessary after taking the derivative so that the noise will not hinder the curvature visualization [25]. As seen in Fig. 3C, the peak was asymmetric with a dip that was indicative of the peak tail. Other asymmetries, peak 1 and peak 2, were identified with the first derivative. Also, a shoulder was determined to be characteristic of a largely overloaded peak and was not seen with lower concentration bands. To further enhance the peak 1 shoulder, the second derivative was taken (Fig. 3D). Another shoulder was identified, which was also determined to be from the overloaded conditions and not an impurity (Fig. 3D). Therefore, there were idiosyncrasies observed when using the derivative test for this experiment. When overloading to the point of retention time shift, the derivative test can show splits, resulting in false positive results (Fig. 3C and 3D). Overloaded peaks are commonly described to make splits and other structures, which further explains this result [9, 31-32]. Therefore, assigning shoulders as detected by the first and the second derivatives as impurities or other components should be done carefully, especially under overload conditions. It should also be noted that Chromeleon software offers the first and second derivatives during data analysis along with smoothing options. In the Supplementary Material, the first and second derivatives of the data from Fig. 3B were compared between the numerical approach (based on the definitions of the first and second derivatives) reported in Figs. 3C and 3D to the output of the Chromeleon software [27-28]. The magnitudes of the y-axes were different indicating that the Chromeleon software does not take the time

interval into account. Additionally, there is an embedded smoothing procedure in the derivative taken by Chromeleon, which showed differences in noise levels. It should be remarked, since the derivative test was only used for qualitative purposes, this did not hinder the results of the approach since only the shape was of interest.

8.4.3 Quantitation of embedded peaks in nearby signals with the normalized power law

Like case 2, rac-4-phenyl-2-oxazolidinone was separated with the superficially porous particle TeicoShell column. However, in this investigation, the normalized power law was utilized to enhance the visualization as well as accurately quantitate a trace impurity (Fig. 4).



Chapter 8 Figure 4. Visualization and quantitation of the trace enantiomeric component hidden in the other enantiomer's tail. **A)** Enantiomeric separation of 99.99:0.01 (*S/R*)-4-phenyl-2-oxazolidinone under overload conditions. **B)** A polynomial baseline of degree 5 was developed using iterative curve fitting to subtract the baseline. **C)** The remaining smoothed trace component data once subtracted. **D)** Use of normalized power law to enhance peak shape for visualization and quantification. Chromatographic conditions: Same as Fig. 2. Sample conditions: 5 mg/mL (*S*)-4-phenyl-2-oxazolidinone and 0.0005 mg/mL (*R*)-4-phenyl-2-oxazolidinone, injection volume: 2.5 μ L. See Section 1.2 for normalized power law protocol.

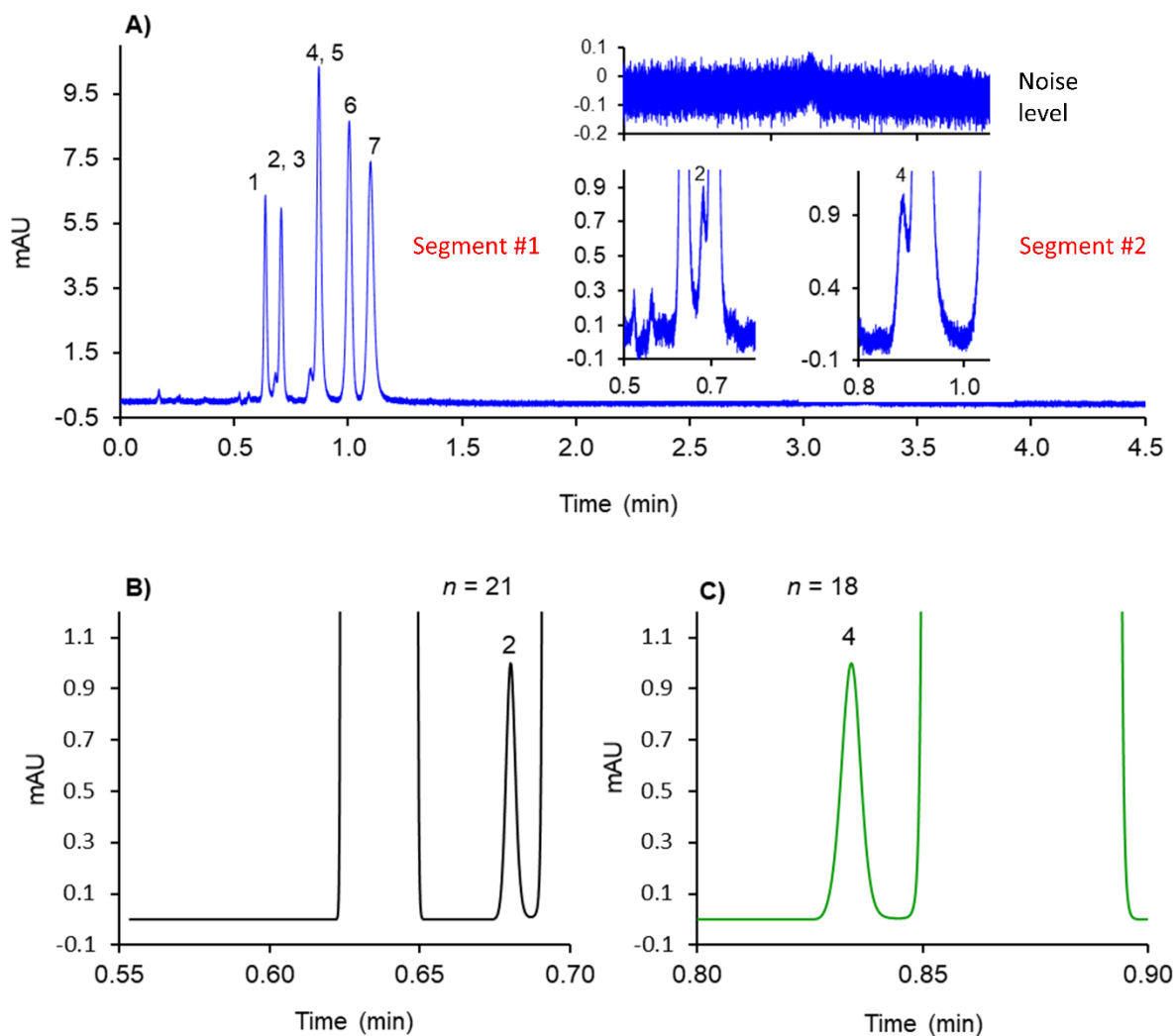
A mixture of 99.99:0.01 of (*S/R*)-4-phenyl-2-oxazolidinone was made and enantiomerically separated (Fig. 4A). The trace component (*R* enantiomer) was only visible when increasing the injection volume to the

point of overload conditions. Simple integration was difficult since the component was embedded in the tail of the larger peak (S enantiomer) with large noise. However, iterative curve fitting with PeakFit was used to estimate the peak area of the trace component. The limitations of PeakFit include that the number of peaks present, and a model must be selected by the user. Also, it cannot model complex overload peaks with concurrent fronting/tailing. Since the choice of models and number of peaks was subjective, it might not be the best choice for an unknown sample but was a good benchmark for comparison of the normalized power law. Using the protocol outlined in Section 1.2, the raw data was smoothed then baseline corrected using a polynomial baseline of degree 5 (Fig. 4B). The key point behind choosing a certain function as a baseline is that it should fit the “local” baseline very well. Many instruments offer only an exponential skim, which can have high error in some situations [33]. As we have seen here, under overload conditions peak shapes can acquire various shapes. Overall, the trace component was now more viewable, but noise was still apparent since it was at a low concentration (Fig. 4C). Using the normalized power law, the peak was visually enhanced to ease integration (Fig. 4D). The recovered area was 0.00993 maU·min, compared to the PeakFit iterative curve fitting, which estimated an area of 0.00959 maU·min with an R^2 value of 0.9942. It took nine iterations in fitting an exponentially modified Gaussian model to the peaks after using an inbuilt (undisclosed) baseline function of the selected region as shown in Fig. 4B. As seen, by applying a normalized power law it is far more convenient to integrate after using a polynomial baseline in the region of interest.

8.4.4 Segmented normalized power law for multiple overlapped critical pairs

In a complex chromatogram, the number of critical pairs will increase, and have less chromatographic resolution than the previously discussed cases. Herein, we introduce the concept of segmented normalized power law, which is useful for complicated cases. As an illustrative example we have investigated a mixture of 7 hormones, including 17α -ethynylestradiol, estrone, estriol, estradiol, androstadienone (androsta-4,16-dien-3-one), progesterone, and testosterone. Different than previous enantiomeric analyses, this mix contained closely related compounds with similar masses hence m/z values of parent ions. Such components

can still pose problems for MS differentiation, like epimers and enantiomers. Androstadienone and estrone have the same mass, but in this case, CDSshell-RSP easily separated them, like other estrogen epimers with a β -cyclodextrin column (Fig. 5A) [34].



Chapter 8 Figure 5. Utilizing a “segmented” normalized power law approach with trace and overlapping components. **A)** Raw separation data of 7 hormones (in order of elution): 17α -ethynylestradiol, estrone, estriol, estradiol, androstadienone (androsta-4,16-dien-3-one), progesterone, and testosterone. CDSshell-RSP, 2.7 μ m particle size, 100 x 4.6 mm (i.d.), 50:50, acetonitrile:water, 2.0 mL/min. Sample conditions: 1.0 mg/mL of each component except peaks 2 and 4, which were 0.1 mg/mL, injection volume 0.3 μ L. **B)** Segment 1 with $n = 21$ of peak 2. **C)** Segment 2 with $n = 18$ of peak 4. See Results and Discussion for more information about the “segmented” normalized power law approach compared to the normalized power law protocol described in Section 1.2.

In this separation, there were two overlapping pairs, estrone and estriol (peaks 2 and 3, segment 1: 0.50 – 0.75 min) and estradiol and androstadienone (peaks 4 and 5, segment 2: 0.80 – 1.00 min) (Fig. 5A). One of the components of each pair were mixed at significantly lower concentrations compared to the other components. Additionally, significant peak to peak noise, ± 0.18 mAU (E1657-98 ASTM standard), was present and representative of high-throughput and high-efficiency conditions. Compared to the previous protocol where the same power is used for each peak area recovery, different powers are applied in various segments of a given chromatogram. A power of 21 was needed to baseline separate estrone and estriol (peaks 2 and 3, segment 1), which had a R_s of 0.74 (Fig. 5B). The recovered area was 0.01402 maU·min, which was comparable to the result from iterative curve fitting (using the exponentially modified Gaussian model), which was 0.01431 maU·min. Therefore, the difference between the two values was $\pm 2.0\%$. Again, this approach was applied to the second critical pair (estradiol and androstadienone, peaks 4 and 5, segment 2), which had a R_s of 0.88 (Fig. 5C). A lower power of 18 was needed, compared to segment 1, due to slightly higher R_s . The recovered area was 0.02186 maU·min, which was compared to the result from iterative curve fitting, which was 0.02152 maU·min. The difference was $\pm 1.6\%$, which was lower than the first overlapped pair due to the higher initial resolution. These results correlate very well with the simulated data shown in Table 1. It is important to note that the data from Table 1 corresponds to a peak to peak area ratio on the order of 1 to 99. The R_s of an overlapping pair with this peak ratio must be > 0.9 to perform accurate quantitation. However, as seen in the case of Fig. 5, accuracy can be maintained with a $R_s < 0.9$ when the peak areas are less disproportionate. Since peak overlap can be different between critical pairs, it was appropriate to utilize the normalized power in segments (segmented normalized power law). It provided enhanced visualization of the trace components an accurate quantification comparable to or better than other conventional integration methods in the presence of high noise [33] without requiring any sophisticated software or mathematical tools.

8.5 Conclusions

Conventional power law offers advantages such as peak sharpening and noise reduction, so it has become a common resolution enhancement technique in chromatography, especially ultrafast chromatography where high noise is present. However, it is limited by quantitative applications of unknown species since the areas and heights of chromatographic peaks change in a complex fashion. The normalized power law approach utilized in this study overcame the limitations of the simple power law, providing a route to determine original peak characteristics. This was shown in chromatographic environments where the resolution was typically substantial, but trace enantiomeric components were present in noisy and “difficult to integrate” environments. With several overlapped peaks or critical pairs, it might be more appropriate to utilize the segmented power law approach. If necessary, the derivative test was utilized in this study to determine the presence of overlapping trace peaks before quantification. Further error analysis, especially in low signal to noise environments are needed. Undoubtedly other uses of these protocols exist, but this application was critical in the sense that differentiation of barely visible and overlapping trace enantiomeric components is difficult and requires much more effort than a simple mathematical procedure.

8.6 References

- [1] J. Namieśnik, Trace analysis – challenges and problems, *Crit. Rev. Anal. Chem.* 32 (2002) 271–300.
- [2] N. Hermes, K.S. Jewell, A. Wick, T.A. Ternes, Quantification of more than 150 micropollutants including transformation products in aqueous samples by liquid-chromatography-tandem mass spectrometry using scheduled multiple reaction monitoring, *J. Chromatogr. A* 1531 (2018) 64-73.
- [3] D.K. Bryant, M.D. Kingswood, A. Belenguer, Determination of liquid chromatographic peak purity by electrospray ionization mass spectrometry, *J. Chromatogr. A* 721 (1996) 41-51.
- [4] C.L. Barhate, D.A. Lopez, A.A. Makarov, X. Bu, W.J. Morris, A. Lekhal, R. Hartman, D.W. Armstrong, E.L. Regalado, Macrocyclic glycopeptide chiral selectors bonded to core-shell particles enables enantiopurity analysis of the entire verubecestat synthetic route, *J. Chromatogr. A* 1539 (2018) 87-92.
- [5] C.L. Barhate, L.A. Joyce, A.A. Makarov, K. Zawatzky, F. Bernardoni, W.A. Schafer, D.W. Armstrong, C.J. Welch, E.L. Regalado, Ultrafast chiral separations for high throughput enantiopurity analysis, *Chem. Commun.* 53 (2016) 509–512.
- [6] M.F. Wahab, Z.S. Breitbach, D.W. Armstrong, R. Strattan, A. Berthod, Problems and pitfalls in the analysis of amygdalin and its epimer, *J. Agric. Food. Chem.* 63 (2015) 8966-8973.
- [7] R.E. Boehm, D.E. Martire, D.W. Armstrong, Theoretical considerations concerning the separation of enantiomeric solutes by liquid chromatography, *Anal. Chem.* 60 (1988) 522-528.
- [8] D.W. Armstrong, J.D. Duncan, S.H. Lee, Evaluation of D-amino acid levels in human urine and in commercial L-amino acid samples, *Amino Acids* 1 (1991) 97-106.

- [9] M.F. Wahab, J.K. Anderson, M. Abdelrady, C.A. Lucy, Peak distortion effects in analytical ion chromatography, *Anal. Chem.* 86 (2014) 559-566.
- [10] S. Golshan-Shirazi, G. Guiochon, Theoretical explanation of the displacement and tag-along effects, *Chromatographia* 30 (1990) 613-617.
- [11] G. Hellinghausen, D. Roy, J.T. Lee, Y. Wang, C.A. Weatherly, D.A. Lopez, K.A. Nguyen, J.D. Armstrong, D.W. Armstrong, Effective methodologies for enantiomeric separations of 150 pharmacology and toxicology related 1°, 2°, and 3° amines with core-shell chiral stationary phases, *J. Pharm. Biomed. Anal.* 155 (2018) 70-81.
- [12] T.E. Beesley, J.T. Lee, Method development strategy and applications update for CHIROBIOTIC chiral stationary phases, *J. Liq. Chromatog. Rel. Technol.* 32 (2009) 1733-1767.
- [13] D.A. Spudeit, M.D. Dolzan, Z.S. Breitbach, W.E. Barber, G.A. Micke, D.W. Armstrong, Superficially porous particles vs. fully porous particles for bonded high performance liquid chromatographic chiral stationary phases: isopropyl cyclofructan 6, *J. Chromatogr. A* 1363 (2014) 89-95.
- [14] D.C. Patel, Z.S. Breitbach, M.F. Wahab, C.L. Barhate, D.W. Armstrong, Gone in seconds: praxis, performance, and peculiarities of ultrafast chiral liquid chromatography with superficially porous particles, *Anal. Chem.* 87 (2015) 9137-9148.
- [15] D.C. Patel, M.F. Wahab, D.W. Armstrong, Z.S. Breitbach, Advances in high-throughput and high-efficiency chiral liquid chromatographic separations, *J. Chromatogr. A* 1467 (2016) 2-18.
- [16] M.F. Wahab, R.M. Wimalasinghe, Y. Wang, C.L. Barhate, D.C. Patel, D.W. Armstrong, Salient sub-second separations, *Anal. Chem.* 88 (2016) 8821-8826.
- [17] D.C. Patel, M.F. Wahab, T.C. O'Haver, D.W. Armstrong, Separations at the speed of sensors, *Anal. Chem.* 90 (2018) 3349-3356.
- [18] M.F. Wahab, P.K. Dasgupta, A.F. Kadjo, D.W. Armstrong, Sampling frequency, response times and embedded signal filtration in fast, high-efficiency liquid chromatography: A tutorial. *Anal. Chim. Acta* 907 (2016) 31-44.
- [19] C.L. Barhate, M.F. Wahab, D.J. Tognarelli, T.A. Berger, D.W. Armstrong, Instrumental idiosyncrasies affecting the performance of ultrafast chiral and achiral sub/supercritical fluid chromatography, *Anal. Chem.* 88 (2016) 8864-8672.
- [20] R.A. Shalliker, P.G. Stevenson, D. Shock, M. Mnatsakanyan, P.K. Dasgupta, G. Guiochon, Application of power functions to chromatographic data for the enhancement of signal to noise ratios and separation resolution, *J. Chromatogr. A* 1217 (2010) 5693-5699.
- [21] P.K. Dasgupta, Y. Chen, C.A. Serrano, G. Guiochon, H. Liu, J.N. Fairchild, R.A. Shalliker, Black box linearization for greater linear dynamic range: the effect of power transforms on the representation of data, *Anal. Chem.* 82 (2010) 10143-10150.
- [22] M.F. Wahab, D.C. Patel, D.W. Armstrong, Total peak shape analysis: detection and quantitation of concurrent fronting, tailing, and their effect on asymmetry measurements, *J. Chromatogr. A* 1509 (2017) 163-170.
- [23] M.F. Wahab, D.C. Patel, D.W. Armstrong, Peak shapes and their measurements: The need and the concept behind total peak shape analysis, *LC GC N. Am.* 35 (2017) 846-853.
- [24] S. Ebel, Validation of analysis methods, *Fresenius J. Anal. Chem.* 342 (1992) 769-778.
- [25] T.C. O'Haver, G.L. Green, Numerical error analysis of derivative spectrometry for the quantitative analysis of mixtures, *Anal. Chem.* 48 (1976) 312-318.
- [26] G. Vivó-Truyols, J.R. Torres-Lapasió, A.M. van Nederkassel, Y. Vander Heyden, D.L. Massart, Automatic program for peak detection and deconvolution of multi-overlapped chromatographic signals Part I: Peak detection, *J. Chromatogr. A* 1096 (2005) 133-145.

- [27] Difference equations, in: D. Zwillinger (Ed.), CRC Standard Mathematical Tables and Formulas, 33rd ed., New York: Chapman and Hall/CRC, 2018, pp. 184-188.
- [28] C.F. Gerald, P.O. Wheatley, Numerical differentiation and numerical integration, in: T.N. Taylor (Ed.), Applied Numerical Analysis, fourth ed., Menlo Park, CA: Addison-Wesley Publishing Company, 1990, pp. 264-346.
- [29] A. Cichocki, I. Sabala, S. Choi, B. Orsier, R. Szupiluk, Self-adaptive independent component analysis for sub-Gaussian and super-Gaussian mixtures with an unknown number of sources and additive noise, Proc. NOLTA. 97 (1997) 731-734.
- [30] D.W. Armstrong, Y. Liu, K.H. Ekborg-Ott, A covalently bonded teicoplanin chiral stationary phase for HPLC enantioseparations, Chirality 7 (1995) 474-497.
- [31] S. Golshan-Shirazi, G. Guiochon, Theoretical study of system peaks and elution profiles for large concentration bands in the case of a binary eluent containing a strongly sorbed additive, J. Chromatogr. A 461 (1989) 1-18.
- [32] S. Jacobson, S. Golshan-Shirazi, G. Guiochon, Chromatographic band profiles and band separation of enantiomers at high concentration, J. Am. Chem. Soc. 112 (1990) 6492-6498.
- [33] M.K.L. Bicking, Integration errors in chromatographic analysis, Part II: Large peak size ratios, LC GC N. Am. 24 (2006) 605-616.
- [34] D.W. Armstrong, W. DeMond, A. Alak, W.L. Hinze, T. Riehl, K.H. Bui, Liquid chromatographic separation of diastereomers and structural isomers on cyclodextrin-bonded phases, Anal. Chem. 57 (1985) 234-237.

Chapter 9

Progress in Peak Processing

9.1 Abstract

Despite advanced separation technologies and extensive method development knowledge, peak overlap is still commonly observed. Peak integration becomes more challenging as chromatographic resolution decreases, especially with asymmetric peaks. Post-acquisition signal processing, well established in optical spectroscopy and NMR, is now being utilized in liquid chromatography. Mathematical operations can be applied on raw chromatographic data to enhance resolution of overlapping peaks and reduce peak widths. These techniques can maintain original area information needed for quantitation after some modifications. This article gives a brief overview of recently introduced mathematical procedures such as the Fourier deconvolution of extra-column effects, iterative curve fitting, multivariate curve resolution, modified power law, and use of first and second derivatives in enhancing resolution. Advantages and limitations of each technique are presented. Many of these tools only require ubiquitous Microsoft Excel, but some techniques require more advanced software. Implementation of these techniques in chromatography data software would undoubtedly be feasible in the future. Surely, high-throughput analyses in gas, liquid, and supercritical fluid chromatography, will benefit from these simple and effective approaches in many challenging separations.

9.2 Introduction

Some analytical chemists often wonder, what is the future direction of separation science? One school of thought holds that this field is mature and not much remains to be done. Spectroscopy went through a similar phase a few decades ago, but the introduction of digital signal processing revolutionized the whole field of molecular spectroscopy and nuclear magnetic resonance (NMR) spectroscopy. It is impossible to imagine any modern infrared or NMR spectrum that has not undergone a Fourier transform and other mathematical manipulations. Separation scientists have been quite hesitant to adapt mathematical

techniques to enhance peak resolution but perhaps we can extract more from less, even if the physical separation is not fully developed. The purpose of analytical separations (e.g., chromatography, electrophoresis) is to obtain useful information. This can be qualitative and/or quantitative in nature. Things that enhance the speed of the process and the accuracy of the information are highly desirable.

Advancements in chromatography have led to highly efficient separations and we are finally beginning to grasp the science behind high efficiency columns (1-3). At best, randomly packed beds consisting of non-porous, superficially porous, and fully porous particles can produce reduced plate heights h (equal to the theoretical plate height divided by the particle diameter, H/d_p) as low as 0.5, 0.7, and 0.9, respectively (4), whereas in practice we are currently half-way there. Davis and Giddings, on the basis of statistical theory of overlap, predicted that a multicomponent chromatogram should be roughly 95% empty in order to provide a 90% probability that a given analyte of interest will appear as an isolated peak (5). Even with modern high efficiency separations, there are cases where one or two critical pairs have resolution problems e.g., deuterated vs. non-deuterated molecules, enantiomeric or cases where there are large number of peaks. More often, in enantiomeric separations the entire separation window is empty and yet the enantiomers have poor resolution. Usually, there is an ambiguity in the integration of overlapped chromatographic peaks when using routine drop perpendicular, skimming methods. Thus, the development and use of a method that suitably separates all the components necessary for quantitation (usually with the aim of a baseline separation, resolution = 1.5) commonly becomes the bottleneck of chromatographic analysis in research work as well as in the pharmaceutical industry. What if, *with a click of a button*, resolution was instantaneously improved, and there was no need to go through the arduous process of method development (switching stationary phases, mobile phases, etc.)?

The primary concern is: can we mathematically improve chromatographic resolution while maintaining critical peak information necessary for quantitation? Also, it would be preferred if the protocol was simple and straightforward. Herein, we provide the fundamental ideas that govern new signal processing protocols

including deconvolution e.g., via Fourier transformation (6,7), iterative curve fitting and multivariate curve resolution (8-10), power laws (11,12) and derivatives (13). These are shown in Table 1.

Chapter 9 Table 1. Overview of advanced signal processing techniques.

	Technique	Requirements	Advantages
a.	Fourier transform deconvolution	<ul style="list-style-type: none"> • Data with & w/o column • Advanced software (MATLAB) 	<ul style="list-style-type: none"> • Remove extra-column band broadening • Corrects time delay from system volume • Increases resolution
b.	Iterative curve fitting	<ul style="list-style-type: none"> • Known number of components • Single channel data • Advanced software (PeakFit, OriginPro) • Computationally heavy 	<ul style="list-style-type: none"> • Area extraction of partial overlapped peaks (quantitation subjective to user*)
c.	Multivariate curve resolution	<ul style="list-style-type: none"> • Known number of components • Multidimensional data • Advanced software (MATLAB) • Computationally heavy 	<ul style="list-style-type: none"> • Area extraction of completely overlapped peaks in complex matrices (quantitation subjective to user*)
d.	Modified power law	<ul style="list-style-type: none"> • Smoothed single channel data • Repeat for each peak, resolution ~ 0.8 for error $\leq \sim 1\%$ (proportionate peaks) 	<ul style="list-style-type: none"> • Directly increases resolution by reducing peak width and tailing • Improves S/N • Simple software (Microsoft Excel) • Quick procedure
e.	Even derivative peak sharpening	<ul style="list-style-type: none"> • Smoothed single channel data • Resolution ~ 0.7 for error $\leq \sim 1\%$ (proportionate peaks) 	<ul style="list-style-type: none"> • Directly increases resolution by reducing peak width • Simple software (Microsoft Excel) • Quick procedure

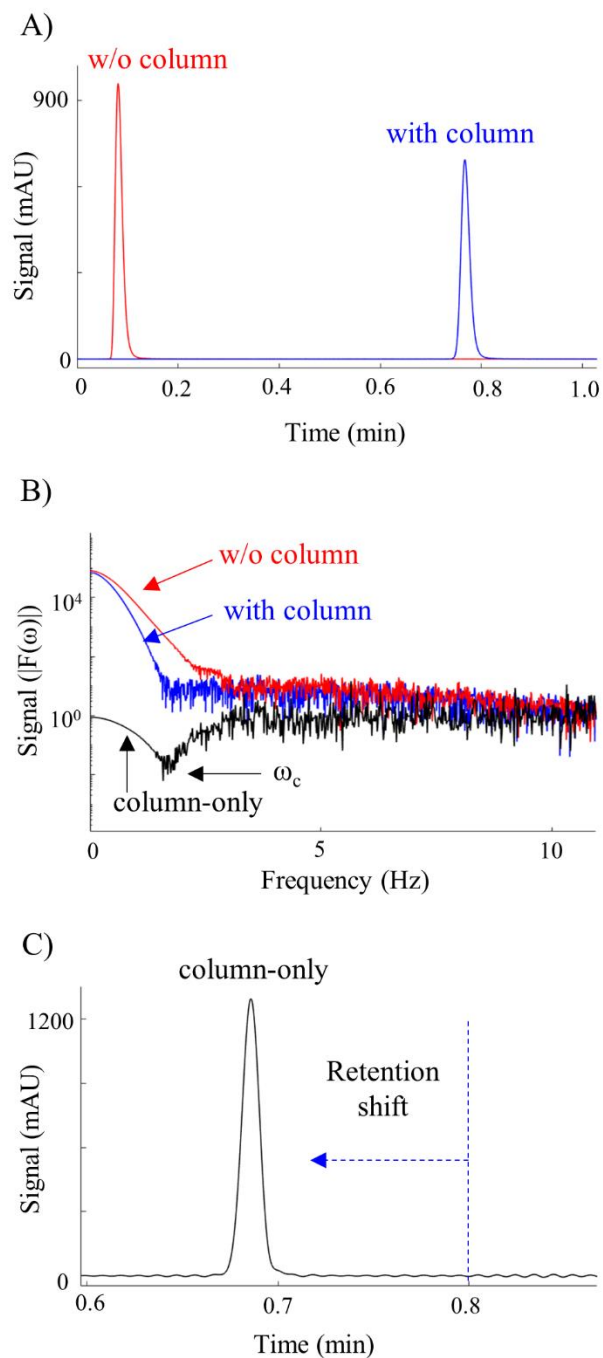
* User must choose model/constraints used for this operation.

They fall under three general categories: 1) elimination of extra-column band broadening 2) extracting peak areas by curve fitting 3) directly enhancing resolution by reducing peak widths. The following sections describe these strategies with their advantages and limitations as per the maxim *when we gain something, in turn we can lose something else*. These resolution enhancement strategies mostly only require ubiquitous software (e.g. Microsoft Excel), single channel data, and surely will be implemented into chromatography data software in future. Once fully automated, their true power will be most apparent in ultrafast (< 1 min), hyperfast (< 1 sec) liquid chromatography and high peak capacity separations.

9.3 Discussion

9.3.1 Deconvolution of extracolumn effects by Fourier transformation (FT)

A chromatograph that does not contribute to band broadening has yet to be invented. Thus, the recorded signal from the instrument is convoluted with broadening by the injector, connection tubings and the detector design. Deconvoluting this effect would remove these extra-column effects from the chromatogram. Resolution would also increase if the separation was compromised by the hardware and software. FT deconvolution was first described chromatography in the early 1980s (7). Recent work evaluated the band broadening elimination by FT deconvolution on modern UHPLCs and narrow bore columns as shown in Figure 1 (6).



Chapter 9 Figure 1. Removal of extra-column band broadening effects by Fourier transform deconvolution (6). Panel A shows the collection of a chromatogram with and without the column. Then, each dataset is converted to the frequency domain as shown in panel B. Next, they are divided, with the result shown as “column-only”. This is converted back to the time domain as shown in panel C. The retention time of the chromatographic peak has also shifted accounting for the system volume. (Figures in MATLAB provided by Y. Vanderheyden).

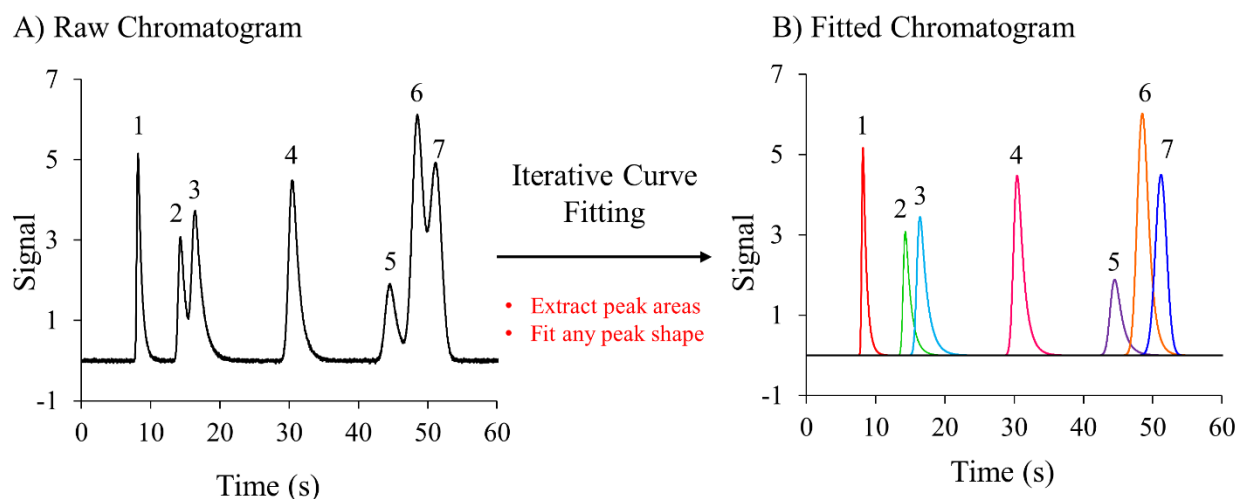
The protocol for FT deconvolution is a three-step process. First, a chromatogram must be collected with and without the column (panel A). Then, both chromatograms are converted to the frequency domain by Fourier transformation (panel B). Next, the frequency transformed data from the chromatogram with the column is divided by the frequency transformed data collected without the column. The resulting quotient is converted back to the time domain by inverse Fourier transform (6). This yields a chromatogram which is free of extra-column band broadening effects (panel C). Note, that there is a shift in peak retention time resulting from the time needed for the injected analyte to reach the detector without the column i.e., system volume effect is also corrected. Baseline noise increases as a result of division in frequency domain because division by very small numbers as well as oscillations are seen, which can easily be decreased by digital smoothing or cutting off all high frequency noise (ω_c). Fourier transform deconvolution has also been applied while working with 1 cm columns at extremely high flow rates (14).

9.3.2 Peak area extraction by iterative curve fitting

Iterative curve fitting is a versatile approach for extracting peak areas from partially overlapping peaks, especially when multiple components are overlapping to some extent. The chromatogram containing time and single channel signal is exported into a curve fitting software e.g., or OriginPro, PeakFit™, which considers the entire chromatogram as a sum of exponentially modified peaks. It is assumed that a single peak represents a pure component. The number of components (peaks) are proposed by the user, then the chromatogram is fitted according to the chosen peak model by method of minimization of residuals. There are several peak functions, but for liquid chromatography, usually an exponentially decaying tail is observed. Thus, the most useful model for these purposes has been determined as the bi-directional exponentially modified Gaussian (BI-EMG), which is a Gaussian function with a one-sided exponentially decaying tail or front as a function of time (15). For simple chromatograms, one can conveniently obtain a fit with a coefficient of determination (R^2) close to 1 (if $R^2 = 1$, then it is a perfect fit). This is a trial and error approach where the user continues to adjust the initial parameters of the model iteratively improving the fit until they find it acceptable. Caution should be exercised that an iterative curve fitting procedure

may yield several mathematically correct answers. Similarly, it is ambiguous to fit several peaks under a single peak, which is mathematically possible, but it will not reflect the reality.

Once a suitable fit is determined for the separation, a baseline must be established to extract each underlying peak area. In most cases, a simple linear baseline is sufficient. However, in gradient elution or multidimensional separations, a non-linear baseline could be utilized by choosing it from the software. The use of iterative curve fitting to extract peak areas from overlapping peaks is illustrated in Figure 2.



Chapter 9 Figure 2. Iterative curve fitting of 7 simulated peaks with different peak heights, areas, and shapes. Panel A shows the raw chromatogram obtained from the simulation. After fitting, using a bidirectional exponentially modified Gaussian model, and a linear baseline, each peak area can be extracted. Customization can be made to the constraints, which improves the fit and allows the user to fit any peak shape.

A simulated separation of 7 peaks in under a minute is shown (Figure 2). There are two sets of overlapping segments with differing degree of tailing and efficiencies. Since it was simulated, their true area of each peak was known. The *exact* peak areas of peaks 1 to 7 were 4, 3, 6, 8, 5, 10, 9 area units in the absence of noise, respectively. Using the BI-EMG model, this separation was fitted with an R^2 of 0.9996. After this mathematical fitting, we can extract peak areas, as well as other peak information including efficiency, tailing factors, peak height, zeroth, first, second, and statistical moments. In this case, the extracted areas are in order of peaks 1-7, 3.99, 2.99, 5.99, 7.99, 5.01, 9.98, and 9.02 respectively, with an excellent match of theoretical areas in the presence of random noise. Overall, curve fitting procedures are powerful for extracting peak areas when it is clear that there are no hidden peak under the

peak of interest. One aspect should be kept in mind that choosing a Gaussian peak is only a limiting case as real peaks are rarely pure Gaussians.

9.3.3 Model-free approaches for peak information extraction

Various powerful methods exist besides iterative curve fitting for extracting peak information even when the peak overlap completely, where an iterative curve fitting method mentioned above will fail (16).

Unlike iterative curve fitting, these methods require multidimensional data, i.e. various signals are acquired at the same time. Secondly, these signals must be specific to the molecule of interest. For example, a photodiode array generates an entire spectrum of a given component, similarly mass spectrometry generates analyte specific signal. Thirdly, in order to identify multiple peaks in a completely coeluting peak envelope the key requirements are that the compounds that are coeluting must be known and their *pure* spectra must be present in the software library. A latest example is that of the vacuum UV (VUV) GC detector. The mathematical technique is termed as “linear combination of weighted reference spectra.” The VUV software can extract complete peak information of coeluting compounds if the spectra of co-eluting compounds are known and they are sufficiently distinct. The observed spectrum at each data point is treated as the sum of pure spectra for the coeluting compounds following Equation (1):

$$\text{Observed spectrum at a given data point} = f_1A_1 + f_2A_2 + \dots \quad \text{Eq [1]}$$

A_1 and A_2 are the pure absorbance spectra of each components, and f_1 and f_2 are corresponding scaling factors. These scaling factors are determined by linear regression by minimization of residuals. The fit coefficients f_1 and f_2 plotted over the time region of a coelution event represent chromatographic signals for each of the coeluting compounds. Measured VUV absorbance spectra can be converted into chromatographic signals using spectral filters (16).

Multivariate curve resolution (MCR-ALS) is another tool that can estimate underlying elution and spectral profiles for a chromatogram even in the case of completely overlap of peaks ($R_s = 0$). The main requirement from a chromatographic point of view is to collect data from multiple channels with time like

the case of VUV. The availability of photodiode array detectors in HPLCs has made this procedure convenient as it allows the construction of a two-dimensional data matrix. The goal of MCR-ALS is to decompose the observed data matrix (D) of a chromatogram into elution (C) and pure spectral profiles (S^T) that optimally fit the data matrix as shown in Equation 2. E is the experimental error in the estimated convergence.

$$\text{Data matrix } (D) = \text{Elution profile } (C) * \text{Spectral profile } (S^T) + \text{Error } (E) \quad [\text{Eq 2}]$$

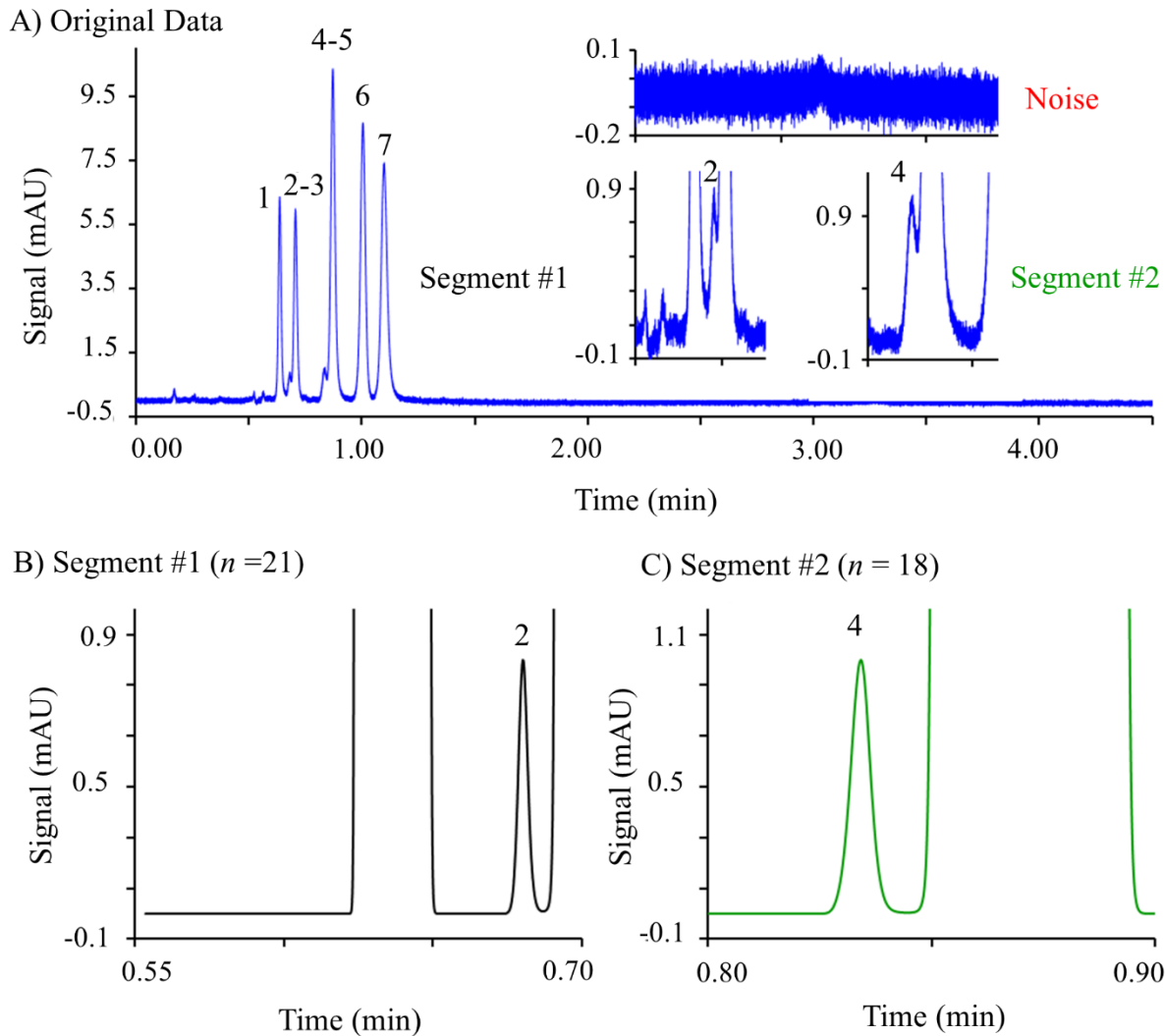
MCR-ALS requires an initial estimation of pure spectral profiles (S^T). Perhaps, the fastest way to get the initial estimate is if the components are known and a pure spectrum is available for each component. If the components and their pure spectral profiles are not available, then the most common way is to estimate the concentration profiles using evolving factor analysis (EFA) (17). The details on EFA can be found in the seminal work by Maeder (17), and examples in previous LCGC reviews on MCR-ALS (18) for peak purity analysis. Since MCR-ALS and the linear combination of weighted reference spectra approach used in VUV requires an initial estimate of concentration or spectral profile, enantiomers might be more difficult to differentiate, especially if there is no separation because their UV-Vis absorbance and their MS spectra would be identical. Similarly, universal response detectors cannot be used with MCR-ALS, which essentially eliminates all data from flame ionization detectors (FID), thermal conductivity detectors (TCD), barrier discharge ionization detectors (BID), conductivity detectors and refractive index (RI) detectors. However, MCR-ALS technique is not limited UV-Vis or mass spectrometry. Also, this procedure is subjective to the user because the constraints can be inappropriately chosen and lead to unrealistic peak shapes. Most MCR methods utilize non-negativity and unimodality, but other various constraints like closure, trilinearity, selectivity, and other shape constraints make MCR the most sophisticated technique among all described herein. When multiple peaks are determined under a similar curve, computation is more difficult and can increase post-processing time. Commercial spectroscopy software has already implemented MCR-ALS, but most chromatography data software has not except for Shimadzu Lab Solutions (patented under i-PDEA). For research work, MCR can be also be accomplished with MATLAB software.

9.3.4 Direct resolution enhancement by power law

Unlike MCR-ALS, the power law approach is a single channel approach and it can be applied on any detectors which are not amenable to MCR-ALS. The power law directly increases chromatographic resolution (R_s) of overlapping peaks to baseline separation ($R_s = 1.5$) so they are easier and more accurately visualized and integrated (11,12). The fundamental principle of a recently proposed power law is that raising a given number to a power, n (where n is an integer > 1) increases the signal magnitude if it is > 1 or decreases the signal magnitude if it is < 1 (11). The power law (a.k.a. as power transform) reduces tailing, noise, maintains retention time, and increase resolution between overlapping chromatographic peaks. Already, a simpler version of power law is integrated in some software, i.e., Chromeleon, where collected chromatographic signal data can be raised to a power (max of $n = 3$) then integrated normally. However the simple law is not suitable for quantitation because the area of a exponentially enhanced peaks have changed after the mathematical operations relative to the original peaks (12). As a result modified power law approach was introduced in 2019, which maintained peak area integrity and offers all the benefits of a simple power law (11).

The modified power law relies on this fundamental characteristic by normalizing the peak of interest's maximum to a value of 1 (and the rest of the chromatogram accordingly) before raising the chromatographic signal to a power that provides the desired resolution. The chromatographic data can be exported to Excel and the peak area quantitated with an external method either in Excel in our template or by numerical integration in OriginPro/MATLAB. It is desirable to smooth the raw data and correct the baseline if needed from a drifting baseline resulting from a gradient method. Each peak in a critical pair is first normalized to unit height followed by raising the chosen peak signal to a desired power. It is recommended to have $R_s \geq 0.8$. The area recovery is described below in equation (3).

To visualize this method, an example from one of our recent works is shown where 2 critical overlapping pairs are present, which we identify as segment 1 and segment 2 (Figure 3) (19).



Chapter 9 Figure 3. Directly increasing resolution of two overlapping pairs by modified power law. Panel A shows the original separation data of hormones (in order of elution): 17α -ethynylestadiol, estrone, estriol, estradiol, androstadienone (androsta-4,16-dien-3-one), progesterone, and testosterone. See reference (4) for chromatographic information. Panels B and C show each overlapping pair baseline separated of each segment; segment 1 with a power (n) of 21 and segment 2 with a power (n) of 18. The area of peaks 2 and 4 can be recovered using Equation 3. Reprinted from reference (19), with permission from Elsevier.

Noise is high, and all chromatographic peaks are tailing, making integration difficult (panel A). After applying powers in each segment (panels B and C) peak widths are reduced, and signal-to-noise is significantly increased. After raising these segments to powers, it is much easier to integrate, and the original peak area can be back-calculated using the equation (3) below where n = the power used to get baseline resolution.

$$\text{Original Area} = \text{Height (original peak)} * \text{Area(normalized powered peak)} * \sqrt{n} \quad [\text{Eq. 3}]$$

Questions that remain are: how is the correct power chosen, and how much error is there?

Originally, each pair had different magnitudes of overlap (more or less resolution) so different powers were needed to get a baseline resolution ($R_s = 1.5$). Choosing what power of n to use is somewhat arbitrary, i.e., two overlapping peaks might be baseline separated by using a power of 3, but if you used a power of 10, one would still get higher resolution. Where do we stop? Since the chosen n is limitless (limit towards infinity), very large powers could be chosen. However, if such large powers are needed to get $R_s = 1.5$, then error might be very large. To determine the constraints of this method, errors have been reported according to changing resolution when quantitating proportionate as well as disproportionate overlapping chromatographic peaks (11,19). Peak area quantification was accurate within 1% error when R_s was >0.8 for 2 overlapping proportionate peaks (50:50 area ratio) (19). With overlapping peaks of area in proportion of 1:99, error was much higher at similar resolution (19). Depending on the case, some method development might be necessary to obtain a resolution around 0.8 before applying power transformation.

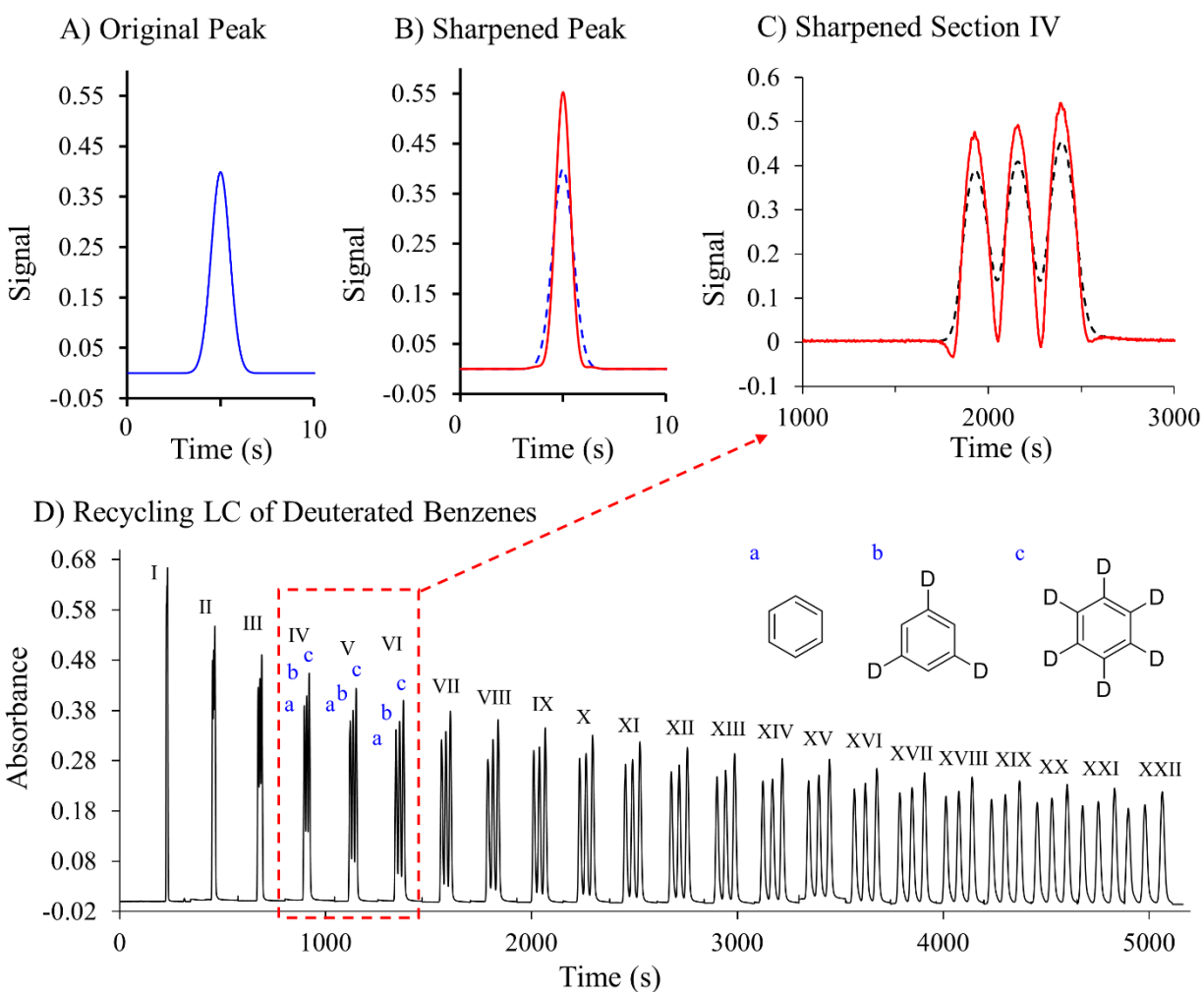
9.3.5 Direct resolution enhancement by even derivative peak sharpening

Using even derivatives to enhance chromatographic resolution is another example of directly increasing the resolution of chromatographic peaks post-data acquisition. The fundamental property of sharpening peaks is that for a symmetric peak function, the area under a derivative is zero (13). Real chromatographic peaks are rarely symmetric, but the area under a derivative for a tailing or fronting peak is negligible (on the order of 10^{-11}). Therefore, if we add or subtract even time-derivatives of peaks from the raw chromatographic data, the peaks areas should not change. The result is a sharper peak, which increases the chromatographic resolution between adjacent peaks. It is important to smooth the data, so the noise is minimal before subtraction or addition. The idea can be expressed mathematically as shown in equation 4.

$$\text{Sharp Peak} = \text{Signal} - K_2 (\text{second derivative}) + K_4 (\text{fourth derivative}) \quad [\text{Eq. 4}]$$

K_2 and K_4 are constant multipliers with consistent units to make the derivatives dimensionless. The user can empirically tune these values until the desired peak widths are obtained. Commonly, small dips are observed at the front and back of the chromatographic envelope, but do not change the peak area or interfere with integration if properly included in integration (13). An Excel template was created to automate this process, such that a chromatogram could be exported and then resolved (13).

To visualize this technique, a simulated Gaussian peak with an area of 1 is shown in panel A of Figure 4.



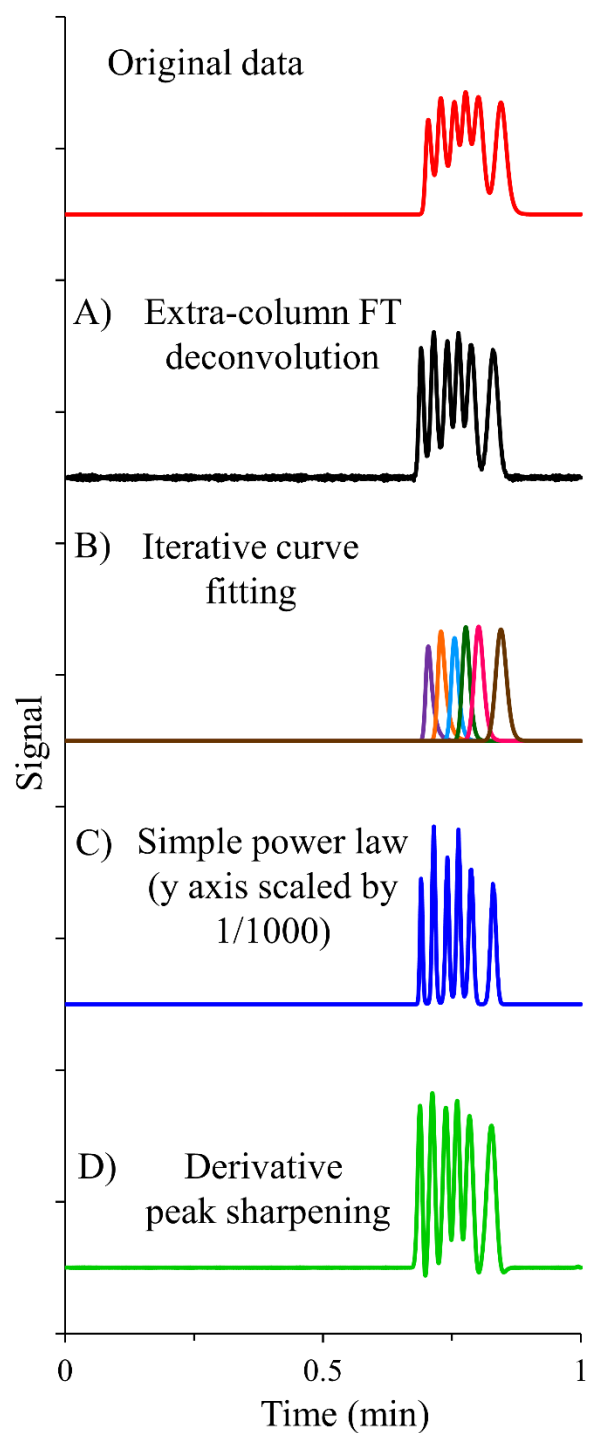
Chapter 9 Figure 4. Sharpening peaks with even derivatives. Panel A shows a simulated Gaussian peak (in blue). Panel B then shows the effect of sharpening the simulated peak (in blue) by reducing the peak width (in red). This is done by subtracting the second and adding the fourth derivatives with their appropriate multipliers. The area of the peak is conserved. Panels C and D show the separation of an isotope mixture containing benzene (a), 1,3,5-benzene-d₃ (b), and benzene-d₆ (c). See reference (13) for

chromatographic information. The separation takes up to 1.5 hours to get baseline resolution needed for quantitation. However, using even derivative peak sharpening (in Panel C), section IV (in black) can be baseline resolved (in red) increasing throughput by ~1 hour. Reprinted from reference (13), with permission from Elsevier.

The result of subtracting the second derivative and adding the fourth derivative (each with an appropriate multiplier) is shown in panel B of Figure 4. The sixth derivative was also added but its effect is negligible. The peak width is reduced, and the peak height increased while the area remains unity. Thus, the even derivative method is a peak shaping protocol to make the peaks narrow. This method can operate on all components of a chromatogram simultaneously unlike the modified power law where each peak has to be treated individually (19). In panel C of Figure 4, a twin-column recycling HPLC chromatogram separating d_3 and d_6 -benzenes from ordinary benzene is shown (13). In recycling HPLC, the analytes are continuously injected and detected i.e., recycled in the chromatograph until the desired resolution is obtained. For this separation, it takes about 1.5 h to separate deuterated benzenes completely (panel D of Figure 4). Instead of waiting for 1.5 h for baseline resolution, a faster approach would be to determine each peak area by equation 3. Panel C of Figure 4 shows the peak sharpening of the fourth recycled chromatogram (segment IV from Panel D of Figure 4). From this point onwards, accurate peak area estimation ($< \sim 1\%$ error) can be obtained even before the physical separation is complete. Error for peak area determination of 2 overlapping proportionate peaks was determined to be within 1% if the chromatographic resolution was > 0.7 (13).

9.3.6 A quick comparison of peak resolution methods

Figure 5 illustrates a quick overview of four new methods discussed above when multidimensional data is not available or when it is not applicable.



Chapter 9 Figure 5. Overview of each signal processing technique. Original data simulated of 6 components partially separated in a under a minute. a) Fourier Transform Deconvolution: dead volume of an Agilent 1290 UHPLC was determined at 3 mL/min and used to remove the extra-column band broadening. b). Iterative Curve Fitting: the chromatogram was fitted using a bidirectional exponentially

modified Gaussian model providing the extracted areas of each peak under the curve. c) Simple power law: the data was raised to power = 3 then scaled down to fit in the same signal window as other methods. The modified power law could be used to quantitate the individual peak areas one at a time. d) Derivative peak sharpening: adding the first and subtracting the second derivatives with constants K_1 and K_2 of 0.0051, and 0.000005 respectively.

These techniques can be applied on any single channel data in any mode of chromatography (GC/LC/SFC) and capillary electrophoresis with any detector. The original data (Figure 5A) consists of six overlapping peaks with noise. The instrumental band broadening can be removed by FT deconvolution. As is evident Figure 5A increases the resolution by removing the tailing caused by instrument itself. The iterative curve fitting procedure can resolve the six peaks baseline with accurate areas as exponentially modified peaks (Figure 5C). MCR-ALS provides similar results of iterative curve fitting however it is more powerful and does not need a peak model In order to easily visualize all the six peak, one can apply a positive integer power by raising the signal to power 3 (12) on Figure 5B. Finally, the first and second derivative sharpening method (13) can be applied be on Figure 5B to make the peaks baseline for convenient integration. Further studies are underway to improve these resolution enhancing procedures.

9.4 Conclusions

Resolution enhancement strategies seem to be the next step to improving chromatographic separations, not only to determine peak areas of overlapping peaks, but to deconvolute system effects, reduce noise, and fix asymmetry. These strategies aim to increase throughput and offer cost-effective solutions compared to traditional method development. Surely, their automation will make them extremely useful to the chromatography community-hence this intelligent peak processing is the future of chromatography. In general, the techniques described in this review either remove extra-column band broadening (Fourier transform deconvolution), extract peak area from under a curve (iterative curve fitting and multivariate curve resolution), or directly enhance chromatographic resolution (modified power law and even derivative peak sharpening). There are benefits and limitations of each technique so one might be more

favorable than another for a specific application and the users have to apply their own judgement on the choice of resolution enhancing methods.

9.5 References

1. S. Bruns, E. G. Franklin, J. P. Grinias, J. M. Godinho, J. W. Jorgenson and U. Tallarek, *Journal of Chromatography A*, **1318**, 189-197 (2013)
2. A. E. Reising, S. Schlabach, V. Baranau, D. Stoeckel and U. Tallarek, *Journal of Chromatography A*, **1513**, 172-182 (2017)
3. M. F. Wahab, D. C. Patel, R. M. Wimalasinghe and D. W. Armstrong, *Analytical chemistry*, **89**, 8177-8191 (2017)
4. F. Gritti and M. F. Wahab, *LCGC Europe*, **31**, 90-101 (2018)
5. J. M. Davis and J. C. Giddings, *Analytical Chemistry*, **55**, 418-424 (1983)
6. Y. Vanderheyden, K. Broeckhoven and G. Desmet, *Journal of Chromatography A*, **1465**, 126-142 (2016)
7. N. A. Wright, D. C. Villalanti and M. F. Burke, *Analytical Chemistry*, **54**, 1735-1738 (1982)
8. H. Parastar and R. Tauler, *Journal*, 2013.
9. S. N. Chesler and S. P. Cram, *Analytical Chemistry*, **45**, 1354-1359 (1973)
10. A. De Juan and R. Tauler, *Critical Reviews in Analytical Chemistry*, **36**, 163-176 (2006)
11. M. F. Wahab, F. Gritti, T. C. O'Haver, G. Hellinghausen and D. W. Armstrong, *Chromatographia*, **82**, 211-220 (2019)
12. P. K. Dasgupta, Y. Chen, C. A. Serrano, G. Guiochon, H. Liu, J. N. Fairchild and R. A. Shalliker, *Analytical chemistry*, **82**, 10143-10150 (2010)
13. M. F. Wahab, T. C. O'Haver, F. Gritti, G. Hellinghausen and D. W. Armstrong, *Talanta*, **192**, 492-499 (2019)
14. D. C. Patel, M. F. Wahab, T. C. O'Haver and D. W. Armstrong, *Analytical chemistry*, **90**, 3349-3356 (2018)
15. S. Misra, M. F. Wahab, D. C. Patel and D. W. Armstrong, *Journal of Separation Science*, **0**,
16. J. Schenk, J. X. Mao, J. Smuts, P. Walsh, P. Kroll and K. A. Schug, *Analytica chimica acta*, **945**, 1-8 (2016)
17. M. Maeder, *Analytical Chemistry*, **59**, 527-530 (1987)
18. S. C. Daniel W Cook; Rutan, D. R. Stoll and C. Venkatramani, *LCGC North America*, **36**, 248-255 (2018)
19. G. Hellinghausen, M. F. Wahab and D. W. Armstrong, *Journal of Chromatography A*, **1574**, 1-8 (2018)

Chapter 10

Separating 101 Compounds in Less than 60 Seconds: *Operating Above Normal Peak Capacity Limits with Signal Processing*

10.1 Abstract

A primary focus in liquid chromatography analysis of complex samples is high peak capacity separations. Using advanced instrumentation and optimal small, high-efficiency columns, complex multicomponent mixtures can now be analyzed in relatively short times. Despite these advances, chromatographic peak overlap is still observed. Recently, attention has shifted from improvements in chromatographic efficiency and selectivity to enhancing data processing after collection. Many processing methods have been adapted from those used in spectroscopy, like Fourier transform deconvolution. Curve fitting methods can be used to trace underlying peaks, but do not directly enhance chromatographic resolution. Methods based on the properties of derivatives and power transform were recently shown to enhance chromatographic peak resolution while maintaining critical peak information (peak areas and retention times). These methods offer other benefits important to fast liquid chromatography such as improving signal-to-noise ratios and peak asymmetry. These protocols have been extensively investigated for their fundamental properties, advantages, and limitations, but they have not been evaluated with complex chromatograms. Herein, we evaluate the use of deconvolution via Fourier transform, even-derivative peak sharpening, and power law with the fast separation (< 60 seconds) of a 101-component mixture using ultra-high-pressure liquid chromatography. High noise and peak overlap are present in this gradient separation, which is representative of fast chromatography. Chromatographic resolution enhancement is demonstrated and described. Further, accurate quantitation is maintained and shown with representative examples. Enhancements in peak capacity and peak-to-peak resolutions are discussed as well.

10.2 Introduction

State-of-the-art instrumentation and high-efficiency columns have provided the infrastructure for extremely fast liquid chromatographic (LC) separations [1-5]. Typically, these columns are short, 0.5 – 5 cm, and are packed with sub-2 μm fully porous particles (FPPs) or $\leq 2.7 \mu\text{m}$ superficially porous particles (SPPs). Several SPP chiral stationary phases (CSPs) have been reported to have over 200,000 plate m^{-1} [6,7]. These high-efficiency columns are particularly useful for enantiomeric separations because enantiomers usually require physical or chemical separation to be effectively identified and efficiently quantitated. Often, this requires extensive method development [8]. Patel, et al. reported the separation of 10 components in under a second [9]. The speed of chromatography is now comparable to that of sensors and offers high selectivity and accurate quantitation. High-throughput screening also benefits from faster chromatography. Other applications, like 2D-LC, profit from fast chiral separations in the 2nd dimension [10]. However, these fast separations require advanced high efficiency instrumentation and chromatographic overlap is still observed.

Recently, parameters important to fast separations like detector response times and sampling frequencies, extra-column band broadening, and noise have been investigated [11-12]. Instead of focusing on the separation occurring in the column, subsequent studies investigated how the signal data is collected and processed [13-17]. Extra-column variance (band broadening) can be removed using Fourier transform deconvolution, resulting in a retention time change and increased chromatographic resolution by removing the peak broadening caused by the extra-column hardware [17-18]. Higher sampling frequencies provide more accurate representations of the signal, but potentially decrease the signal to noise ratio. This noise can be removed using various filtering (smoothing) techniques [19]. However, with most modern instrumentation, these parameters do not substantially increase chromatographic resolution. Thus, other approaches like curve fitting have been used to estimate underlying peak profiles of overlapping chromatographic peaks [13,20]. These approaches benefit analyses where advanced chromatography instrumentation is not ubiquitous and when separations cannot be optimized easily. For example, iterative curve fitting was used to estimate underlying peak areas for the enantiomeric

separation of pyrethroids with 8 stereoisomers [13]. Further, it was noted that curve fitting techniques require a model and a known number of components in the chromatogram [13]. Therefore, it is subjective to the user and requires time to get accurate information. A more problematic aspect of curve fitting is that there can be several “mathematically” correct solutions, and this can provide misleading results.

More recent work has explored the use of derivatives and power transform to reduce chromatographic peak widths, and directly enhance resolution [14-16]. The fundamentals and requirements of these mathematical treatments have been thoroughly evaluated elsewhere [14-16]. It was clear from those studies that a moderate resolution ($\sim 0.7 - 1.0$) is needed to get accurate ($< 1\%$ error in peak area) peak area information [14-16]. A recent report focused on decreasing the required resolution and correcting potential errors arising of severe peak overlaps [21]. Power transform increases signal-to-noise and improves peak shapes by exponentially raising the signal data to a certain power [22-23]. The fundamental principle is that raising a given output signal to a power, n , (where n is an integer > 1) increases the signal magnitude if it is > 1 or decreases the signal magnitude if it is < 1 [22-23]. However, the power law used in these reports requires a back-calculation of the area because the original chromatographic peak areas will change after being raised to a power [5,14,16]. Derivatives, well-known for their use in optical spectroscopy, have been reported to enhance resolution of overlapping peaks while maintaining all critical peak information (peak areas and retention times), clarify shoulders for peak purity analysis, and are useful for peak shape analysis [14,15]. Even-derivative peak sharpening operates by adding a fraction of the signal's 2nd derivative and subtracting a fraction of the signal's 4th derivative from the original collected data [15].

These signal processing methods have been introduced with liquid chromatography but can be applied to any chromatography technique (gas, liquid, supercritical fluid, and capillary electrophoresis). Signal processing methods have been extensively investigated for their fundamental use with simple examples [13-17]. In this work, we evaluate the use of Fourier transform deconvolution, derivatives, and power law with a complex case: a 101-component mixture separated in less than 60 seconds. Peak capacity is

generally influenced by column length, particle size, flow rate, etc. [24]. Herein, we also consider the gain in peak capacity using signal processing. Additionally, quantitation for representative peaks is shown and discussed as a function of resolution.

10.3 Materials and methods

10.3.1 Chromatographic conditions

The CORTECS T3 C18 column (50 x 3.0 mm i.d., 2.7 μm SPP) was obtained from Waters (Milford, MA, USA). The Vanquish UHPLC instrument (Thermo Fisher Scientific, Waltham, MA) was utilized for all HPLC experiments. This instrument is custom configured to by-pass the column oven to minimize extra-column effects. The column was connected to the injector and the 2.5 μL UV-Vis detector with 100 μm diameter nanoviper tubing. HPLC grade acetonitrile and formic acid were obtained from Sigma-Aldrich (St. Louis, MO, USA). Water was purified by a Milli-Q water purification system (Millipore, Billerica, MA, USA). The following mobile phases A and B (MPA and MPB) were utilized in gradient elution: MPA – acetonitrile, MPB – 0.1% formic acid in water. The following step gradient was utilized: 1) $t = 0$ min, MPA = 30%, MPB = 70%, 2) $t = 0.6$ min, MPA = 70%, MPB = 30%, 3) $t = 0.8$ min, MPA = 100%, MPB = 0%, 4) $t = 1.45$ min, MPA = 100%, MPB = 0%, 5) $t = 1.50$ min, MPA = 30%, MPB = 70%.

10.3.2 Analytes and sample preparation

All analytes were obtained from Sigma-Aldrich (St. Louis, MO, USA). Each analyte was dissolved in acetonitrile at a concentration ~ 1 mg/mL and shot individually. Each analyte was diluted by height to the lowest observed peak height. 50 μL of each diluted sample was mixed, resulting in a mixture of 101 compounds in 5050 μL . Representative standards were made by distributing 50 μL of the sample into 5050 μL using diluent (acetonitrile). The standards were injected three times each, at the same volume as the mix to provide a true peak area for quantitation. The mixture was injected 6 times and the total peak area of the chromatogram had a % RSD < 0.1.

The following analytes were used in the 101 component mixture (in order of their elution): 1) nicotine-1-oxide, 2) nicotinic acid, 3) 5-nitouracil, 4) 1,3-dimethyluracil, 5) mandelamide, 6) 5-hydroxyindole-3-acetic acid, 7) hippuric acid, 8) clopyralid, 9) catechol, 10) N-acetylphenylalanine, 11) trans-4-hydroxy-3-methoxy cinnamic acid, 12) vanillin, 13) phenyl succinic anhydride, 14) 4-phenyl-2-oxalidinone, 15) acetyl salicylic acid, 16) phenol, 17) benzoic acid, 18) 4-benzyl-2-oxalidinone, 19) chloramphenicol, 20) 4-(1H-indol-3-ylmethyl)-2-oxazolidinone, 21) α -methyl- α -phenyl succinimide, 22) 4-nitrophenol, 23) 1-benzoylcyclobutene carboxylic acid, 24) hydrocortisone, 25) m-cresol, 26) cis-2-methoxycinnamic acid, 27) 4-benzyl-2-oxalidinone-thione, 28) 2-nitroaniline, 29) ethyl-4-hydroxybenzoate, 30) hydrobenzoin, 31) 3-chlorophenoxy benzoic acid, 32) 5,5-diphenylhydantoin, 33) indole 3-butyric acid, 34) N-pthaloyl-methionine, 35) α -methylhydrocinnamic acid, 36) 2,2-chlorophenoxypropionic acid, 37) indole, 38) 2-naphthol, 39) 2-naphthoyl chloride, 40) glycosyl tosylate, 41) sulindac, 42) 7-chloro-4-nitrobenz-2-oxa-1,3-diazole, 43) N-3,5-dinitrobenzoyl phenylglycine, 44) bisphenol A, 45) 5-phenylvaleric acid, 46) 4,5,6,7,8-hexahydronaphthalene, 47) 2,2-diphenylethanol, 48) 4-nitrotoluene, 49) benzo(b)furan, 50) 3-phenylphenol, 51) phenetole, 52) 4-tert butyl phenol, 53) 4-nitrobenzyl bromide, 54) 4-(2,4-dichlorophenoxy)butyric acid, 55) furalaxyl, 56) dimethenamid, 57) benoxacor, 58) fenamidophos, 59) benzophenone, 60) 3-methylbenzofuran, 61) Fmoc-methionine, 62) napropamid, 63) flavanone, 64) valerophenone, 65) 3-chlorotoluene, 66) haloxyfop, 67) 2,5-dichlorothiophene, 68) 3-methylbenzothiophene, 69) 2-methylthianaplene, 70) mecoprop methyl ester, 71) 2,2,2-trifluoro-1-anthryl ethanol, 72) 4,5-diphenyl-1,3-dioxal-2-one, 73) chlormadinone, 74) dinoseb, 75) hexanophenone, 76) acenaphthene, 77) 1Hbenzo(a)carbazole, 78) 1-bromonaphthalene, 79) benzyl cinnamate, 80) phenanthrene, 81) 1,4-dimethylnaphthalene, 82) 1,3-dimethylnaphthalene, 83) 2,6-dimethylnaphthalene, 84) cloquintocet mexyl, 85) 3,3-dibromo-1-naphthol, 86) 2,2-dimethoxy-1,1-binaphthyl, 87) 6,6-dibromo-1,1-bi-2-naphthol, 88) pyrene, 89) diclofop methyl, 90) benzo(b)naphth(1,2,d)furan, 91) Fmoc-beta-alanine O-pfp, 92) triphenylene, 93) benz(c)phenanthrene, 94) etoxazole, 95) VANOL, 96) 2,6-ditert butyl-4-methylphenol, 97) fenpropathrin, 98) benzo(k)fluoranthrene, 99) benzo(a)pyrene, 100) fenvalerate, and 101) closantel.

10.3.3 Data processing

All data was collected at 254 nm and sampled at 100 Hz with a response time of 0.05 s. A blank injection was used to correct the baseline drift observed from the gradient. Chromeleon 7.2 ST4 software (Thermo Fisher Scientific 2009-2016) controlled the Vanquish system. MATLAB version R2018b (MathWorks Inc, 1984 – 2018) was used to perform all signal processing protocols (Fourier transform deconvolution, even-derivative peak sharpening, and normalized power law), which are discussed in Table 1. An injection delay of 20 seconds was used to collect the no-column data for deconvolution by Fourier transform. The chromatographic resolutions of each chromatogram (original and processed data) and peak areas were determined using PeakFit version 4.12 (SeaSolv Software Inc. 1999 – 2003).

Chapter 10 Table 1. Signal processing protocols.

A) Deconvolution by Fourier Transform		
<ol style="list-style-type: none"> 1) Collect chromatogram with and without the column using the same method then export data into external software (i.e., MATLAB). 2) Convert both chromatograms to the frequency domain using Fourier transform. 3) Divide the transformed column data (FT_c) by the transformed no-column data (FT_{nc}) (shown in equation 1). The number of data-points should be identical. 4) Convert the resulting data back into the time domain using inverse Fourier transform (IFT). 5) Multiply all the IFT data points by the peak area obtained without the column. 6) If needed, remove noise with a centered moving average. 		
$\text{Deconvoluted data} = \text{IFT}\left[\frac{FT_c}{FT_{nc}}\right] \times A_{nc}$		Equation 1
B) Even-Derivative Peak Sharpening		
<ol style="list-style-type: none"> 1) Calculate the second and fourth derivatives of the signal data. 2) Remove noise from the calculated derivatives with a centered moving average. 3) Subtract the second and add the fourth derivative with appropriate K_2 and K_4 values according to equation 2. These values should be appropriately chosen to avoid significant negative dips in the baseline. 4) Determine resolved peak areas of the sharpened chromatogram using numerical integration. Include any dips in the baseline as part of the peak. 		
$\text{Sharpened Peak} = \text{Signal} - K_2(\text{2nd Derivative}) + K_4(\text{4th Derivative})$		Equation 2
C) Normalized Power Law		
<ol style="list-style-type: none"> 1) Measure all peak heights (H'_i) (i.e., $i = 1-101$) of the signal data. 		

- 2) Locate the shortest peak of the chromatogram (peak 5 for our case) and normalize its original peak height (H'_s) to unity. If the resolution is low ($R_s < 0.7$) for the shortest peak other height corrections can be done according to ref. 21.
- 3) Apply the same division in step 2 to the rest of the chromatogram.
- 4) Raise the entire chromatogram's signal data to a power, where n is an integer >1 and continue increasing n until desired R_s (i.e., $R_s = 1.5$) is achieved.
- 5) Measure all peak areas of the powered chromatogram, A_i^n , with numerical integration (A_s^n is the shortest peak's area of the powered chromatogram).
- 6) For the shortest peak, calculate the original area (A_s^o) using Equation 3.
- 7) Calculate the original areas (A_i^o) of the remaining peaks in the chromatogram using Equation 4.

$$A_s^o = H'_s A_s^n \sqrt{n} \quad \text{Equation 3}$$

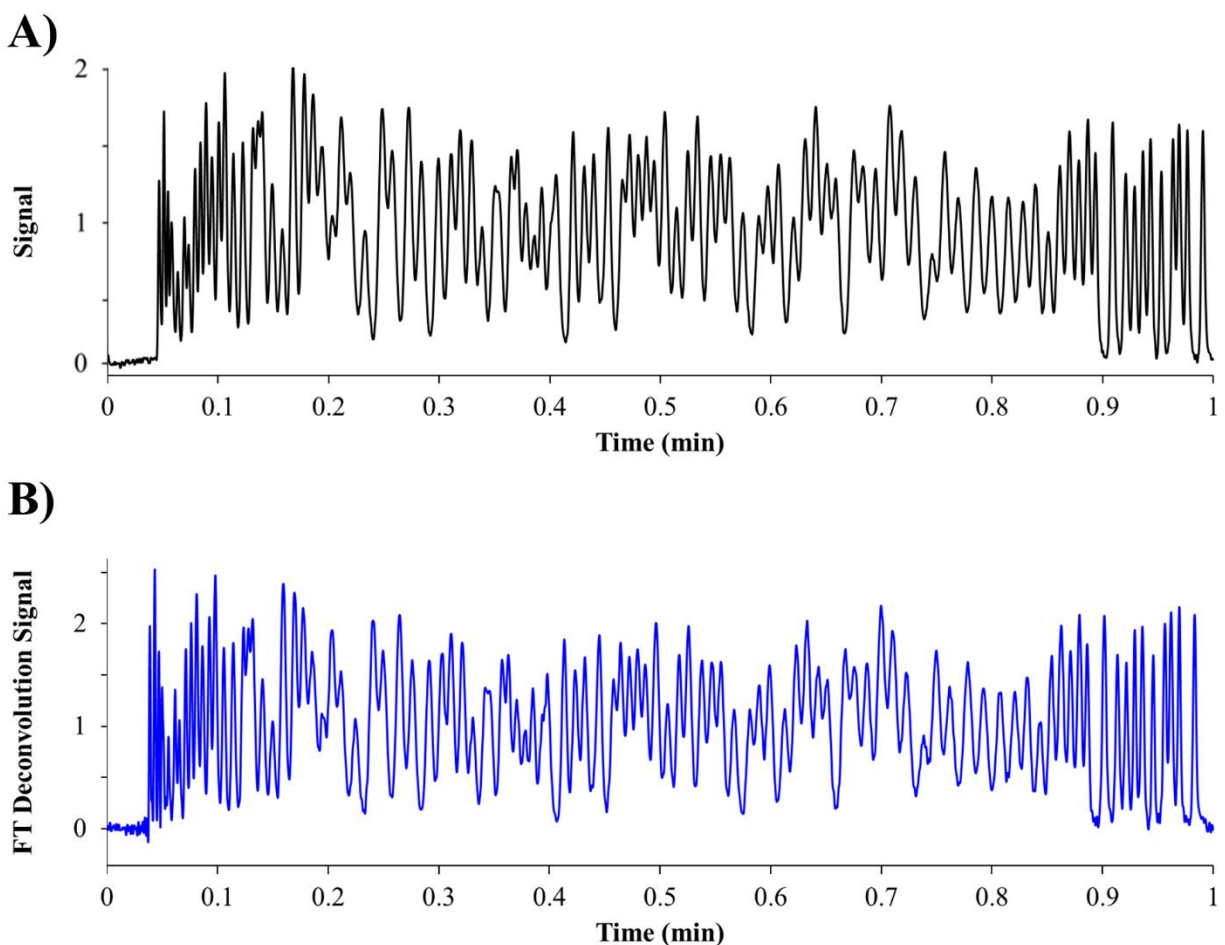
$$A_i^o = A_i^n H'_s \sqrt{n} \left(\frac{H'_s}{H'_i} \right)^{n-1} \quad \text{Equation 4}$$

Peak capacity (P_c) was calculated according to Equation 5 [25]. This expression determines the peak capacity, for a gradient elution, in terms of the gradient time (t_G) and average peak width (w) assuming a resolution = 1 for all peaks. Typically, the average peak width can be estimated by the average of the first and last peaks' width. In this calculation, the widths of the most narrow and wide peaks (peak 101 and peak 24 for each set of data) were averaged to provide a rough estimation.

$$P_c \approx 1 + \frac{t_G}{w} \quad \text{Equation 5}$$

10.4 Results and discussion

To push the limits of fast chromatography with the best current instrumentation and to concurrently evaluate recent signal processing methods, a complex chromatogram of 101 components separated in < 60 seconds was developed (Fig. 1A).



Chapter 10 Figure 1. The separation of 101 components in under 60 seconds: A) original signal chromatogram, B) original signal processed chromatogram by deconvolution with Fourier transform.

Each of the 101 compounds in Fig. 1A are listed in the Materials and Methods in order of their elution time. The basic requirement is that each components' chromatographic peak maximum be distinguishable ($R_s > 0.3$). This is necessary for the derivative and power-based signal processing methods to be effective [14-16]. The Fig. 1A chromatogram has various peak resolutions, heights, areas, and shapes representative of a complex analysis, much like a complex biological analysis. The mixture was injected six times and was reproducible (see Materials and Methods). Additionally, the position of each analyte was confirmed with individual standards by their retention time. After confirmation, the chromatographic R_s of each adjacent peak was determined and reported in ranges as shown in Table 2. Most components in the original chromatogram had overlapping chromatographic peaks, with a $R_s < 1.0$. Signal processing

methods like even-derivative peak sharpening and normalized power methods have been shown to be highly accurate (<1 % error in peak area) when the original chromatogram has a $R_s > 0.7$ for the overlapping pair of peaks [14-16]. Therefore, at least 62% of this chromatogram could be quantitated accurately.

Chapter 10 Table 2. Gain in chromatographic resolution and peak capacity using signal processing approaches.

Resolution ^a	Original ^{b1}	Fourier Transform ^{b2}	Derivative ^{b3}	Power ^{b4}
0 – 0.7	36%	26%	5%	3%
0.7 – 1.0	55%	48%	42%	14%
1 – 1.25	2%	16%	33%	18%
1.25 – 1.5	3%	3%	14%	19%
≥ 1.5	2%	7%	6%	46%

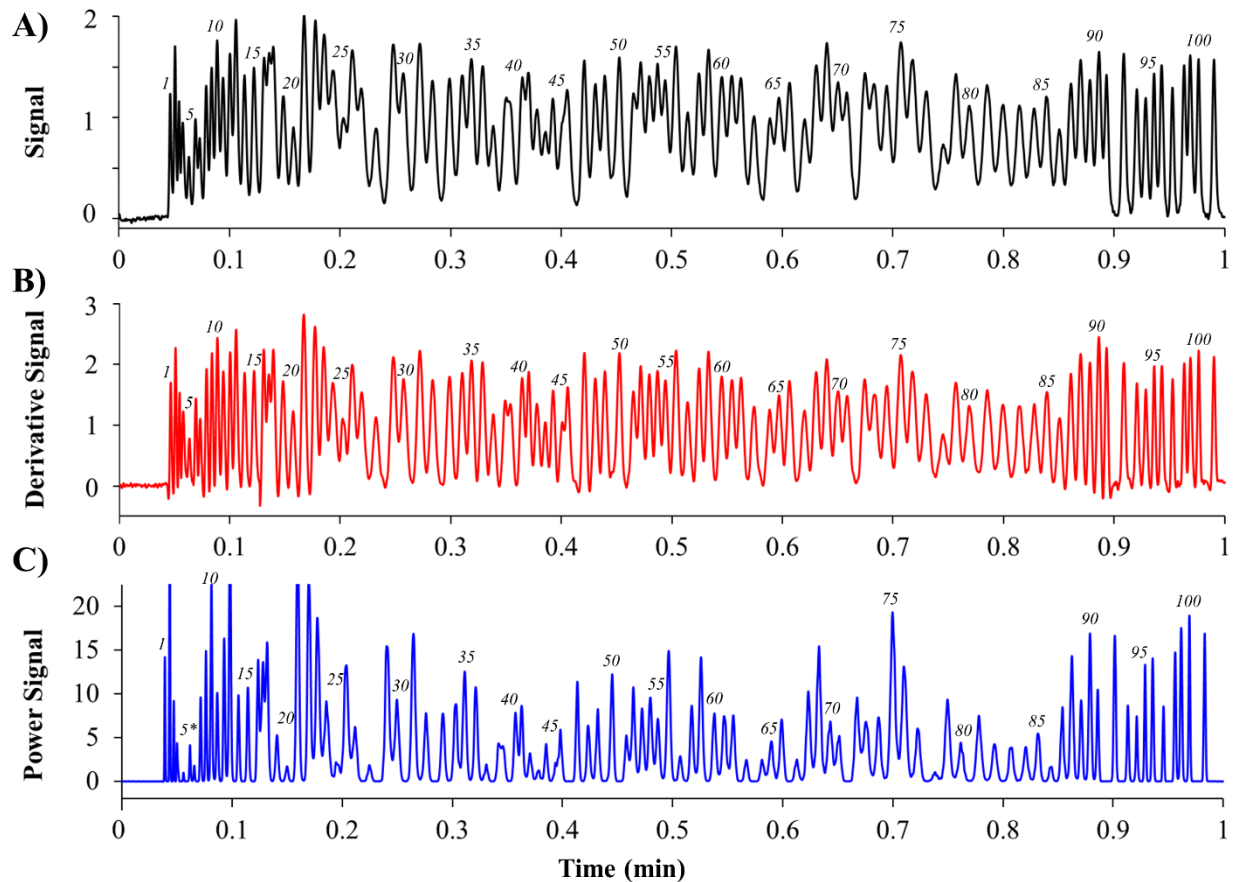
^a The percentage of chromatographic resolution from each signal data: original data, Fourier transform deconvoluted data (FT), even-derivative sharpening (Derivative), and normalized power law (Power).

^b The chromatographic resolution was calculated using PeakFit (see Materials and Methods).

Before applying derivatives or powers, Fourier transform deconvolution was performed to remove extra column variance (band broadening). Table 1 explains this process and the resulting chromatogram is shown in Fig. 1B. When compared to the original signal, the Fourier transform deconvoluted signal has slightly decreased retention times. The peak capacity (P_c) of the column was determined according to Equation 5 in the Materials and Methods. Typically, the column's peak capacity describes the maximum theoretical number of components that can be separated with $R_s = 1$ [25]. Peak capacity is highly dependent on chromatographic peak width, and since signal processing techniques reduce peak width, we expect an increase in P_c . With deconvolution by Fourier transform, the peak capacity would remain constant if there was no extra-column band broadening present. However, this was not the case since the peak capacity increased from 78 to 93 with the Fourier transform procedure (calculated by Equation 5 in Materials and Methods). Relative to other signal processing procedures, which will be discussed, this gain in peak capacity is minimal, which indicates the UHPLC instrument used in this study has low but non-

zero extra-column volume. After deconvolution via Fourier transform, chromatographic R_s slightly increased; i.e., fewer separations with a R_s of 0 – 0.7 and 0.7 – 1.0 (26% and 48%, respectively), and more with a R_s of 1.0 – 1.25, 1.25 – 1.5, and ≥ 1.5 (16%, 3%, 7%, respectively) (Table 2). However, the Fourier transform deconvolution added significant noise to the chromatogram (Fig. 1B) and a cut-off filtering was required in the frequency domain.

After completing the Fourier transform deconvolution, even-derivative peak sharpening was used to process the data [15]. Table 1 explains the application of derivatives on the Fourier transformed data. However, the Fourier transform deconvolution process decreased the signal-to-noise, which resulted in the formation of additional chromatographic peaks after even-derivative sharpening. Therefore, the original chromatographic data was determined to be better suited for derivative-based signal processing. The resulting chromatogram of the derivative sharpening procedure on the original signals (not the Fourier transform deconvoluted signals) is shown in Fig. 2B and compared to the original chromatogram (Fig. 2A).

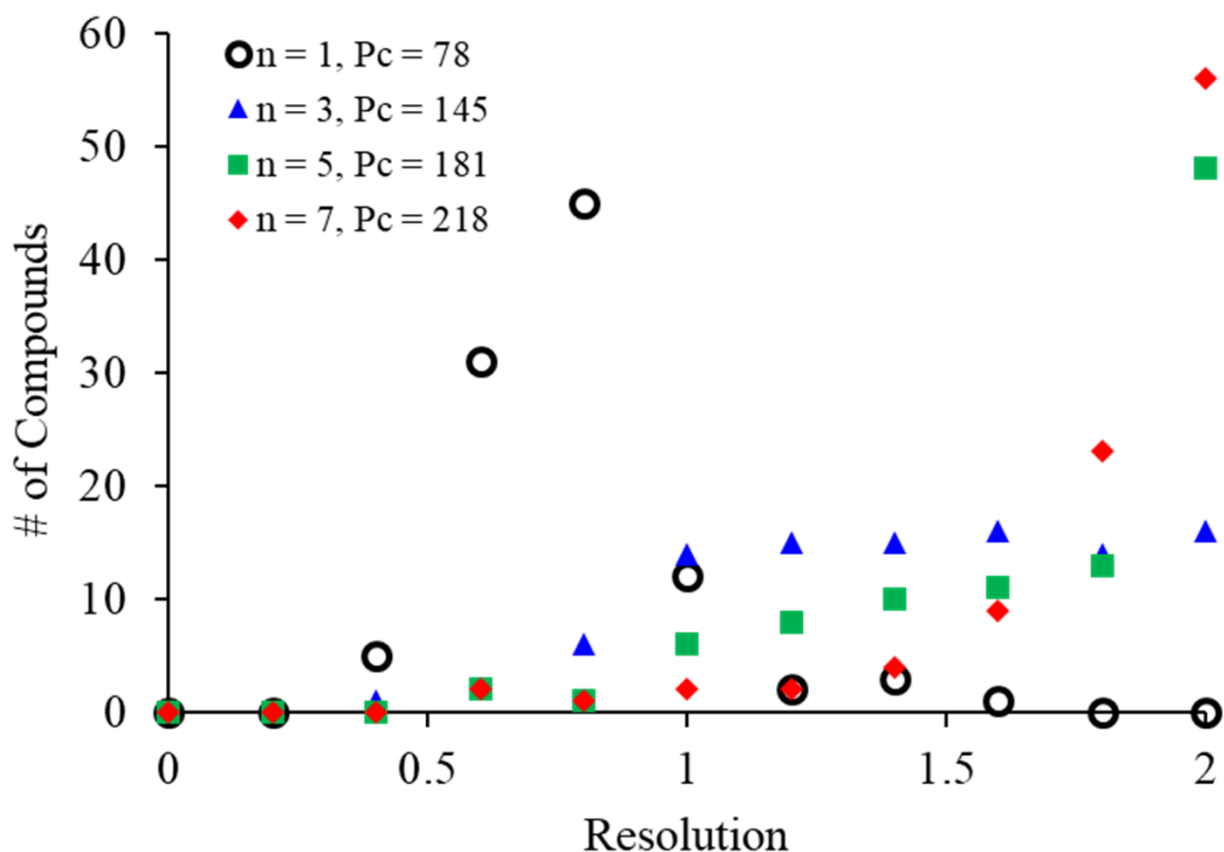


Chapter 10 Figure 2. Signal processing of the separation of 101 components in under 60 seconds: A) original chromatogram, B) signal processed chromatogram by even-sharpening derivatives, and C) signal processed by deconvolution using Fourier transform, normalized to peak 5*, and raised to a power, $n = 3$. The components 1-101 are listed in Materials and Methods in order of their elution.

When applying the protocol to the complex set of data, it was observed that one set of K values (K_2 and K_4 coefficients determine the amount of sharpening) was not going to be optimal for processing. This was indicated by several negative dips in the signal at the beginning and end of the chromatogram where R_s is higher than in the middle. Avoiding negative dips in the chromatogram typically makes quantitation easier and more accurate [15]. Therefore, different K_2 values were utilized in segments of the chromatogram, which has been reported as segmented even-derivative peak sharpening [15]. In Figure 2B, 4 sections were made with various K_2 values chosen empirically ($K_2 = 3.5$ for 0.05 – 0.07 min, $K_2 = 7$ for 0.07 – 0.13 min, $K_2 = 20$ for 0.13 – 0.90 min, and $K_2 = 6$ for 0.90 – 1.00 min). K_4 values were kept constant ($K_4 = 0.001$ for 0 – 1.0 min), since minimal chromatographic R_s gain was observed when

changing this coefficient. Smaller K_2 values were used in higher R_s areas, while larger K values were needed in lower R_s areas. This empirical optimization required more time than just using one coefficient value and the choice in K value was not always clear. However, more sharpening can be achieved with fewer negative dips using segmented even-derivatives compared to the typical even-derivatives protocol (one set of K values for the entire chromatogram). After segmented even-derivative sharpening, significant increases in chromatographic resolution (R_s) were observed, with an increased peak capacity equal to 107 (P_c calculated by Equation 5 in Materials and Methods, see Table 2 for R_s). Over 30% of the original peak overlaps with chromatographic $R_s < 0.7$ were increased to > 0.7 and approximately 50% of the entire chromatogram had a chromatographic $R_s > 1$. It should be noted that more improvement in chromatographic R_s might have been observed with additional segments.

Unlike derivatives, the power law was applied to the Fourier transform deconvoluted data because it improves the signal-to-noise. Table 1 explains the protocol for the normalized power law, which provides a back-calculation of the original area underlying the overlapping peaks. The Fourier transform deconvoluted signal was normalized to the shortest peak, peak 5, and raised to the power, $n = 3$. (Figure 2C). Higher powers could have been used but were not needed to significantly enhance chromatographic R_s . The power law process increases the original signal's peak capacity as a function of \sqrt{n} , resulting in a peak capacity of 145 (calculated by Equation 5 in Materials and Methods). Therefore, several more components could have been included in the original chromatogram. Almost 50% of the entire chromatogram was baseline resolved with a power of 3 on the Fourier transformed data (Table 2). The power law method seems to be more powerful than derivatives for complex chromatograms and works well with Fourier transform deconvoluted data that may have significant noise. Additionally, larger powers can be used to further enhance chromatographic R_s . The difference in chromatographic R_s between the original signal, and different powers ($n = 3, 5, \text{ and } 7$) is shown in Fig. 3.



Chapter 10 Figure 3. The increased chromatographic resolution of the original chromatogram of 101 components ($n = 1$) when powered by $n = 3, 5$, and 7 . The power law process increases the original signal's peak capacity as a function of \sqrt{n} . Peak capacity (P_c) was calculated according to equation 5 in Materials and Methods. *Resolution values at 2.0 represent chromatographic $R_s \geq 2.0$.

Values at R_s of 2.0 represent chromatographic $R_s \geq 2.0$. Original data is represented by black circles in Fig. 3 show a maximum at a R_s of ~ 0.8 . By raising the signal to a power, $n = 3$, the majority of chromatographic R_s shifts to $R_s > 1$. The slope of the powered, $n = 3$ signal data (blue triangles) seems to plateau over a R_s of 1 . However, with increasing powers, $n = 5$ and $n = 7$, the shift is more pronounced, with an exponential rise. With $n = 7$, $\sim 90\%$ of all components are baseline separated ($R_s \geq 1.5$). The peak capacity, P_c , was calculated for $n = 5$ and $n = 7$, and increased to 181 and 218 , respectively (see Fig. 3). Thus, the original peak capacity obtained with no signal processing could be increased ~ 3 -fold by processing it with a power, $n = 7$.

Representative chromatographic pairs from the 101-component separation that had overlap in the R_s ranges mentioned in Table 1 were chosen for quantitation evaluation. Their peak areas were determined (as described in Table 1) and compared to the true peak areas (as described in Materials and Methods) in Table 3. The areas determined by even-derivative peak sharpening and the normalized power law procedures were very close to true areas for peaks with $R_s = 0.8$. For the overlapping pair with $R_s \sim 0.5$, the peak areas for the derivatives and powers techniques had errors from 2 – 15%. It should be noted that this pair was not optimized to a baseline separation using higher powers or K values, which would improve the quantitation. Additionally, error corrections have been reported for the power law procedure, which allows its use for lower original chromatographic R_s [21]. However, as seen for this complex example of 101 components in less than a minute, the majority of R_s was 0.7 – 0.8, where these signal processing techniques have high accuracy in peak area quantitation.

Chapter 10 Table 3. Representative quantitation evaluation of signal processing techniques.

Peak # ^a	R_s ^b	A_{True} ^c	$A_{\text{Derivative}}$ ^d	A_{Power} ^e
26	0.53	0.0142	0.0121	0.0135
27		0.0087	0.0089	0.0097
4	0.84	0.0035	0.0033	0.0026
5		0.0016	0.0019	0.0014
32	1.07	0.0102	0.0106	0.0098
33		0.0099	0.0102	0.0093
92	1.34	0.0075	0.0078	0.0076
93		0.0058	0.0059	0.0057
101	Baseline	0.0059	0.0063	0.0061

^a The name of the peak according to peak # can be found in Experimental.

^b The chromatographic resolution (R_s) in the original chromatogram of adjacent peaks.

^c The true area of each peak (A_{True}) was determined with a separate injection of a standard that had the same concentration of that component as in the mixture of 101 components.

^d The areas determined by the even-derivative sharpening approach ($A_{\text{Derivative}}$).

^e The areas determined by the height correlation equation (Equation 4) from the normalized power law approach that only normalizes the shortest peak of the chromatogram (A_{Power}).

10.5 Conclusions

New signal processing protocols can be used to enhance resolution, peak capacities, and signal-to-noise ratios of complex chromatograms. Deconvolution by Fourier transform produced small improvements in chromatographic Rs but added significant noise. Signal processing with segmented even-derivative peak sharpening required more time and resulted in less enhancement than the power law approach. The normalized power procedure was simple and effective, providing baseline separation for ~90% of the chromatogram (with $n = 7$). Power processing also increases signal-to-noise, so it is well suited for fast liquid chromatography data of complex biological samples. Signal processing also allows users to operate above normal column peak capacities, which will surely benefit complex multicomponent separations.

10.6 References

27. Patel DC, Breitbach ZS, Wahab MF, Barhate CL, Armstrong DW. Gone in seconds: praxis, performance, and peculiarities of ultrafast chiral liquid chromatography with superficially porous particles. *Anal Chem.* 2015;87:9137-9148.
28. Patel DC, Wahab MF, Armstrong DW, Breitbach ZS. Advances in high-throughput and high-efficiency chiral liquid chromatographic separations. *J Chromatogr A.* 2016;1467:2-18.
29. Barhate CL, Joyce LA, Makarov AA, Zawatzky K, Bernardoni F, Schafer WA, Armstrong DW, Welch CJ, Regalado EL. Ultrafast chiral separations for high throughput enantiopurity analysis. *Chem Commun.* 2016;53:509-512.
30. Barhate CL, Wahab MF, Breitbach ZS, Bell DS, Armstrong DW. High efficiency, narrow particle size distribution, sub-2 μm based macrocyclic glycopeptide chiral stationary phases in HPLC and SFC. *Anal Chim Acta.* 2015;898:128-137.
31. Wahab MF, Wimalasinghe RM, Wang Y, Barhate CL, Patel DC, Armstrong DW. Salient sub-second separations. *Anal Chem.* 2016;88:8821-8826
32. Spudeit DA, Dolzan MD, Breitbach ZS, Barber WE, Micke GA, Armstrong DW. Superficially porous particles vs. fully porous particles for bonded high performance liquid chromatographic chiral stationary phases: isopropyl cyclofructan 6. *J Chromatogr A.* 2014;1363:89-95.
33. Wahab MF, Patel DC, Wimalasinghe RM, Armstrong DW. Fundamental and practical insights on the packing of modern high-efficiency analytical and capillary columns. *Anal Chem.* 2017;89:8177-8191.
34. Hellinghausen G, Roy D, Lee JT, Wang Y, Weatherly CA, Lopez DA, Nguyen KA, Armstrong JD, Armstrong DW. Effective methodologies for enantiomeric separations of 150

- pharmacology and toxicology related 1°, 2°, and 3° amines with core-shell chiral stationary phases. *J Pharm Biomed Anal.* 2018;155:70-81.
35. Patel DC, Wahab MF, O'Haver TC, Armstrong DW. Separations at the speed of sensors. *Anal Chem.* 2018;90:3349-3356.
 36. Barhate CL, Regalado EL, Contrella ND, Lee J, Jo J, Makarov AA, Armstrong DW, Welch CJ. Ultrafast chiral chromatography as the second dimension in two-dimensional liquid chromatography experiments. *Anal Chem.* 2017;89:3545-3553.
 37. Wahab MF, Dasgupta PK, Kadjo AF, Armstrong DW. *Anal Chim Acta.* Sampling frequency, response times and embedded signal filtration in fast, high efficiency liquid chromatography: A tutorial. 2016;907:31-44.
 38. Barhate CL, Wahab MF, Tognarelli DJ, Berger TA, Armstrong DW. Instrumental idiosyncrasies affecting the performance of ultrafast chiral and achiral sub/supercritical fluid chromatography. *Anal Chem.* 2016;88: 8864-8672.
 39. Hellinghausen G, Readle ER, Wahab MF, Lee JT, Lopez DA, Weatherly CA, Armstrong DW. Mass spectrometry-compatible enantiomeric separations of 100 pesticides using core-shell chiral stationary phases and evaluation of iterative curve fitting models for overlapping peaks. *Chromatographia* 2019;82:221-233.
 40. Hellinghausen G, Wahab MF, Armstrong DW. Improving visualization of trace components for quantification using a power law based integration approach. *J Chromatogr A.* 2018;1574:1-8.
 41. Wahab MF, O'Haver TC, Gritti F, Hellinghausen G, Armstrong DW. Increasing chromatographic resolution of analytical signals using derivative enhancement approach. *Talanta.* 2019;192:492-499.
 42. Wahab MF, Gritti F, O'Haver TC, Hellinghausen G, Armstrong DW. *Chromatographia.* 2019;82:211-220.
 43. Wahab MF, Hellinghausen G, Armstrong DW. Progress in peak processing. *LC GC Eur.* 2019;32:22 – 28.
 44. Vanderheyden Y, Broeckhoven K, Desmet G. Peak deconvolution to correctly assess the band broadening of chromatographic columns. *J Chromatogr A.* 2016;1465:126-142.
 45. Savitzky A, Golay MJE. Smoothing and diffraction of data by simplified least squares procedures. *Anal Chem.* 1964;36:1627-1639.
 46. Cook DW, Rutan SC, Stoll DR, Venkatramani C. Peak purity in liquid chromatography, Part II: Potential of curve resolution techniques. *LC GC N Am.* 2018;36:248–255.
 47. Wahab MF, Berthod A, Armstrong DW. Extending the power transform approach for recovering areas of overlapping peaks. *J Sep Sci.* 2019; <https://doi.org/10.1002/jssc.201900799>
 48. Shalliker RA, Stevenson PG, Shock D, Mnatsakanyan M, Dasgupta PK, Guiochon G. Application of power functions to chromatographic data for the enhancement of signal to noise ratios and separation resolution. *J Chromatogr A.* 2010;1217:5693-5699.
 49. Dasgupta PK, Chen Y, Serrano CA, Guiochon G, Liu H, Fairchild JN, Shalliker RA. Black box linearization for greater linear dynamic range: the effect of power transforms on the representation of data. *Anal Chem.* 2010;82:10143-10150.
 50. Gilar M, Daly AE, Kele M, Neue UD, Gelber JC. Implications of column peak capacity on the separation of complex peptide mixtures in single- and two-dimensional high-performance liquid chromatography. *J Chromatogr A.* 2004;1061:183 – 192.

51. Li X, Stoll DR, Carr PW. Equation for peak capacity estimation in two-dimensional liquid chromatography. *Anal Chem.* 2009;81:845 – 850.

Chapter 11

Summary and Future Outlook

Separation science has progressed toward using short, high-efficiency columns packed with small, often superficially porous particles for liquid chromatographic analysis. This dissertation focused on providing methodologies for hundreds of small molecules using several existing and new high-efficiency chiral stationary phases (Chapters 2-6). The fundamental methodologies led to universal methods, including the enantiomeric separation of 18 racemic controlled substances in 35 minutes (Chapter 2) or 32 fungicide enantiomers in less than 20 minutes (Chapter 6), each with a single method using LC-MS. While these methodologies did advance the literature with fast and effective separations, peak overlap was still observed. This led to the introduction of post-acquisition signal processing, which can be used in any type of chromatography, to enhance chromatographic resolution. Indirect and direct methods, specifically iterative curve fitting, Fourier transform, power law, and derivatives were evaluated and discussed (Chapters 6-10). Signal processing presents an effective and simple platform for extracting more and better information from any given chromatogram. However, it will be most useful in high-throughput screening applications and for complex sample analysis. The separation of 101 components in under a minute provides the ultimate example of the power of these signal processing techniques (Chapter 10). Surely, future automation will make them extremely useful to the chromatography community-hence this intelligent peak processing is the future of chromatography.

Appendix A: Chapter co-authors & citations

Chapter 2: G. Hellinghausen, D. Roy, J.T. Lee, Y. Wang, C.A. Weatherly, D.A. Lopez, K.A. Nguyen, J.D. Armstrong, D.W. Armstrong, *J. Pharm. Biomed. Anal.* **155**, 70-81 (2018).

Chapter 3: G. Hellinghausen, D.A. Lopez, J.T. Lee, Y. Wang, C.A. Weatherly, A.E. Portillo, A. Berthod, D.W. Armstrong, *Chirality* **30**, 1067-1078 (2018).

Chapter 4: G. Hellinghausen, J.T. Lee, C.A. Weatherly, D.A. Lopez, D.W. Armstrong, *Drug Test. Anal.* **9** (2017) 944-948.

Chapter 5: G. Hellinghausen, D. Roy, Y. Wang, J.T. Lee, D.A. Lopez, C.A. Weatherly, D.W. Armstrong, *Talanta* **181**, 132-141 (2018).

Chapter 6: G. Hellinghausen, E.R. Readell, M.F. Wahab, J.T. Lee, D.A. Lopez, C.A. Weatherly, D.W. Armstrong, *Chromatographia* **82** (2018) 221-233.

Chapter 7: M.F. Wahab, T.C. O'Haver, F. Gritti, G. Hellinghausen, D.W. Armstrong, *Talanta* **192** (2019) 492-499.

Chapter 8: G. Hellinghausen, M.F. Wahab, D.W. Armstrong, *J. Chromatogr. A* **1574** (2018) 1-8.

Chapter 9: M.F. Wahab, G. Hellinghausen, D.W. Armstrong, *LC GC Eur* **32** (2019) 22-28.

Chapter 10: G. Hellinghausen, M.F. Wahab, D.W. Armstrong, *Anal. Bioanal. Chem.* (submitted).

Appendix B: Rights and permissions

Chapter 2



RightsLink®

Home

Account Info

Help



Title: Effective methodologies for enantiomeric separations of 150 pharmacology and toxicology related 1°, 2°, and 3° amines with core-shell chiral stationary phases

Author: Garrett Hellinghausen, Daipayan Roy, Jauh T. Lee, Yadi Wang, Choyce A. Weatherly, Diego A. Lopez, Kate A. Nguyen, John D. Armstrong, Daniel W. Armstrong

Publication: Journal of Pharmaceutical and Biomedical Analysis

Publisher: Elsevier

Date: 5 June 2018

© 2018 Elsevier B.V. All rights reserved.

Logged in as:

Garrett Hellinghausen
University of Texas at
Arlington

Account #:
3001303587

LOGOUT

Please note that, as the author of this Elsevier article, you retain the right to include it in a thesis or dissertation, provided it is not published commercially. Permission is not required, but please ensure that you reference the journal as the original source. For more information on this and on your other retained rights, please visit: <https://www.elsevier.com/about/our-business/policies/copyright#Author-rights>

BACK

CLOSE WINDOW

Copyright © 2019 Copyright Clearance Center, Inc. All Rights Reserved. [Privacy statement](#). [Terms and Conditions](#).
Comments? We would like to hear from you. E-mail us at customercare@copyright.com

Chapter 3

JOHN WILEY AND SONS LICENSE TERMS AND CONDITIONS

Oct 25, 2019

This Agreement between University of Texas at Arlington -- Garrett Hellinghausen ("You") and John Wiley and Sons ("John Wiley and Sons") consists of your license details and the terms and conditions provided by John Wiley and Sons and Copyright Clearance Center.

License Number	4696090073475
License date	Oct 25, 2019
Licensed Content Publisher	John Wiley and Sons
Licensed Content Publication	Chirality
Licensed Content Title	Evaluation of the Edman degradation product of vancomycin bonded to core-shell particles as a new HPLC chiral stationary phase
Licensed Content Author	Garrett Hellinghausen, Diego A. Lopez, Jauh T. Lee, et al
Licensed Content Date	Jul 3, 2018
Licensed Content Volume	30
Licensed Content Issue	9
Licensed Content Pages	12
Type of use	Dissertation/Thesis
Requestor type	Author of this Wiley article
Format	Print and electronic
Portion	Full article
Will you be translating?	No
Title of your thesis / dissertation	DEVELOPMENT, EVALUATION, AND APPLICATION OF CHROMATOGRAPHIC RESOLUTION ENHANCEMENT STRATEGIES
Expected completion date	Dec 2019
Expected size (number of pages)	200
Requestor Location	University of Texas at Arlington Department of Chemistry and Biochemistry The University of Texas at Arlington ARLINGTON, TX 76019 United States Attn: University of Texas at Arlington
Publisher Tax ID	EU826007151
Total	0.00 USD
Terms and Conditions	

**JOHN WILEY AND SONS LICENSE
TERMS AND CONDITIONS**

Oct 25, 2019

This Agreement between University of Texas at Arlington -- Garrett Hellinghausen ("You") and John Wiley and Sons ("John Wiley and Sons") consists of your license details and the terms and conditions provided by John Wiley and Sons and Copyright Clearance Center.

License Number	4696090760855
License date	Oct 25, 2019
Licensed Content Publisher	John Wiley and Sons
Licensed Content Publication	Drug Testing and Analysis
Licensed Content Title	Evaluation of nicotine in tobacco-free-nicotine commercial products
Licensed Content Author	Daniel W. Armstrong, Diego A. Lopez, Choyce A. Weatherly, et al
Licensed Content Date	Jan 25, 2017
Licensed Content Volume	9
Licensed Content Issue	6
Licensed Content Pages	5
Type of use	Dissertation/Thesis
Requestor type	Author of this Wiley article
Format	Print and electronic
Portion	Full article
Will you be translating?	No
Title of your thesis / dissertation	DEVELOPMENT, EVALUATION, AND APPLICATION OF CHROMATOGRAPHIC RESOLUTION ENHANCEMENT STRATEGIES
Expected completion date	Dec 2019
Expected size (number of pages)	200
Requestor Location	University of Texas at Arlington Department of Chemistry and Biochemistry The University of Texas at Arlington ARLINGTON, TX 76019 United States Attn: University of Texas at Arlington
Publisher Tax ID	EU826007151
Total	0.00 USD
Terms and Conditions	

Chapter 5



RightsLink®

Home

Account Info

Help



Title: A comprehensive methodology for the chiral separation of 40 tobacco alkaloids and their carcinogenic E/Z-(R,S)-tobacco-specific nitrosamine metabolites

Author: Garrett Hellinghausen, Daipayan Roy, Yadi Wang, Jauh T. Lee, Diego A. Lopez, Choyce A. Weatherly, Daniel W. Armstrong

Publication: Talanta

Publisher: Elsevier

Date: 1 May 2018

© 2017 Elsevier B.V. All rights reserved.

Logged in as:
Garrett Hellinghausen
University of Texas at
Arlington
Account #:
3001303587

LOGOUT

Please note that, as the author of this Elsevier article, you retain the right to include it in a thesis or dissertation, provided it is not published commercially. Permission is not required, but please ensure that you reference the journal as the original source. For more information on this and on your other retained rights, please visit: <https://www.elsevier.com/about/our-business/policies/copyright#Author-rights>

BACK

CLOSE WINDOW

Copyright © 2019 [Copyright Clearance Center, Inc.](#) All Rights Reserved. [Privacy statement](#). [Terms and Conditions](#).
Comments? We would like to hear from you. E-mail us at customercare@copyright.com

Chapter 6

SPRINGER NATURE LICENSE TERMS AND CONDITIONS

Oct 25, 2019

This Agreement between University of Texas at Arlington -- Garrett Hellinghausen ("You") and Springer Nature ("Springer Nature") consists of your license details and the terms and conditions provided by Springer Nature and Copyright Clearance Center.

License Number	4696091187849
License date	Oct 25, 2019
Licensed Content Publisher	Springer Nature
Licensed Content Publication	Chromatographia
Licensed Content Title	Mass Spectrometry-Compatible Enantiomeric Separations of 100 Pesticides Using Core-Shell Chiral Stationary Phases and Evaluation of Iterative Curve Fitting Models for Overlapping Peaks
Licensed Content Author	Garrett Hellinghausen, Elizabeth R. Readel, M. Farooq Wahab et al
Licensed Content Date	Jan 1, 2018
Licensed Content Volume	82
Licensed Content Issue	1
Type of Use	Thesis/Dissertation
Requester type	academic/university or research institute
Format	print and electronic
Portion	full article/chapter
Will you be translating?	no
Circulation/distribution	1 - 29
Author of this Springer Nature content	yes
Title	DEVELOPMENT, EVALUATION, AND APPLICATION OF CHROMATOGRAPHIC RESOLUTION ENHANCEMENT STRATEGIES
Institution name	n/a
Expected presentation date	Dec 2019
Requester Location	University of Texas at Arlington Department of Chemistry and Biochemistry The University of Texas at Arlington ARLINGTON, TX 76019 United States Attn: University of Texas at Arlington
Total	0.00 USD
Terms and Conditions	

Chapter 7



RightsLink®

[Home](#)[Account Info](#)[Help](#)

Title: Increasing chromatographic resolution of analytical signals using derivative enhancement approach

Author: M. Farooq Wahab, Thomas C. O'Haver, Fabrice Gritti, Garrett Hellinghausen, Daniel W. Armstrong

Publication: Talanta

Publisher: Elsevier

Date: 15 January 2019

© 2018 Elsevier B.V. All rights reserved.

Logged in as:

Garrett Hellinghausen
University of Texas at
Arlington

Account #:
3001303587

[LOGOUT](#)

Please note that, as the author of this Elsevier article, you retain the right to include it in a thesis or dissertation, provided it is not published commercially. Permission is not required, but please ensure that you reference the journal as the original source. For more information on this and on your other retained rights, please visit: <https://www.elsevier.com/about/our-business/policies/copyright#Author-rights>

[BACK](#)

[CLOSE WINDOW](#)

Copyright © 2019 [Copyright Clearance Center, Inc.](#) All Rights Reserved. [Privacy statement](#). [Terms and Conditions](#).
Comments? We would like to hear from you. E-mail us at customercare@copyright.com

Chapter 8



RightsLink®

Home

Account Info

Help



Title: Improving visualization of trace components for quantification using a power law based integration approach

Author: Garrett Hellinghausen, M. Farooq Wahab, Daniel W. Armstrong

Publication: Journal of Chromatography A

Publisher: Elsevier

Date: 2 November 2018

© 2018 Elsevier B.V. All rights reserved.

Logged in as:

Garrett Hellinghausen
University of Texas at
Arlington

Account #:
3001303587

LOGOUT

Please note that, as the author of this Elsevier article, you retain the right to include it in a thesis or dissertation, provided it is not published commercially. Permission is not required, but please ensure that you reference the journal as the original source. For more information on this and on your other retained rights, please visit: <https://www.elsevier.com/about/our-business/policies/copyright#Author-rights>

BACK

CLOSE WINDOW

Copyright © 2019 Copyright Clearance Center, Inc. All Rights Reserved. [Privacy statement](#). [Terms and Conditions](#).
Comments? We would like to hear from you. E-mail us at customer@copyright.com

Chapter 9

Copyright Permissions for Dissertation from LCGC



Laura Bush <LBush@mmhgroup.com>

Fri 10/25/2019 4:17 PM

Hellinghausen, Garrett ✓



Dear Garrett,

As a co-author, you, along with your co-authors, retained your copyright over the unedited, original version, and thus you have full permission to use that version as you wish.

We are also happy to have you use the edited version for the purposes of your dissertation.

Best regards,

Laura Bush, Editorial Director, LCGC & Spectroscopy
485F US Highway 1 S, Ste 210, Iselin, NJ 08830-3009
Office: +1.732.346.3020; Mobile: +1.908.963.0058

LCGC and Spectroscopy are now part of the MMH Group.

Please note my new email address:

lbush@MMHGroup.com

www.chromatographyonline.com

www.spectroscopyonline.com

...

Chapter 10

Unpublished work.

Biographical information

Garrett Hellinghausen obtained his Bachelor of Science Degree in Biochemistry from the University of Texas at Austin in 2015. He worked at a CRO called the Drug Dynamics Institute that collaborated with the College of Pharmacy at the University of Texas at Austin where his passion for separations began. He joined Professor Daniel W. Armstrong's research group in 2015. He developed hundreds of chiral separation methodologies using several newly synthesized chiral stationary phases. The focus of his recent work has been on the investigation of signal processing techniques that can be applied to fast chromatography. He has presented his work in numerous conferences like Pittcon and HPLC and received the Analytical Bioanalytical Award for his work on signal processing at the ISCC & GCxGC conference (Fort Worth, TX) in 2019. He also received the Graduate Student Teaching Award in 2017 and the Charles K. Baker Scholarship in 2019 for his character during his time at the University of Texas at Arlington.